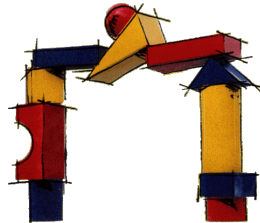![JGU Universitätsmedizin Mainz logo]

Modulation of intrahepatic immune responses through nanoparticle-mediated delivery of drugs, adjuvants, and antigens

Dissertation zur Erlangung des Grades

„Doktor der Naturwissenschaften"

am Fachbereich Biologie

der Johannes Gutenberg-Universität Mainz

vorgelegt von Michael Fichter

geboren am 03.04.1987 in Zweibrücken

Mainz, März 2016

D77

Dekan: Prof. Dr. rer. nat. Hans Zischler

Erster Gutachter:

Zweiter Gutachter:

Tag der mündlichen Prüfung: 11.11.2016

PREFACE

The present PhD thesis is the result of research performed between December 2011 and December 2015 at the laboratory for Pediatric Immunology and Infectious Diseases headed by Univ.-Prof. Dr. med. Stephan Gehring at the Children´s Hospital of the Johannes Gutenberg University Mainz, Germany. The obtained data have been presented in six publications and one submitted manuscript attached to this thesis (see Appendix 1-7).

1. **Fichter M**, Baier G, Dedters M, Pretsch L, Pietrzak-Nguyen A, Landfester K, Gehring S.

   Nanocapsules generated out of a polymeric dexamethasone shell suppress the inflammatory response of liver macrophages.

   Nanomedicine, 2013. **9**(8): p. 1223-34.

2. Pietrzak-Nguyen A, **Fichter M**, Dedters M, Pretsch L, Gregory SH, Meyer CU, Doganci A, Diken M, Landfester K, Baier G, Gehring S.

   Enhanced *in vivo* targeting of murine nonparenchymal liver cells with monophosphoryl lipid A functionalized microcapsules.

   Biomacromolecules, 2014. **15**(7): p. 2378-88.

3. **Fichter M***, Dedters M*, Pietrzak-Nguyen A, Pretsch L, Meyer CU, Strand S, Zepp F, Baier G, Landfester K, Gehring S.

   Monophosphoryl lipid A coating of hydroxyethyl starch nanocapsules drastically increases uptake and maturation by dendritic cells while minimizing the adjuvant dosage.

   Vaccine, 2015. **33**(7): p. 838-46.

   * Shared first authorship

4. Piradashvili K, **Fichter M**, Mohr K, Gehring S, Wurm FR, Landfester K.

   Biodegradable protein nanocontainers.

   Biomacromolecules, 2015. **16**(3): p. 815-21.

5. Baier G, Winzen S, Messerschmidt C, Frank D, **Fichter M**, Gehring S, Mailänder V, Landfester K.

   Heparin-based nanocapsules as potential drug delivery systems.

   Macromol Biosci, 2015. **15**(6): p. 765-76.

6. Baier G, **Fichter M**, Kreyes A, Klein K, Mailander V, Gehring S, Landfester K.

   Glutathione responsive hyaluronic acid nanocapsules obtained by bioorthogonal interfacial "click" reaction.

   Biomacromolecules, 2016. **17**(1): p. 148-53.

7. **Fichter M**, Piradashvili K, Pietrzak-Nguyen A, Pretsch L, Kuhn G, Strand S, Zepp F, Wurm FR, Mailänder V, Landfester K, Gehring S.

   Polymeric hepatitis C virus non-structural protein 5A nanocapsules induce intrahepatic antigen-specific immune responses.

   submitted manuscript

Significant findings along with their scientific relevance are summarized in the following sections.

Mainz, March 2016

Michael Fichter

TABLE OF CONTENTS

LIST OF FIGURES

LIST OF TABLES

ABSTRACT

Targeted delivery of drugs, antigens, or adjuvants to organs and cells of interest is a promising concept for the development of novel drug or vaccine formulations. Benefits arising from this approach include protection of agents from degradation, increased drug bioavailability, and reduced systemic adverse effects. Polymeric nanocapsules are particularly suited for the application as vaccine delivery systems, since they facilitate combined delivery of antigens along with adjuvants to antigen-presenting cells (APCs). Intravenous administration of these nanocarriers enables targeting of liver APCs subsequently inducing intrahepatic T cellular immune responses essential for eradication and control of viral infections, e.g. hepatitis C virus (HCV). Aim of the present study was the modulation of intrahepatic immune responses using functionalized nanocapsules.

Polymeric nanocapsules (NCs) were synthesized of hydroxyethyl starch (HES), dexamethasone (DXM), heparin (HEP), hyaluronic acid (HA), ovalbumin (OVA), and HCV non-structural protein 5A (NS5A) by a polyaddition reaction in an inverse miniemulsion process. Nanocapsule formulations were characterized with respect to biodistribution, cargo release, and the biological activity of nanocapsule cargo.

Intravenous administration of NCs led to a preferential deposition in the liver, targeting mainly dendritic cells and Kupffer cells. Intracellular release of encapsulated cargo was documented for NCs made of the model antigen OVA or glutathione-responsive HA-NCs using protease-sensitive fluorescent dyes. In addition, release of NC content and biological activity of the encapsulated compound was observed through suppression of inflammatory responses by Kupffer cells following uptake of DXM-NCs *in vitro*. In parallel, polymeric HEP-NCs exhibited anti-coagulative properties even after polymerization.

The final goal of this thesis, the induction of intrahepatic HCV antigen-specific immune responses, was achieved by surface functionalization of NS5A nanocapsules with monophosphoryl lipid A (MPLA). Uptake of these NC formulations by dendritic cells induced vigorous maturation reducing the required equipotent MPLA dosage by more than 15 times. Immunization with MPLA-supplemented NS5A nanocapsules exclusively synthesized of the antigen generated robust intrahepatic T cellular immune responses and substantial levels of antigen-specific antibodies.

In summary, polymeric nanocapsules, made of immunosuppressive drugs or antigens, represent a novel approach for an effective and targeted treatment of inflammatory and infectious liver diseases such as autoimmune hepatitis, HCV, or Malaria.

1 INTRODUCTION

1.1 Nanoformulations for biomedical applications

Over the past 20 years the interest in nanoparticle research for biomedical applications steadily increased, with more than 16.000 publications in 2015 (Figure 1). The size of nanoparticles was specified by the United States Food and Drug Administration (FDA) and the European Medicine Agency (EMA) to range from 1 nm to 1000 nm [1, 2]. In addition, nanoparticles can be categorized based on their morphology, chemical composition, and physico-chemical properties. Different nanotechnological formulations applied to various biomedical applications include liposomes, solid-lipid nanoparticles, micelles, nanocrystals, dendrimers, iron oxide or gold nanoparticles, polymeric nanoparticles or nanocapsules, and nanoemulsions [2-6]. Nanoformulations of drugs and vaccines inherit the potential to optimize delivery to specified cells and organs, bioavailability, and compound stability, concurrently avoiding systemic side effects [7]. Consequently, applications in different disciplines are diverse, ranging from iron oxide nanoparticles utilized for imaging of cancer and thermal treatment of tumors [8] to self-assembling virus-like particles used for immunization [9].
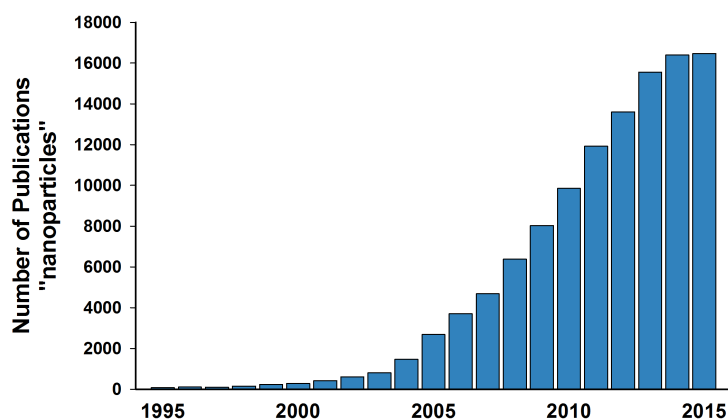
Figure 1: Number of publications in the field of nanoparticles. Publication frequency was estimated based on a literature search with the term: "nanoparticles" using the PubMed platform (www.pubmed.gov, effective January 7, 2016).

Nanocrystals are able to enhance solubility and bioavailability, e.g. in the case of sirolimus, a water-insoluble immunosuppressive drug often applied in patients receiving kidney transplants [10]. Liposomes, another very successful nanoformulation composed of amphiphilic lipid molecules forming a bilayer structure, have been widely tested in clinical trials for drug delivery to target cells and have been approved by regulatory authorities [11]. The formation of bilayer structures with an aqueous core is attributed to amphiphilic lipid molecules providing the possibility to entrap hydrophilic and hydrophobic drugs. Nanoemulsions, in particular oil-in-water emulsions, are often utilized for delivery of water-insoluble drugs in order to improve bioavailability. Recently, several

formulations, based on nanoemulsions, have been introduced to the pharmaceutical market, e.g. the formulation of water-insoluble agents, including vitamins A, D, E, K (Vitalipid® by Fresenius Kabi) for parenteral nutrition, or propofol (Diprivan® by AstraZeneca) [12]. However, stabilization of nanoemulsions can be challenging and needs additional emulsifiers to prevent breakdown by re-coalescence or aggregation [13].

1.1.1 Drug delivery with polymeric nanoparticles

Polymeric nanoparticles play a significant role in biopharmaceutical development. A wide range of synthetic or natural substances have been investigated for the synthesis of polymeric nanoparticles, including chitosan, gelatin, starch, poly(cyanoacrylates) (PACA), polylactic acid (PLA), and poly(lactic-*co*-glycolic acid) (PLGA) [14, 15]. PLGA nanoparticles have been used extensively for the delivery and release of drugs due to their excellent biocompatibility and the ability to precisely modulate their physico-chemical properties. Certain PLGA nanoparticle formulations are already approved by regulatory authorities (FDA / EMA) [16].

Polymeric nanoparticles are classified into *nanospheres*, consisting of an uniform structure (matrix) and the entrapped drug, in contrast to *nanocapsules,* characterized by a polymeric shell with cross-linked carrier molecules and a fluidic, drug-containing core [17]. An efficient and controlled release of encapsulated drugs is a prerequisite of every drug delivery system. Release properties of nanocapsules can be precisely adjusted, since they strongly depend on the physico-chemical characteristics of the capsule shell, including the type of polymer used for synthesis, molecular weight, and thickness [6]. A targeted drug delivery is essential in order to prevent unintended side effects caused by systemic distribution of the drug while maintaining similar therapeutic effects on the organ or cells of interest. Thus, nanocapsules are very well suited as delivery vehicles due to the potential of surface functionalization with targeting moieties such as antibodies, proteins, or peptides [18, 6]. Further advantages of polymeric nanocapsules include: (1) protection of antigens from proteolysis by encapsulation [19, 20]; (2) enhanced phagocytosis [21-24]; and (3) prolonged release and presentation of antigens by dendritic cells [25-27].

1.1.2 Nanoparticulate vaccines

Polymeric PLGA particles are one of the most studied formulations in the field of vaccinology. Vaccination approaches based on PLGA particles have been performed against viral antigens derived from HIV [28] and influenza virus [29], and tumor antigens

overexpressed by certain cancer types [30-32]. Liposomes and virus-like particles (VLP) have also been introduced as particulate vaccine formulations [33]. Self-assembling viral structural proteins form VLPs, which lack viral nucleic acid and are thus safe and non-infectious antigen delivery vehicles. VLPs mimic viruses in terms of size, morphology and antigen composition making them ideal vaccine candidates [34, 35]. Few VLP-based vaccines have already been approved for prophylactic immunizations against viral infections like hepatitis B virus (Engerix®, GlaxoSmithKline and Recombivax HB®, Merck and Co., Inc.) or human papilloma virus (Cervarix®, GlaxoSmithKline and Gardasil®, Merck and Co., Inc.) [36, 37].

1.1.3 Adjuvant supplementation of nanoparticulate vaccines

In most cases, despite the high immunogenicity VLPs elicit, additional adjuvant supplementation is required for the induction of robust and long-lasting protective immunity [38, 39]. Several vaccines licensed for the use in humans, such as HPV, HBV, HAV, TBE, Polio, Diphteria, Tetanus, and Pertussis, are supplemented with aluminum salts (aluminum hydroxide or phosphate), often referred to as alum [40]. However, alum preferentially induces T_h2-directed immune responses (humoral immunity) characterized by the secretion of antigen-specific (neutralizing) antibodies [41, 42]. Unfortunately, humoral immune responses are not sufficient for effective protection against pathogens requiring strong T_h1-mediated immunity, e.g. hepatitis C virus (HCV), Plasmodia (Malaria parasites) or the human immunodeficiency virus (HIV) [43, 41, 44]. Consequently, alternative adjuvants promoting T_h1-directed differentiation are needed. Monophosphoryl lipid A (MPLA), a synthetic Toll-like receptor 4 (TLR4) agonist and low toxicity derivative of lipopolysaccharide (LPS), enhances T_h1-directed immune responses [45]. MPLA adsorbed on alum (referred to as AS04) is currently approved for the use as adjuvant in GlaxoSmithKline´s HBV (Fendrix®) and HPV (Cervarix®) vaccines [46, 47].

The benefit of combined and simultaneous delivery of antigens along with adjuvants to dendritic cells, resulting in robust and sustained immune responses, has been documented in several studies [48-50]. Polymeric nanocapsules are perfectly suited delivery vehicles due to the possibility of combining antigens and adjuvants in a single particle system [24, 51, 52]. Antigens and adjuvants can be associated with nanocapsules by encapsulation or coupling to the capsule surface. Combining two or more adjuvants in the same particle enables to precisely modulate the type of immune response (T_h1 / T_h2) or the magnitude of response that is required [53]. For example, LPS and IFNγ induced a substantial secretion of interleukin-12 (IL-12), a T_h1-promoting cytokine, by human dendritic cells, whereas single components did not [54].

1.2 Hepatitis C virus infection

Approximately 3% of the world's population is infected with the hepatitis C virus, accounting for more than 184 million people worldwide [55]. Regions with high prevalence (> 3.5%) include Central and East Asia, the Middle East, and North Africa. However, there are no robust epidemiologic data for most of the sub-Saharan African countries [56]. Particular high prevalences are reported for Egypt and Cameroon with about 14% [57]. The largest population of infected individuals is located in China (29.8 million), India (18.2 million), Egypt (11.8 million), Pakistan (9.4 million), and Indonesia (9.4 million) [58]. Worldwide, genotype 1 is the most prevalent strain, whereas genotypes 2 and 4 are predominantly present in African countries (Figure 2). Genotype 3 is the most prevalent strain in India, Pakistan and Thailand [58].
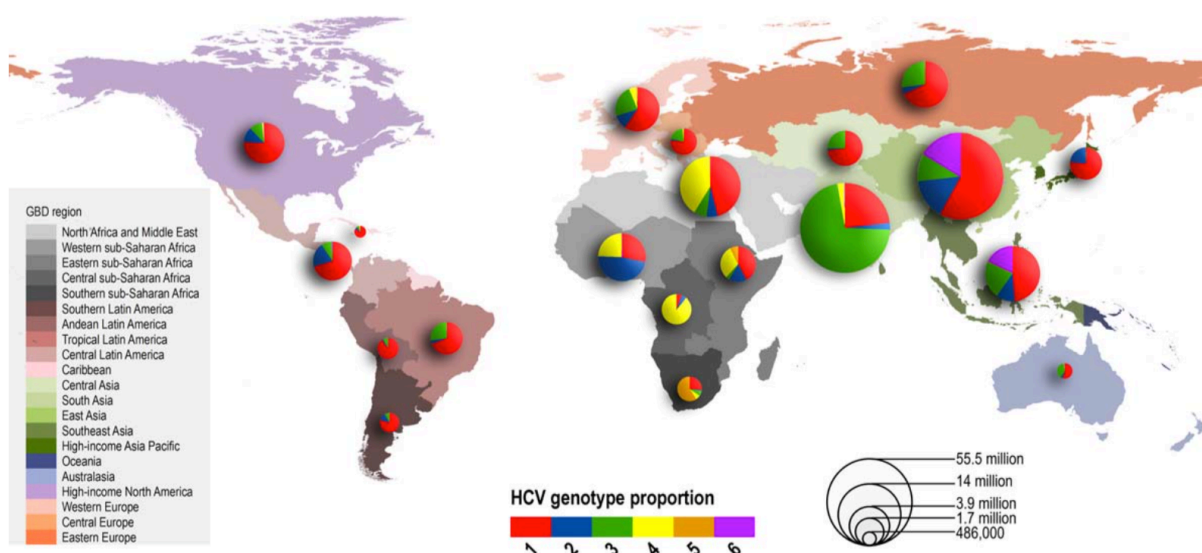
Figure 2: Global prevalence of HCV genotypes. Regions were determined by guidelines of the Global Burden of Disease, Injuries and Risk Factors 2010 (GBD2010) study. Pie charts represent the relative seroprevalence based on estimation of Mohd Hanafiah et al. (2013). Figure from Messina et al. (2015).

Incidence rates are likely underestimated due to the lack of epidemiologic data and the predominantly asymptomatic course of acute HCV infection [58]. Infection rates dropped dramatically since the discovery of HCV in 1989 by Choo et al. [60, 61]. Nevertheless, HCV still represents one of the major health issues with a significant global disease burden. 350,000 deaths per year are attributed to HCV-related liver diseases [62].

1.2.1 Natural history of HCV infection

Hepatitis C virus is a single-stranded RNA virus of the *Flaviviridae* family [63]. Transmission of HCV occurs through parenteral exposure to blood, e.g. through blood transfusion or needlestick injury [64, 65]. In general, HCV RNA can be detected as early

as 2 weeks post infection followed by the appearance of anti-HCV antibodies (seroconversion) approximately 7 to 8 weeks later [66]. Serum alanine aminotransferase (ALT) increases dramatically during the acute phase of infection (4 - 6 weeks), but drops again to only slightly elevated levels [67]. Approximately 20 - 30% of acutely infected patients spontaneously clear infection, which is associated with seroconversion (appearance of anti-HCV IgM and later IgG antibodies) and the disappearance of HCV RNA. Unfortunately, 70 - 80% of patients develop chronic infection defined by the persistence of HCV RNA for more than 6 months after infection [68]. Chronic HCV infection (CHC) induces an ongoing intrahepatic inflammation associated with the development of liver fibrosis, leading to cirrhosis in 20 - 30% of all CHC patients [64, 69]. Approximately 30% of patients with severe liver fibrosis or cirrhosis develop a hepatocellular carcinoma (HCC) [70, 71].

1.2.2 Treatment of HCV infection

Until a few years ago the standard of care treatment was the combined administration of interferon-α (IFNα) or pegylated IFNα and ribavirin (RBV) with sustained virological response (SVR) rates of 30 - 40% for patients infected with HCV genotype 1 (about 80% for genotypes 2 and 3). This treatment is associated with severe side effects including autoimmune activation, general malaise, and depression [72-74]. Recently, treatment options dramatically improved due to the development of novel direct acting antiviral drugs (DAAs). SVR rates of over 95% could be achieved with combinations including sofosbuvir/ledipasvir, sofosbuvir/daclatasvir, and ombitasvir/paritaprevir/ritonavir + dasabuvir (3D) [75-77]. Notably, all of the outlined DAA combinations exclude the use of IFNα. However, the expenses for a 12-week therapy with sofosbuvir or sofosbuvir/ledipasvir are extraordinary high, amounting up to $94,500 in the US [78]. Access to this costly treatment is limited not only in the western world, but also in countries with limited resources, most often particularly stricken with a high HCV prevalence [79]. Moreover, DAA treatment promotes the appearance of resistant viral strains due to drug induced evolutionary pressure, the high mutational rate of HCV, and the pre-existing genetic variability of HCV [80-85].

Intravenous drug users (IVDU) have a particular high risk for HCV infection, documented by a global seroprevalence of 51% [86]. Even after successful DAA treatment, IVDUs are at high risk to be reinfected in case of continued drug abuse [87].

The costly HCV treatment, resistant viral strains, and the risk of reinfection in populations with high HCV exposure provide a strong rationale for research efforts aiming to develop a prophylactic and/or therapeutic HCV vaccine.

1.2.3   The liver as an immunological organ

The liver is essential for detoxification and degradation of endogenous and exogenous waste products and is highly involved in protein, carbohydrate and lipid metabolism [88]. The microanatomy of the liver is characterized by multiple repetitive units - hexagonal lobules - with radially arranged cords of hepatocytes surrounded by vasculatory sinusoids, effectively providing blood supply (Figure 3). Moreover, the liver exerts important immunological functions. Liver function is reflected by its cellular composition with 60 - 80% hepatocytes, representing parenchymal cells, and 20 - 40% non-hepatocytic cells, the so-called "non-parenchymal liver cells" (NPCs) [89].
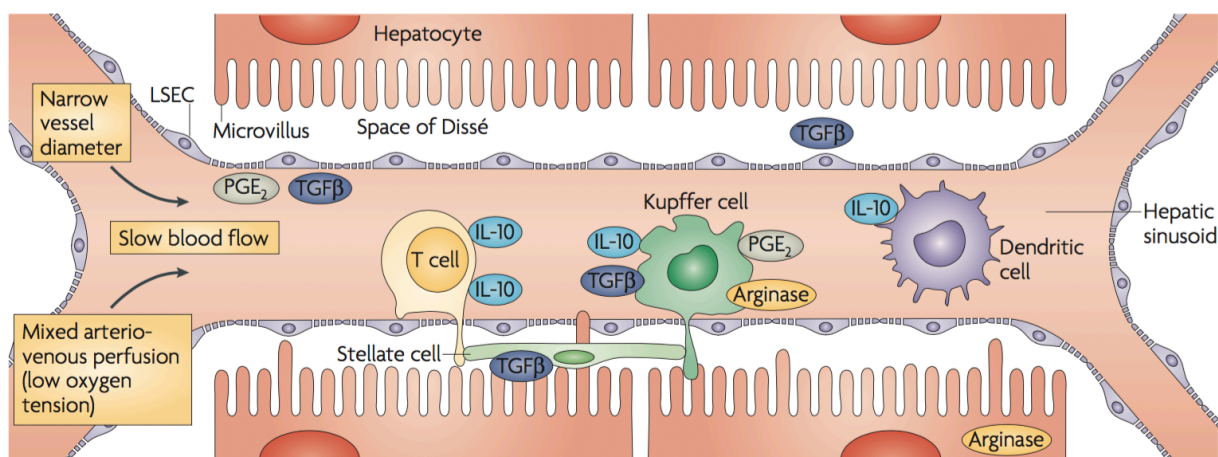
Figure 3: Microanatomy of the liver sinusoids and immunological cells. Liver sinusoidal endothelial cells (LSECs) form a fenestrated endothelial barrier between sinusoids and the parenchyma (hepatocytes). Hepatic stellate cells reside within the Space of Dissé located between the endothelial barrier and hepatocytes. Dendritic cells and Kupffer cells are located in the sinusoids but are able to migrate through LSECs into the Space of Dissé. Hepatic antigen-presenting cells exert tolerogenic functions due to the secretion of IL-10, TGFβ, and prostaglandin E_2. *IL-10: interleukin-10, TGFβ: transforming growth factor-β, PGE$_2$: prostaglandin E$_2$.* Figure from Thomson et al. (2010).

NPCs can be further classified in liver sinusoidal endothelial cells (LSECs), about 50% of NPCs, Kupffer cells (≈ 20%) constituting the immobile macrophage population in the liver, biliary cells (≈ 5%), hepatic stellate cells (< 1%), and dendritic cells with different subsets (≈ 1%) (Figure 4) [89, 91]. In addition, 25% of NPCs are lymphocytes, which can be further subdivided in conventional (CD4$^+$ and CD8$^+$) and unconventional T cells (e.g. classical and non-classical natural killer T cells), natural killer cells (NKs), and B cells [89].

Dendritic cells, Kupffer cells and LSECs form the hepatic reticulo-endothelial system (scavenger cells), clearing the sinusoidal blood stream from bacterial and food-derived

degradation products, antigens, and toxins via endocytosis receptors [90]. The liver is exposed to large amounts of endotoxins originating from the gastrointestinal tract (up to 1 ng/ml of lipopolysaccharide) leading to a hyporesponsiveness of scavenger cells, in particular of hepatic myeloid DCs [92, 93].
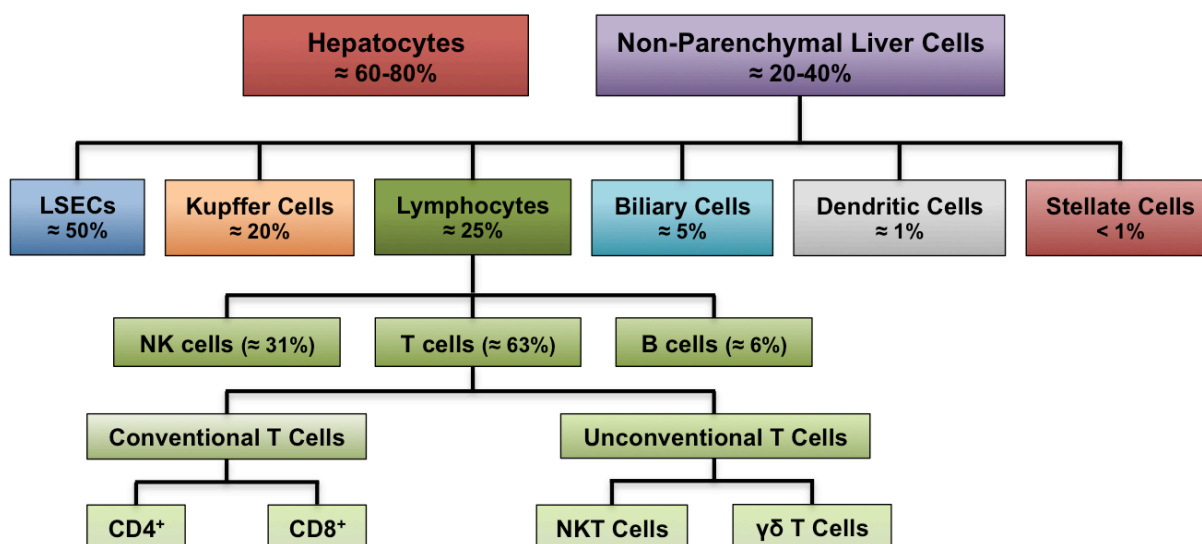
Figure 4: Cellular composition of the liver. Frequencies of cell populations are related to the respective parent population. LSEC: liver sinusoidal endothelial cell, NK (T) cell: natural killer (T) cell. Figure adapted from Racanelli et al. (2006).

The endotoxin tolerance phenomenon contributes to the predominating tolerogenic microenvironment of the liver. The ligation of interleukin-6 (IL-6), IL-10, and transforming growth factor-β (TGFβ), which are secreted by different cell populations in the liver following LPS stimulation, leads to a suppressed activation of nuclear factor-κB (NF-κB) by downstream signaling, and subsequently to the inhibition of DC maturation [90]. This in turn increases the secretion of IL-10 parallel to a reduced production of IL-12 leading to a tolerogenic DC phenotype. Moreover, intrahepatic IL-10 secretion induces an antigen-specific T cell hyporesponsiveness and the differentiation to T_{reg} and T_h2 cells, subsequently suppressing T cell-mediated immune responses [94]. The tolerogenic liver environment is essential to prevent exaggerating inflammatory responses caused by bacterial debris from the gut. However, the same environment represents a great challenge for the development of vaccines against pathogens affecting the liver, such as HCV or Malaria parasites, with humoral immune responses providing only insufficient protection.

1.2.4 Hepatitis C virus vaccine development

The introduction of novel therapy regimens tremendously improved the outcome of hepatitis C virus-infected patients. However, the development of an effective prophylactic

vaccine is still an essential medical need, since prevention of infection is the most efficient measure to control infectious diseases. Following the discovery of the hepatitis C virus in 1989, formerly named "non-A, non-B hepatitis" (NANBH) virus, scientists have been working on the development of prophylactic vaccines. Nevertheless, to this day, there is no effective vaccine in sight. Several challenges account for this phenomenon. First, the hepatitis C virus has a tremendous replication rate and is equipped with an RNA polymerase that lacks proofreading activity. Consequently, evolutionary pressure induced by the host immunity leads to a rapid sequence drift and the generation of multiple quasispecies [95, 96]. The genetic variability of the virus enables the escape from CD8^{+} T cell activity and neutralizing antibody responses [97, 98]. Second, the virus is decorated with lipoproteins, shielding the epitopes of envelope glycoproteins E1 and E2 from recognition and binding of neutralizing antibodies [99, 100]. Third, translation of non-structural protein 3-4A in infected hepatocytes leads to the cleavage of mitochondrial antiviral-signaling protein (MAVS) and Toll/interleukin-1 receptor domain-containing adapter-inducing interferon-β (TRIF) protein involved in TLR3 (Toll-like receptor 3) and RIG-I (retinoic acid inducible gene I) signaling pathways. Thus, inhibition of IFNβ production upon recognition of HCV RNA by intracellular TLR3 and RIG-I results in reduced restriction of viral replication and delayed induction of CD8^{+} T cell responses [101-103]. Fourth, HCV inherits the capability to induce the loss of CD4^{+} T cell help leading to an exhaustion of CD8^{+} effector T cell function [98]. However, the involved pathways underlying this mechanism remain unclear [104]. In summary, HCV has evolved several very effective evading mechanisms, making it a challenging pathogen to control.

The lack of adequate rodent models susceptible to persistent HCV infections represents an additional obstacle contributing to the slow progression of vaccine development.

Recent clinical studies of the acute phase of infection clearly document the immunological prerequisites needed for eradication of HCV [105]. Broad intrahepatic CD8^{+} T cell responses directed against epitopes less prone to viral evasion, maintained by a vigorous CD4^{+} T cell-mediated immune response, are essential for viral clearance [106, 107]. A missing CD4^{+} T cell help leads to the functional exhaustion of effector CD8^{+} T cells and is a reliable predictor for a chronic course of infection [108, 44]. In contrast, strong T$_h$1-mediated immunity has been observed in patients with a sustained virological response [109]. The relevance of neutralizing antibodies against envelope proteins is controversially discussed. However, there is evidence that anti-envelope neutralizing antibodies have the capacity to aid protection from persistent infection [110-112]. Thus,

most of the recent studies focused on the induction of humoral responses against the structural proteins envelope 1 (E1) and envelope 2 (E2) [105].

Nanoparticulate structures were applied in pre-clinical vaccination approaches. Polymeric PLGA nanoparticles carrying plasmid DNA, encoding for different structural and non-structural proteins of the HCV polyprotein, induced humoral and T cell-mediated immune responses in mice after intramuscular administration [113, 114]. Moreover, hepatitis C virus-like particles consisting of the core, E1, and E2 proteins were successfully tested in chimpanzees leading to protective immunity after viral challenge [115].

1.2.5 HCV vaccine candidates in clinical trials

Two promising prophylactic vaccines that were successfully tested in chimpanzees have been introduced to clinical trials. Both elicited robust immune responses providing protection from chronic hepatitis after challenge of chimpanzees with HCV [97]. The vaccine developed by Chiron (now Novartis) consists of recombinant envelope glycoproteins E1 and E2 and is supplemented with the oil-in-water emulsion MF59 adjuvant [116]. This approach induced neutralizing antibodies reactive to different genotypes and a strong $CD4^+$ T cell response in a phase I clinical study, but did not proceed to a phase II study due to financial and human resource issues [117, 97, 118].

The Okairos (now GlaxoSmithKline) vaccine targets T cellular immunity by administration of chimpanzee adenovirus 3 (ChAd3) and modified vaccinia Ankara (MVA), both encoding the HCV non-structural proteins 3A-5B, applying a prime-boost regimen [119, 112]. In a phase I trial, the Okairos vaccine generated broad $CD4^+$ and $CD8^+$ T cell immune responses with a high magnitude [119]. This success led to the initiation of a follow-up phase I/II study in individuals at high risk (intravenous drug users) and first results are expected for 2016 [97, 112].

However, there are limitations in the application of adenoviral vectors as vaccine delivery vehicles with respect to pre-existing immunity even against adenoviruses with low seroprevalence in humans [120]. This phenomenon can reduce vaccine efficacy due to the presence of neutralizing antibodies against adenoviral vectors [121, 119].

The success and limitations of prophylactic vaccines, recently tested in clinical trials, emphasizes the need for vaccines inducing both, T cell immunity and neutralizing antibodies, in order to optimize protection against HCV infection [122, 112].

1.3   Aims of the PhD thesis

Focus of the present PhD thesis was the synthesis and subsequent investigation of polymeric nanocapsules targeting liver antigen-presenting cells in order to modulate intrahepatic immune responses.

Characterization of the synthesized nanocapsules followed three steps:

1) biodistribution of nanocapsules
2) release of nanocapsule cargo
3) biological activity of nanocapsule cargo (drug, antigen and/or adjuvant under *in vitro* and *in vivo* conditions)

The provided nanocapsule formulations were tested for efficient uptake by antigen-presenting cells such as liver dendritic cells or Kupffer cells *in vitro*. Moreover, a liver-specific targeting of nanocapsules was analyzed *in vivo* in order to pave the way for intrahepatic deposition of antigen-containing or immunosuppressive nanocapsules in vaccination approaches or in models of intrahepatic inflammation, respectively.

The extra- and intracellular release of cargo was investigated using encapsulated enzyme-sensitive fluorescent dyes. In addition, the intracellular release of the glucocorticoid dexamethasone (DXM) was analyzed regarding the suppression of inflammatory responses by hepatic Kupffer cells.

Biological activity of nanocapsule cargo was analyzed by functionalization with the Toll-like receptor 4 (TLR4) agonist monophosphoryl lipid A (MPLA) and/or αCD40, and subsequent activation of dendritic cells.

Finally, immunizations of mice with nanocapsules made of antigen were performed in order to induce intrahepatic T cellular immune responses against proteins originated from the hepatitis C virus. The nanocapsule-based vaccination of mice was the main focus of the present thesis.

2 RESULTS

Data summarized in the present thesis have already been published or submitted to scientific journals. Significant findings are summarized in the following sections, while publications and the submitted manuscript are attached (see Appendix).

2.1 Synthesis and characterization of polymeric nanocapsules

Polymeric nanocapsules were synthesized via inverse miniemulsion polymerization through an interfacial polyaddition reaction, adapted from Baier et al. [123]. Nanocapsule formulations were prepared of dexamethasone (DXM), hydroxyethyl starch (HES), heparin (HEP), hyaluronic acid (HA), ovalbumin (OVA), and the hepatitis C virus non-structural protein 5A (NS5A). The resulting polymeric nanocapsules displayed a core-shell morphology evaluated by transmission and scanning electron microscopy (Figure 5). Further characterization was performed using zeta potential measurements and dynamic light scattering, determining the average diameter and size distribution of nanocapsules [124-130]. Different fluorescent dyes, such as cy5-labeled oligonucleotides, IRdye 800CW, sulforhodamine 101, CellTracker™ Green CMFDA, or DQ™ ovalbumin, were encapsulated for subsequent intracellular detection and *in vivo* tracking. Encapsulation efficiencies and stability evaluations were performed on the basis of encapsulated fluorescence dyes, demonstrating high integrity of the capsule shell [129, 130]. Moreover, nanocapsules were further functionalized by adsorption of monophosphoryl lipid A (MPLA) or covalent coupling of antibodies onto the NC surface. Table 1 summarizes nanocapsule formulations and characteristics based on colloid chemical analyses.

Table 1: Characterization of nanocapsule formulations.

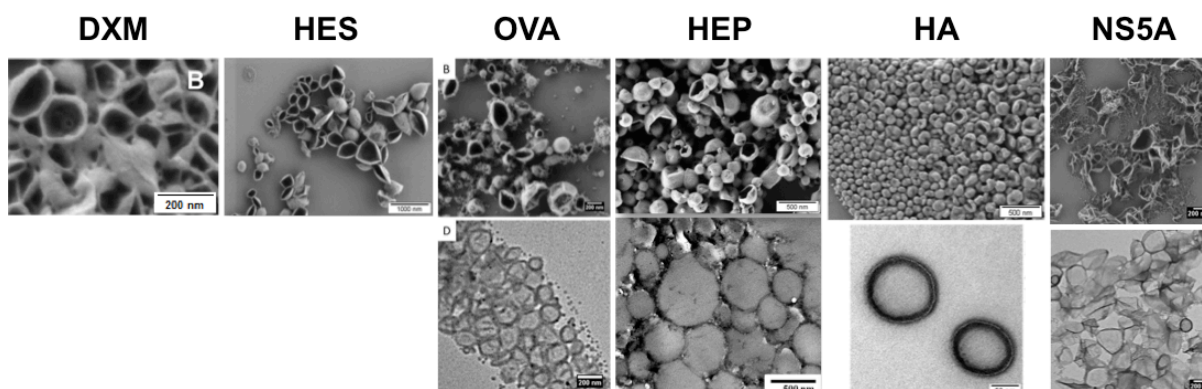| Nanocapsule formulation	Average diameter [nm]	Zeta potential [mV]	Reference
DXM	240	-22	[126]
HES	230	-24	[129, 127]
HES+MPLA	235	-32	[127, 129]
OVA	175	-19	[130]
HEP	180	-48	[125]
HA	160	-35	[124]
NS5A	410	-32	[128]

Figure 5: Electron microscopy of different polymeric nanocapsules. *Upper panel:* Scanning electron microscopy (SEM) images of dexamethasone (DXM), hydroxyethyl starch (HES), ovalbumin (OVA), heparin (HEP), hyaluronic acid (HA), and HCV non-structural protein 5A (NS5A) nanocapsules. *Lower panel:* Transmission electron microscopy (TEM) images of OVA, HEP, HA, and NS5A nanocapsules. Figure modified from Fichter et al. (2013), Pietrzak-Nguyen et al. (2014), Piradashvili et al. (2015), Baier et al. (2015), Baier et al. (2016), Fichter et al. (submitted manuscript).

2.2 Nanocapsule uptake by antigen-presenting cells and liver-specific targeting

The main prerequisite for delivery of encapsulated material is the efficient uptake of nanocapsules by target cells. Kupffer cells preferentially ingested polymeric hydroxyethyl starch nanocapsules. In contrast, dexamethasone nanocapsules were phagocytized by Kupffer cells and liver sinusoidal endothelial cells (LSECs) [126]. Targeting of murine and human dendritic cells (DCs), representing the key players for the induction of T cellular immune responses, was achieved by functionalization of HES-NCs with DC-specific antibodies αCD40 or αDEC205 [129, 127]. In order to expand the intrahepatic population of dendritic cells (from 1% up to about 60%) for targeting studies *in vivo*, mice were pre-treated with a plasmid encoding the human Fms-like tyrosine kinase 3 ligand (hFlt3l) through hydrodynamic tail vein injections [129, 128].

Adsorption of MPLA onto the NC surface (HES+MPLA-NCs) even surpassed the effect of antibody coupling with respect to the overall uptake by non-parenchymal liver cells (NPCs) *in vitro*. Intravenous administration of HES+MPLA-NCs led to a significantly increased incorporation in NPCs, compared to non-functionalized HES-NCs, in hFlt3l-treated mice [129]. This effect was also detected after intravenous administration of IRdye 800CW-labeled nanocapsules, synthesized of the hepatitis C virus non-structural protein 5A and coated with MPLA, and subsequent *in vivo* imaging (Figure 6). Both formulations (NS5A-NCs and NS5A+MPLA-NCs) were almost exclusively deposited in the liver. Just a minute fraction of NCs was found in the spleen [128]. Moreover, MPLA-functionalized NCs led to a significantly enhanced fluorescence signal in the liver at 30 min and 3 h post injection (Figure 6) [128]. Isolation of NPCs after NC injection identified dendritic cells and Kupffer cells as the primarily ingesting cell populations.
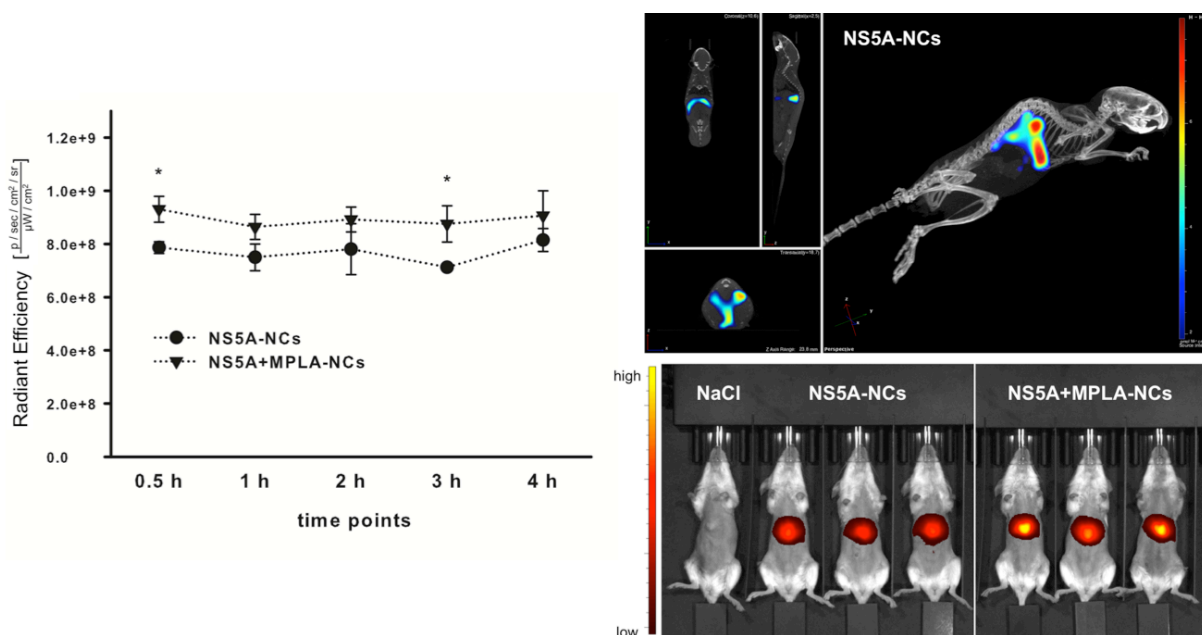
Figure 6: Biodistribution of NS5A-based nanocapsules. *In vivo* imaging of NS5A- and NS5A+MPLA-NCs labeled with IRdye 800CW was performed at different time points (30 min / 1 h / 2 h / 3 h / 4 h) after intravenous injection into B6N-Tyr$^{c\text{-}Brd}$/BrdCrCrl albino mice (n = 3). *left:* Fluorescence signal intensities (radiant efficiency) of IRdye-labeled NCs deposited in the liver compartment. Comparisons between NS5A- and NS5A+MPLA-NCs were performed using a non-paired Student's *t*-test and significance was given with p < 0.05 (*). *Right, upper panel:* representative image of an albino mouse 4 h after injection of NS5A-NCs analyzed using fluorescence intensity tomography (FLIT) and 3D reconstruction. Co-registration of bones and fluorescence signals is depicted. *Right, lower panel:* Epi-illumination image of mice 4 h after NC injection. NaCl served as negative control. Figure modified from Fichter et al. (submitted manuscript).

Confocal laser scanning microscopy of NPCs was performed, confirming intracellular localization of DXM-, HES-, OVA-, and NS5A-NCs (Figure 7) [126, 127, 130, 128].

In conclusion, all evaluated nanocapsule formulations were efficiently phagocytized by antigen-presenting cells. Additionally, HES- and NS5A-NCs showed a preferential intrahepatic deposition, representing prerequisites for the delivery of antigens, adjuvants, or immunosuppressive drugs into the liver compartment [128, 129].
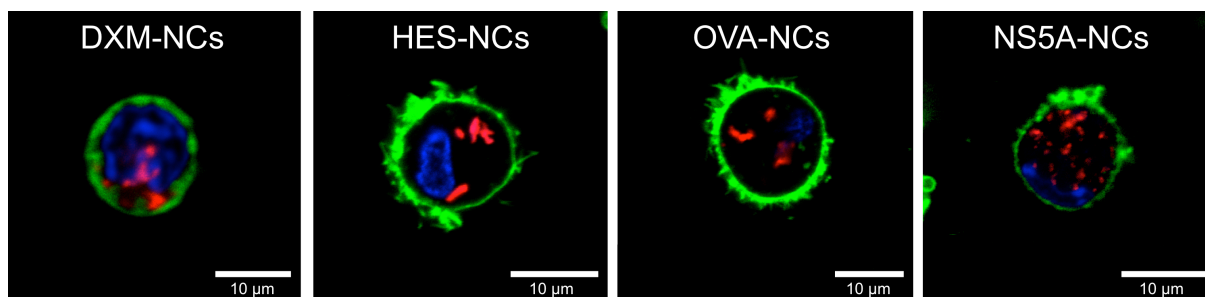
Figure 7: Confocal laser scanning microscopy illustrates the intracellular uptake of polymeric nanocapsules. DXM-, HES-, OVA-, or NS5A-NCs labeled with cy5-oligonucleotides (pseudocoloured in red) were co-incubated with murine non-parenchymal liver cells (DXM- and NS5A-NCs) or human monocyte-derived dendritic cells (HES- and OVA-NCs), respectively. Plasma membrane staining was performed using CellMask™ Orange (pseudocoloured in green) and nuclei were stained using Hoechst 33342 (pseudocoloured in blue). Figure modified from Fichter et al. (2013), Fichter et al. (2015), Piradashvili et al. (2015), Fichter et al. (submitted manuscript).

14

2.3 Release of nanocapsule cargo

2.3.1 Intracellular degradation of nanocapsules and cargo release

The ability of polymeric nanocapsules to release encapsulated cargo after intracellular delivery was evaluated with ovalbumin (OVA) and hyaluronic acid (HA) as carrier substances. Therefore, the fluorescent dyes CellTracker™ Green CMFDA or BODIPY-conjugated ovalbumin (DQ™ ovalbumin), only emitting fluorescence signals following cleavage by intracellular esterase or proteases, were encapsulated in HA- or OVA-NCs, respectively. Both NC formulations demonstrated bright fluorescence after ingestion by dendritic cells, verifying intracellular cleavage and release of NC cargo [130, 124]. Due to a distinct synthetic approach, the so-called "click" reaction, hyaluronic acid molecules were functionalized with an azide (-N$_3$) leading to cross-linking via disulfide bonds. This in turn led to a sensitivity of HA-NCs to glutathione. The glutathione-triggered release of the fluorescent dye sulforhodamine 101 (SR101) out of HA-NCs could be additionally confirmed in a cell-free assay [124].

2.3.2 Dexamethasone nanocapsules suppress inflammatory responses

Aside from macromolecules like proteins, the intracellular release of molecules with low molecular weight out of nanocapsules was investigated. The glucocorticoid dexamethasone was used due to its easily detectable immunosuppressive properties. DXM-NCs displayed biological effects despite polymerization of dexamethasone molecules forming the capsule shell. Figure 8 illustrates the potential of DXM-NCs to suppress the inflammatory response of NPCs (in particular Kupffer cells) following stimulation with lipopolysaccharide (LPS) [126]. Furthermore, dexamethasone encapsulated in hydroxyethyl starch nanocapsules (HES-DXM-NCs) exhibited similar anti-inflammatory effects to DXM-NCs, when co-incubated with NPCs.
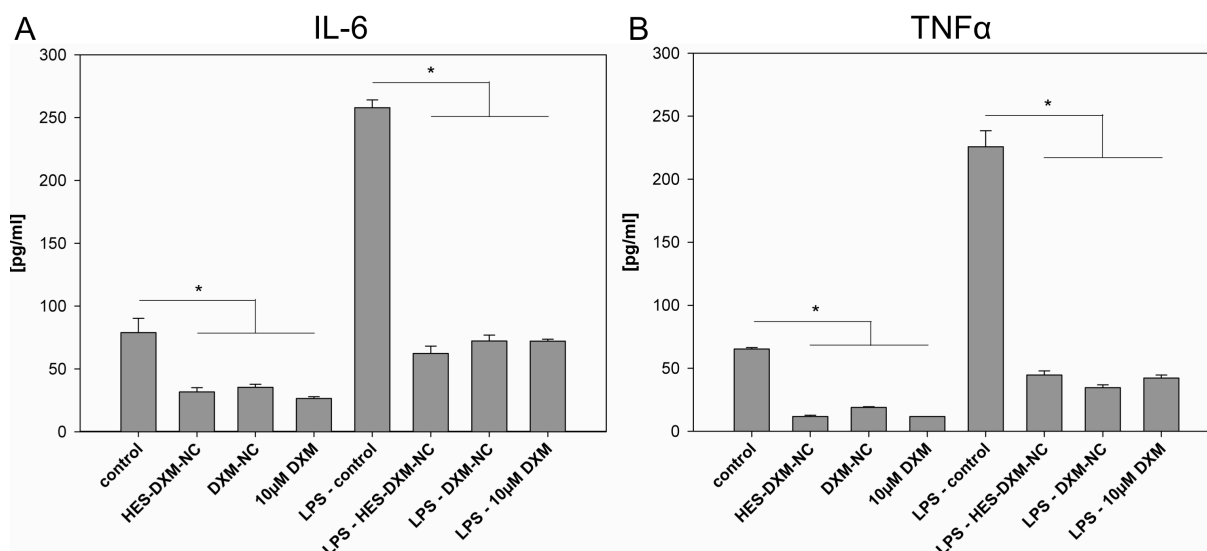
Figure 8: Dexamethasone nanocapsules feature anti-inflammatory properties. Suppression of cytokine response after uptake of hydroxyethyl starch NCs loaded with DXM (HES-DXM-NCs) or DXM-NCs *in vitro* was determined by secretion of IL-6 (A) or TNFα (B) into the supernatant. Dexamethasone (10 µM) in solution served as positive control. Data represents the mean ± standard deviation of three independent experiments. *Significance was given with $p < 0.001$ (One way ANOVA). Figure modified from Fichter et al. (2013).

2.4 Biological activity of nanocapsule cargo

2.4.1 Heparin nanocapsules feature anti-coagulative properties

Heparin (HEP) nanocapsules were synthesized with different chain densities and evaluated regarding their anti-coagulative properties. Activated clotting time of human blood in the presence of HEP-NCs was significantly prolonged compared to untreated blood or blood treated with control NCs based on hexanediol. This finding evidenced the biological activity of heparin even after polymerization forming heparin nanocapsules [125].

2.4.2 Adjuvant-supplemented nanocapsules modulate immune responses

The induction of robust T cellular immune responses requires the activation and maturation of dendritic cells. Thus, different nanocapsule formulations, presented in this thesis, were additionally functionalized by covalent coupling of the antibody αCD40 and/or adsorption of MPLA onto the NC surface [127-129]. MPLA-coated HES- and NS5A-NCs demonstrated a substantial enhancement of dendritic cell activation with respect to surface marker expression (CD40, CD80, CD83, and CD86) [127, 128] and secretion of pro-inflammatory cytokines (IL-6, TNFα, and IL-12p70 – Figure 9) in human and murine studies [129, 127, 128]. IL-12, a cytokine promoting T_h1-directed responses, could even be induced *in vivo* after intravenous (IV) administration of NS5A-NCs functionalized with MPLA (Figure 9 D), while IL-10, a predictor cytokine for T_h2-

16

associated immune responses, could not be detected [128]. The functionalization of HES nanocapsules with the antibody αCD40 did not induce substantial activation of dendritic cells, while a combined adjuvant supplementation with MPLA led to significantly enhanced secretion of pro-inflammatory cytokines. However, the strongest impact on DC activation and maturation was achieved by supplementation of NCs exclusively with MPLA even surpassing the effect detected after stimulation with 1 µg/ml or 4 µg/ml MPLA in solution (positive control).
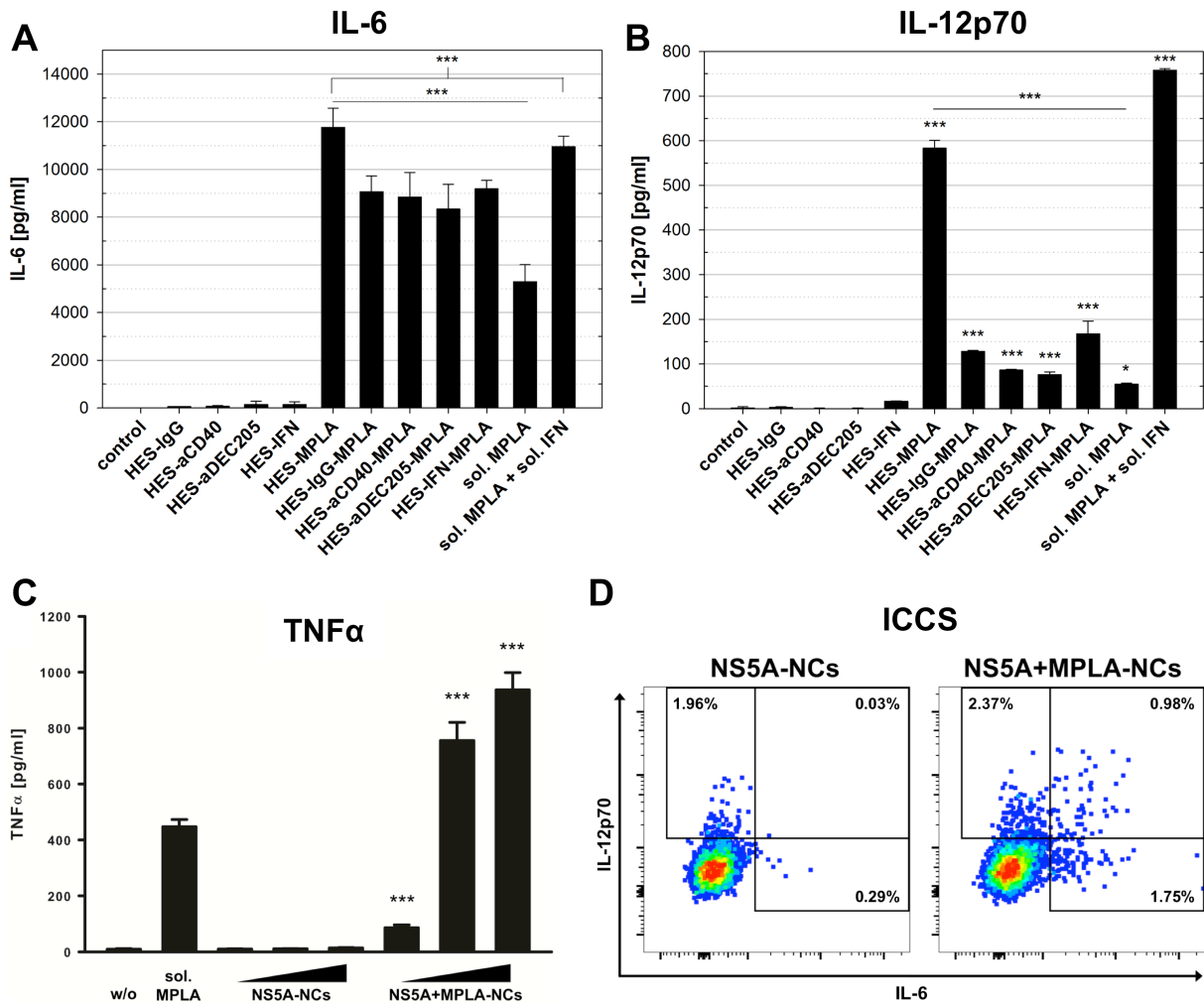
Figure 9: Monophosphoryl lipid A-functionalized nanocapsules induce vigorous activation of dendritic cells and non-parenchymal liver cells. (A, B) Cytokine secretion of human monocyte-derived dendritic cells was analyzed after co-incubation with different HES-based nanocapsule formulations (7.5 µg/ml) for 24 hours. IFNγ (50 ng/ml) and/or MPLA (4 µg/ml) in solution served as positive controls. (C) Murine NPCs were co-incubated with different concentrations of NS5A- or NS5A+MPLA-NCs (1 / 10 / 100 µg/ml) for 24 h following analysis of TNFα secretion. MPLA (1 µg/ml) in solution served as positive control. (D) NS5A- or NS5A+MPLA-NCs were intravenously administered into hFlt3l-treated mice and CD11c^{+} NC^{+} NPCs isolated 4 h post injection were analyzed using intracellular cytokine staining for IL-12p70 and IL-6. Figure modified from Fichter et al. (2015), Fichter et al. (submitted manuscript).

2.4.3 HCV antigen nanocapsules induce intrahepatic immune responses

The primary aim of the present thesis was the induction of intrahepatic antigen-specific immune responses against hepatitis C virus proteins using polymeric nanocapsules. Therefore, the HCV non-structural protein 5A was expressed in the yeast Pichia pastoris, purified and used for the synthesis of polymeric NCs (NS5A-NCs) without additional carrier substances. Mice were pre-treated with a plasmid encoding the secreted portion of human Fms-like tyrosine kinase 3 ligand (hFlt3l). This leads to the expansion of the dendritic cell population in the liver, promoting antigen-specific immunity [131]. Mice were immunized three times by intravenous administration of different NS5A-NC formulations [128]. NPCs and splenocytes derived from immunized mice exhibited substantial production of T_h1-associated cytokines IFNγ and IL-2 after re-stimulation with NS5A *ex vivo* (Figure 10). This effect was confirmed by intracellular IFNγ staining of CD4^{+} T cells. The supplementation of NS5A-NCs with MPLA resulted in a slight increase in T_h1 cytokine secretion. The additional administration of αCD40 surpassed the effect of MPLA adsorption. Moreover, adsorption of MPLA onto the NC surface evoked a vigorous NS5A-specific antibody response even in the absence of αCD40 (Figure 10 C).
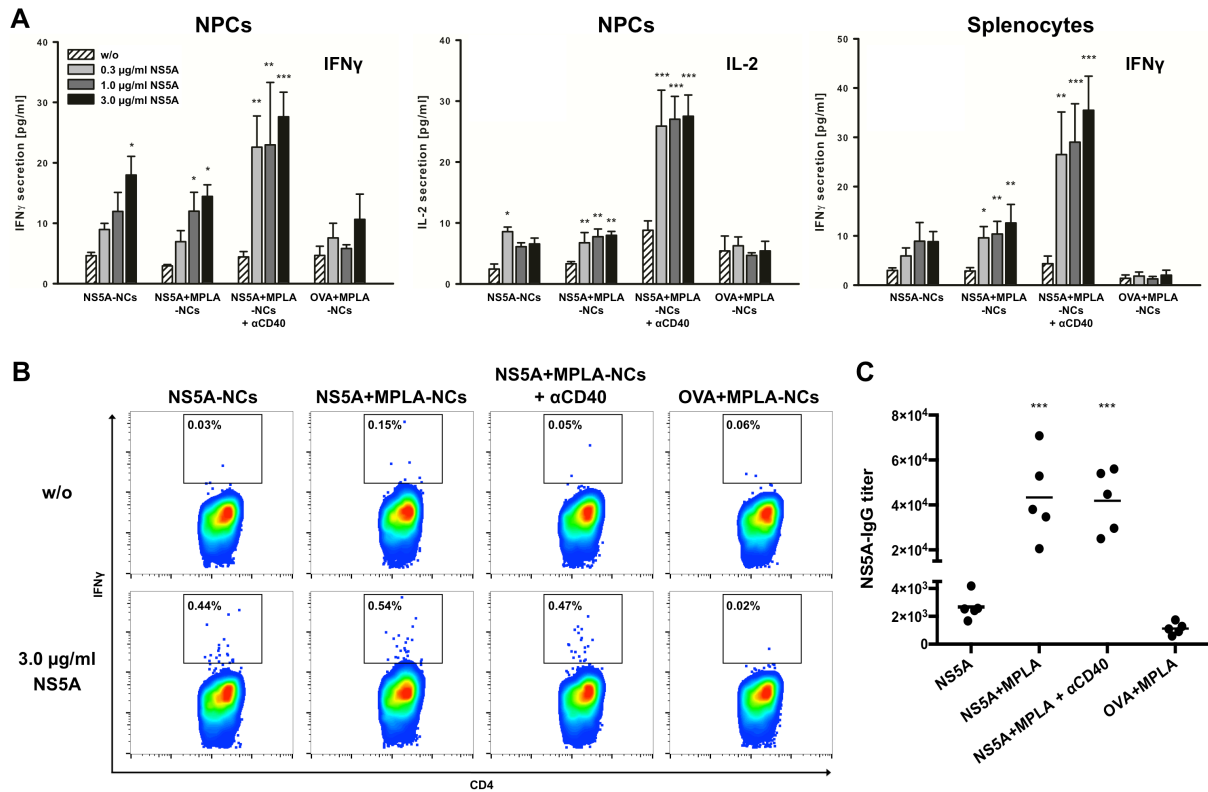
Figure 10: MPLA-functionalized NS5A-NCs induce intrahepatic T cellular and humoral immune responses. NPCs and splenocytes obtained from mice immunized three times with different NC formulations were cultured with recombinant HCV NS5A at indicated concentrations. (A) Culture supernatants were collected after 24 h; IFNγ, IL-2 concentrations were quantified by an enzyme-linked immunosorbent assay. (B) NPCs were incubated for a total of 16 h, in the presence of GolgiPlug™ during the last 4 h, following intracellular cytokine staining of IFNγ and flow cytometric analysis. (C) Antibody responses were evaluated after serum collection from immunized mice. NS5A-specific antibody titers were determined using an enzyme-linked immunosorbent assay. Data represents the mean ± SD derived from five mice. All conditions were compared to the negative control (without stimulation) or to the OVA+MPLA-NCs group for antibody responses. Significance was given with $p < 0.05$ (*), $p < 0.01$ (**), $p < 0.001$ (***) (One way ANOVA). Figure from Fichter et al. (submitted manuscript).

3 DISCUSSION

3.1 Synthesis of polymeric nanocapsules as delivery vehicles

Nanoformulations for drug delivery and vaccination approaches are currently a primary research focus. Nanoformulated drugs enable efficient delivery to target cells while reducing systemic side effects. However, there are safety concerns about nano-sized particulate structures, mostly attributed to inorganic, non-degradable nanoparticles [132]. Inert materials for nanomedical applications can accumulate in organs or cells leading to long-term cytotoxicity [133, 132]. Notably, nanoparticulate vaccines require a high safety profile due to their intended use in healthy individuals. Side effects caused by accumulation might be avoidable with biodegradable nanoparticles [134]. Polymeric nanoparticles and -capsules are particularly suited for the synthesis with biodegradable compounds [135, 14].

In the present study, different biodegradable formulations of polymeric nanocapsules were synthesized and provided by the group of Prof. Dr. Katharina Landfester at the Max Planck Institute for Polymer Research in Mainz, Germany.

The required nanocapsule properties included:

1) excellent biocompatibility in terms of biodegradability and low cytotoxicity as described above [132]

2) high stability of nanocapsule formulations *in vitro* ("shelf life") [7]

3) high encapsulation efficiency of drugs or antigens in order to increase the amount of delivered cargo [136, 3]

4) appropriate size of capsules (150 - 500 nm) for optimized uptake by antigen-presenting cells [137, 138]

5) intracellular release of cargo (drugs / antigens) [139]

6) functionalization of nanocapsules with adjuvants or antibodies in order to achieve activation of APCs or targeting of organs and cell types [21, 18]

Dendritic cells preferentially ingest nanoparticles with a size range from 20 - 500 nm [137, 138, 140]. Macrophages, in contrast, are professional phagocytes typically phagocytizing larger particles sizing 0.5 - 5 µm [33]. The size of nanocapsules, synthesized using the miniemulsion polymerization process, can be adjusted through the modification of ultrasonication conditions (amplitude, shear rate), the type and load of surfactant, and the volumetric ratio of oil and water phase [6]. Accordingly, nanocapsules

were synthesized within a size range from 160 to 410 nm as indicated in table 1. Efficient uptake by antigen-presenting cells was detected for all investigated nanocapsule formulations (see Fichter et al. (2013), Pietrzak-Nguyen et al. (2014), Fichter et al. (2015), Piradashvili et al. (2015), Fichter et al. (submitted manuscript)). Further characterization of nanocapsules included zeta potential measurements documenting negative values for all synthesized formulations (see table 1). The negative values resulted from anionic groups present at the nanocapsule surface leading to electrostatic repulsive forces between nanocapsules. This in turn prevented aggregation while providing a high stability of nanocapsule dispersions [141].

3.2 Targeting of nanocapsules to antigen-presenting cells in the liver

The liver *per se* exerts important functions regarding clearance of gut-derived endotoxins, microbiota, and microbial debris from the blood stream [142, 143]. Liver phagocytes (Kupffer cells and dendritic cells) are situated in hepatic microvessels at periportal areas facilitating access to passing microorganisms or particulate structures [89]. This localization enables efficient phagocytosis, which can be exploited in terms of a passive targeting of the liver following intravenous administration of nanoparticles [144-146]. All investigated nanocapsule formulations, including hydroxyethyl starch (HES), HCV non-structural protein 5A (NS5A), and even dexamethasone (DXM; unpublished data) nanocapsules, exhibited preferential deposition in the liver after intravenous administration (Figure 6).

In addition to efforts for passive targeting, functionalization of hydroxyethyl starch nanocapsules with targeting moieties was performed (see Pietrzak-Nguyen et al. (2014) and Fichter et al. (2015)). Different antibodies (αCD40 and αDEC205) targeting dendritic cell receptors were covalently coupled to the nanocapsule surface [147-149]. Antibody coupling induced an accelerated uptake of HES nanocapsules by murine non-parenchymal liver cells, mainly Kupffer cells and dendritic cells, and by human monocyte-derived dendritic cells *in vitro* (see Pietrzak-Nguyen et al. (2014), Fichter et al. (2015)). Intracellular localization of nanocapsules was verified by confocal laser scanning microscopy (Figure 7). However, the targeting effects observed *in vitro* could not be confirmed after intravenous administration in a mouse model presumably due to a rapid coverage of nanocapsules by serum proteins impeding protrusion and binding of antibodies to dendritic cells. Additionally, an aligned coupling of the carboxy-terminal Fc region could not be ensured with the applied coupling method possibly leading to diminished access to the antibody binding sides.

In contrast to antibody coupling, efficient targeting was achieved with nanocapsules functionalized with the Toll-like receptor 4 (TLR4) agonist monophosphoryl lipid A (MPLA). Due to its amphiphilic characteristics, MPLA was coated onto the nanocapsule surface by adsorption [150]. MPLA adsorption onto HES nanocapsules drastically increased the overall uptake of nanocapsules by murine non-parenchymal liver cells or human monocyte-derived dendritic cells *in vitro* (see Pietrzak-Nguyen et al. (2014) and Fichter et al. (2015)). Moreover, MPLA coating of HES and NS5A nanocapsules led to a preferential deposition in the liver, especially in Kupffer cells and dendritic cells (see Pietrzak-Nguyen et al. (2014) and Fichter et al. (submitted manuscript)). To our knowledge, these studies, for the first time, describe a direct effect of MPLA regarding targeting of antigen-presenting cells, whereas several studies described an enhancement of immune responses after incorporation in nanoparticles [24, 151, 152].

3.3 Release of nanocapsule cargo

3.3.1 Intracellular release of encapsulated cargo

The intracellular release of encapsulated proteins after nanocapsule uptake was evaluated using ovalbumin nanocapsules. This nanocapsule formulation was applied as a proof-of-concept to analyze release properties and was not intended for the use as vaccine delivery system. The application of proteins as carrier substances for later vaccinations with specific antigens is not recommendable due to the generation of unintended immune responses against carrier proteins. Nevertheless, OVA nanocapsules exhibited excellent biodegradability determined through the release of an encapsulated fluorescent protein (DQ™ ovalbumin) after uptake by dendritic cells (see Piradashvili et al. (2015)). DQ™ ovalbumin is a conjugate of ovalbumin with multiple BODIPY fluorochrome molecules leading to fluorescence quenching. After proteolytic degradation into peptides, labeled with single BODIPY molecules, a restoration of fluorescence occurs [153]. With these properties, DQ™ ovalbumin is an excellent sensor for intracellular nanocapsule degradation and protein release.

In addition to OVA-NCs, a nanocapsule formulation based on hyaluronic acid (HA) synthesized with an alternative polymerization method was investigated. An azidation of HA molecules was performed, followed by cross-linking of monomers and the introduction of disulfide bonds in the capsule shell ("click-chemistry"). HA nanocapsules featured a strong sensitivity to glutathione, which is the major reducing agent in biochemical processes and is found in intracellular compartments at concentrations of up to 10 mM [154]. HA-NCs were taken up by human monocyte-derived dendritic cells after

co-incubation *in vitro*, followed by degradation in intracellular compartments and the release of a fluorescent dye (see Baier et al. (2016)). The intracellular release of nanocapsule cargo was detected with a CellTracker™ dye eliciting a bright fluorescence signal only after cleavage by intracellular esterases. Thus, additionally to the detection of protein release using DQ™ ovalbumin, the release of a dye with low molecular weight was observed after ingestion of NCs by antigen-presenting cells. Glutathione-sensitive hyaluronic acid nanocapsules are perfectly qualified for the delivery and subsequent release of biomacromolecules, such as proteins or nucleic acids, and will be investigated in future studies.

3.3.2 Dexamethasone-based nanocapsules suppress inflammation

In addition to ovalbumin-based formulations, cargo release was investigated with nanocapsules synthesized of dexamethasone (DXM), a synthetic glucocorticoid. DXM has potent immunosuppressive properties, which can be easily detected through the suppression of pro-inflammatory cytokine expression by antigen-presenting cells following stimulation with lipopolysaccharides [155-157].

Immunosuppression with glucocorticoids is a common treatment option of autoimmune liver diseases and standard of care even in pediatric patients [158]. However, systemic administration of dexamethasone is associated with severe side effects such as hypertension, hyperglycemia, intestinal bleeding, delayed wound healing, and gastric ulcers [159, 160]. Therefore, targeting DXM to cells involved in driving intrahepatic inflammation, e.g. Kupffer cells or monocytes, is a particularly promising approach to reduce systemic adverse effects [157]. Several studies described the conjugation of DXM to polymeric nanoparticles consisting of PLGA [161], Chitosan [162], or Poly(ethylene glycol) (PEG) [163] targeting different diseases. In the current study, polymeric DXM nanocapsules induced a significant suppression of pro-inflammatory cytokines secreted by Kupffer cells after ingestion (Figure 8). These findings encourage to study the immunosuppressive effects of DXM-NCs in *in vivo* models of liver inflammation. Suitable mouse models include an LPS- and D-galactosamine-induced inflammation model of autoimmune hepatitis, or a model of cholestatic liver injury through bile duct ligation [164, 165].

3.4 Biological activity of nanocapsule cargo

3.4.1 Polymerization maintains anti-coagulative properties of heparin

The glycosaminoglycan heparin (HEP) is an anti-coagulative drug with polymeric structure and varying chain length. Binding of heparin to the serine-protease antithrombin III (AT III) induces a conformational change of AT III. Activated AT III inhibits thrombin and thus prevents the cleavage of fibrinogen to fibrin [166]. Polymerization of heparin molecules forming HEP nanocapsules maintained the anti-thrombogenic properties determined by measurements of the activated clotting time (see Baier et al. (2015)). Heparin is a frequently used drug, included in the World Health Organization´s List of Essential Medicines [167]. It induces fairly low side effects but has a very short half-life [168]. Heparin-containing nanoparticles have been successfully applied as delivery vehicles [169]. Nanoparticles coated with heparin significantly prolonged the circulation time in blood from a few minutes up to 72 h [170]. This effect is attributed to the inhibition of plasma protein adsorption on heparin-functionalized nanoparticles. In contrast, uncoated nanoparticles are prone to the formation of a protein corona, which activates the complement system and ultimately leads to the recognition and elimination by the mononuclear phagocyte system [171, 172]. The "stealth" properties of heparin nanoparticles can potentially be exploited in order to increase the bioavailability and half-life after parenteral administration. Accordingly, the application of polymeric HEP nanocapsules for targeted drug delivery is a very promising approach in order to avoid early phagocytic uptake.

3.4.2 Nanocapsules functionalized with MPLA efficiently activate dendritic cells

MPLA, a low toxicity TLR4 agonist and synthetic derivate of lipopolysaccharide (LPS), mediates its activity through "Toll/interleukin-1 receptor domain-containing adapter inducing interferon-β" (TRIF) suppressing the expression of myeloid differentiation factor 88 (MyD88) [173]. This leads to a decreased secretion of pro-inflammatory cytokines, which correlates with the abrogated toxicity compared to LPS or other lipid A derivates [45, 174]. Notably, MPLA induces the secretion of T_h1-related cytokines [45]. However, in humans, without further co-stimulation, MPLA also promotes strong T_h2-directed responses, including the secretion of IL-4 and IL-10 along with the induction of humoral immune responses [175, 176].

Here, the effects of MPLA adsorption on HES and NS5A nanocapsules were investigated with respect to the activation of dendritic cells (see Fichter et al. (2015), Fichter et al. (submitted manuscript), Pietrzak-Nguyen et al. (2014)). Both nanocapsule

formulations induced a vigorous secretion of pro-inflammatory cytokines (IL-6 and TNFα) (Figure 9 A and C). Notably, the secretion of IL-12 by activated dendritic cells is required for the induction of a strong T_h1 response leading to the resolution of acute HCV infection [109]. Thus, the main goal of the current study was to activate and mature dendritic cells. All MPLA-coated nanocapsule formulations induced a significant expression of IL-12 even under *in vivo* conditions (Figure 9 B and D). In contrast, substantial secretion of IL-10, a cytokine promoting T_h2 responses, could not be detected in the murine model. The activation of DCs by MPLA-coated nanocapsules was additionally determined by the upregulation of surface markers, such as CD80, CD83, or CD86 (see Fichter et al. (2015) and Fichter et al. (submitted manuscript)), which are attributed to DC activation [177].

3.4.3 Immobilization on nanocapsules potentiates the effects of MPLA

The adsorption of MPLA on NS5A nanocapsules was determined in order to quantify the administered amount of the adjuvant (see Fichter et al. (submitted manuscript)). MPLA in solution (1 µg/ml) served as a positive control in cell culture experiments. A concentration of only 66 ng/ml adsorbed on NS5A nanocapsules induced similar or even higher levels of DC activation compared to the positive control (Figure 9 C and D). Consequently, a dose-sparing effect of more than 15 times was demonstrated due to the immobilization of MPLA at the nanocapsule surface (see Fichter et al. (submitted manuscript)). Similar effects were observed for HES nanocapsules (see Fichter et al. (2015)).

Beneficial effects by combination of antigens along with adjuvants have been reported for immunizations with different nanoparticle formulations [24, 48-50]. Tacken et al. described a dose-sparing potential of up to 100-fold by incorporation of adjuvant (R848) and antigen (ovalbumin) in PLGA nanoparticles [48]. Such dose-sparing strategies are essential for the development of novel vaccines, reducing systemic and local side effects caused by MPLA or other adjuvants [178-180].

3.4.4 HCV NS5A+MPLA nanocapsules induce intrahepatic immune responses

Successful eradication of hepatitis C virus infections depends on the induction of intrahepatic immunity [44]. Thus, delivery of nanoparticulate vaccines to the liver is a promising approach for the development of prophylactic or therapeutic vaccines. In addition, it has been shown that intravenous administration of protein particles generated stronger immune responses compared to subcutaneous injections in a mouse model [181]. With respect to the development of a prophylactic vaccine against Malaria,

intravenous but not subcutaneous injection of live-attenuated *Plasmodium falciparium* sporozoites (PfSPZ) induced robust and sustained intrahepatic T cell responses in non-human primates [182]. These findings led to a phase I clinical trial testing intravenous administration of PfSPZ in 40 healthy adults [183].

According to these observations, the final goal of this study was the induction of intrahepatic antigen-specific T cellular immune responses against hepatitis C virus proteins. Preliminary experiments with HCV NS5A antigen encapsulated in hydroxyethyl starch failed to induce robust immunity. In contrast, nanocapsules synthesized exclusively of HCV non-structural protein 5A (NS5A) and administered intravenously generated substantial intrahepatic antigen-specific T cell and humoral immune responses (see Fichter et al. (submitted manuscript)). Nanocapsules solely made of viral antigen avoid side effects caused by additional compounds needed for the stabilization of the nanocapsule structure, e.g. unintended immune responses or toxicity [3, 184, 185]. Moreover, these nanocapsules deliver high antigen payloads to antigen-presenting cells, which is essential for the induction of robust and sustained cellular immunity [136].

Mice did not develop any detectable clinical symptoms after intravenous injection of NS5A nanocapsules. Though, adjuvant supplementation with adsorbed MPLA was accompanied by a mild fatigue, enduring for about two hours. These moderate symptoms correspond to the slightly increased adverse effects described in clinical studies investigating the safety profile of a MPLA-supplemented hepatitis B virus vaccine (Fendrix®) [186].

Intrahepatic cellular immunity was determined through antigen-specific cytokine secretion (IFNγ and IL-2) by CD4$^+$ T cells (Figure 10) [187]. Immunization with MPLA-functionalized OVA nanocapsules served as antigen control and failed to induce IFNγ or IL-2 production. In addition to T cell responses, immunization with MPLA-supplemented NS5A nanocapsules generated robust levels of NS5A-specific antibodies (humoral immunity) (see Fichter et al. (submitted manuscript)). NS5A is a non-structural protein only translated after infection of hepatocytes and consequently no primary target of neutralizing antibodies present in the blood [188]. Nevertheless, in this proof-of-concept study the generation of combined immune responses (T cellular and antibody-mediated) was demonstrated. In future studies it is intended to investigate immune responses to structural proteins of the hepatitis C virus, e.g. envelope I or II. The results of two phase I clinical trials of prophylactic HCV vaccines underlined the relevance of both, the induction of humoral and T cell immune responses for the generation of robust protective immunity against HCV virus challenges [112, 122]. Notably, MPLA-supplemented

nanocapsules, exclusively made of HCV-derived antigens, address the requirements for a successful prophylactic vaccine.

4 OUTLOOK

The present PhD thesis demonstrated the potential of polymeric nanocapsules to deliver immunosuppressive drugs or antigens along with adjuvants to antigen-presenting cells. Future studies should investigate the biological impact of dexamethasone-based nanocapsules in models of intrahepatic inflammation. Excellent mouse models mimicking diseases, such as autoimmune hepatitis or biliary atresia, enable to assess the potential of dexamethasone nanocapsules to suppress inflammatory processes in the liver.

Immunization with nanocapsules synthesized of the hepatitis C virus non-structural protein 5A induced $CD4^+$ T cell-mediated immunity along with humoral responses. However, significant $CD8^+$-related responses of cytotoxic T cells remained elusive. Therefore, modulation of immune responses with respect to the adjuvant composition and the optimization of readout assays should be the major focus of subsequent vaccination studies.

Substantial efforts investigating the epitope composition of the HCV polyprotein, revealed a significant proportion of epitopes promoting regulatory T cell responses [189, 190]. It is thus intended, in cooperation with Prof. Dr. Stephen H. Gregory (Rhode Island Hospital and The Warren Alpert Medical School of Brown University, Providence, USA), to investigate the effects of encapsulated recombinant HCV proteins only comprising epitopes that promote T_h1-directed immunity.

Moreover, several applications for the delivery of biomacromolecules are projected for investigation, including the targeted delivery of enzymes to hepatocytes in order to treat congenital metabolic diseases, e.g. phenylketonuria or tyrosinemia.

Nanocapsule formulations, established in this thesis, provide a platform for subsequent studies focusing on intrahepatic targeting of antigens, enzymes, or drugs to specific cell populations. It was demonstrated that specifically designed nanocapsules are able to suppress or induce immune responses. These observations document the tremendous number of opportunities to apply nanocapsules in novel therapeutic or prophylactic applications.

5 REFERENCES

1.   Rao, J.P. and Geckeler, K.E., *Polymer nanoparticles: Preparation techniques and size-control parameters.* Progress in Polymer Science, 2011. **36**(7): p. 887-913.

2.   Smith, D.M., Simon, J.K., and Baker, J.R., Jr., *Applications of nanotechnology for immunology.* Nat Rev Immunol, 2013. **13**(8): p. 592-605.

3.   De Jong, W.H. and Borm, P.J., *Drug delivery and nanoparticles:Applications and hazards.* Int J Nanomedicine, 2008. **3**(2): p. 133-49.

4.   Laurent, S., Bridot, J.L., Elst, L.V., and Muller, R.N., *Magnetic iron oxide nanoparticles for biomedical applications.* Future Med Chem, 2010. **2**(3): p. 427-49.

5.   Conde, J., Doria, G., and Baptista, P., *Noble metal nanoparticles applications in cancer.* J Drug Deliv, 2012. **2012**: p. 751075.

6.   Musyanovych, A. and Landfester, K., *Polymer micro- and nanocapsules as biological carriers with multifunctional properties.* Macromol Biosci, 2014. **14**(4): p. 458-77.

7.   Muller, R.H. and Keck, C.M., *Challenges and solutions for the delivery of biotech drugs--a review of drug nanocrystal technology and lipid nanoparticles.* J Biotechnol, 2004. **113**(1-3): p. 151-70.

8.   Gobbo, O.L., Sjaastad, K., Radomski, M.W., Volkov, Y., and Prina-Mello, A., *Magnetic nanoparticles in cancer theranostics.* Theranostics, 2015. **5**(11): p. 1249-63.

9.   Kang, S.M., Kim, M.C., and Compans, R.W., *Virus-like particles as universal influenza vaccines.* Expert Rev Vaccines, 2012. **11**(8): p. 995-1007.

10.   Shen, L.J. and Wu, F.L., *Nanomedicines in renal transplant rejection--focus on sirolimus.* Int J Nanomedicine, 2007. **2**(1): p. 25-32.

11.   Allen, T.M. and Cullis, P.R., *Liposomal drug delivery systems: From concept to clinical applications.* Adv Drug Deliv Rev, 2013. **65**(1): p. 36-48.

12.   Ganta, S., Talekar, M., Singh, A., Coleman, T.P., and Amiji, M.M., *Nanoemulsions in translational research-opportunities and challenges in targeted cancer therapy.* AAPS PharmSciTech, 2014. **15**(3): p. 694-708.

13.   Odriozola-Serrano, I., Oms-Oliu, G., and Martin-Belloso, O., *Nanoemulsion-based delivery systems to improve functionality of lipophilic components.* Front Nutr, 2014. **1**: p. 24.

14.   Kumari, A., Yadav, S.K., and Yadav, S.C., *Biodegradable polymeric nanoparticles based drug delivery systems.* Colloids Surf B Biointerfaces, 2010. **75**(1): p. 1-18.

15.   Smith, J.D., Morton, L.D., and Ulery, B.D., *Nanoparticles as synthetic vaccines.* Curr Opin Biotechnol, 2015. **34**: p. 217-24.

16.   Danhier, F., Ansorena, E., Silva, J.M., Coco, R., Le Breton, A., and Preat, V., *Plga-based nanoparticles: An overview of biomedical applications.* J Control Release, 2012. **161**(2): p. 505-22.

17.   Mora-Huertas, C.E., Fessi, H., and Elaissari, A., *Polymer-based nanocapsules for drug delivery.* Int J Pharm, 2010. **385**(1-2): p. 113-42.

18.   Cruz, L.J., Tacken, P.J., Rueda, F., Domingo, J.C., Albericio, F., and Figdor, C.G., *Targeting nanoparticles to dendritic cells for immunotherapy.* Methods Enzymol, 2012. **509**: p. 143-63.

19.   Gregory, A.E., Titball, R., and Williamson, D., *Vaccine delivery using nanoparticles.* Front Cell Infect Microbiol, 2013. **3**: p. 13.

20.   Marasini, N., Skwarczynski, M., and Toth, I., *Oral delivery of nanoparticle-based vaccines.* Expert Rev Vaccines, 2014. **13**(11): p. 1361-76.

21.   Leleux, J. and Roy, K., *Micro and nanoparticle-based delivery systems for vaccine immunotherapy: An immunological and materials perspective.* Adv Healthc Mater, 2013. **2**(1): p. 72-94.

22.   Akagi, T., Wang, X., Uto, T., Baba, M., and Akashi, M., *Protein direct delivery to dendritic cells using nanoparticles based on amphiphilic poly(amino acid) derivatives.* Biomaterials, 2007. **28**(23): p. 3427-36.

23.   Uto, T., Wang, X., Sato, K., Haraguchi, M., Akagi, T., et al., *Targeting of antigen to dendritic cells with poly(gamma-glutamic acid) nanoparticles induces antigen-specific humoral and cellular immunity.* J Immunol, 2007. **178**(5): p. 2979-86.

24.   Elamanchili, P., Diwan, M., Cao, M., and Samuel, J., *Characterization of poly(d,l-lactic-co-glycolic acid) based nanoparticulate system for enhanced delivery of antigens to dendritic cells.* Vaccine, 2004. **22**(19): p. 2406-12.

25.   Waeckerle-Men, Y. and Groettrup, M., *Plga microspheres for improved antigen delivery to dendritic cells as cellular vaccines.* Adv Drug Deliv Rev, 2005. **57**(3): p. 475-82.

26.   Audran, R., Peter, K., Dannull, J., Men, Y., Scandella, E., et al., *Encapsulation of peptides in biodegradable microspheres prolongs their mhc class-i presentation by dendritic cells and macrophages in vitro.* Vaccine, 2003. **21**(11-12): p. 1250-5.

27.   Kwon, Y.J., Standley, S.M., Goh, S.L., and Frechet, J.M., *Enhanced antigen presentation and immunostimulation of dendritic cells using acid-degradable cationic nanoparticles.* J Control Release, 2005. **105**(3): p. 199-212.

28.   Otten, G.R., Schaefer, M., Doe, B., Liu, H., Srivastava, I., et al., *Enhanced potency of plasmid DNA microparticle human immunodeficiency virus vaccines in rhesus macaques by using a priming-boosting regimen with recombinant proteins.* J Virol, 2005. **79**(13): p. 8189-200.

29.   Rajapaksa, T.E., Stover-Hamer, M., Fernandez, X., Eckelhoefer, H.A., and Lo, D.D., *Claudin 4-targeted protein incorporated into plga nanoparticles can mediate m cell targeted delivery.* J Control Release, 2010. **142**(2): p. 196-205.

30.   Luby, T.M., Cole, G., Baker, L., Kornher, J.S., Ramstedt, U., and Hedley, M.L., *Repeated immunization with plasmid DNA formulated in poly(lactide-co-glycolide) microparticles is well tolerated and stimulates durable t cell responses to the tumor-associated antigen cytochrome p450 1b1.* Clin Immunol, 2004. **112**(1): p. 45-53.

31.   McKeever, U., Barman, S., Hao, T., Chambers, P., Song, S., et al., *Protective immune responses elicited in mice by immunization with formulations of poly(lactide-co-glycolide) microparticles.* Vaccine, 2002. **20**(11-12): p. 1524-31.

32.   Zhang, Z., Tongchusak, S., Mizukami, Y., Kang, Y.J., Ioji, T., et al., *Induction of anti-tumor cytotoxic t cell responses through plga-nanoparticle mediated antigen delivery.* Biomaterials, 2011. **32**(14): p. 3666-78.

33.   Zhao, L., Seth, A., Wibowo, N., Zhao, C.X., Mitter, N., et al., *Nanoparticle vaccines.* Vaccine, 2014. **32**(3): p. 327-37.

34.   Zhang, L.F., Zhou, J., Chen, S., Cai, L.L., Bao, Q.Y., et al., *Hpv6b virus like particles are potent immunogens without adjuvant in man.* Vaccine, 2000. **18**(11-12): p. 1051-8.

35.   Noad, R. and Roy, P., *Virus-like particles as immunogens.* Trends in Microbiology, 2003. **11**(9): p. 438-444.

36. Grgacic, E.V. and Anderson, D.A., *Virus-like particles: Passport to immune recognition.* Methods, 2006. **40**(1): p. 60-5.

37. Roldao, A., Mellado, M.C., Castilho, L.R., Carrondo, M.J., and Alves, P.M., *Virus-like particles in vaccine development.* Expert Rev Vaccines, 2010. **9**(10): p. 1149-76.

38. Madrid-Marina, V., Torres-Poveda, K., Lopez-Toledo, G., and Garcia-Carranca, A., *Advantages and disadvantages of current prophylactic vaccines against hpv.* Arch Med Res, 2009. **40**(6): p. 471-7.

39. Saade, F., Honda-Okubo, Y., Trec, S., and Petrovsky, N., *A novel hepatitis b vaccine containing advax, a polysaccharide adjuvant derived from delta inulin, induces robust humoral and cellular immunity with minimal reactogenicity in preclinical testing.* Vaccine, 2013. **31**(15): p. 1999-2007.

40. Mbow, M.L., De Gregorio, E., Valiante, N.M., and Rappuoli, R., *New adjuvants for human vaccines.* Curr Opin Immunol, 2010. **22**(3): p. 411-6.

41. Aimanianda, V., Haensler, J., Lacroix-Desmazes, S., Kaveri, S.V., and Bayry, J., *Novel cellular and molecular mechanisms of induction of immune responses by aluminum adjuvants.* Trends Pharmacol Sci, 2009. **30**(6): p. 287-95.

42. Marrack, P., McKee, A.S., and Munks, M.W., *Towards an understanding of the adjuvant action of aluminium.* Nat Rev Immunol, 2009. **9**(4): p. 287-93.

43. Seder, R.A. and Hill, A.V., *Vaccines against intracellular infections requiring cellular immunity.* Nature, 2000. **406**(6797): p. 793-8.

44. Thimme, R., Binder, M., and Bartenschlager, R., *Failure of innate and adaptive immune responses in controlling hepatitis c virus infection.* FEMS Microbiol Rev, 2012. **36**(3): p. 663-83.

45. Bohannon, J.K., Hernandez, A., Enkhbaatar, P., Adams, W.L., and Sherwood, E.R., *The immunobiology of toll-like receptor 4 agonists: From endotoxin tolerance to immunoadjuvants.* Shock, 2013. **40**(6): p. 451-62.

46. Kundi, M., *New hepatitis b vaccine formulated with an improved adjuvant system.* Expert Rev Vaccines, 2007. **6**(2): p. 133-40.

47. Harper, D.M., *Currently approved prophylactic hpv vaccines.* Expert Rev Vaccines, 2009. **8**(12): p. 1663-79.

48. Tacken, P.J., Zeelenberg, I.S., Cruz, L.J., van Hout-Kuijer, M.A., van de Glind, G., et al., *Targeted delivery of tlr ligands to human and mouse dendritic cells strongly enhances adjuvanticity.* Blood, 2011. **118**(26): p. 6836-44.

49. Blander, J.M. and Medzhitov, R., *Toll-dependent selection of microbial antigens for presentation by dendritic cells.* Nature, 2006. **440**(7085): p. 808-12.

50. Kratky, W., Reis e Sousa, C., Oxenius, A., and Sporri, R., *Direct activation of antigen-presenting cells is required for cd8+ t-cell priming and tumor vaccination.* Proc Natl Acad Sci U S A, 2011. **108**(42): p. 17414-9.

51. Standley, S.M., Mende, I., Goh, S.L., Kwon, Y.J., Beaudette, T.T., et al., *Incorporation of cpg oligonucleotide ligand into protein-loaded particle vaccines promotes antigen-specific cd8 t-cell immunity.* Bioconjug Chem, 2007. **18**(1): p. 77-83.

52. Bershteyn, A., Hanson, M.C., Crespo, M.P., Moon, J.J., Li, A.V., et al., *Robust igg responses to nanograms of antigen using a biomimetic lipid-coated particle vaccine.* J Control Release, 2012. **157**(3): p. 354-65.

53. Krumbiegel, D., Zepp, F., and Meyer, C.U., *Combined toll-like receptor agonists synergistically increase production of inflammatory cytokines in human neonatal dendritic cells.* Hum Immunol, 2007. **68**(10): p. 813-22.

54.   Krumbiegel, D., Rohr, J., Schmidtke, P., Knuf, M., Zepp, F., and Meyer, C.U., *Efficient maturation and cytokine production of neonatal dcs requires combined proinflammatory signals.* Clin Dev Immunol, 2005. **12**(2): p. 99-105.

55.   Mohd Hanafiah, K., Groeger, J., Flaxman, A.D., and Wiersma, S.T., *Global epidemiology of hepatitis c virus infection: New estimates of age-specific antibody to hcv seroprevalence.* Hepatology, 2013. **57**(4): p. 1333-42.

56.   Mohamed, A.A., Elbedewy, T.A., El-Serafy, M., El-Toukhy, N., Ahmed, W., and Ali El Din, Z., *Hepatitis c virus: A global view.* World J Hepatol, 2015. **7**(26): p. 2676-80.

57.   Lavanchy, D., *Evolving epidemiology of hepatitis c virus.* Clin Microbiol Infect, 2011. **17**(2): p. 107-15.

58.   Hajarizadeh, B., Grebely, J., and Dore, G.J., *Epidemiology and natural history of hcv infection.* Nat Rev Gastroenterol Hepatol, 2013. **10**(9): p. 553-62.

59.   Messina, J.P., Humphreys, I., Flaxman, A., Brown, A., Cooke, G.S., et al., *Global distribution and prevalence of hepatitis c virus genotypes.* Hepatology, 2015. **61**(1): p. 77-87.

60.   Razavi, H., Elkhoury, A.C., Elbasha, E., Estes, C., Pasini, K., et al., *Chronic hepatitis c virus (hcv) disease burden and cost in the united states.* Hepatology, 2013. **57**(6): p. 2164-70.

61.   Choo, Q.L., Kuo, G., Weiner, A.J., Overby, L.R., Bradley, D.W., and Houghton, M., *Isolation of a cdna clone derived from a blood-borne non-a, non-b viral hepatitis genome.* Science, 1989. **244**(4902): p. 359-62.

62.   Perz, J.F., Armstrong, G.L., Farrington, L.A., Hutin, Y.J., and Bell, B.P., *The contributions of hepatitis b virus and hepatitis c virus infections to cirrhosis and primary liver cancer worldwide.* J Hepatol, 2006. **45**(4): p. 529-38.

63.   Appleby, T.C., Perry, J.K., Murakami, E., Barauskas, O., Feng, J., et al., *Viral replication. Structural basis for rna replication by the hepatitis c virus polymerase.* Science, 2015. **347**(6223): p. 771-5.

64.   Lauer, G.M. and Walker, B.D., *Hepatitis c virus infection.* N Engl J Med, 2001. **345**(1): p. 41-52.

65.   Falagas, M.E., Karydis, I., and Kostogiannou, I., *Percutaneous exposure incidents of the health care personnel in a newly founded tertiary hospital: A prospective study.* PLoS One, 2007. **2**(2): p. e194.

66.   Bowen, D.G. and Walker, C.M., *Adaptive immune responses in acute and chronic hepatitis c virus infection.* Nature, 2005. **436**(7053): p. 946-52.

67.   Racanelli, V. and Rehermann, B., *Hepatitis c virus infection: When silence is deception.* Trends Immunol, 2003. **24**(8): p. 456-64.

68.   Webster, D.P., Klenerman, P., and Dusheiko, G.M., *Hepatitis c.* Lancet, 2015. **385**(9973): p. 1124-35.

69.   Westbrook, R.H. and Dusheiko, G., *Natural history of hepatitis c.* J Hepatol, 2014. **61**(1 Suppl): p. S58-68.

70.   Fattovich, G., Stroffolini, T., Zagni, I., and Donato, F., *Hepatocellular carcinoma in cirrhosis: Incidence and risk factors.* Gastroenterology, 2004. **127**(5 Suppl 1): p. S35-50.

71.   El-Serag, H.B. and Rudolph, K.L., *Hepatocellular carcinoma: Epidemiology and molecular carcinogenesis.* Gastroenterology, 2007. **132**(7): p. 2557-76.

72. Fried, M.W., Shiffman, M.L., Reddy, K.R., Smith, C., Marinos, G., et al., *Peginterferon alfa-2a plus ribavirin for chronic hepatitis c virus infection.* N Engl J Med, 2002. **347**(13): p. 975-82.

73. Manns, M.P., McHutchison, J.G., Gordon, S.C., Rustgi, V.K., Shiffman, M., et al., *Peginterferon alfa-2b plus ribavirin compared with interferon alfa-2b plus ribavirin for initial treatment of chronic hepatitis c: A randomised trial.* Lancet, 2001. **358**(9286): p. 958-65.

74. Righi, E., Londero, A., Carnelutti, A., Baccarani, U., and Bassetti, M., *Impact of new treatment options for hepatitis c virus infection in liver transplantation.* World J Gastroenterol, 2015. **21**(38): p. 10760-75.

75. Lawitz, E., Poordad, F.F., Pang, P.S., Hyland, R.H., Ding, X., et al., *Sofosbuvir and ledipasvir fixed-dose combination with and without ribavirin in treatment-naive and previously treated patients with genotype 1 hepatitis c virus infection (lonestar): An open-label, randomised, phase 2 trial.* Lancet, 2014. **383**(9916): p. 515-23.

76. Sulkowski, M.S., Gardiner, D.F., Rodriguez-Torres, M., Reddy, K.R., Hassanein, T., et al., *Daclatasvir plus sofosbuvir for previously treated or untreated chronic hcv infection.* N Engl J Med, 2014. **370**(3): p. 211-21.

77. Walker, D.R., Pedrosa, M.C., Manthena, S.R., Patel, N., and Marx, S.E., *Early view of the effectiveness of new direct-acting antiviral (daa) regimens in patients with hepatitis c virus (hcv).* Adv Ther, 2015. **32**(11): p. 1117-27.

78. Hill, A., Khoo, S., Fortunak, J., Simmons, B., and Ford, N., *Minimum costs for producing hepatitis c direct-acting antivirals for use in large-scale treatment access programs in developing countries.* Clin Infect Dis, 2014. **58**(7): p. 928-36.

79. Hill, A. and Cooke, G., *Medicine. Hepatitis c can be cured globally, but at what cost?* Science, 2014. **345**(6193): p. 141-2.

80. Paolucci, S., Fiorina, L., Mariani, B., Landini, V., Gulminetti, R., et al., *Development and persistence of daa resistance associated mutations in patients failing hcv treatment.* J Clin Virol, 2015. **72**: p. 114-8.

81. Yoshimi, S., Imamura, M., Murakami, E., Hiraga, N., Tsuge, M., et al., *Long term persistence of ns5a inhibitor-resistant hepatitis c virus in patients who failed daclatasvir and asunaprevir therapy.* J Med Virol, 2015. **87**(11): p. 1913-20.

82. Chayama, K. and Hayes, C.N., *Hcv drug resistance challenges in japan: The role of pre-existing variants and emerging resistant strains in direct acting antiviral therapy.* Viruses, 2015. **7**(10): p. 5328-42.

83. Poveda, E., Wyles, D.L., Mena, A., Pedreira, J.D., Castro-Iglesias, A., and Cachay, E., *Update on hepatitis c virus resistance to direct-acting antiviral agents.* Antiviral Res, 2014. **108**: p. 181-91.

84. Sarrazin, C., *The importance of resistance to direct antiviral drugs in hcv infection in clinical practice.* J Hepatol, 2016. **64**(2): p. 486-504.

85. Bartolini, B., Selleri, M., Garbuglia, A.R., Giombini, E., Taibi, C., et al., *Hcv ns3 quasispecies in liver and plasma and dynamics of telaprevir-resistant variants in breakthrough patients assessed by udps: A case study.* J Clin Virol, 2015. **72**: p. 60-5.

86. Ruta, S. and Cernescu, C., *Injecting drug use: A vector for the introduction of new hepatitis c virus genotypes.* World J Gastroenterol, 2015. **21**(38): p. 10811-23.

87. Hickman, M., De Angelis, D., Vickerman, P., Hutchinson, S., and Martin, N.K., *Hepatitis c virus treatment as prevention in people who inject drugs: Testing the evidence.* Curr Opin Infect Dis, 2015. **28**(6): p. 576-82.

88.   Crispe, I.N., *Liver antigen-presenting cells.* J Hepatol, 2011. **54**(2): p. 357-65.

89.   Racanelli, V. and Rehermann, B., *The liver as an immunological organ.* Hepatology, 2006. **43**(2 Suppl 1): p. S54-62.

90.   Thomson, A.W. and Knolle, P.A., *Antigen-presenting cell function in the tolerogenic liver environment.* Nat Rev Immunol, 2010. **10**(11): p. 753-66.

91.   Hsu, W., Shu, S.A., Gershwin, E., and Lian, Z.X., *The current immune function of hepatic dendritic cells.* Cell Mol Immunol, 2007. **4**(5): p. 321-8.

92.   Lumsden, A.B., Henderson, J.M., and Kutner, M.H., *Endotoxin levels measured by a chromogenic assay in portal, hepatic and peripheral venous blood in patients with cirrhosis.* Hepatology, 1988. **8**(2): p. 232-6.

93.   Biswas, S.K. and Lopez-Collazo, E., *Endotoxin tolerance: New mechanisms, molecules and clinical significance.* Trends Immunol, 2009. **30**(10): p. 475-87.

94.   Bamboat, Z.M., Stableford, J.A., Plitas, G., Burt, B.M., Nguyen, H.M., et al., *Human liver dendritic cells promote t cell hyporesponsiveness.* J Immunol, 2009. **182**(4): p. 1901-11.

95.   Neumann, A.U., Lam, N.P., Dahari, H., Gretch, D.R., Wiley, T.E., et al., *Hepatitis c viral dynamics in vivo and the antiviral efficacy of interferon-alpha therapy.* Science, 1998. **282**(5386): p. 103-7.

96.   Bowen, D.G. and Walker, C.M., *Mutational escape from cd8+ t cell immunity: Hcv evolution, from chimpanzees to man.* J Exp Med, 2005. **201**(11): p. 1709-14.

97.   Zingaretti, C., De Francesco, R., and Abrignani, S., *Why is it so difficult to develop a hepatitis c virus preventive vaccine?* Clin Microbiol Infect, 2014. **20 Suppl 5**: p. 103-9.

98.   Dustin, L.B., Cashman, S.B., and Laidlaw, S.M., *Immune control and failure in hcv infection-tipping the balance.* J Leukoc Biol, 2014. **96**(4): p. 535-48.

99.   Shimizu, Y., Hishiki, T., Ujino, S., Sugiyama, K., Funami, K., and Shimotohno, K., *Lipoprotein component associated with hepatitis c virus is essential for virus infectivity.* Curr Opin Virol, 2011. **1**(1): p. 19-26.

100.   Lindenbach, B.D. and Rice, C.M., *The ins and outs of hepatitis c virus entry and assembly.* Nat Rev Microbiol, 2013. **11**(10): p. 688-700.

101.   Li, X.D., Sun, L., Seth, R.B., Pineda, G., and Chen, Z.J., *Hepatitis c virus protease ns3/4a cleaves mitochondrial antiviral signaling protein off the mitochondria to evade innate immunity.* Proc Natl Acad Sci U S A, 2005. **102**(49): p. 17717-22.

102.   Li, K., Foy, E., Ferreon, J.C., Nakamura, M., Ferreon, A.C., et al., *Immune evasion by hepatitis c virus ns3/4a protease-mediated cleavage of the toll-like receptor 3 adaptor protein trif.* Proc Natl Acad Sci U S A, 2005. **102**(8): p. 2992-7.

103.   Meylan, E., Curran, J., Hofmann, K., Moradpour, D., Binder, M., et al., *Cardif is an adaptor protein in the rig-i antiviral pathway and is targeted by hepatitis c virus.* Nature, 2005. **437**(7062): p. 1167-72.

104.   Callendret, B. and Walker, C., *A siege of hepatitis: Immune boost for viral hepatitis.* Nat Med, 2011. **17**(3): p. 252-3.

105.   Ghasemi, F., Rostami, S., and Meshkat, Z., *Progress in the development of vaccines for hepatitis c virus infection.* World J Gastroenterol, 2015. **21**(42): p. 11984-2002.

106.   Diepolder, H.M., Zachoval, R., Hoffmann, R.M., Wierenga, E.A., Santantonio, T., et al., *Possible mechanism involving t-lymphocyte response to non-structural protein 3 in viral clearance in acute hepatitis c virus infection.* Lancet, 1995. **346**(8981): p. 1006-7.

107. Thimme, R., Oldach, D., Chang, K.M., Steiger, C., Ray, S.C., and Chisari, F.V., *Determinants of viral clearance and persistence during acute hepatitis c virus infection.* J Exp Med, 2001. **194**(10): p. 1395-406.

108. Grakoui, A., Shoukry, N.H., Woollard, D.J., Han, J.H., Hanson, H.L., et al., *Hcv persistence and immune evasion in the absence of memory t cell help.* Science, 2003. **302**(5645): p. 659-62.

109. Flynn, J.K., Dore, G.J., Hellard, M., Yeung, B., Rawlinson, W.D., et al., *Maintenance of th1 hepatitis c virus (hcv)-specific responses in individuals with acute hcv who achieve sustained virological clearance after treatment.* J Gastroenterol Hepatol, 2013. **28**(11): p. 1770-81.

110. Morin, T.J., Broering, T.J., Leav, B.A., Blair, B.M., Rowley, K.J., et al., *Human monoclonal antibody hcv1 effectively prevents and treats hcv infection in chimpanzees.* PLoS Pathog, 2012. **8**(8): p. e1002895.

111. Lavillette, D., Morice, Y., Germanidis, G., Donot, P., Soulier, A., et al., *Human serum facilitates hepatitis c virus infection, and neutralizing responses inversely correlate with viral replication kinetics at the acute phase of hepatitis c virus infection.* J Virol, 2005. **79**(10): p. 6023-34.

112. Walker, C.M. and Grakoui, A., *Hepatitis c virus: Why do we need a vaccine to prevent a curable persistent infection?* Curr Opin Immunol, 2015. **35**: p. 137-43.

113. O'Hagan, D.T., Singh, M., Dong, C., Ugozzoli, M., Berger, K., et al., *Cationic microparticles are a potent delivery system for a hcv DNA vaccine.* Vaccine, 2004. **23**(5): p. 672-80.

114. Yang, Y., Kuang, Y., Liu, Y., Li, W., Jiang, Z., et al., *Immunogenicity of multiple-epitope antigen gene of hcv carried by novel biodegradable polymers.* Comp Immunol Microbiol Infect Dis, 2011. **34**(1): p. 65-72.

115. Elmowalid, G.A., Qiao, M., Jeong, S.H., Borg, B.B., Baumert, T.F., et al., *Immunization with hepatitis c virus-like particles results in control of hepatitis c virus infection in chimpanzees.* Proc Natl Acad Sci U S A, 2007. **104**(20): p. 8427-32.

116. Houghton, M., *Prospects for prophylactic and therapeutic vaccines against the hepatitis c viruses.* Immunol Rev, 2011. **239**(1): p. 99-108.

117. Frey, S.E., Houghton, M., Coates, S., Abrignani, S., Chien, D., et al., *Safety and immunogenicity of hcv e1e2 vaccine adjuvanted with mf59 administered to healthy adults.* Vaccine, 2010. **28**(38): p. 6367-73.

118. Eisenstein, M., *Vaccines: A moving target.* Nature, 2011. **474**(7350): p. S16-7.

119. Swadling, L., Capone, S., Antrobus, R.D., Brown, A., Richardson, R., et al., *A human vaccine strategy based on chimpanzee adenoviral and mva vectors that primes, boosts, and sustains functional hcv-specific t cell memory.* Sci Transl Med, 2014. **6**(261): p. 261ra153.

120. Buchbinder, S.P., Mehrotra, D.V., Duerr, A., Fitzgerald, D.W., Mogg, R., et al., *Efficacy assessment of a cell-mediated immunity hiv-1 vaccine (the step study): A double-blind, randomised, placebo-controlled, test-of-concept trial.* Lancet, 2008. **372**(9653): p. 1881-93.

121. Barnes, E., Folgori, A., Capone, S., Swadling, L., Aston, S., et al., *Novel adenovirus-based vaccines induce broad and sustained t cell responses to hcv in man.* Sci Transl Med, 2012. **4**(115): p. 115ra1.

122. Chmielewska, A.M., Naddeo, M., Capone, S., Ammendola, V., Hu, K., et al., *Combined adenovirus vector and hepatitis c virus envelope protein prime-boost regimen elicits t cell and neutralizing antibody immune responses.* J Virol, 2014. **88**(10): p. 5502-10.

123. Baier, G., Musyanovych, A., Dass, M., Theisinger, S., and Landfester, K., *Cross-linked starch capsules containing dsdna prepared in inverse miniemulsion as "nanoreactors" for polymerase chain reaction.* Biomacromolecules, 2010. **11**(4): p. 960-8.

124. Baier, G., Fichter, M., Kreyes, A., Klein, K., Mailander, V., et al., *Glutathione responsive hyaluronic acid nanocapsules obtained by bioorthogonal interfacial "click" reaction.* Biomacromolecules, 2016. **17**(1): p. 148-53.

125. Baier, G., Winzen, S., Messerschmidt, C., Frank, D., Fichter, M., et al., *Heparin-based nanocapsules as potential drug delivery systems.* Macromol Biosci, 2015. **15**(6): p. 765-76.

126. Fichter, M., Baier, G., Dedters, M., Pretsch, L., Pietrzak-Nguyen, A., et al., *Nanocapsules generated out of a polymeric dexamethasone shell suppress the inflammatory response of liver macrophages.* Nanomedicine, 2013. **9**(8): p. 1223-34.

127. Fichter, M., Dedters, M., Pietrzak-Nguyen, A., Pretsch, L., Meyer, C.U., et al., *Monophosphoryl lipid a coating of hydroxyethyl starch nanocapsules drastically increases uptake and maturation by dendritic cells while minimizing the adjuvant dosage.* Vaccine, 2015. **33**(7): p. 838-46.

128. Fichter, M., Piradashvili, K., Pietrzak-Nguyen, A., Pretsch, L., Kuhn, G., et al., *Polymeric hepatitis c virus non-structural protein 5a nanocapsules induce intrahepatic antigen-specific immune responses.* submitted manuscript.

129. Pietrzak-Nguyen, A., Fichter, M., Dedters, M., Pretsch, L., Gregory, S.H., et al., *Enhanced in vivo targeting of murine nonparenchymal liver cells with monophosphoryl lipid a functionalized microcapsules.* Biomacromolecules, 2014. **15**(7): p. 2378-88.

130. Piradashvili, K., Fichter, M., Mohr, K., Gehring, S., Wurm, F.R., and Landfester, K., *Biodegradable protein nanocontainers.* Biomacromolecules, 2015. **16**(3): p. 815-21.

131. Wintermeyer, P., Gehring, S., Eken, A., and Wands, J.R., *Generation of cellular immune responses to hcv ns5 protein through in vivo activation of dendritic cells.* J Viral Hepat, 2010. **17**(10): p. 705-13.

132. Stark, W.J., *Nanoparticles in biological systems.* Angew Chem Int Ed Engl, 2011. **50**(6): p. 1242-58.

133. Koch, A.M., Reynolds, F., Kircher, M.F., Merkle, H.P., Weissleder, R., and Josephson, L., *Uptake and metabolism of a dual fluorochrome tat-nanoparticle in hela cells.* Bioconjug Chem, 2003. **14**(6): p. 1115-21.

134. Limbach, L.K., Grass, R.N., and Stark, W.J., *Physico-chemical differences between particle- and molecule-derived toxicity: Can we make inherently safe nanoparticles?* CHIMIA International Journal for Chemistry, 2009. **63**(1): p. 38-43.

135. Hans, M.L. and Lowman, A.M., *Biodegradable nanoparticles for drug delivery and targeting.* Current Opinion in Solid State & Materials Science, 2002. **6**(4): p. 319-327.

136. Burchill, M.A., Tamburini, B.A., Pennock, N.D., White, J.T., Kurche, J.S., and Kedl, R.M., *T cell vaccinology: Exploring the known unknowns.* Vaccine, 2013. **31**(2): p. 297-305.

137. Xiang, S.D., Scholzen, A., Minigo, G., David, C., Apostolopoulos, V., et al., *Pathogen recognition and development of particulate vaccines: Does size matter?* Methods, 2006. **40**(1): p. 1-9.

138. Foged, C., Brodin, B., Frokjaer, S., and Sundblad, A., *Particle size and surface charge affect particle uptake by human dendritic cells in an in vitro model.* Int J Pharm, 2005. **298**(2): p. 315-22.

139. Moon, J.J., Huang, B., and Irvine, D.J., *Engineering nano- and microparticles to tune immunity.* Adv Mater, 2012. **24**(28): p. 3724-46.

140. Joshi, V.B., Geary, S.M., and Salem, A.K., *Biodegradable particles as vaccine delivery systems: Size matters.* AAPS J, 2013. **15**(1): p. 85-94.

141. Clogston, J.D. and Patri, A.K., *Zeta potential measurement.* Methods Mol Biol, 2011. **697**: p. 63-70.

142. Fox, E.S., Thomas, P., and Broitman, S.A., *Comparative studies of endotoxin uptake by isolated rat kupffer and peritoneal cells.* Infect Immun, 1987. **55**(12): p. 2962-6.

143. Billiar, T.R., Maddaus, M.A., West, M.A., Dunn, D.L., and Simmons, R.L., *The role of intestinal flora on the interactions between nonparenchymal cells and hepatocytes in coculture.* J Surg Res, 1988. **44**(4): p. 397-403.

144. Crispe, I.N., *The liver as a lymphoid organ.* Annu Rev Immunol, 2009. **27**: p. 147-63.

145. Jenne, C.N. and Kubes, P., *Immune surveillance by the liver.* Nat Immunol, 2013. **14**(10): p. 996-1006.

146. Ossipov, D.A., *Nanostructured hyaluronic acid-based materials for active delivery to cancer.* Expert Opin Drug Deliv, 2010. **7**(6): p. 681-703.

147. Cella, M., Scheidegger, D., Palmer-Lehmann, K., Lane, P., Lanzavecchia, A., and Alber, G., *Ligation of cd40 on dendritic cells triggers production of high levels of interleukin-12 and enhances t cell stimulatory capacity: T-t help via apc activation.* J Exp Med, 1996. **184**(2): p. 747-52.

148. Guo, M., Gong, S., Maric, S., Misulovin, Z., Pack, M., et al., *A monoclonal antibody to the dec-205 endocytosis receptor on human dendritic cells.* Hum Immunol, 2000. **61**(8): p. 729-38.

149. Tacken, P.J. and Figdor, C.G., *Targeted antigen delivery and activation of dendritic cells in vivo: Steps towards cost effective vaccines.* Semin Immunol, 2011. **23**(1): p. 12-20.

150. Garcon, N., *Preclinical development of as04.* Methods Mol Biol, 2010. **626**: p. 15-27.

151. Weilhammer, D.R., Blanchette, C.D., Fischer, N.O., Alam, S., Loots, G.G., et al., *The use of nanolipoprotein particles to enhance the immunostimulatory properties of innate immune agonists against lethal influenza challenge.* Biomaterials, 2013. **34**(38): p. 10305-18.

152. Sarti, F., Perera, G., Hintzen, F., Kotti, K., Karageorgiou, V., et al., *In vivo evidence of oral vaccination with plga nanoparticles containing the immunostimulant monophosphoryl lipid a.* Biomaterials, 2011. **32**(16): p. 4052-7.

153. Santambrogio, L., Sato, A.K., Carven, G.J., Belyanskaya, S.L., Strominger, J.L., and Stern, L.J., *Extracellular antigen processing and presentation by immature dendritic cells.* Proc Natl Acad Sci U S A, 1999. **96**(26): p. 15056-61.

154. Schafer, F.Q. and Buettner, G.R., *Redox environment of the cell as viewed through the redox state of the glutathione disulfide/glutathione couple.* Free Radic Biol Med, 2001. **30**(11): p. 1191-212.

155. Meikle, A.W. and Tyler, F.H., *Potency and duration of action of glucocorticoids. Effects of hydrocortisone, prednisone and dexamethasone on human pituitary-adrenal function.* Am J Med, 1977. **63**(2): p. 200-7.

156. Lowenberg, M., Verhaar, A.P., van den Brink, G.R., and Hommes, D.W., *Glucocorticoid signaling: A nongenomic mechanism for t-cell immunosuppression.* Trends Mol Med, 2007. **13**(4): p. 158-63.

157. Urbanska, J., Karewicz, A., and Nowakowska, M., *Polymeric delivery systems for dexamethasone.* Life Sci, 2014. **96**(1-2): p. 1-6.

158. Mieli-Vergani, G. and Vergani, D., *Autoimmune liver diseases in children - what is different from adulthood?* Best Pract Res Clin Gastroenterol, 2011. **25**(6): p. 783-95.

159. Doyle, L.W., Ehrenkranz, R.A., and Halliday, H.L., *Dexamethasone treatment in the first week of life for preventing bronchopulmonary dysplasia in preterm infants: A systematic review.* Neonatology, 2010. **98**(3): p. 217-24.

160. Ho, C.M., Wu, H.L., Ho, S.T., and Wang, J.J., *Dexamethasone prevents postoperative nausea and vomiting: Benefit versus risk.* Acta Anaesthesiol Taiwan, 2011. **49**(3): p. 100-4.

161. Gomez-Gaete, C., Tsapis, N., Besnard, M., Bochot, A., and Fattal, E., *Encapsulation of dexamethasone into biodegradable polymeric nanoparticles.* Int J Pharm, 2007. **331**(2): p. 153-9.

162. Turkoglu, O.F., Eroglu, H., Okutan, O., Burul, E., Sargon, M.F., et al., *The efficiency of dexamethasone sodium phosphate-encapsulated chitosan microspheres after cold injury.* Surg Neurol, 2005. **64 Suppl 2**: p. S11-6.

163. Liu, X.M., Quan, L.D., Tian, J., Laquer, F.C., Ciborowski, P., and Wang, D., *Syntheses of click peg-dexamethasone conjugates for the treatment of rheumatoid arthritis.* Biomacromolecules, 2010. **11**(10): p. 2621-8.

164. Emoto, M., Emoto, Y., Brinkmann, V., Miyamoto, M., Yoshizawa, I., et al., *Increased resistance of lfa-1-deficient mice to lipopolysaccharide-induced shock/liver injury in the presence of tnf-alpha and il-12 is mediated by il-10: A novel role for lfa-1 in the regulation of the proinflammatory and anti-inflammatory cytokine balance.* J Immunol, 2003. **171**(2): p. 584-93.

165. Gehring, S., Dickson, E.M., San Martin, M.E., van Rooijen, N., Papa, E.F., et al., *Kupffer cells abrogate cholestatic liver injury in mice.* Gastroenterology, 2006. **130**(3): p. 810-22.

166. Linhardt, R.J., *2003 claude s. Hudson award address in carbohydrate chemistry. Heparin: Structure and activity.* J Med Chem, 2003. **46**(13): p. 2551-64.

167. World Health Organization, *Who model list of essential medicines*, October 2013

168. Horwitz, O., Johnson, W.T., Sayen, J.J., Roberts, B., and Whereat, A.F., *Heparin for oral use: Preliminary studies.* Trans Am Clin Climatol Assoc, 1993. **104**: p. 94-102; discussion 102-3.

169. Kemp, M.M. and Linhardt, R.J., *Heparin-based nanoparticles.* Wiley Interdiscip Rev Nanomed Nanobiotechnol, 2010. **2**(1): p. 77-87.

170. Passirani, C., Barratt, G., Devissaguet, J.P., and Labarre, D., *Long-circulating nanoparticles bearing heparin or dextran covalently bound to poly(methyl methacrylate).* Pharm Res, 1998. **15**(7): p. 1046-50.

171. Ritz, S., Schottler, S., Kotman, N., Baier, G., Musyanovych, A., et al., *Protein corona of nanoparticles: Distinct proteins regulate the cellular uptake.* Biomacromolecules, 2015. **16**(4): p. 1311-21.

172. Treuel, L., Docter, D., Maskos, M., and Stauber, R.H., *Protein corona - from molecular adsorption to physiological complexity.* Beilstein J Nanotechnol, 2015. **6**: p. 857-73.

173. Mata-Haro, V., Cekic, C., Martin, M., Chilton, P.M., Casella, C.R., and Mitchell, T.C., *The vaccine adjuvant monophosphoryl lipid a as a trif-biased agonist of tlr4.* Science, 2007. **316**(5831): p. 1628-32.
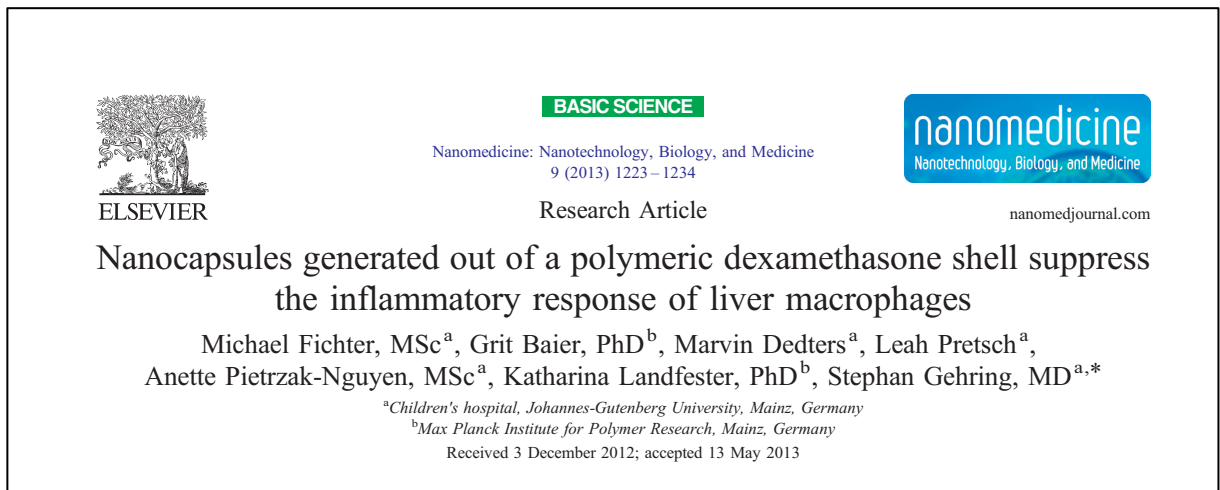
174. Casella, C.R. and Mitchell, T.C., *Inefficient tlr4/md-2 heterotetramerization by monophosphoryl lipid a.* PLoS One, 2013. **8**(4): p. e62622.

175. Moon, J.J., Suh, H., Li, A.V., Ockenhouse, C.F., Yadava, A., and Irvine, D.J., *Enhancing humoral responses to a malaria antigen with nanoparticle vaccines that expand tfh cells and promote germinal center induction.* Proc Natl Acad Sci U S A, 2012. **109**(4): p. 1080-5.

176. Moon, J.J., Suh, H., Polhemus, M.E., Ockenhouse, C.F., Yadava, A., and Irvine, D.J., *Antigen-displaying lipid-enveloped plga nanoparticles as delivery agents for a plasmodium vivax malaria vaccine.* PLoS One, 2012. **7**(2): p. e31472.

177. Hubo, M., Trinschek, B., Kryczanowsky, F., Tuettenberg, A., Steinbrink, K., and Jonuleit, H., *Costimulatory molecules on immunogenic versus tolerogenic human dendritic cells.* Front Immunol, 2013. **4**: p. 82.

178. Pasquale, A.D., Preiss, S., Silva, F.T., and Garcon, N., *Vaccine adjuvants: From 1920 to 2015 and beyond.* Vaccines (Basel), 2015. **3**(2): p. 320-43.

179. Reed, S.G., Orr, M.T., and Fox, C.B., *Key roles of adjuvants in modern vaccines.* Nat Med, 2013. **19**(12): p. 1597-608.

180. The European Medicines Agency, *Guideline on adjuvants in vaccines for human use*, January 20th 2005

181. Christie, M., Torres, R.M., Kedl, R.M., Randolph, T.W., and Carpenter, J.F., *Recombinant murine growth hormone particles are more immunogenic with intravenous than subcutaneous administration.* J Pharm Sci, 2014. **103**(1): p. 128-39.

182. Epstein, J.E., Tewari, K., Lyke, K.E., Sim, B.K., Billingsley, P.F., et al., *Live attenuated malaria vaccine designed to protect through hepatic cd8(+) t cell immunity.* Science, 2011. **334**(6055): p. 475-80.

183. Seder, R.A., Chang, L.J., Enama, M.E., Zephir, K.L., Sarwar, U.N., et al., *Protection against malaria by intravenous immunization with a nonreplicating sporozoite vaccine.* Science, 2013. **341**(6152): p. 1359-65.

184. Dobrovolskaia, M.A., Shurin, M., and Shvedova, A.A., *Current understanding of interactions between nanoparticles and the immune system.* Toxicol Appl Pharmacol, 2015.

185. Elsabahy, M. and Wooley, K.L., *Cytokines as biomarkers of nanoparticle immunotoxicity.* Chem Soc Rev, 2013. **42**(12): p. 5552-76.

186. Beran, J., *Safety and immunogenicity of a new hepatitis b vaccine for the protection of patients with renal insufficiency including pre-haemodialysis and haemodialysis patients.* Expert Opin Biol Ther, 2008. **8**(2): p. 235-47.

187. Gehring, S., Gregory, S.H., Wintermeyer, P., Aloman, C., and Wands, J.R., *Generation of immune responses against hepatitis c virus by dendritic cells containing ns5 protein-coated microparticles.* Clin Vaccine Immunol, 2009. **16**(2): p. 163-71.

188. Bartenschlager, R., Lohmann, V., and Penin, F., *The molecular and structural basis of advanced antiviral therapy for hepatitis c virus infection.* Nat Rev Microbiol, 2013. **11**(7): p. 482-96.

189. Losikoff, P.T., Mishra, S., Terry, F., Gutierrez, A., Ardito, M.T., et al., *Hcv epitope, homologous to multiple human protein sequences, induces a regulatory t cell response in infected patients.* J Hepatol, 2015. **62**(1): p. 48-55.

190. Moise, L., Terry, F., Gutierrez, A.H., Tassone, R., Losikoff, P., et al., *Smarter vaccine design will circumvent regulatory t cell-mediated evasion in chronic hiv and hcv infection.* Front Microbiol, 2014. **5**: p. 502.

6 APPENDIX

6.1 Publication 1

Nanocapsules generated out of a polymeric dexamethasone shell suppress the inflammatory response of liver macrophages

Published in: *Nanomedicine*, 2013. **9**(8): p. 1223-34.

Nanocapsules generated out of a polymeric dexamethasone shell suppress the inflammatory response of liver macrophages

Michael Fichter, MSc[a], Grit Baier, PhD[b], Marvin Dedters[a], Leah Pretsch[a], Anette Pietrzak-Nguyen, MSc[a], Katharina Landfester, PhD[b], Stephan Gehring, MD[a,*]

[a]*Children's hospital, Johannes-Gutenberg University, Mainz, Germany*
[b]*Max Planck Institute for Polymer Research, Mainz, Germany*
Received 3 December 2012; accepted 13 May 2013

Summary:

Polymeric nanocapsules were generated exclusively of dexamethasone (DXM) and suppressed the pro-inflammatory response of non-parenchymal liver cells derived from C57B6/J mice *in vitro*. DXM-NCs were ingested primarily by liver sinusoidal endothelial cells (LSECs) and Kupffer Cells (KCs) and released their content intracellularly. DXM-NCs effectively suppressed the secretion of pro-inflammatory cytokines (IL-6 and TNFα), thus efficiently slowing down inflammatory processes.

Author contribution:

- Design, conduction and evaluation of all biological experiments
- Preparation of graphs and figures
- Preparation of the manuscript together with Prof. Dr. Stephan Gehring

Nanocapsules generated out of a polymeric dexamethasone shell suppress the inflammatory response of liver macrophages

Michael Fichter, MSc[a], Grit Baier, PhD[b], Marvin Dedters[a], Leah Pretsch[a],
Anette Pietrzak-Nguyen, MSc[a], Katharina Landfester, PhD[b], Stephan Gehring, MD[a,*]

[a]Children's hospital, Johannes-Gutenberg University, Mainz, Germany
[b]Max Planck Institute for Polymer Research, Mainz, Germany
Received 3 December 2012; accepted 13 May 2013

Abstract

Dexamethasone (DXM) is a synthetic glucocorticoid with anti-inflammatory properties. Targeted delivery of dexamethasone to inflammatory cells, e.g. macrophages and Kupffer cells represents a promising approach to minimize side effects. The aim of the present study was to induce a targeted transport of novel DXM-based biodegradable nanocapsules to phagocytic cells. Nanocapsules (NCs) consisting of a hydroxyethylated glucose polymer (hydroxyethyl starch, HES) shell with encapsulated DXM and NCs synthesized exclusively in inverse miniemulsion out of DXM were investigated. Non-parenchymal murine liver cells served as target cells. HES-DXM NCs were predominantly incorporated by Kupffer cells (KCs). In contrast, DXM NCs were phagocytized by KCs and endothelial cells. The release of the NC-content was confirmed by incorporation of CellTracker™ into the NCs. Uptake of DXM NCs by Kupffer cells reduced significantly the release of inflammatory cytokines in response to LPS stimulation. Importantly, the DXM NCs consisting exclusively out of a dexamethasone shell offer the potential to serve as carriers for additional therapeutics.

From the Clinical Editor: In this paper, nanocapsule-based targeted delivery of dexamethasone to inflammatory cells is presented as a promising approach to minimize side effects and increase efficacy of this anti-inflammatory clinically used corticosteroid.
© 2013 Elsevier Inc. All rights reserved.

Key words: Dexamethasone nanocapsules; Kupffer cells; Liver sinusoid endothelial cells; Cytokines

There is a growing interest in colloidal nanocarriers such as liposomes, micelles, dendrimers, polymeric particles or capsules composed of biocompatible and biodegradable materials for biomedical applications.[1–5] The encapsulation of bioactive compounds in polymeric nanocapsules provides protection for sensitive biomolecules (e.g. proteins, dsDNA). The synthesis of nanocapsules made of natural biomolecules (e.g. starch) could be successfully performed using the miniemulsion process. This technique allows the formation of stable nanocapsules, whose properties can be tailored individually according to the specific requirements.[6,7] The nanocapsule size (between 150 and 500 nm) and stability of the system can be adjusted by varying the amount of biomolecule, surfactant and cross-linker.

Following the synthesis, the nanocapsules can be redispersed in an aqueous phase, which provides an opportunity to employ them as nanocarriers for various biomedical reactions. Recently, a polymerase chain reaction was performed into a single shielded and stable nanocapsule, thus protecting the biological material from the influence of the environment. Each capsule can be seen as a separate "nanocontainer".[8] The encapsulation of water-soluble fluorescent or infrared dyes, drugs or biomolecules enables the usage of the obtained nanocapsules for imaging or targeted drug delivery within the living organism. The latter bears the striking potential to minimize potential side effects.

In this context, dexamethasone (DXM), a synthetic glucocorticoid with vigorous anti-inflammatory and immunosuppressive properties and broad clinical application, is of particular interest. Compared to endogenous synthesized cortisol, DXM is estimated to be at least 30 times more potent.[9] However, systemic administration of DXM is associated with severe side-effects, such as hyperglycemia, hypertension, and intestinal bleeding.[10] Targeted delivery of dexamethasone to key cells

regulating inflammation, such as macrophages, monocytes, and Kupffer cells, represents a promising approach to avoid unintended treatment effects. Recently, several polymeric DXM formulations have been developed, including the encapsulation of DXM in poly(D,L-lactide-*co*-glycolide) (PLGA) nanoparticles,[11] in biodegradable polyurethane,[12] in poly(phenylacetylene) (PPA),[13] in block copolymer,[14] coupled to mannosylated albumin,[15] and in a nanostructured lipid carrier system consisting of soybean oil and lecithin.[16]

The aim of the present study was to induce a targeted transport of novel DXM-based nanocapsules in order to suppress the inflammatory response of phagocytic cells. Nanocapsules (NCs) consisting of a hydroxyethylated glucose polymer (hydroxyethyl starch, HES) shell with encapsulated DXM (HES-DXM NCs) and NCs synthesized exclusively out of DXM (DXM NCs) were investigated. The biocompatible hydroxyethylated glucose polymer HES which is a naturally derived substitute for the often used synthetic water-soluble PEG was chosen because of its common usage in medicine. In general, polysaccharides have proven to be a good alternative for the reduction or prevention of protein adsorption.[17,18] Because of its similarity with human glycogen, HES is considered to be a low toxicity compound. Compared with dextran serious anaphylactic reactions are clearly less prevalent.[19] Furthermore, HES is considered to have a low pro-thrombogenic potential.[20]

Our interest to compare the HES-DXM nanocapsule with a nanocapsule solely generated out of DXM was triggered by two apparent advantages: First, avoiding additional compounds (e.g. PLGA, PU, and lipids) reduces the risk of toxicity and unintended immune responses, second, the nanocapsule structure allows the combination with other therapeutic compounds, commonly used in combination with steroids (e.g. immunosuppressive drugs or chemotherapeutics).

All types of nanocapsules were synthesized in inverse (water-in-oil) miniemulsion through interfacial polyaddition reaction. After the synthesis the nanocapsules were characterized in terms of size, size distribution and morphology. Furthermore, the embedded amount of dexamethasone was determined from absorbance measurements.

The biologic properties of our DXM NC formulations were evaluated using primary cell cultures generated out of non-parenchymal murine liver cells (NPCs). The latter were chosen, due to the fact, that most particulate carriers administered intravenously (iv) usually accumulate in the liver.[21] Approximately one third of the NPCs are Kupffer cells, which are resident tissue macrophages that line the liver sinusoids, and are responsible for clearing the blood stream from large particles.[22] In addition, Kupffer cells are involved in the pathogenesis of liver injury through the release of biological cytokines (e.g. IL-6, TNF-α), superoxide, nitric oxide, eicosanoids, and chemokines.[23] In contrast, small particles are preferentially ingested by endothelial cells which contribute to another third of liver NPCs. The distribution of our DXM nanocapsules among the heterogeneous liver NPC population, the release of nanocapsule content, toxicity and the ability to suppress the secretion of inflammatory cytokines by NPCs were the focus of the biological part of the present study.
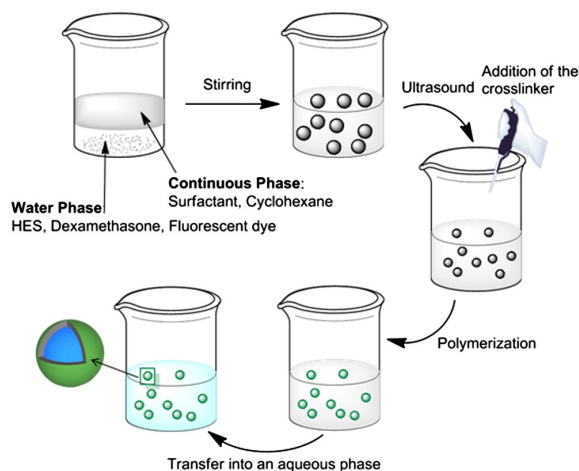

Figure 1. Scheme of nanocapsule synthesis using the inverse (water-in-oil) miniemulsion process.

Methods

NC synthesis

Materials used for the NCs synthesis

Hydroxyethyl starch (HES, 10%, degree of molar substitution = 0.5, M_w = 200,000 g·mol^{-1}) and sodium chloride (NaCl 0.9%) were purchased from Fresenius Kabi. Dexamethasone (M_w = 392.46 g·mol^{-1}), 2,4-toluene diisocyanate (TDI, M_w = 174.16 g·mol^{-1}) and cyclohexane (>99.9%) were purchased from Sigma Aldrich. The oil-soluble surfactant poly((ethylene-co-butylene)-*b*-(ethylene oxide)), P(E/B-*b*-EO), consisting of a poly(ethylene-co-butylene) block (M_w = 6796 g·mol^{-1}) and a poly(ethylene oxide) block (M_w = 8785 g·mol^{-1}) was synthesized starting from ω-hydroxypoly(ethylene-co-butylene), which was dissolved in toluene after addition of ethylene oxide under anionic polymerization conditions.[24] The anionic surfactant sodium dodecyl sulfate (SDS) was purchased from Fluka. The osmotic reagent sodium chloride (>99%) salt was purchased from Fischer. The cy5-labeled oligonucleotide with the sequence cy5-CCA CTC CTT TCC AGA AAA CT-3′ was synthesized by Thermo Scientific Ulm. The CellTracker™ Green CMFDA (M_w = 464.86 g·mol^{-1}) was purchased from Life Technologies (Molecular Probes). The magnesium- and calcium-free phosphate buffered solution (PBS) was purchased from Life Technologies (Molecular Probes). Demineralized water was used during the experiments.

Preparation of NCs

A setup of seven nanocapsules was prepared by a polyaddition reaction performed at the miniemulsion droplet's interface following a previously published slightly changed procedure[25] (Figure 1). Briefly, an aqueous phase consisting of the ingredients listed in Table 1 and 20 mg NaCl were added to a mixture of 100 mg of surfactant P(E/B-*b*-EO) dissolved in 7.5 g cyclohexane and stirred over 1 h at 25 °C. After the homogenization step (ultrasonication: 180 s at 90% amplitude in a pulse regime (20 s sonication, 10 s pause) using a Branson Sonifier

Table 1
Composition of the aqueous phase and amount of the crosslinker TDI.

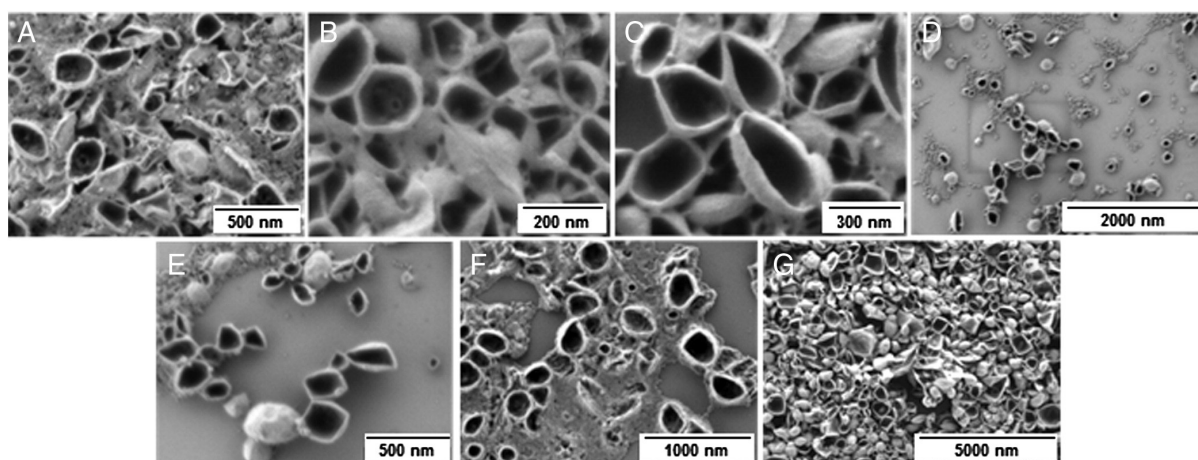| Samples	Amount of				
	HES (100 mg/ml) µl	DXM (10 mg/ml) µl	fluorescent dye µl	PBS buffer µl	TDI, mg
HES	1400	-	-	-	100
HES-cy5	1200	-	200 (100 pmol/µl)	-	100
HES-DXM	720	680	-	-	100
HES-CellTracker™	1200	-	200 (2.15 nmol/µl)	-	100
DXM	-	1000	-	400	40
DXM-cy5	-	1000	200 (100 pmol/µl)	200	40
DXM-CellTracker™	-	1000	200 (2.15 nmol/µl)	200	40

Figure 2. SEM micrographs of nanocapsules synthesized using the inverse miniemulsion process **(A)** DXM NCs, **(B)** DXM-cy5 NCs, **(C)** HES-DXM NCs, **(D)** HES-CellTracker™ NCs, **(E)** HES-cy5 NCs, **(F)** HES NCs and **(G)** DXM-CellTracker™ NCs.

W-450-Digital and a ½″ tip under ice cooling) a solution consisting of 5 g cyclohexane, 30 mg P(E/B-*b*-EO) and TDI (amounts are given in Table 1) was added dropwise over 5 min to the earlier prepared mixture I at 25 °C. The reaction was performed for 24 h at 25 °C under stirring. After the synthesis the nanocapsules were cleaned by centrifugation (two times, 20 min, Sigma 3 k-30, RCF 1467) in order to remove residuals of P(E/B-*b*-EO) and were redispersed in cyclohexane. Then, they were transferred into an aqueous phase using the following procedure: 1 g of the nanocapsules dispersion in cyclohexane (polymer solid content around 3 wt%) was mixed with 5 g SDS aqueous solution (0.1 wt%) under mechanical stirring for 24 h at 25 °C. Afterwards, the samples were redispersed for 15 min at 50 °C in a sonication bath (power 50%, 25 kHz). Then, they were dialyzed for 24 h (MWCO: 12,000 g·mol^{-1}) in order to remove residuals. Finally, the nanocapsules dispersion was centrifuged (20 min, Sigma 3 k-30, RCF 1467), the supernatant was removed and the nanocapsules were redispersed in NaCl 0.9%.

The non-encapsulated or non-crosslinked ("free") amount of dexamethasone was measured in the supernatant using a plate reader (Infinite M1000, Tecan, Switzerland). The maximum of absorbance of dexamethasone was detected at 240 nm. After the synthesis and redispersion, the nanocapsules were centrifuged (20 min using Sigma 3 k-30, RCF 1467) and the amount of dexamethasone present in the supernatant was calculated from the absorbance data. For the calculations a calibration curve obtained from different amounts of dissolved dexamethasone was used. For each sample the encapsulation efficiency was calculated from six single measurements.

Methods of the characterization of NCs

The average size and the size distribution of nanocapsules were analyzed by means of dynamic light scattering (DLS) at 25 °C using a Nicomp 380 submicron particle sizer equipped with a detector at a 90° angle to the incident beam (Nicomp Particle Sizing Systems, USA) at 20 °C. The zeta potential of nanocapsules was measured in 10^{-3} M potassium chloride solution at pH 6.8 with a Malvern Zeta sizer (Malvern Instruments, U.K.) at 20 °C. Morphological studies were performed with scanning electron microscopy (SEM). The images were recorded by using a field emission microscope (LEO (Zeiss) 1530 Gemini, Oberkochen, Germany) operated at an accelerating voltage of 170 V. Generally, the samples were prepared by diluting the capsule dispersion in cyclohexane or demineralized water (for redispersed samples) to about 0.01% solid content. A droplet of dispersion was placed onto silica wafers and dried under ambient conditions.

Table 2
Data obtained from dynamic light scattering and zeta potential measurements.

Samples	Diameter, nm/ STD% in cyclohexane	Diameter, nm/ STD% in water	Zeta potential, mV at pH 6.8 after dialyzation
HES	220/28	220/29	−28
HES-cy5	205/27	210/28	−30
HES-DXM	230/30	215/33	−28
HES-CellTracker™	175/26	175/28	−28
DXM	240/32	240/33	−22
DXM-cy5	215/32	240/31	−24
DXM-CellTracker™	245/33	220/33	−22

Table 3
Data obtained from absorbance measurements (240 nm).

Samples	Supernatant, %	Nanocapsules, %
HES-DXM	7.4 (±0.1)	92.6 (±5.3)
DXM	13.6 (±0.3)	86.4 (± 4.7)
DXM-cy5	11.9 (± 0.3)	88.1 (±4.5)
DXM-CellTracker™	11.6 (±0.4)	88.4 (±5.0)

Biological analysis

Mice

Five to 6-week old female C57BL/6 J mice were obtained from the Zentrale Versuchstiereinrichtung Mainz, Germany and kept under a 12 h dark, 12 h light cycle (with food and water supply at every time) in the animal facility of the University Hospital Mainz. The animals were treated in accordance with NIH publications entitled "Principles for Use of Animals" and "Guide for the Care and Use of Laboratory Animals." All protocols have been approved by the local Animal Care and Use Committee ("Landesuntersuchungsamt Rheinland-Pfalz").

Isolation of liver non-parenchymal cells (NPCs)

The NPC population consisting mainly of Kupffer cells, endothelial cells and hepatic stellate cells was isolated from livers of female C57BL/6 J mice using a modified method previously described.[26] Briefly, mice were anesthetized with Ketamin/Rompun®. Livers were perfused through the portal vein with 20 ml Ca^{2+}- and Mg^{2+}-free Hank's Balanced Salt Solution (PAN Biotech) containing 100 U/l collagenase (Sigma-Aldrich, C9891), 5% fetal calf serum (Hyclone, heat-inactivated) and 10 µg/ml DNase I (AppliChem). After dissection, the liver was incubated for 15 min at 37 °C. Single cell suspension was generated by grinding the livers through a 70 µm cell strainer. The parenchymal cell fraction (hepatocytes) was discarded following centrifugation for 15 min at 4 °C and 30 × g. The NPCs remaining in the supernatant were purified by centrifugation at 300 × g, resuspended in ice cold Histodenz solution (30%

in Ca^{2+}-and Mg^{2+}-free Hank's Balanced Salt Solution, PAN Biotech) and overlaid with ice cold Hank's Balanced Salt Solution, followed by another centrifugation step at 1500 × g at 4 °C for 20 min. NPCs were collected at the HBSS/Histodenz interface using a Pasteur pipette and resuspended with washing medium (HEPES buffered RPMI 1640 containing 10% fetal calf serum, 1% penicillin/streptomycin). The resulting NPC population was 95% viable or more and free of hepatocyte contamination. The cell suspension was then cultured in HEPES buffered RPMI 1640 medium containing 10% FCS, 1% penicillin/streptomycin, 1 mM L-glutamine, 1% essential and non-essential amino acids, 50 µM 2-mercaptoethanol and with or without 2.5 µg/ml bacterial endotoxin (LPS).

Confocal laser scanning microscopy (CSLM)

Intracellular uptake of nanocapsules by NPCs and a release of encapsulated substances were analyzed using a Zeiss LSM 710 NLO confocal laser scanning microscope. Freshly isolated NPCs were cultured with a density of 5×10^5 in 300 µl culture medium at 37 °C (in 8-Well-Chamberslides) in the presence of 25 µg/ml HES-cy5, DXM-cy5, HES-CellTracker™ or DXM-CellTracker™ capsules, respectively. An incubation time of three hours was assessed to ensure nanocapsule uptake by NPCs. Nuclei were stained with 2 µg/ml Hoechst 33342 (molecular probes) for 30 min. Immediately before analysis 2 µg/ml CellMask™ Orange (molecular probes) was added in order to perform plasma membrane staining.

Intracellular cytokine staining (ICCS) and flow cytometric cell analysis

Freshly isolated NPCs were cultured in a density of 1×10^6/ ml in the presence of different concentrations of HES-cy5, DXM-cy5 or HES-DXM-cy5. Phenotypic characterization of nanocapsule positive cells was performed after three hours of incubation with 0.25 µg/ml, 2.5 µg/ml or 25 µg/ml HES-cy5 or DXM-cy5; intracellular cytokine expression was determined after a six hour incubation period with 25 µg/ml of nanocapsules. ICCS and flow cytometric analysis were performed using

Figure 3. Confocal laser scanning microscopy (CLSM) was performed in order to document the uptake of HES-cy5 **(B)** and DXM-cy5 **(C)** nanocapsules (red) by non-parenchymal liver cells. The release of content out of NCs was analysed using the CellTracker™ Green CMFDA dye (green) which becomes fluorescent upon cleavage by cellular esterases **(D)**. Pseudocolor images which document the release of CellTracker™ dye out of HES **(E)** and DXM **(F)** NCs. Flow cytometric analysis was performed to quantify the uptake of nanocapsules at different concentrations by NPCs **(G)**. *Significance was given with $P < 0.001$ (Student's t test).
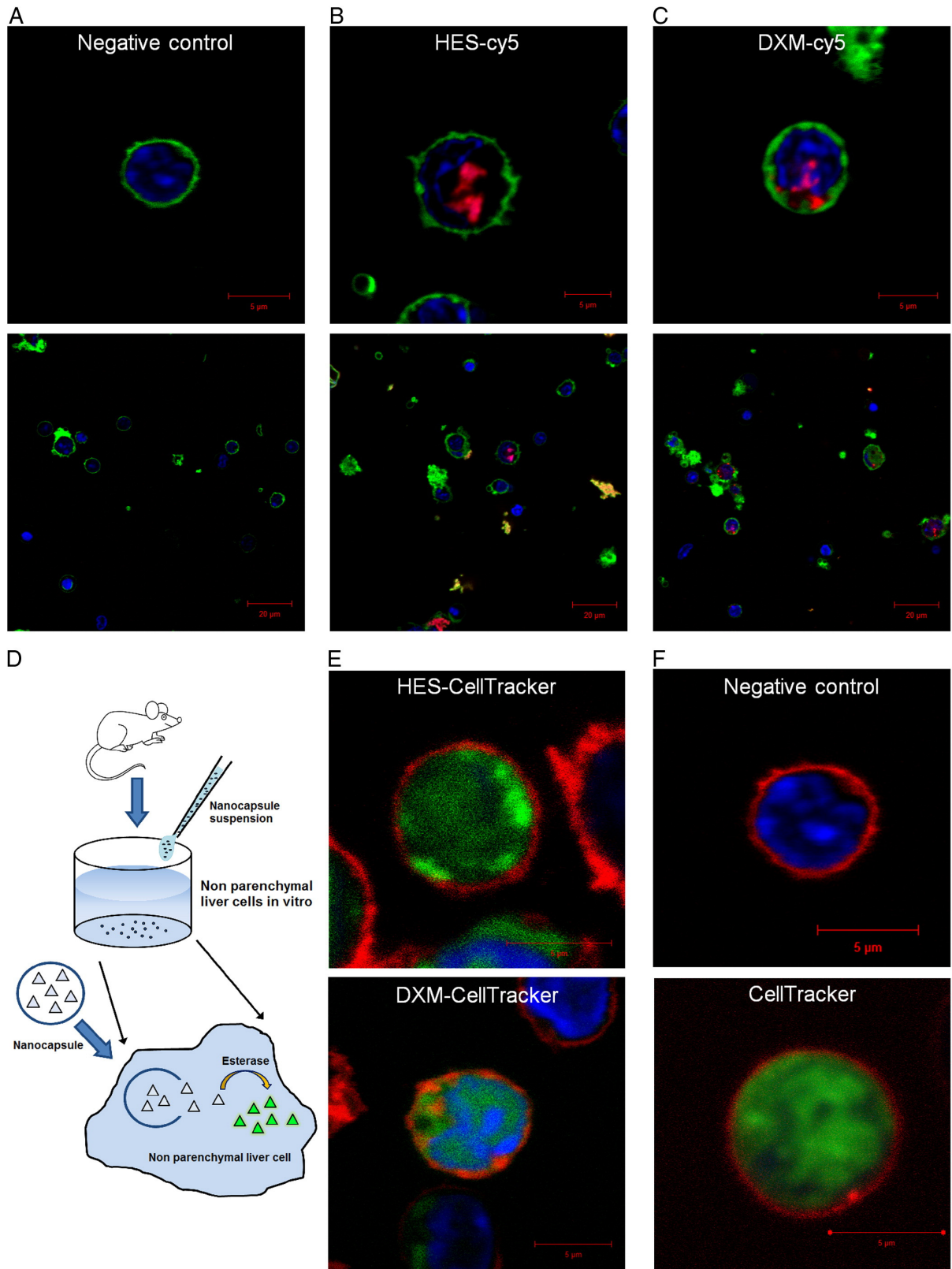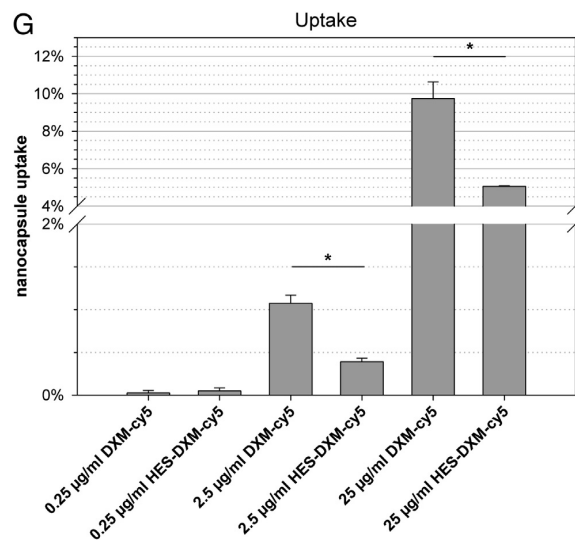
Figure 3. (*continued*).

the multi-channel cytometer BD LSR II (BD Biosciences) equipped with FACSDiva software (BD Biosciences) in accordance to methods we previously described.[26] Briefly, 1×10^6 cells were incubated for 15 min with excess anti-mouse CD16/32 (Clone 2.4G2, rat isotype) in order to block the Fc receptor followed by a 30 min incubation with fluorochrome-conjugated antibodies CD45 (Pacific Blue or APC, clone 30-F11), F4/80 (APC-cy7, clone BM8), or CD31 (PE, clone 390). ICCS was performed with anti-IL-6 (V450, clone MP5-20 F3) using a cytofix/cytoperm kit (BD Pharmingen) according to the manufacturer's instructions.

Analysis of nanocapsule toxicity

Toxicity of nanocapsules was evaluated by propidium iodide (PI; BD Pharmingen) staining, and subsequent flow cytometric quantification of PI positive cells. NPCs (1×10^6 per ml) were incubated with different capsule concentrations (0.25/2.5/25 µg/ml) and stained with 5 µl PI after 3, 8 or 24 h incubation according to the manufacturer's instructions.

Measurement of cytokine secretion

In order to quantify cytokine secretion, 5×10^5 NPCs/ml were cultured in the presence of 25 µg/ml HES, DXM or HES-DXM nanocapsules and/or 2.5 µg/ml LPS in 96-well, flat-bottom plates at 37 °C. After 24 h incubation, the supernatants were collected and the levels of IL-6 and TNF-α were measured using enzyme-linked immunosorbent assay kits (eBiosciences) according to the manufacturer's instructions.

Statistical analysis

Experiments were performed in triplicates and analyzed using SigmaStat 4.0 Software (Systat Software Inc). When more than two groups were compared with each other, a one way ANOVA test was performed followed by a Holm–Sidak test to determine which groups differed significantly ($P < 0.001$). For comparisons between two groups only a non-paired Student's t test was performed ($P < 0.001$).

Results

NC Synthesis

The nanocapsules were synthesized by interfacial polyaddition reaction in inverse miniemulsion as displayed in Figure 1. The obtained nanocapsules are colloidally stable and no precipitation or aggregation was observed within 2 months of storage under ambient conditions. SEM studies of the nanocapsules (Figure 2) confirm the formation of a core-shell morphology. The characteristics of the nanocapsules after synthesis and redispersion in an aqueous phase in terms of size, size distribution and zeta potential are summarized in Table 2. After synthesis the average size of nanocapsules was between 175 and 240 nm. The zeta potential of the dialyzed nanocapsules was negative due to the presence of anionic surfactant used for the redispersion process (SDS-solution 0.1 wt%; Table 2).

The total amount of dexamethasone encapsulated inside the nanocapsules was determined using UV spectroscopy evaluated by measuring the DXM absorbance maximum at 240 nm. The results either for total amount of dexamethasone encapsulated inside the nanocapsules (core or shell) or found in the supernatant are shown in Table 3.

Biological analysis

Uptake of nanocapsules by NPCs and release of content

Confocal microscopy measurements were performed to ensure uptake of NCs rather than just adherence to the cell surface. Figure 3, *B* and *C* clearly document the uptake of NCs (red), which appear to be compartmentalized. In addition, the capability of NCs to release their content into the cell plasma was determined by the encapsulation of CellTracker™. As depicted in Figure 3, *D* cell plasma esterases alter the CellTracker™ conformation leading to the emission of fluorescence. Figure 3, *E* displays non-parenchymal cells completely filled with the fluorescent dye. In order to rule out that non-encapsulated free CellTracker™ outside of the nanocapsules of the NC suspension is responsible for the observed fluorescence signal we used the supernatants of sedimented nanocapsules after centrifugation as control. Free CellTracker™ was used as positive control. In addition, fluorescence inside the NCs ingested by NPCs was observed, which possibly can be attributed to the influx of cell plasma esterases into NCs. In addition, a quantitative analysis was performed in order to determine the uptake behavior of different nanocapsule concentrations. Figure 3, *G* shows a concentration dependent increase of NPCs ingesting nanocapsules from 0.25 to 25 µg/ml. Furthermore, incubation with DXM NCs resulted in a significant higher uptake at concentrations of 2.5 µg/ml and 25 µg/ml of about 1% and 9.7%, respectively, compared to HES-DXM NCs with an uptake of 0.4% and 5%, respectively.

Phenotypic characterization of cells that take up NCs

Flow cytometry was performed to determine the phenotype of NPCs preferentially ingesting the NCs. The non-parenchymal liver cell population can be distinguished between bone marrow derived cells (CD45 positive), e.g. Kupffer cells and lympho-
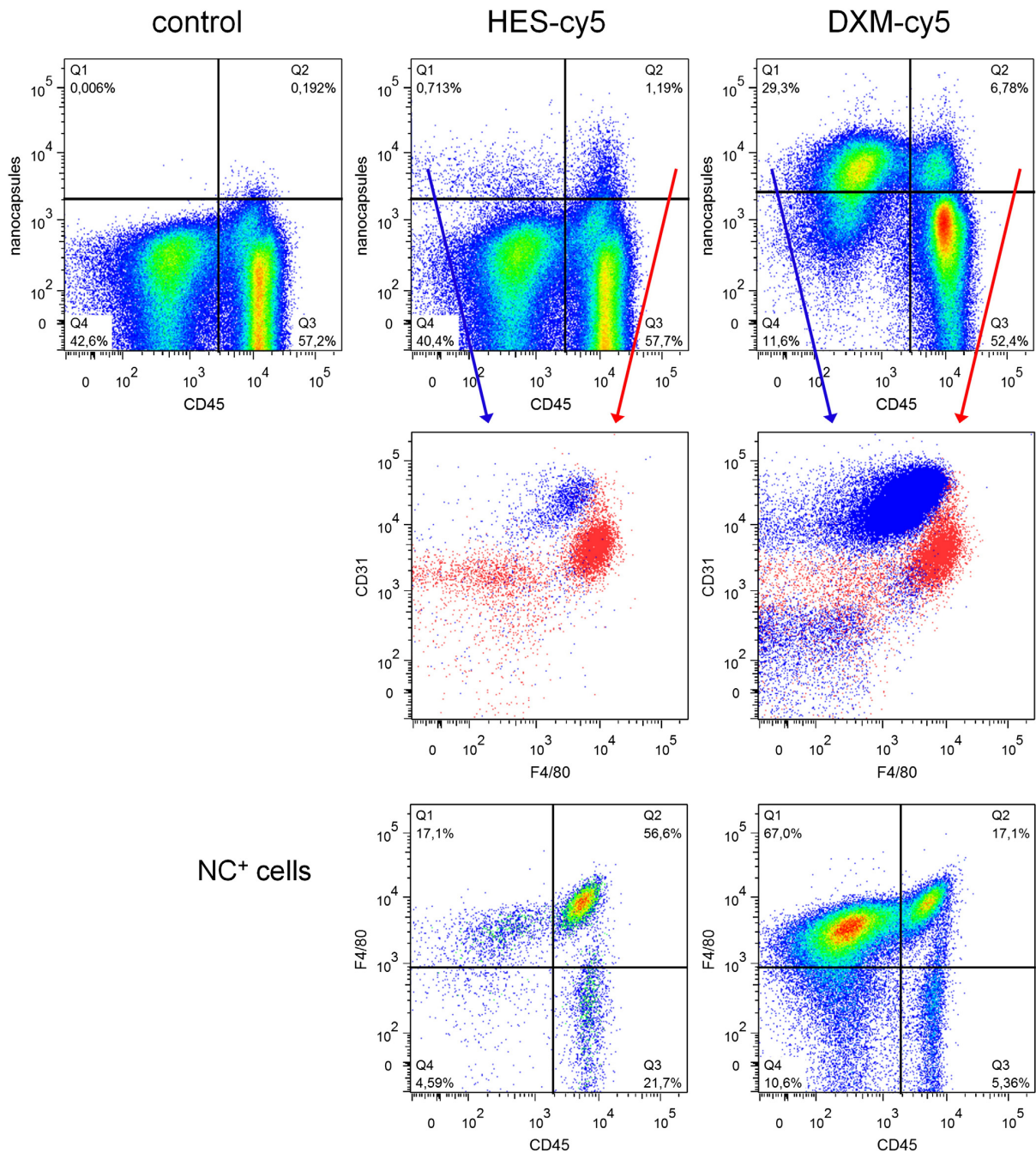
Figure 4. Phenotypic characterization of NPCs preferentially ingesting DXM-cy5 NCs or HES-cy5 NCs using flow cytometric analysis. NPCs were co-incubated with NCs (25 μg/ml) for 3 h and stained using fluorochrome labeled antibodies against surface proteins (CD45, CD31, F4/80). Data shown are representative for three individual experiments.

cytes, and CD45 negative cells (endothelial cells (LSECs), biliary cells).[23] Interestingly, the overall uptake of DXM NCs was significantly higher and exceeded 30% of the total NPC population in contrast to 2% in the case of HES NCs (Figure 4). Notably, DXM NCs were preferentially ingested by CD45 negative cells whereas 70% of HES NCs positive cells belonged to the CD45$^+$F4/80$^+$ population (KCs). Despite the preferential uptake of DXM NCs by CD45$^-$CD31$^+$ cells (LSECs) the absolute amount of KCs ingesting DXM NCs exceeded the number of KCs ingesting HES NCs.

Figure 5. Toxicity of HES, HES-DXM and DXM NCs was documented by PI-staining and subsequent flow cytometric analysis. NPCs were co-incubated with NCs at different concentrations (0.25, 2.5 or 25 µg/ml) for 3, 8 and 24 h. *Significance was given with $P < 0.001$ (One way ANOVA).

Viability of NPCs after co-cultivation with NCs
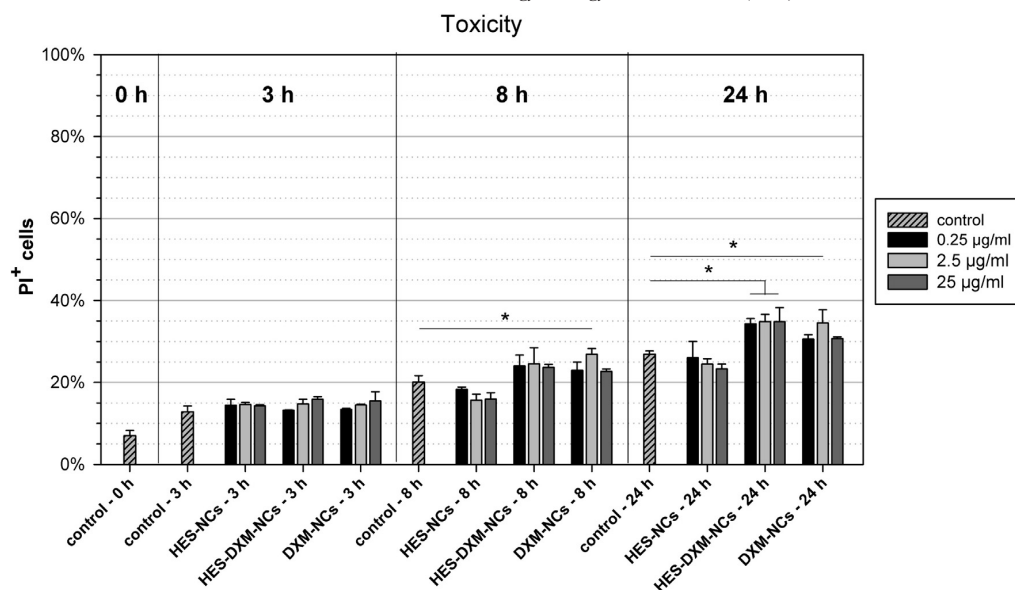
The toxicity of nanocapsules at different concentrations was analyzed using propidium iodide staining after incubation with NPCs for 3, 8 and 24 h. As shown in Figure 5, a time dependent increase in PI$^+$ (dead) cells up to 35% for HES-DXM NCs was detected throughout all concentrations. HES NCs served as a nanocapsule control and showed no increase in toxicity at all investigated concentrations when compared to cells without any NCs. After 3 h of incubation no significant difference between the HES control and the nanocapsules with DXM could be detected. However, after 8 h and 24 h of co-cultivation HES-DXM and DXM NCs showed a significantly reduced viability of about 5%-12%, in particular at a concentration of 2.5 and 25 µg/ml, when compared to HES NCs. Importantly, the cultured non-parenchymal liver cells cultured are primary cells displaying without any treatment 25% reduced viability after 24 h.

*Efficient suppression of cytokine production by NPCs*

In order to compare the ability of encapsulated DXM (HES-DXM), polymerized DXM (DXM NCs) and soluble DXM to suppress immune responses by NPCs, the latter were isolated and co-cultured for 24 h with NCs and soluble DXM as depicted in Figure 6, A and B. ELISA analysis of cell culture supernatants showed significantly lower levels of IL-6 and TNF-α when NPCs were co-cultured with HES-DXM or DXM NCs. Soluble DXM (10 µM) served as positive control and

induced an similar reduction of cytokine levels compared to HES-DXM or DXM NCs.

Additional stimulation with lipopolysaccharides (LPS) (2.5 µg/ml) resulted in elevated IL-6 and TNF-α secretion by NPCs. Accordingly, the suppressive capabilities of HES-DXM or DXM NCs were even more prominent with an 5-8 fold decrease in IL-6 and TNF-α levels. HES NCs without any DXM served as a nanocapsule control and had no influence on IL-6 and TNF-α secretion compared to cells without any NCs. Therefore, possible suppressive effects of HES NCs could be ruled out. Supplementary experiments over an incubation period of 8 h and with additional nanocapsule concentrations of 0.25 µg/ml and 25 µg/ml were performed to determine a possible time- or concentration-dependent manner of reduced cytokine secretion. However, these approaches showed similar results compared to 24 h incubation and a concentration of 25 µg/ml (data not shown).

Intracellular cytokine staining was performed in order to confirm that Kupffer cells (F4/80$^+$) are responsible for IL-6 and TNF-α production detected by ELISA measurements and that ingestion of DXM NCs and HES-DXM NCs (by NPCs) resulted in a decreased production of the inflammatory cytokine IL-6. HES-cy5 NCs without encapsulated DXM were used as control in order to evaluate the cytokine suppressive capability of DXM containing NCs. As displayed in Figure 6, C, DXM-cy5 and HES-DXM-cy5 NCs significantly decreased the percentage of IL-6$^+$ cells of the

Figure 6. Suppression of cytokine response after uptake of NCs (2.5 µg/ml) *in vitro* was determined by IL-6 **(A)** or TNF-α **(B)** cytokine release into the supernatant using enzyme-linked immunosorbent assays. Data represent the mean ± standard deviation of four wells for each condition. Another two experiments were performed with similar results. *Significance was given with $P < 0.001$ (One way ANOVA). Intracellular cytokine stainings **(C-D)** were performed in order to analyze whether Kupffer cells are responsible for IL-6 production. Consistent results were obtained in a second experiment. *Significance was given with $P < 0.001$ (One way ANOVA).
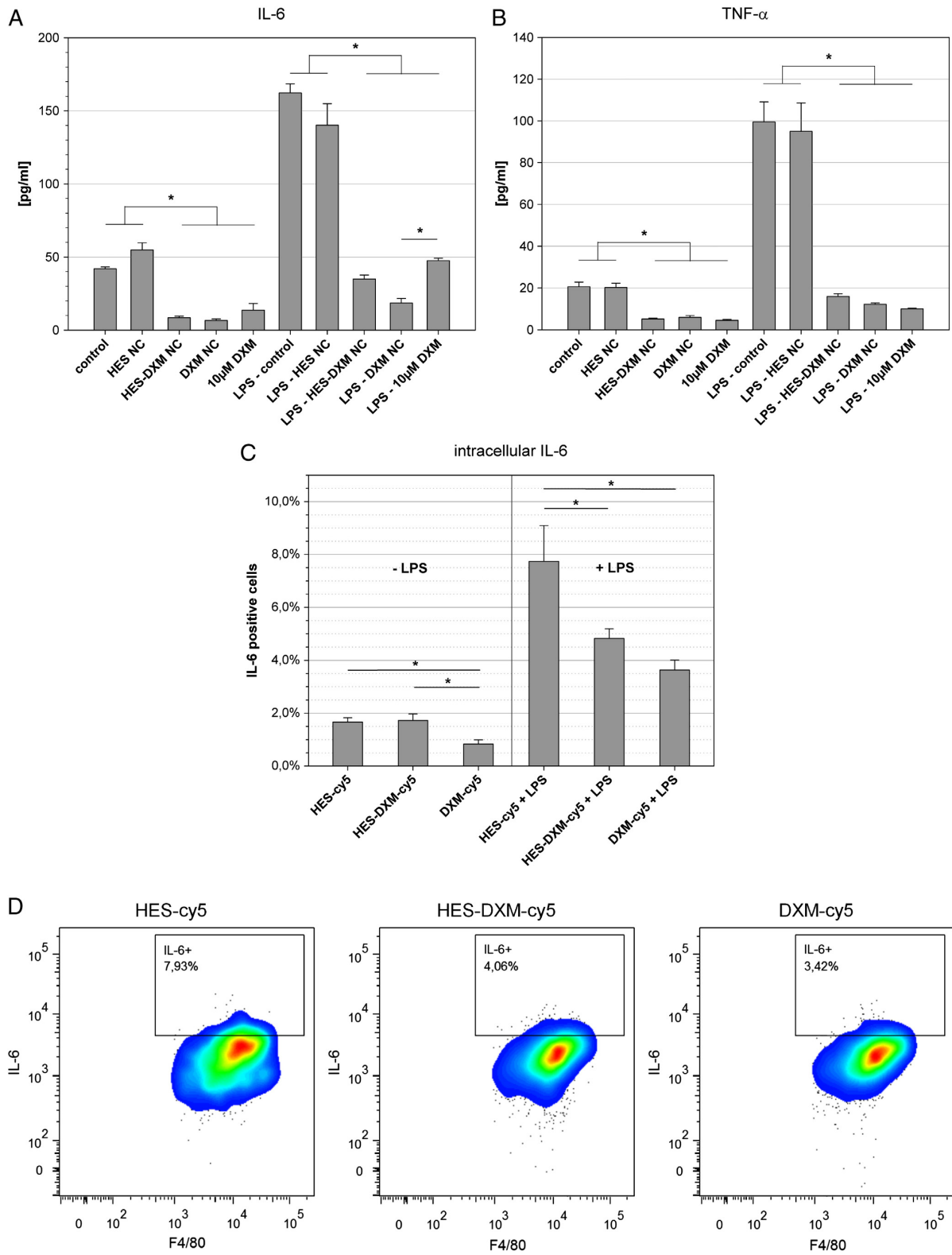
NC^+ population from 7.74% to 4.83% and 3.63%, respectively, after stimulation with lipopolysaccharide. In addition, even without LPS-stimulation DXM NCs had the potential to significantly reduce the IL-6 producing cell population from 1.67% to 0.84%. Figure 6, *D* shows that an uptake of DXM-cy5 and HES-DXM-cy5 resulted in a slight shift of the NC^+ population compared to an ingestion of HES-cy5 control capsules.

Discussion

Our present study was designed to evaluate the ability of a dexamethasone nanocapsule synthesized exclusively out of dexamethasone to suppress the inflammatory response of phagocytic liver cells. Dexamethasone encapsulated in a HES-shell served as a reference nanocapsule. The formation of a crosslinked polymeric shell resulted from the reaction between −OH groups originated either from HES or DXM and −NCO groups originated from TDI and occurred at the water-in-oil droplet interface. The size of nanocapsules after redispersion (175-240 nm) in water slightly increased, which could be due to the surface-attached hydration layer. The size polydispersity (standard deviation) was approximately the same for all described samples. The fairly broad size distribution could be due to the presence of the surfactant on the nanocapsule surface. The mobile chains of the surfactant molecules are free to move, and therefore they protrude differently far into the continuous phase, causing the diameter variability. Generally, the nanocapsule diameter was bigger without the presence of HES molecules. This fact can be due to the difference in the concentration of hydrophilic compounds. Without HES molecules, the effect of Ostwald ripening is less suppressed, and therefore the droplet collisions take place leading to larger droplets formation. The total amount of DXM encapsulated inside the nanocapsules was measured by UV (240 nm). The obtained results (see Table 3) indicate that the polymeric shell of the HES-DXM nanocapsules possesses high compactness and resistance. Only 7.4% dexamethasone was found in supernatant which corresponds to an encapsulation efficiency of 92.6%. The absorbance found in the supernatant of DXM-cy5 and DXM-CellTracker™ NCs was 1.7% and 2.0% lower compared to DXM NCs without any fluorescent dye. This could be due to the fact that fluorescent dye molecules are amphiphilic and therefore dye molecules bring additional stabilization to the droplets and later on to the nanocapsules. The absorbance measured in the supernatant could be referred to the trace dexamethasone molecules released from the nanocapsules which were broken during the redispersion step.

Biological evaluation of the synthesized NCs was performed using primary murine non-parenchymal liver cells (NPCs). Approximately 30% of the NPC population are Kupffer cells which reside within the sinusoidal vascular space. Here, they are perfectly situated to clear endotoxins from the blood, and to phagocytose microorganisms and debris.[27] Accordingly, non-specific phagocytosis of particles taken up in the liver is mediated primarily by Kupffer cells.[28] Activated Kupffer cells release pro-inflammatory cytokines, including IL-6. The latter phenomenon is associated with activation of Hepatic Stellate cells inducing collagen synthesis, which subsequently leads to fibrosis.[29] The liver is affected by a variety of diseases triggered and sustained by overwhelming inflammatory immune responses, e.g. primary biliary cirrhosis (PBC), primary sclerosing cholangitis (PSC), and autoimmune hepatitis (AIH). Each of these diseases accounts for approximately 5% of liver transplants per year performed in the United States and Europe.[30] Immunosuppressive treatment is a key element of therapeutic approaches targeting autoimmune liver diseases and is essential after liver transplant. Despite their potential side effects, corticosteroids remain to be a corner stone in immunosuppressive treatment of autoimmune diseases and after liver transplant even in pediatric patients.[31] Minimizing side effects of corticosteroid treatment through local delivery and/or cell directed targeting represents an important improvement of current treatment options, promising dose reduction and extension of corticosteroid-therapy to other entities such as biliary atresia.[32–34]

In a first step we analyzed the ability of non-parenchymal liver cells (NPCs) to phagocytize nanocapsules and release their content. Hydroxyethyl starch (HES) has been used in a variety of clinical settings, e. g. as volume expander.[35] Even though the benefit of HES is under discussion when given in large quantities,[36] HES is considered a safe and biodegradable compound. Degradation is catalyzed via amylase activity, which is present in a variety of tissues, cells and blood plasma, including the liver.[37] Notably, liver macrophages (e. g. Kupffer cells, infiltrating monocytes) take up cellular debris including amylase.[38] The latter phenomenon provides a rationale how HES nanocapsules release their content after phagocytosis by liver macrophages. In our experimental approach phagocytosis and release of capsule content were evidenced by confocal microscopy and staining of cell plasma through release of CellTracker™ encapsulated into NCs (Figure 3).

Interestingly, DXM NCs were taken up at a significantly higher level compared to HES NCs. There are two possible explanations for this observation: first, the synthetic glucocorticoid DXM is a hydrophobic bioactive compound[39]; second, the HES NCs are specifically designed to avoid unspecific uptake.[40]

In addition, DXM NCs were preferentially ingested by the $CD45^-CD31^+$ population, phenotypically assigned to the liver endothelial cells (LSECs). Primary roles of LSECs include scavenger function and blood clearance. LSECs are capable to endocytose low density lipoprotein and mannosylated proteins, and are involved in elimination of viruses, colloids, and macromolecular waste from the circulation.[41] Importantly, LSECs have immunological properties including antigen uptake, presentation and are associated with hepatic immunologic tolerance.[42] In contrast, Kupffer cells which are found in close proximity to the LSECs and reside in between the hepatic sinusoid, constantly exposed to the intra-hepatic blood circulation, are associated to both tolerance and induction of inflammatory responses.[43,44]

Both, DXM NCs and HES NCs were phagocytized by KCs, even though the absolute amount of DXM NC positive KCs exceeded the number of KCs ingesting HES NCs (Figure 4).

In order to assess the biological properties of the two DXM formulations, NPCs were stimulated with LPS and cytokine release was determined as outlined in Figure 6. Interestingly, the effect on the overall suppression of cytokine release (IL-6

and TNF-α) by LPS stimulated NPCs was similar between the two nanoparticle formulations, despite their different uptake behaviour. Noteworthy, cytokine release can be mainly attributed to Kupffer cells,[45,46] indicating, that only nanocapsules incorporated by the CD45$^+$F4/80$^+$ population contribute to the reduction of cytokine release. In accordance with this hypothesis our intracellular cytokine staining experiments evidenced a significant reduction of the IL-6 positive CD45$^+$F4/80$^+$ population (Figure 6).

The larger number of DXM NC positive Kupffer cells had no significant influence on cytokine release. An explanation for this phenomenon might be, that polymerization of Dexamethasone reduces the biological activity of this compound. However the suppression of cytokine release could be due to the presence of the DXM molecules on the nanocapsule surface. We assume, that on one hand there are mobile chains of the DXM molecule which are free to move, due to their partially hydrophilic character, and therefore protrude into the continuous phase, causing the suppression of the release of inflammatory cytokines. On the other hand the density of the DXM NC shell is lower compared to the shell density of the HES NCs due to fewer OH groups per molecule resulting in a lower degree of cross-linkage. This explains the better release of the encapsulated DXM molecules from the inner core.

In the present publication, polymeric nanocapsules were synthesized using the inverse (water-in-oil) miniemulsion process. The nanocapsules have core-shell morphology and an average size between 175 and 240 nm with a size distribution of about 30%. Both formulations of biodegradable dexamethasone nanocapsules were efficiently incorporated mainly by two cell types: Kupffer cells and LSECs. Incorporation of nanocapsules containing dexamethasone by Kupffer cells significantly suppressed the release of inflammatory cytokines. A variety of diseases affecting the liver are an interesting target for dexamethasone nanocapsules, prompting us to apply these formulations to *in vivo* models. Of particular interest are the dexamethasone nanocapsules, consisting exclusively out of a dexamethasone shell, bearing the potential to serve as a carrier for additional therapeutics.

Acknowledgments

References

1. Liu SQ, Tong YW, Yang YY. Incorporation and in vitro release of doxorubicin in thermally sensitive micelles made from poly(N-isopropylacrylamide-co-N, N-dimethylacrylamide)-b-poly(D, L-lactide-co-glycolide) with varying compositions. *Biomaterials* 2005;**26**(24):5064-74.
2. Nanjwade BK, Bechra HM, Derkar GK, Manvi FV, Nanjwade VK. Dendrimers: emerging polymers for drug-delivery systems. *Eur J Pharm Sci* 2009;**38**(3):185-96.
3. Yellepeddi VK, Kumar A, Palakurthi S. Biotinylated poly(amido)amine (PAMAM) dendrimers as carriers for drug delivery to ovarian cancer cells in vitro. *Anticancer Res* 2009;**29**(8):2933-43.
4. Musacchio T, Torchilin VP. Recent developments in lipid-based pharmaceutical nanocarriers. *Front Biosci* 2011;**16**:1388-412.
5. Zhang SF, Uludag H. Nanoparticulate systems for growth factor delivery. *Pharm Res* 2009;**26**(7):1561-80.
6. Landfester K. Miniemulsionspolymerisation und struktur von polymer-und hybridnanopartikeln. *Angewandte Chemie* 2009;**121**(25):4556-76.
7. Landfester K, Musyanovych A, Mailander V. From polymeric particles to multifunctional nanocapsules for biomedical applications using the miniemulsion process. *Journal of Polymer Science Part a-Polymer Chemistry* 2010;**48**(3):493-515.
8. Baier G, Musyanovych A, Mailaender V, Landfester K. Performing encapsulation of dsDNA and a polymerase chain reaction (PCR) inside nanocontainers using the inverse miniemulsion process. *Int J Artif Organs* 2012;**35**(1):77-83.
9. Meikle AW, Tyler FH. Potency and duration of action of glucocorticoids. Effects of hydrocortisone, prednisone and dexamethasone on human pituitary–adrenal function. *Am J Med* 1977;**63**(2):200-7.
10. Doyle LW, Ehrenkranz RA, Halliday HL. Dexamethasone treatment in the first week of life for preventing bronchopulmonary dysplasia in preterm infants: a systematic review. *Neonatology* 2010;**98**(3):217-24 [Epub 2010/04/15].
11. Gomez-Gaete C, Tsapis N, Besnard M, Bochot A, Fattal E. Encapsulation of dexamethasone into biodegradable polymeric nano-particles. *Int J Pharm* 2007;**331**(2):153-9 [Epub 2006/12/13].
12. Da Silva GR, Ayres E, Orefice RL, Moura SA, Cara DC, Cunha Ada Jr S. Controlled release of dexamethasone acetate from biodegradable and biocompatible polyurethane and polyurethane nanocomposite. *J Drug Target* 2009;**17**(5):374-83 [Epub 2009/06/27].
13. Fratoddi I, Venditti I, Cametti C, Palocci C, Chronopoulou L, Marino M, et al. Functional polymeric nanoparticles for dexamethasone loading and release. *Colloids Surf B Biointerfaces* 2012;**93**:59-66 [Epub 2012/01/10].
14. Krishnan V, Xu X, Barwe SP, Yang X, Czymmek K, Waldman SA, et al. Dexamethasone-loaded block copolymer nanoparticles induce leukemia cell death and enhance therapeutic efficacy: a novel application in pediatric nanomedicine. *Mol Pharm* 2012 [Epub 2012/12/01].
15. Melgert BN, Olinga P, Van Der Laan JM, Weert B, Cho J, Schuppan D, et al. Targeting dexamethasone to Kupffer cells: effects on liver inflammation and fibrosis in rats. *Hepatology* 2001;**34**(4 Pt 1):719-28 [Epub 2001/10/05].
16. Wang MT, Jin Y, Yang YX, Zhao CY, Yang HY, Xu XF, et al. In vivo biodistribution, anti-inflammatory, and hepatoprotective effects of liver targeting dexamethasone acetate loaded nanostructured lipid carrier system. *Int J Nanomedicine* 2010;**5**:487-97 [Epub 2010/10/20].
17. Marchant RE, Yuan S, Szakalasgratzl G. Interactions of plasma-proteins with a novel polysaccharide surfactant physisorbed to polyethylene. *J Biomater Sci Polym Ed* 1994;**6**(6):549-64.
18. Osterberg E, Bergstrom K, Holmberg K, Schuman TP, Riggs JA, Burns NL, et al. Protein-rejecting ability of surface-bound dextran in end-on and side-on configurations — comparison to PEG. *J Biomed Mater Res* 1995;**29**(6):741-7.
19. Kraft D, Sirtl C, Laubenthal H, Scheiner O, Parth E, Dieterich HJ, et al. No evidence for the existence of preformed antibodies against hydroxyethyl starch in man. *Eur Surg Res* 1992;**24**(3):138-42.
20. Treib J, Baron JF. Hydroxyethyl starches: effects on haemostasis. *Annales Francaises D Anesthesie Et De Reanimation* 1998;**17**(1):72-81.
21. Joshi MD, Muller RH. Lipid nanoparticles for parenteral delivery of actives. *Eur J Pharm Biopharm* 2009;**71**(2):161-72 [Epub 2008/10/01].
22. Ishibashi H, Nakamura M, Komori A, Migita K, Shimoda S. Liver architecture, cell function, and disease. *Semin Immunopathol* 2009;**31**(3):399-409 [Epub 2009/05/27].
23. Racanelli V, Rehermann B. The liver as an immunological organ. *Hepatology* 2006;**43**(2 Suppl 1):S54-62 [Epub 2006/02/01].
24. Schlaad H, Kukula H, Rudloff J, Below I. Synthesis of alpha, omega-heterobifunctional poly(ethylene glycol)s by metal-free anionic ring-opening polymerization. *Macromolecules* 2001;**34**(13):4302-4.
25. Crespy DMA, Landfester K. Synthesis of polymer particles and nanocapsules stabilized with PEO/PPO containing polymerizable surfactants in miniemulsion. *Colloid Polym Sci* 2006;**284**(7):8.

26. Gehring S, Dickson EM, San Martin ME, van Rooijen N, Papa EF, Harty MW, et al. Kupffer cells abrogate cholestatic liver injury in mice. *Gastroenterology* 2006;**130**(3):810-22 [Epub 2006/03/15].

27. Gregory SH, Wing EJ. Neutrophil–Kupffer cell interaction: a critical component of host defenses to systemic bacterial infections. *J Leukoc Biol* 2002;**72**(2):239-48 [Epub 2002/08/01].

28. Parker GA, Picut CA. Liver immunobiology. *Toxicol Pathol* 2005;**33**(1):52-62 [Epub 2005/04/05].

29. Tan HH, Fiel MI, Sun Q, Guo J, Gordon RE, Chen LC, et al. Kupffer cell activation by ambient air particulate matter exposure may exacerbate non-alcoholic fatty liver disease. *J Immunotoxicol* 2009;**6**(4):266-75 [Epub 2009/11/17].

30. Mendes F, Couto CA, Levy C. Recurrent and de novo autoimmune liver diseases. *Clin Liver Dis* 2011;**15**(4):859-78 [Epub 2011/10/29].

31. Mieli-Vergani G, Vergani D. Autoimmune liver diseases in children — what is different from adulthood? *Best Pract Res Clin Gastroenterol* 2011;**25**(6):783-95 [Epub 2011/11/29].

32. London NJ, Chiang A, Haller JA. The dexamethasone drug delivery system: indications and evidence. *Adv Ther* 2011;**28**(5):351-66 [Epub 2011/04/16].

33. Meyers RL, Book LS, O'Gorman MA, Jackson WD, Black RE, Johnson DG, et al. High-dose steroids, ursodeoxycholic acid, and chronic intravenous antibiotics improve bile flow after Kasai procedure in infants with biliary atresia. *J Pediatr Surg* 2003;**38**(3):406-11 [Epub 2003/03/13].

34. Hegeman MA, Cobelens PM, Kamps J, Hennus MP, Jansen NJ, Schultz MJ, et al. Liposome-encapsulated dexamethasone attenuates ventilator-induced lung inflammation. *Br J Pharmacol* 2011;**163**(5):1048-58 [Epub 2011/03/12].

35. Ogilvie MP, Pereira BM, McKenney MG, McMahon PJ, Manning RJ, Namias N, et al. First report on safety and efficacy of hetastarch solution for initial fluid resuscitation at a level 1 trauma center. J Am Coll Surg. 2010;210(5):870–80, 80–2. Epub 2010/04/28.

36. Lissauer ME, Chi A, Kramer ME, Scalea TM, Johnson SB. Association of 6% hetastarch resuscitation with adverse outcomes in critically ill trauma patients. *Am J Surg* 2011;**202**(1):53-8 [Epub 2011/05/24].

37. Arnold M, Rutter WJ. Liver amylase. III. Synthesis by the perfused liver and secretion into the perfusion medium. *J Biol Chem* 1963;**238**:2760-5 [Epub 1963/08/01].

38. Dubuisson L, Bioulac-Sage P, Boussarie L, Quinton A, Saric J, de Mascarel A, et al. Removal of cellular debris formed in the Disse space in patients with cholestasis. *Virchows Arch A Pathol Anat Histopathol* 1987;**410**(6):501-7 [Epub 1987/01/01].

39. van Kooten C, Stax AS, Woltman AM, Gelderman KA. Handbook of experimental pharmacology "dendritic cells": the use of dexamethasone in the induction of tolerogenic DCs. 2009;188:233–49.

40. Baier G, Baumann D, Siebert JM, Musyanovych A, Mailander V, Landfester K. Suppressing unspecific cell uptake for targeted delivery using hydroxyethyl starch nanocapsules. *Biomacromolecules* 2012 [Epub 2012/08/01].

41. Connolly MK, Bedrosian AS, Malhotra A, Henning JR, Ibrahim J, Vera V, et al. In hepatic fibrosis, liver sinusoidal endothelial cells acquire enhanced immunogenicity. *J Immunol* 2010;**185**(4):2200-8 [Epub 2010/07/20].

42. Knolle PA, Limmer A. Control of immune responses by savenger liver endothelial cells. *Swiss Med Wkly* 2003;**133**(37–38):501-6 [Epub 2003/12/04].

43. Klein I, Cornejo JC, Polakos NK, John B, Wuensch SA, Topham DJ, et al. Kupffer cell heterogeneity: functional properties of bone marrow derived and sessile hepatic macrophages. *Blood* 2007;**110**(12):4077-85 [Epub 2007/08/11].

44. Roberts RA, Ganey PE, Ju C, Kamendulis LM, Rusyn I, Klaunig JE. Role of the Kupffer cell in mediating hepatic toxicity and carcinogenesis. *Toxicol Sci* 2007;**96**(1):2-15 [Epub 2006/11/24].

45. Kolios G, Valatas V, Kouroumalis E. Role of Kupffer cells in the pathogenesis of liver disease. *World J Gastroenterol* 2006;**12**(46):7413-20 [Epub 2006/12/15].

46. Gehring S, Sabo E, San Martin ME, Dickson EM, Cheng CW, Gregory SH. Laser capture microdissection and genetic analysis of carbon-labeled Kupffer cells. *World J Gastroenterol* 2009;**15**(14):1708-18 [Epub 2009/04/11].

6.2   Publication 2

Enhanced *in vivo* targeting of murine nonparenchymal liver cells with monophosphoryl lipid A functionalized microcapsules

Published in: *Biomacromolecules*, 2014. **15**(7): p. 2378-88.

BioMACROMOLECULES

Article

pubs.acs.org/Biomac

Enhanced in Vivo Targeting of Murine Nonparenchymal Liver Cells with Monophosphoryl Lipid A Functionalized Microcapsules

Anette Pietrzak-Nguyen,[†] Michael Fichter,[†] Marvin Dedters,[†] Leah Pretsch,[†] Stephen H. Gregory,[§] Claudius Meyer,[†] Aysefa Doganci,[†] Mustafa Diken,[‖] Katharina Landfester,[‡] Grit Baier,[‡] and Stephan Gehring*,[†]

[†]Children's Hospital, University Medical Center, Johannes Gutenberg University, Mainz 55131, Germany

[‡]Max-Planck Institute for Polymer Research, Mainz 55128, Germany

[§]Department of Medicine, Rhode Island Hospital and the Warren Alpert Medical School at Brown University, Providence, Rhode Island 02903, United States

[‖]In Vivo Imaging Core Facility, TRON - Translational Oncology, University Medical Center, Johannes Gutenberg University, Mainz 55131, Germany

Summary:

Hydroxyethyl starch nanocarriers were prepared by the inverse miniemulsion technique resulting in polymeric HES microcapsules (MC) with core-shell morphology and an average diameter of about 230 nm. HES-MCs preferentially accumulated in the liver after intravenous injection. Further surface modification with antibodies αCD40 or αDEC205 and monophosphoryl lipid A (MPLA) led to enhanced uptake by non-parenchymal liver cells *in vivo* and the induction of pro-inflammatory cytokines IL-6, IL-12 and IFNγ. Targeting intrahepatic Kupffer cells and dendritic cells with simultaneous activation is a promising approach for vaccination strategies against pathogens affecting the liver.

Author contribution:

- Assistance in experimental design
- Conduction of preliminary tests using surface-modified HES nanocapsules *in vitro* and *in vivo*
- Contribution to analysis and interpretation of results
- Proofreading of the submitted manuscript

Enhanced in Vivo Targeting of Murine Nonparenchymal Liver Cells with Monophosphoryl Lipid A Functionalized Microcapsules

Anette Pietrzak-Nguyen,[†] Michael Fichter,[†] Marvin Dedters,[†] Leah Pretsch,[†] Stephen H. Gregory,[§] Claudius Meyer,[†] Aysefa Doganci,[†] Mustafa Diken,[‖] Katharina Landfester,[‡] Grit Baier,[‡] and Stephan Gehring*,[†]

[†]Children's Hospital, University Medical Center, Johannes Gutenberg University, Mainz 55131, Germany

[‡]Max-Planck Institute for Polymer Research, Mainz 55128, Germany

[§]Department of Medicine, Rhode Island Hospital and the Warren Alpert Medical School at Brown University, Providence, Rhode Island 02903, United States

[‖]In Vivo Imaging Core Facility, TRON - Translational Oncology, University Medical Center, Johannes Gutenberg University, Mainz 55131, Germany

S *Supporting Information*

ABSTRACT: A broad spectrum of infectious liver diseases emphasizes the need of microparticles for targeted delivery of immunomodulatory substances to the liver. Microcapsules (MCs) are particularly attractive for innovative drug and vaccine formulations, enabling the combination of antigen, drugs, and adjuvants. The present study aimed to develop microcapsules characterized by an enhanced liver deposition and accelerated uptake by nonparenchymal liver cells (NPCs). Initially, two formulations of biodegradable microcapsules were synthesized from either hydroxyethyl starch (HES) or mannose. Notably, HES-MCs accumulated primarily in the liver, while mannose particles displayed a lung preference. Functionalization of HES-MCs with anti-CD40, anti-DEC205, and/or monophosphoryl lipid A (MPLA) enhanced uptake of MCs by nonparenchymal liver cells in vitro. In contrast, only MPLA-coated HES-MCs promoted significantly the in vivo uptake by NPCs. Finally, HES-MCs equipped with MPLA, anti-CD40, and anti-DEC205 induced the secretion of TNF-α, IL-6 by Kupffer cells (KCs), and IFN-γ and IL-12p70 by liver dendritic cells (DCs). The enhanced uptake and activation of KCs by MPLA-HES-MCs is a promising approach to prevent or treat infection, since KCs are exploited as an entry gate in various infectious diseases, such as malaria. In parallel, loading and activating liver DCs, usually prone to tolerance, bears the potential to induce antigen specific, intrahepatic immune responses necessary to prevent and treat infections affecting the liver.
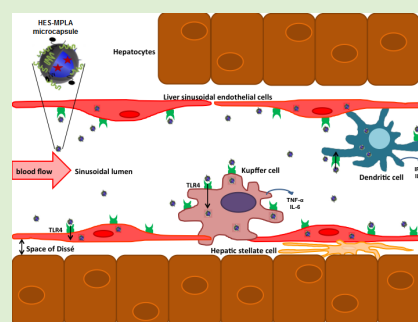
1. INTRODUCTION

Targeted delivery of bioactive compounds within the living organism and minimizing toxic side effects drives the growing interest in the development of colloidal microcarriers.[1,2] Synthesis of microcarriers made of natural biomolecules (e.g., starch, gelatin, chitosan) has been successfully performed using different preparation methods (e.g., nanoprecipitation, emulsion−diffusion, double emulsification) and polymerization techniques (polyaddition reaction, radical polymerization).[3] Due to their potential in diagnostics, imaging, and targeted therapy, colloidal microcarriers, especially liposomes,[4] polymeric particles and capsules,[5] micelles,[6] and dendrimers[7] have recently gained great attention. Of high interest are microcarriers that are able to transport bioactive compounds within the human body and release them without causing any toxic effects. Especially encapsulation in polymeric microcapsules has an advantage providing protection for sensitive biomolecules.[8] Furthermore, microcapsules can be functionalized for targeting to specific organs, tissues, and cells. This can be achieved by

different approaches including (a) size and shape of particles,[9] (b) surface engineering, and (c) receptor-based approaches.[10] Size- and shape-based targeting is triggered by the observation that phagocytic capabilities of cells differ between cell populations. A compelling example is the observation that large particles (200 nm to 1 μm) are preferentially cleared from the bloodstream by Kupffer cells (KC) in the liver, whereas small nanoparticles (20−200 nm) are ingested by liver endothelial cells.[11] Surface engineered microcarriers offer the opportunity to exploit shell compounds to target cell surface molecules involved in receptor-mediated uptake. Biomaterials used for enhanced uptake include mannose, targeting the mannose receptor (CD206),[12] human serum albumin, specific for folate receptor beta (FR-β) positive macrophages,[13] and folic acid, also enhancing uptake by FR-β positive macrophages.[14] Receptor-mediated targeting is achieved by immobi-

lization of antibodies onto the polymer surface. This approach is often exploited in dendritic cell (DC)-based immunizations. DCs are of particular interest for vaccines, due to their ability to induce vigorous antigen specific cellular immunity.[15,16] Commonly targeted DC receptors[10] include CD205 (DEC-205),[17] CD209 (DC-Sign),[18] and CD40.[19] Importantly, receptor-mediated targeting not only enhances uptake but is also capable to induce activation of cells, for example, in CD40-mediated phagocytosis.

Targeting antigens in conjunction with activation of professional antigen presenting cells are key requisites necessary for the induction of protective and therapeutic cellular immunity.[16] This is in particular challenging in the setting of infectious liver diseases, since the liver is prone to induce tolerance.[20] The latter contributes to the fact that the liver is the target and host of various pathogens such as hepatitis B/C, cytomegalovirus, and malaria for which effective preventive or therapeutic vaccines have been difficult to develop.[21]

The aim of the present study was to evaluate the uptake behavior of biodegradable microcapsules (MC) functionalized with two different antibodies, anti-CD40 and anti-DEC205, targeting receptors on macrophages and dendritic cells, by nonparenchymal liver cells (NPCs). In addition, microcapsules were equipped with monophosphoryl lipid A (MPLA), a synthetic toll-like-receptor 4 (TLR4) agonist, with the intention to mature the dendritic cell fraction within the NPC population.

During the course of this investigation, two main observations were made: first, microcapsules synthesized from hydroxyethyl starch (HES) ended up primarily in the liver, while mannose particles displayed a lung preference; second, MPLA coating not only induced maturation of liver dendritic cells, but in addition resulted in accelerated uptake in vitro and in vivo by Kupffer cells and liver DCs, representing a major fraction within liver NPCs. To our knowledge, the herein presented experimental approach for the first time documents the ability of MPLA, a broadly applied vaccine adjuvant, to serve not only as an immune modulator but also as a targeting compound.

2. MATERIALS AND METHODS

2.1. Microcapsule Synthesis. *2.1.1. Materials Used for Synthesis of Microcapsules.* Materials purchased included hydroxyethyl starch (HES, $M_w = 200\,000$ g·mol^{-1} (Fresenius Kabi), mannose, 2,4-toluene diisocyanate (TDI) and cyclohexane (>99.9%) (Sigma-Aldrich), sodium dodecyl sulfate (SDS) (Fluka), *N*-ethyl-*N′*-(3-(dimethylamino)propyl)-carbodiimide (EDC), and monochloroacetic acid (MCA) (Aldrich). The oil-soluble surfactant poly((ethylene-*co*-butylene)-*b*-(ethylene oxide)), P(E/B-*b*-EO), was synthesized under anionic polymerization conditions at the Max Planck Institute (MPI).[22] Cy5-labeled oligonucleotides (5′-Cy5-CCACTCCTTTCC-AGAAAACT-3′) were synthesized by Thermo Scientific (Germany). IRDye 800CW infrared dye was obtained from LI-COR. 4-Sulfotetrafluorophenyl (STP) was synthesized at the MPI.[23]

2.1.2. Preparation of Microcapsules. Microcapsules (MCs) were prepared by a polyaddition reaction applying the inverse miniemulsion procedure.[24−26] Briefly, 1400 mg of an aqueous HES (100 mg·mL^{-1}) solution or 100 mg of mannose solved in 1300 mg of PBS buffer were mixed with the Cy5-labeled oligonucleotides (100 pmol·μL^{-1}) (mixture I). Then 100 mg of the surfactant P(E/B-*b*-EO) was dissolved in 7.5 g of cyclohexane and added to mixture I and stirred over 1 h at 25 °C. After the homogenization step using a Branson Sonifier W-450-Digital apparatus and a 1/2″ tip under ice cooling, a clear solution consisting of 5 g of cyclohexane, 30 mg of P(E/B-*b*-EO),

and 100 mg of TDI was added dropwise over 5 min to the earlier prepared mixture I at 25 °C. The reaction was performed for 1 day at 25 °C under stirring. After synthesis, MCs were purified by repetitive centrifugation (Sigma 3k-30, RCF 1467, 20 min, two times) and redispersed in cyclohexane. Afterward, the MCs were transferred into the aqueous phase using the following procedure: 1 g of the MCs dispersion in cyclohexane (polymer solid content 3 wt %) was mixed with 5 g of SDS/Ampuwa aqueous solution (0.1 wt %) and kept under mechanical stirring conditions for 1 day at 25 °C. Thereafter, the samples were redispersed in a sonication bath. After redispersion, MCs were dialyzed (MWCO: 12 000 g·mol^{-1}) to remove residues of SDS.

2.1.2.1. Carboxymethylation of Microcapsules. The carboxymethylation of HES-MCs was performed using a modified procedure published previously.[27] Briefly, 1.0 g of HES-MCs aqueous dispersion (solid content 1.0 wt %) was mixed with 0.1 mL of NaOH solution (0.1 M) and stirred at 25 °C for 1 day to neutralize the nonreacted hydroxyl groups from the starch molecules on the MC surface. For the carboxymethylation, 10 μL of MCA (20.0 wt %) was mixed with the HES-MCs dispersion (after NaOH addition) and stirred for 1 day at 40 °C. After that, 0.05 mL of a NaOH solution (1.0 M) was added and stirred again for 1 day at 25 °C. Finally, the microcapsule dispersion was centrifuged (20 min, Sigma 3k-30, RCF 1467), the supernatant was removed, and the MCs were redispersed in Ampuwa. The amount of carboxylic groups was determined by polyelectrolyte titration as described below.

2.1.2.2. Coupling of Anti-DEC205, Anti-CD40, or IgG onto HES Microcapsules. A volume of 200 μL of the carboxymethylated HES-MC dispersion (solid content 1.0 wt %, 1.88×10^{14} COOH-groups as determined by particle charge determination (PCD)) was mixed with 20 mg (0.13 mmol) of EDC and 20 mg (0.07 mmol) of STP. After stirring for 30 min, the MCs were centrifuged at 4000 rpm for 30 min (Sigma 3k-30, RCF 1467) to remove residuals of EDC and STP. The supernatant was removed, and the pellet was resuspended in Ampuwa. Then 200 μL of DEC205, CD40, or IgG (8.02×10^{14} molecules) was added, and the mixture was stirred for 1 day at 4 °C. After the coupling procedure, the MCs were centrifuged at 4000 rpm for 20 min, the supernatant was removed, and the pellet was redispersed in Ampuwa to remove residues of nonreacted antibodies.

2.1.2.3. Adsorption of MPLA onto Microcapsule Surface. A volume of 250 μL of microcapsule dispersion (solid content 1.0 wt %) was mixed with 60 μL of MPLA/DMSO solution (0.1%) and stirred over 1 day at 4 °C. Afterward, MCs were centrifuged two times at 4000 rpm for 30 min (Sigma 3k-30, RCF 1467) to remove residues of MPLA. Finally, the supernatant was removed and the pellet was redispersed in 0.9% NaCl.

2.1.3. Microcapsule Characterization. Average size, size distribution, and colloidal stability of MCs were analyzed by means of dynamic light scattering (DLS) at 25 °C using a Nicomp 380 submicrometer particle sizer (Nicomp Particle Sizing Systems) at 20 °C. The zeta potential (ζ) of MCs was measured in 10^{-3} M potassium chloride solution with a Nicomp zeta sizer (Nicomp Particle Sizing Systems) at 20 °C.

The amount of surface charged groups was calculated from the results of the titration experiments performed on a particle charge detector (Mütek GmbH, Germany) in combination with a Titrino Automatic Titrator (Metrohm AG, Switzerland). The carboxylic groups were titrated against the positively charged polycationpoly-(diallyl dimethylammonium chloride) (poly-DADMAC). The amount of groups per gram of polymer was calculated from the consumed volume of the polyelectrolyte solution.[28] Morphological studies were performed using scanning electron microscopy (SEM).

For the determination of the antibody coupling efficiency, the absorption at 280 nm was measured.

The *chemical stability* of microcapsules was studied in Ampuwa, 0.9% NaCl, and DPBS buffer. The release of SR101 from MCs was studied by fluorescence spectroscopy in the supernatant: 500 μL of MCs was mixed with 500 μL of Ampuwa, 0.9% NaCl, or DPBS, incubated at 37 °C for 24 h, and then centrifuged (Sigma 3k-30, RCF 1467, 20 min). The supernatant was removed, and the fluorescent intensities were measured in the supernatant by using a fluorescence
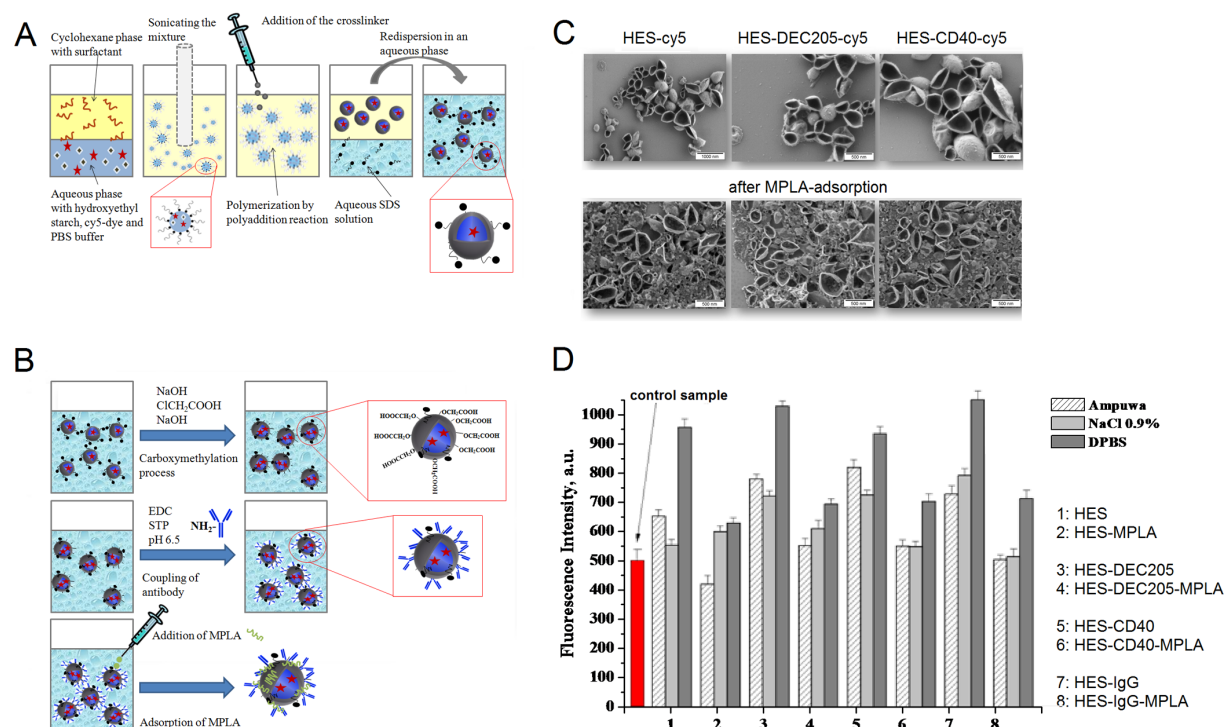
Figure 1. Synthesis of microcapsules (MCs). (A) Scheme of MCs preparation, (B) antibody coupling, and MPLA adsorption. (C) Morphological characterization of HES-cy5-MCs by SEM. (D) Amount of fluorescent dye SR101 released from the MCs after incubation for 24 h at 37 °C in different biological media.

spectrometer (microplate reader, Infinite M1000, Tecan, Switzerland). The fluorescent dye SR101 absorbs light at 580 nm and emits light at 605 nm. For the data normalization, a total amount of 1×10^{12} MCs/mL (solid content 10 mg·mL^{-1}) was used for each experiment. The fluorescence signal was normalized to microcapsules per milliliter at each point of measurement. For each sample, the release of fluorescent dye was calculated from three single measurements and the entire experiment was repeated two times.

The measurements of *colloidal stability* were performed with DLS by keeping the weight to weight capsule to protein ratio similar to the ratio in the performed in vivo experiments. For analysis, the method of Rausch et al. was applied.[29] Briefly, the autocorrelation function of the serum capsule mixture is fitted by a sum of the correlation functions of the respective solutions (serum/capsule). During the fitting process, all parameters of the components are kept fixed and the only fitting parameters are the intensity contributions of the serum and capsule in the serum capsule mixture.

2.2. Biological Analysis. *2.2.1. Mice.* Female C57BL/6J mice of 5−6 weeks of age were obtained from the Zentrale Versuchstiereinrichtung Mainz, Germany and kept under a 12 h dark, 12 h light cycle (with food and water supply at every time) in the animal facility of the University Hospital, Mainz. The animals were treated in accordance with NIH publications entitled "Principles for Use of Animals" and "Guide for the Care and Use of Laboratory Animals". All protocols were approved by the local Animal Care and Use Committee ("Landesuntersuchungsamt Rheinland-Pfalz").

2.2.2. Antibodies. The murine DEC205-antibody was generated in vivo through intraperitoneal injection of the hybridoma cell line NLDC-145/ATCC HB-290 (ATCC) in pristine conditioned nude mice and subsequently purified from the generated ascites. Murine anti-CD40 was purified from the supernate of the hybridoma cell line. Polyclonal murine IgG was purchased from Sigma.

2.2.3. Expansion of the Liver Dendritic Cell Population by Hydrodynamic Gene Delivery of a Human Fms-like Tyrosine Kinase 3 Ligand (hFlT3L) Expressing Plasmid. The cytokine human Fms-like

tyrosine kinase 3 ligand (hFlt3L) mobilizes DCs from bone marrow and can be used to enrich DCs in the liver, enhancing the feasibility of liver DC studies.[30] Liver DCs were expanded in vivo through hydrodynamic gene delivery of the plasmid pUMVC3-hFLex expressing the secreted portion of hFlt3L.[31] Briefly, 10 μg of pUMVC3-hFLex was dissolved in 2 mL of 0.9% NaCl solution and injected into the tail vein of female C57BL/6J mice within 5 s. The injection was repeated on day 6, the liver was dissected on day 12, and the NPC population isolated as described in 2.2.5.

2.2.4. In Vivo Imaging of Microcapsules. In vivo fluorescence imaging of infrared (IR) labeled HES and mannose MCs was performed with the IVIS Spectrum Imaging system (Caliper Life Sciences). The fluorescence source and filters were set for IR-emitting, with excitation at 745 nm and emission at 800 nm, enabling the visualization of IR-MCs in different organs of C57BL/6J mice. Respectively, 1 mg·mL^{-1} MCs in 300 μL of 0.9% NaCl solution was injected through the tail vein into untreated and hFlt3L-treated 8-week old mice. C57BL/6J mice injected with 300 μL of 0.9% NaCl solution without MCs served as negative control. To rule out that free (nonencapsulated) IR-dye, for example, due to microcapsule instability, is responsible for the observed organ specific fluorescence signals, different doses (0.015/0.15/1.5/15.0 μg) of free IR dye were injected as control. Importantly, 0.15 μg of IR-dye correlates with the amount of dye administered via IR-MCs outlined above. At 4 h after injection, mice were anesthetized with isoflurane, sacrificed by cervical dislocation, and dissected to isolate organs. Liver, spleen, lungs, brain, and kidneys were transferred immediately after dissection into the image chamber, and acquisition of the image was performed with an integration time of 3 s.

2.2.5. Isolation of Liver Nonparenchymal Cells (NPCs). The nonparenchymal liver cell (NPC) population was isolated and purified after perfusion of the liver of female C57BL/6J mice with collagenase using methods previously described.[32] In brief, mice were anesthetized with Ketamine/Rompun, the portal vein was cannulated, and the liver perfused with 20 mL of perfusion medium consisting of HBSS (Ca^{2+}-

and Mg^{2+}-free, PAN Biotech), 100 U/mL collagenase (Sigma-Aldrich), 0.001% DNase (AppliChem), and 5% heat inactivated fetal calf serum (FCS). This common practice eliminates cells circulating through the liver and not bound firmly to the tissue. The perfused liver was dissected, teased apart, and incubated for 15 min at 37 °C. Incubated liver sections were passed through a 70 μm nylon cell strainer. The collected cell suspension was centrifuged at 300g for 15 min, and the resulting pellet, containing the parenchymal cells (hepatocytes), was discarded. The NPCs remaining in suspension were purified through centrifugation in a 30% Histodenz-HBSS gradient as previously outlined in detail.[33] The recovered NPC population was >95% viable, was free of hepatocyte contamination, and was subsequently cultured in medium composed of RPMI 1640, 10% FCS, 1% penicillin/streptomycin, 1 mM L-glutamine, 1% essential and nonessential amino acids, and 50 μM 2-mercaptoethanol.

2.2.6. In Vitro and in Vivo Loading of NPCs with Microcapsules and Flow Cytometric Analysis. In vitro loading and phenotypic characterization was initiated through coculturing of a NPC cell suspension (10^{6}cells·mL^{-1}) for 4 h with 10 μg·mL^{-1} of Cy5-labled microcapsules (Cy5-MCs) formulations as depicted below. The in vivo uptake of Cy5-MCs within the NPC population was characterized following intravenous (IV) injection (tail vein of C57BL/6J mice) of 300 μL of 0.9% NaCl solution containing Cy5-MCs in a concentration of 1 mg·mL^{-1}. Quantification of MC uptake and phenotype determination were performed by flow cytometry using methods previously described.[34] Antibodies used for NPC phenotyping included CD45 (clone 30-F11), CD205 (clone NLDC-145), CD40 (clone 1C10), CD11c (clone N418), CD11b (clone M1/70), F4/80 (clone BM8), and CD31 (clone 390). Samples were acquired on a multichannel cytometer BD LSR II (BD Bioscience) equipped with FACS Diva software (BD Bioscience), followed by analyses with FlowJo 7.6.5.

2.2.7. Analysis of Microcapsule Toxicity. Cell toxicity after MC uptake was determined using the fluorescent dye propidium iodide (PI, BD Pharmingen). NPCs (10^6 cells·mL^{-1}) were incubated for 4 h with 10 μg·mL^{-1} MCs and stained for 5 min with 10 μL of PI in the dark according to the manufacturer's instructions. The percentage of apoptotic cells was measured by flow cytometry.

2.2.8. Cytokine Analysis. Cytokine secretion by NPCs was determined with commercial ELISA kits according to the protocols provided by the supplier (eBioscience). NPCs were loaded in vitro and in vivo as described above (2.2.6) and subsequently cultured for 24–48 h in a 96-well, flat-bottom plate at 37 °C. Supernatants were harvested and analyzed for the expression of TNF-α, IL-6, IL-12p70, and IFN-γ.

2.2.9. Statistical Analysis. Experiments were performed in triplicate and analyzed using SigmaPlot 11.0.Ink Software. For the comparison of many groups with each other, a one-way ANOVA test was performed. To determine which groups differed significantly, a Holm-Sidak test ($P < 0.001$) or a Student–Newman–Keuls test ($P < 0.05$) was applied.

3. RESULTS

3.1. Synthesis and Characterization of Nonfunctionalized, Antibody Functionalized, and MPLA-Coated HES Microcapsules. HES- or mannose-MCs were synthesized by interfacial polyaddition. Thereby reaction occurs at the water-in-oil droplet interface resulting in the formation of a cross-linked polymeric shell (Figure 1A). Cy5-labeled oligonucleotide was used for fluorescence labeling of the MCs. The ratio of NCO (from the used cross-linker TDI) to OH groups (in the HES or mannose molecules) was chosen to be lower than 1. After redispersion of the MCs in the aqueous phase, the residual hydroxyl groups could be converted into carboxylic groups by the carboxy-methylation procedure.[27] The reaction between the antibodies and carboxyl groups on the microcapsule surface was achieved using EDC-mediated coupling (Figure 1B). EDC is often combined with *N*-hydroxysuccini-

mide (NHS) or sulfo-NHS (S-NHS) to increase coupling efficiency or create a stable amine-reactive product. The resulting amide link is chemically stable, allowing the long-term use of linked compounds. Unfortunately, NHS and S-NHS are prone to fast hydrolyses and are only reactive for a short time period (<30 min). For that reason, 4-sulfotetrafluorophenyl (STP) coupling was accomplished by mixing the amine groups containing antibodies and the carboxylic groups containing MCs with liquid EDC and adding STP in powder form at a defined concentration. Scanning electron microscopy (SEM) studies of HES-MCs (Figure 1C) confirm the formation of a core−shell structure and the morphology was not changed upon the coupling procedure.

The characteristics of HES-MCs in water phase and after functionalization with covalently coupled anti-DEC205, anti-CD40, and IgG or with adsorbed MPLA in terms of average size, size distribution, and electrokinetic potential (zeta potential) are summarized in Table 1.

Table 1. Characterization of the Microcapsules

	average diameter, nm/standard deviation,%			
samples	in water phase	after antibody coupling	after MPLA adsorption	ζ (pH 7), mV
HES	230/28			−24
HES-MPLA	230/28		235/32	−32
HES-DEC205	230/28	230/30		−16
HES- DEC205-MPLA	230/28	230/30	240/32	−30
HES-CD40	230/28	225/29		−15
HES-CD40-MPLA	230/28	225/29	225/31	−30
HES-IgG	230/28	235/30		−18
HES-IgG-MPLA	230/28	235/30	235/32	−28
HES-IR	265/26			−24
mannose-IR	275/28			−22

The average size of MCs was between 220 and 275 nm. The size distribution (standard deviation) of MCs after antibody coupling and MPLA adsorption slightly increased, which can be attributed to the surface-attached hydration layer. The zeta potential of the redispersed and dialyzed HES- or mannose-MCs was negative (−24 or −22 mV, respectively) due to the presence of anionic surfactant used for the redispersion process (SDS solution 0.1 wt %). After coupling of the antibodies to the HES-MCs, the zeta potential increased between −15 and −18 mV. MPLA adsorption decreased the zeta potential of MCs to values between −28 and −32 mV because of the two phosphate groups linked to the glucosamine lipid A.

The release of SR101 from the microcapsules, which is related to the stability of the capsules' shell, was studied by fluorescence spectroscopy. The measured fluorescence intensities of the supernatant that were obtained after precipitation of the MCs treated with Ampuwa, 0.9% NaCl, or DPBS were compared with the nontreated one (control sample, MCs redispersed in an aqueous SDS solution); see Figure 1D. The fluorescence signal measured in the supernatant for the Ampuwa and 0.9% NaCl treated samples is at comparable levels with respect to the control sample. For HES and HES antibody coupled microcapsules (HES, HES-DEC205, HES-CD40, and HES-IgG) treated with DPBS an increase in fluorescent signal was observed. The latter observation can be attributed to the fact that phosphate buffered saline solution
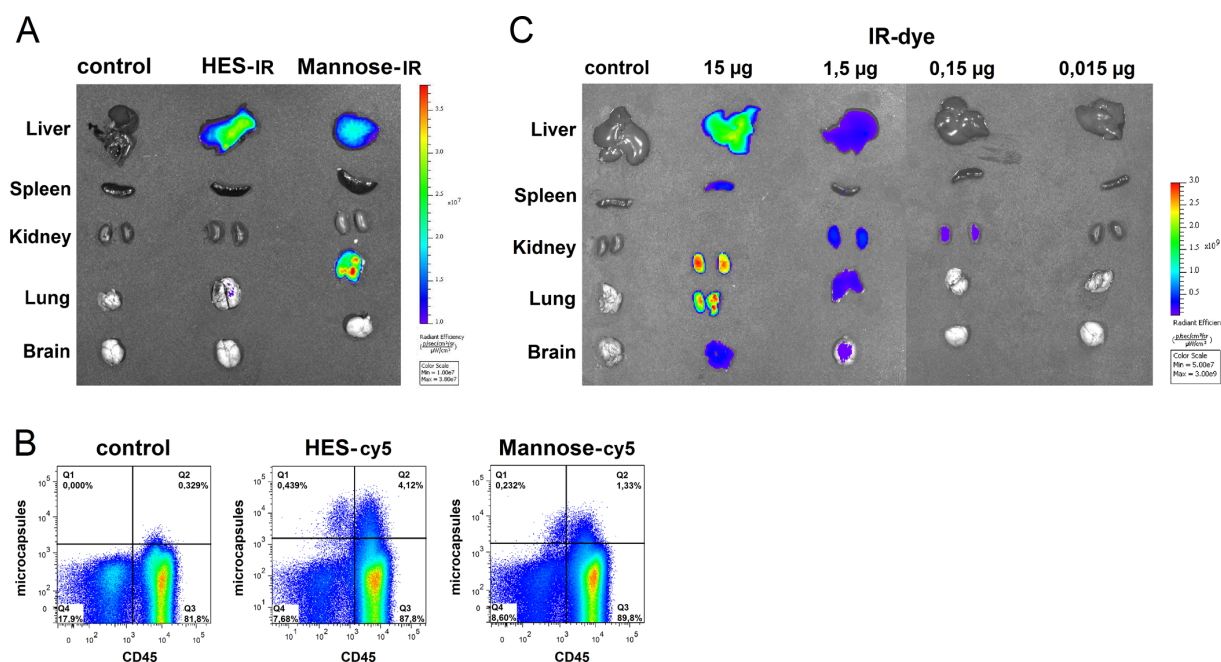
Figure 2. (A) IVIS spectrum images of organs of a C57BL/6J mouse 4 h after IV injection of 1 mg·mL^{-1} HES- and mannose-MCs with an encapsulated infrared dye (IR). (B) FACS analysis of hepatic NPCs after IV administration of HES-cy5- and mannose-cy5-MCs stained with anti-CD45. (C) IVIS spectrum images of organs of a C57BL/6J mouse 4 h after IV injection of nonencapsulated IR-dye. Data shown are representative for three individual experiments.

(12 mM phosphate, present as HPO_4^{2-} and $H_2PO_4^{-}$) interacts with the hydrophilic groups of the proteins.

The colloidal stability of MCs was determined in mouse blood serum at the concentration tested in vivo. As shown in Supporting Information Figure 1, the data points of the microcapsules serum mixture are well described by the parameters of the pure components meaning no aggregation of the capsules in the presence of mouse serum took place.

3.2. HES Microcapsules Are Preferentially Deposited in the Liver after Intravenous Injection. Two formulations of biodegradable MCs were evaluated for organ specific distribution. At 4 h after IV injection, mannose MCs displayed a preferential deposition in the lung (Figure 2A). In contrast, HES-MCs were primarily found in the liver. This observation was paralleled by a 3-fold higher uptake of HES-MCs in CD45$^+$ nonparenchymal liver cells compared to mannose-MCs (Figure 2B). In a first step, HES-MCs were additionally equipped with anti-DEC-205 and anti-CD40. Additional coating of either antibody led to an even enhanced uptake in the liver, but due to the already quite prominent deposition of HES-MCs alone the difference was not significant (data not shown). In addition, we investigated the behavior of HES-MCs in hFlt3L-pretreated animals. Again, the IV administration of HES-MCs displayed a primary deposition in the liver. Release behavior of IR-dye from the capsules was evaluated by injection of different doses of nonencapsulated (free) IR-dye (Figure 2C). Administration of 1.5 and 15.0 μg of free IR-dye distributed equally in all investigated organs, while 0.15 μg accumulated only inside the kidney. Notably, 0.15 μg of free IR-dye correspond with the amount of dye administered via IR containing microcapsules. No signal was detected at 0.015 μg.

3.3. Nonparenchymal Liver Cells Widely Express Both CD205 and CD40 Commonly Used for Dendritic Cell

Targeting Approaches. To assess the potential of HES-MCs functionalized with anti-CD40 or anti-CD205 to target liver cells, involved in the induction of intrahepatic immune responses, we evaluated the expression of both receptors in the immunological relevant nonparenchymal liver cell (NPC) population.

CD45 staining allowed the detection of bone marrow derived cells, which applies for the entire liver leukocyte population within the NPCs (e.g., Kupffer cells (KCs), DCs, and natural killer T cells). CD45 negative cells are cells of structural relevance to the liver, such as biliary cells and liver sinusoidal endothelial cells (LSECs). CD205 positive cells were found in both CD45 positive and negative cells. Interestingly, Kupffer cells (F4/80$^+$ cells) expressed CD205 to an even higher degree than DCs (Figure 3A). Even more surprising was the observation that LSECs (CD45$^-$CD31$^+$ cells) displayed the strongest CD205 expression. This pattern was paralleled by the expression of CD40.

Treatment of animals with hFlt3L induced a significant shift toward the CD45 positive population, combined with the reduction of CD31 expression and a dimmed expression of F4/80 (Figure 3B). The number of DCs (CD11c$^+$ cells) was up regulated at least 7-fold, comprising over 50% of the total NPC population. In addition, hFlt3L treatment induced DCs to highly express both, CD205 and CD40. KCs retained their level of CD40 and CD205 expression.

3.4. Toxicity of Microcapsules. The incubation of NPCs with 10 μg·mL^{-1}HES-MCs for 4 h did not increase toxicity compared to cells without any MCs (Figure 4). Functionalization of HES-MCs with anti-CD205 and the additional adsorption of MPLA resulted in a reduced viability of 5−10% compared to cells without MCs. However, HES-CD40 MCs with or without MPLA did not affect cell viability in a
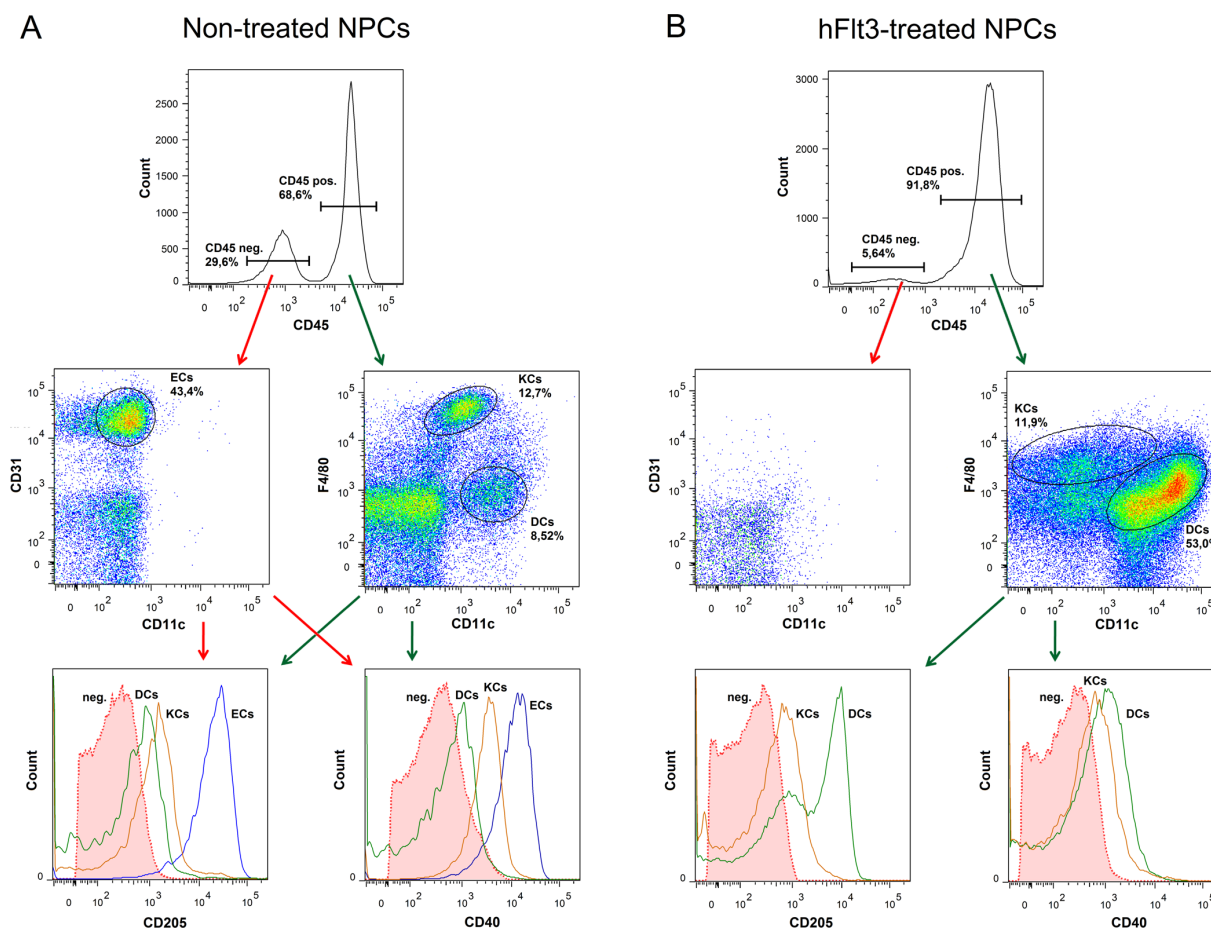
Figure 3. Phenotypic characterization of nontreated (A) and hFlt3L-pretreated (B) hepatic NPC population. Hepatic endothelial cells (ECs; CD31^{+}), Kupffer cells (KCs; F4/80^{+}), and dendritic cells (DCs; CD11c^{+}) were delineated through staining with antibodies against CD45, CD205, CD40, CD11c, F4/80, and CD31. Data shown are representative for three individual experiments.

significant way compared to cells cultured with HES-MCs or without MCs. In addition, viability of NPCs was evaluated for time periods up to 24 h and microcapsule concentrations of maximum 75 μg·mL^{-1}. The results paralleled our previously published observations, with concentrations above 25 μg·mL^{-1} associated with increased toxicity, whereas coincubation of MCs with NPCs for 24 h did not significantly affect viability.[33]

3.5. Microcapsule Uptake. HES-MCs were functionalized with murine anti-CD205, anti-CD40, and MPLA. Coating of either anti-CD205 or anti-CD40 alone induced an increased in vitro uptake of HES-MCs in NPCs derived from untreated and hFlt3L-treated animals (Figure 5A). Notably, MPLA coating alone induced also an increased phagocytosis by NPCs from hFlt3L mice. Surprisingly, the most prominent increase in uptake was observed when HES-MCs were coated with a combination of anti-CD40 or anti-CD205 with MPLA. Unrelated to the type of coating, Kupffer cells (KCs) were in untreated NPCs the most prominent cell population ingesting HES-MCs. The main effect of additional coating with MPLA and/or anti-CD40/anti-CD205 was the increase of MC positive DCs (Figure 5B). In parallel, KCs derived from NPCs after hFlt3L-treatment were the predominant MC positive population. Again, additional coating increased the MC positive DC population (Figure 5B).

Particularly striking was the observation that after IV administration of coated HES-MCs only the MPLA surface modified HES-MCs displayed a significant increase with respect to uptake by NPCs, when compared to all other combinations (Figure 5A). Anti-CD40 coating even displayed a decreased uptake behavior. Combining MPLA with antibody-mediated targeting was not beneficial in the in vivo setting. Only in hFlt3L-treated animals, combined coating induced a slight increase in phagocytosis, which was again exceeded significantly by coating with MPLA alone. With respect to the cell phenotype of MC positive cells in vivo, KCs were the predominant ingesting cell type in untreated animals, with MPLA coating not significantly altering the composition of MC positive cells (Figure 5B). In the case of hFlt3L-treated animals, coating with MPLA increased the uptake by DCs.

Additionally, we investigated the uptake of MCs by hepatocytes, representing the main liver cell population. The uptake of MCs by this cells was minute with only 0.7% of hepatocytes ingesting HES and 2.15% hepatocytes incorporating HES-MPLA-MCs (data not shown).

3.6. Microcapsule Induced Cytokine Profile. The effect of MC functionalization on the cytokine profile released by the cells phagocytizing MCs in vitro and in vivo was determined by ELISA. Consistent with the predominant MC-ingesting cell
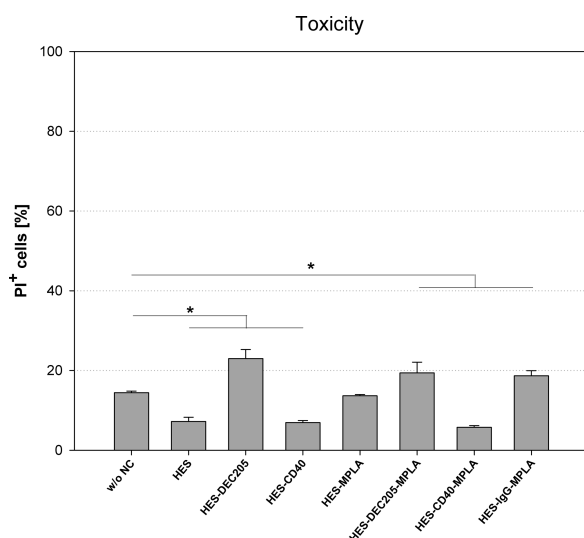
Figure 4. Toxicity of MCs as determined by PI and subsequent flow cytometric analysis. NPCs were cultured with 10 μg·mL^{-1} HES, HES-IgG, HES-αDEC205, and HES-αCD40 microcapsules with and without MPLA for 4 h. Data shown are representative for three individual experiments. *Significance was given with $P < 0.001$ (one-way ANOVA).

type in nontreated NPCs, being Kupffer cells, functionalization induced IL-6 and TNF-α responses both in vitro and in vivo. Clearly, MPLA coating was superior to all other investigated combinations (Figure 6A). In general, additional coating with

either anti-CD40, anti-CD205 or an unspecific IgG reduced the release of cytokines. The same observation was made in vivo differing only with respect to the observation the coating of MCs with anti-CD40 alone induced a cytokine response, again, not reaching the level of MPLA coating. NPCs derived from hFlt3L-treated animals displayed a significant release of IFN-γ and IL-12 when ingesting MPLA coated HES-MCs in vitro. To trace the cell source of the IFN-γ secretion, we purified the DC population from the NPCs using CD11c coated magnetic beads. The results are displayed in Figure 6B supporting that DCs are the primary source of IFN-γ and IL-12 secretion. In vivo, both MPLA and MPLA and anti-CD205 induced a significant IFN-γ secretion by DCs.

4. DISCUSSION

The high prevalence of chronic infectious liver diseases emphasizes the need of designing novel biocompatible and biodegradable microcarrier formulations for targeted delivery of immunemodulatory or antimicrobial substances to the liver. Pathogens that exploit the liver as an entry gate or host include hepatitis B and C, malaria, listeria, and certain herpes virus infections (Epstein−Barr virus, cytomegalovirus).[20,35] The aim of the present study was the development of a microcapsule formulation characterized by an enhanced deposition in the liver, accelerated uptake by nonparenchymal liver cells (Kupffer cells, dendritic cells, and liver sinusoidal endothelial cells (LSECs)), and the capability to activate the targeted cell populations. Microcapsules (MCs) are particularly attractive for innovative vaccine and drug delivery formulations because they allow the combination of antigen, drugs, adjuvants, and the equipment with receptors targeting key cells of the immune
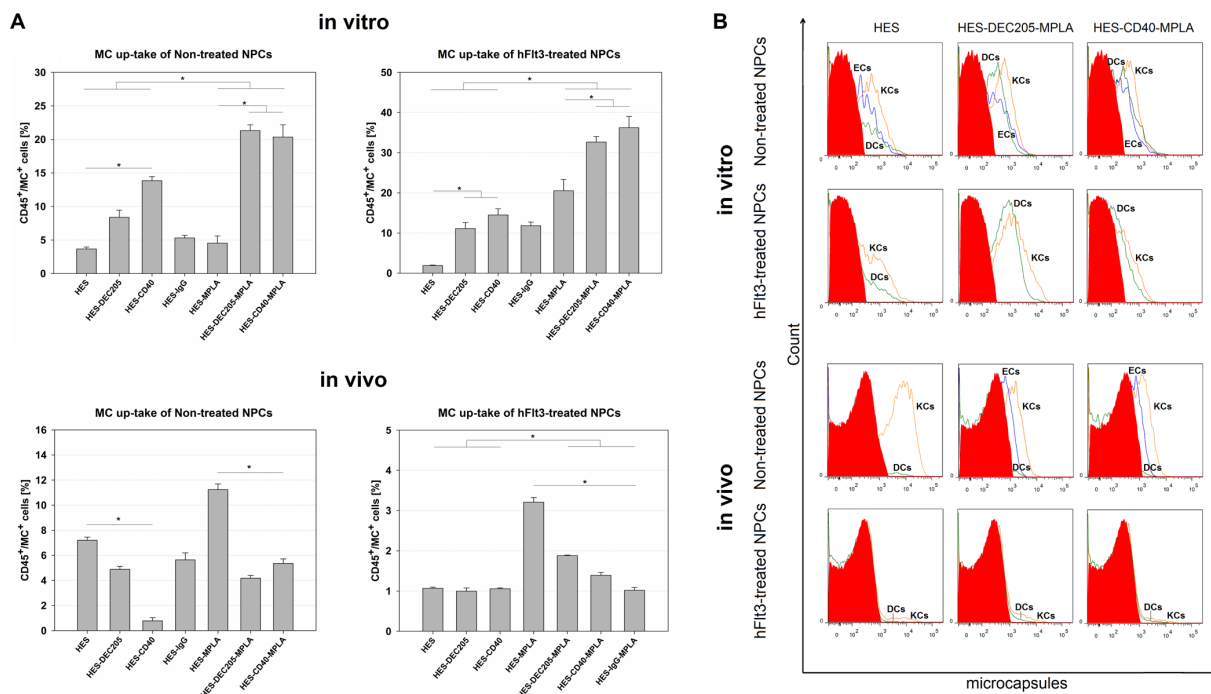

Figure 5. Phenotypic characterization and quantification of MCs-containing cells by flow cytometry. (A) Quantification of in vitro and in vivo MC-uptake by CD45$^+$ NPCs. (B) Distribution of MCs within the different subpopulations of NPCs. Data shown are representative for three individual experiments. *Significance was given with $P < 0.001$ (one-way ANOVA).
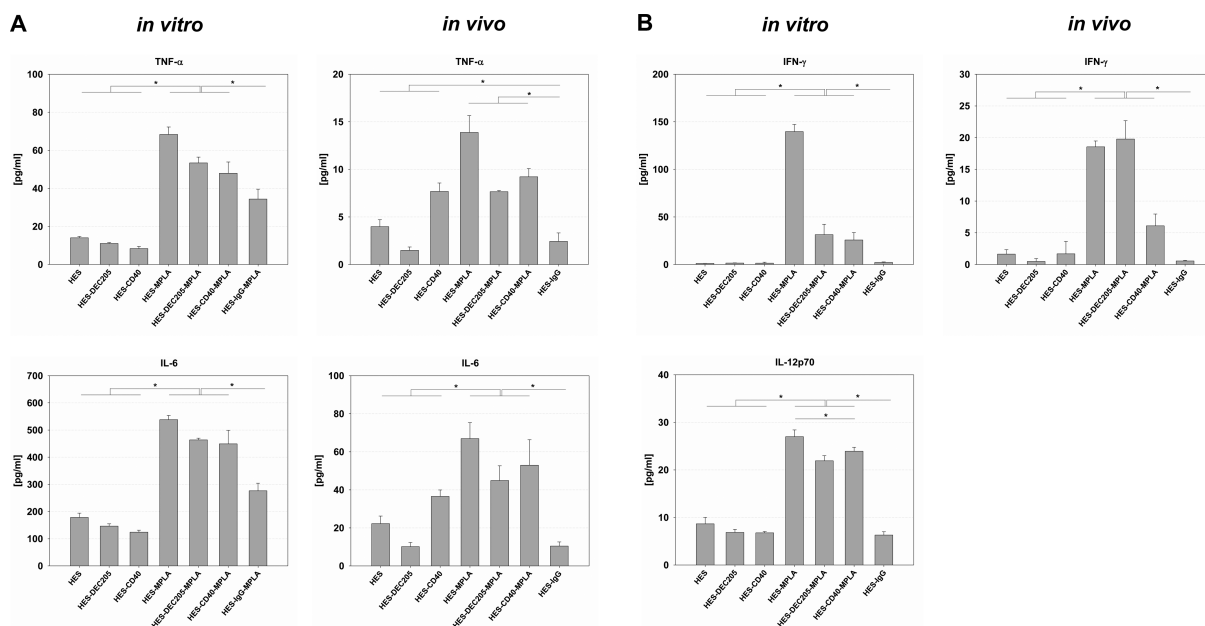
Figure 6. Cytokine release of nontreated NPCs (A) and hFlt3L-pretreated CD11c$^+$ NPCs (B) pulsed with MCs. For in vitro analyses of TNF-α, IL-6, INF-γ, and IL-12 secretion by ELISA, 10 μg·mL^{-1} MCs were cocultured with NPCs for up to 48 h. For in vivo response, cells were isolated 4 h after MC-injection and cultured 24 h at 37 °C. Consistent results were obtained in two additional experiments. *Significance was given with $P < 0.05$ (one-way ANOVA).

system, for example, dendritic cells.[10,21] The latter is crucial for the induction of antigen specific cellular immune responses, necessary to prevent and control chronic viral infections.

Previous work by Landfester et al. documented the ability of microcapsules to encapsulate water-soluble active materials such as dyes and drugs within the inner core, thus serving as an ideal microreactor or microcarriers.[8,36] The inverse miniemulsion method provides an excellent approach for the encapsulation of hydrophilic substances in the aqueous core of MCs, since the activity of proteins and other bioactive compounds is retained as recently documented by our group.[33]

HES- or mannose-MCs with a size between 220 and 275 nm were obtained with the miniemulsion process, providing critically stabilized homogeneous small droplets dispersed in a continuous phase by applying high shear forces. The salt, buffer, or extremely hydrophilic materials (dye molecules), present in aqueous miniemulsion droplets, play a critical role as osmotic controlling agents in inverse miniemulsions, allowing to counteract the Laplace pressure. The colloidal stability of the synthesized MCs was confirmed by Fluorescence spectroscopy in different biological media (Figure 1D). The obtained results for capsules treated in Ampuwa and 0.9% NaCl indicates the high stability of all polymeric microcapsules under the investigated conditions. The enlarged fluorescent signal for MCs treated in DPBS might be due to the fact that phosphate buffered saline solution (12 mM phosphate, present as HPO$_4$$^{2-}$ and H$_2$PO$_4$$^-$) interacts with the hydrophilic groups of the proteins.

To monitor the fate of MCs in vitro and in vivo, fluorescent (Cy5) or infrared dyes (IR) were encapsulated with a high encapsulation yield of over 90%. The achievement of high encapsulation efficiencies can be attributed to the application of a heterophase system[37] and the highly hydrophilic character of the dye molecules. The stability of the microcapsules was

confirmed with the administration of nonencapsulated IR-dye. Accumulation of free IR-dye within the kidneys indicates the renal clearance of this water-soluble substance.

In addition, these results demonstrate the targeting effect of our capsules. Two formulations of biodegradable MCs were synthesized from the polysaccharides hydroxyethyl starch (HES) and mannose. We observed a striking difference in organ deposition with HES preferentially detected in the liver and mannose in the lung. Interestingly, alveolar macrophages (AMϕ), a principal antigen presenting cell population found in the lung, are equipped with C-type lectin receptors (CLRs), which recognize conserved carbohydrate structures, including mannose and galactose.[38] These carbohydrates are found on the surface of many respiratory pathogens, such as *Yersinia pestis*, *Streptococcus* pneumonia, influenza viruses, and *Mycobacterium tuberculosis*.[39] Accordingly, MCs functionalized with mannose have been found to induce an enhanced uptake by AMϕ, for example, with mannosylated liposomes.[40] HES has been widely used as colloidal plasma substitute.[41] In humans, transient tissue deposition of HES after administration as colloidal substitute has been observed in the liver and spleen, and for an extended time period in the muscle and skin.[42] In general, HES is considered to be a low toxicity compound. Compared with dextran, serious anaphylactic reactions are clearly less prevalent.[43]

Prompted by the observation that HES-MCs are primarily deposited in the liver of C57BL/6 mice in parallel with our interest in liver infectious diseases, we further investigated the uptake behavior of HES-MCs and functionalized HES-MCs by the immunological relevant liver NPCs, given that we do not see relevant MCs ingestion within the hepatocytes. Enhanced uptake was observed when HES-MCs were equipped with anti-CD40, anti-DEC205, or MPLA consistent with the expression of these receptors by NPCs (Figures 3 and 5). The most

prominent in vitro effect appeared when MPLA was combined with either anti-CD40 or anti-DEC205. Targeting of dendritic cells with anti-CD40 and anti-CD-205 has been extensively studied.[10,17,38] In contrast, the observation that the vaccine adjuvant MPLA enhances phagocytosis by antigen presenting cells (APCs) has, to our knowledge, not been reported. The enhanced uptake of MPLA-HES-MCs can be in part explained by the fact that MPLA interacts with the toll-like-receptor (TLR) 4 on APCs. TLRs are pathogen recognition receptors expressed on cells of the innate and adaptive immune system including macrophages, and DCs.[39] TLR4 is characterized by the ability to interact with lipopolysaccharides (LPS), found on the outer membrane of Gram negative bacteria.[40] However, the toxicity of LPS precludes its use as a vaccine adjuvant in humans, thus triggering the development of chemical derivatives, such as MPLA, with fewer side effects while maintaining immunogenicity.[44,45] Notably, TLR4 is widely expressed in liver cells, for exampke, Kupffer cells,[46] hepatic stellate cells, LSECs, hepatic dendritic cells, and hepatocytes.[47] This expression pattern correlates with the anatomical location of the liver and function as a primary filter organ for microbial debris absorbed through the gut mucosa and entering the liver via the portal vein.[48] A recent study supports the relevance of TLRs in phagocytosis, observing an enhanced phagocytosis and killing of *Streptococcus pneumoniae* by resident brain macrophages (microglia) after TLR stimulation.[49] The observed in vitro effect of MPLA coating was even more prominent in vivo with MPLA-HES-MCs displaying superior uptake by NPCs in untreated and hFlt3L-treated mice compared to all other formulations (Figure 5). The discrepancy between the in vitro results and the in vivo observations can be explained, first, by the preferential localization of Kupffer cells within the liver architecture and the specific equipment of KCs with TLRs and, second, by the involvement of TLR4 in neutrophil sequestration, which requires rolling and adhesion of leukocytes on endothelial surfaces.[50] Accordingly, we hypothesize that TLR4 activation by MPLA not only enhances cellular uptake and cell activation but also promotes adhesion of MCs in the liver sinusoid as displayed in the graphical abstract.

Finally, functionalization of HES-MCs with MPLA induced a significant cytokine response by ingesting cells with an enhanced secretion of TNF-α and IL-6 by KCs and IFN-γ and IL-12 by DCs.

5. CONCLUSION

HES-MCs display a preferential deposition in the liver after IV administration contrasted by a preferential lung uptake of mannose-MCs. Additional equipment of HES with antibodies targeting the CD40 and CD205 receptor enhances uptake in vitro, which is further promoted when HES-MCs are coated with a combination of anti-CD40 or anti-CD205 and MPLA. Importantly, after IV administration in C57BL/6 mice, only MPLA coating enhances phagocytosis of HES-MCs by KCs and DCs. We assume that TLR4 activation by MPLA not only enhances uptake but also promotes adhesion in the liver sinusoid, explaining the difference between our in vitro and in vivo observations. In addition, coating with MPLA promotes a pro-inflammatory response by the uptaking cell population. In conclusion, the enhanced uptake and activation of KCs by MPLA-HES-MCs is a promising approach to prevent or treat infection, since KCs are exploited as entry gate in various infectious diseases, such as malaria. In parallel, loading and activating liver DCs, usually prone to tolerance, bears the potential to induce antigen specific, intrahepatic immune responses necessary to prevent and treat infections affecting the liver.

■ ASSOCIATED CONTENT

Ⓢ Supporting Information

DLS analysis of microcapsules in mouse serum. This material is available free of charge via the Internet at http://pubs.acs.org.

■ AUTHOR INFORMATION

Corresponding Author

*Tel.: +49 6131 17 3560. E-mail: stephan.gehring@uni-mainz.de.

Notes

The authors declare no competing financial interest.

■ ACKNOWLEDGMENTS

■ REFERENCES

(1) Duncan, R. The dawning era of polymer therapeutics. *Nat. Rev. Drug Discovery* 2003, 2 (5), 347−360.

(2) Haag, R.; Kratz, F. Polymer therapeutics: Concepts and applications. *Angew. Chem., Int. Ed.* 2006, 45 (8), 1198−1215.

(3) Mora-Huertas, C. E.; Fessi, H.; Elaissari, A. Polymer-based nanocapsules for drug delivery. *Int. J. Pharm.* 2010, 385 (1−2), 113−142.

(4) Eldar-Boock, A.; Polyak, D.; Scomparin, A.; Satchi-Fainaro, R. Nano-sized polymers and liposomes designed to deliver combination therapy for cancer. *Curr. Opin. Biotechnol.* 2013, 24 (4), 682−689.

(5) Dawar, S.; Singh, N.; Kanwar, R. K.; Kennedy, R. L.; Veedu, R. N.; Zhou, S. F.; Krishnakumar, S.; Hazra, S.; Sasidharan, S.; Duan, W.; Kanwar, J. R. Multifunctional and multitargeted nanoparticles for drug delivery to overcome barriers of drug resistance in human cancers. *Drug Discovery Today* 2013, 18 (23−24), 1292−1300.

(6) Deng, C.; Jiang, Y.; Cheng, R.; Meng, F.; Zhong, Z. Biodegradable polymeric micelles for targeted and controlled anticancer drug delivery: Promises, progress and prospects. *Nano Today* 2012, 7 (5), 467−480.

(7) Liu, J.; Gray, W. D.; Davis, M. E.; Luo, Y. Peptide- and saccharide-conjugated dendrimers for targeted drug delivery: a concise review. *Interface Focus* 2012, 2 (3), 307−324.

(8) Baier, G.; Musyanovych, A.; Landfester, K.; Best, A.; Lorenz, S.; Mailander, V. DNA amplification via polymerase chain reaction inside miniemulsion droplets with subsequent poly(*n*-butylcyanoacrylate) shell formation and delivery of polymeric capsules into mammalian cells. *Macromol. Biosci.* 2011, 11 (8), 1099−1109.

(9) Manolova, V.; Flace, A.; Bauer, M.; Schwarz, K.; Saudan, P.; Bachmann, M. F. Nanoparticles target distinct dendritic cell populations according to their size. *Eur. J. Immunol.* 2008, 38 (5), 1404−1413.

(10) Tacken, P. J.; de Vries, I. J.; Torensma, R.; Figdor, C. G. Dendritic-cell immunotherapy: from ex vivo loading to in vivo targeting. *Nat. Rev. Immunol.* 2007, 7 (10), 790−802.

(11) Ishibashi, H.; Nakamura, M.; Komori, A.; Migita, K.; Shimoda, S. Liver architecture, cell function, and disease. *Semin. Immunopathol.* 2009, 31 (3), 399−409.

(12) Ezekowitz, R. A.; Williams, D. J.; Koziel, H.; Armstrong, M. Y.; Warner, A.; Richards, F. F.; Rose, R. M. Uptake of *Pneumocystis carinii* mediated by the macrophage mannose receptor. *Nature* 1991, 351 (6322), 155−158.
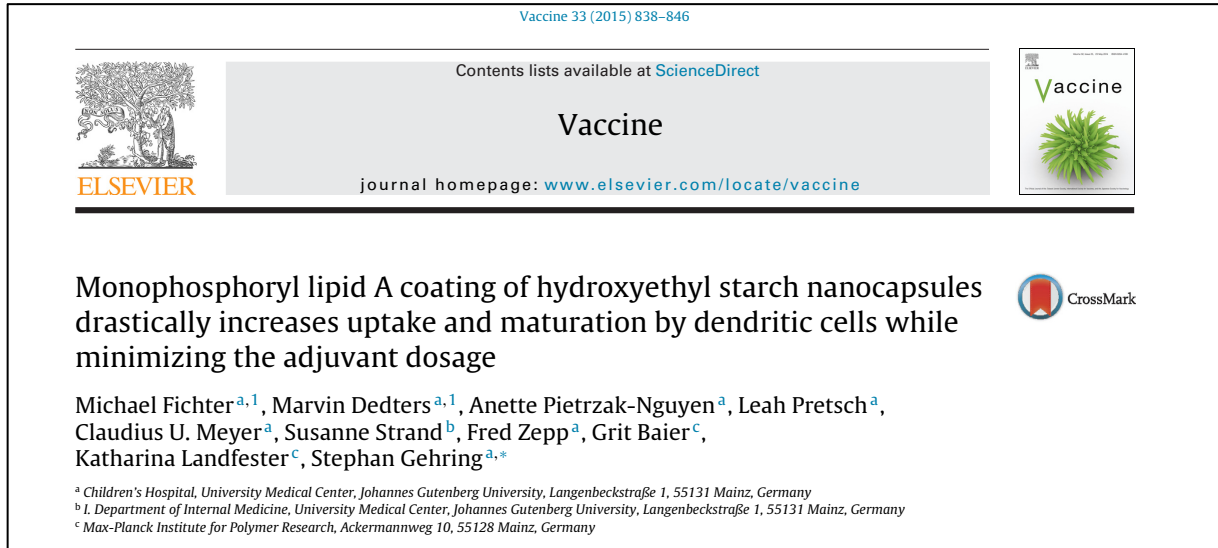
(13) Rollett, A.; Reiter, T.; Nogueira, P.; Cardinale, M.; Loureiro, A.; Gomes, A.; Cavaco-Paulo, A.; Moreira, A.; Carmo, A. M.; Guebitz, G. M. Folic acid-functionalized human serum albumin nanocapsules for targeted drug delivery to chronically activated macrophages. *Int. J. Pharm.* **2012**, *427* (2), 460−466.

(14) van der Heijden, J. W.; Oerlemans, R.; Dijkmans, B. A.; Qi, H.; van der Laken, C. J.; Lems, W. F.; Jackman, A. L.; Kraan, M. C.; Tak, P. P.; Ratnam, M.; Jansen, G. Folate receptor beta as a potential delivery route for novel folate antagonists to macrophages in the synovial tissue of rheumatoid arthritis patients. *Arthritis Rheum.* **2009**, *60* (1), 12−21.

(15) Nabel, G. J. Designing tomorrow's vaccines. *N. Engl. J. Med.* **2013**, *368* (6), 551−560.

(16) Steinman, R. M. Decisions about dendritic cells: past, present, and future. *Annu. Rev. Immunol.* **2012**, *30*, 1−22.

(17) Bonifaz, L. C.; Bonnyay, D. P.; Charalambous, A.; Darguste, D. I.; Fujii, S.; Soares, H.; Brimnes, M. K.; Moltedo, B.; Moran, T. M.; Steinman, R. M. In vivo targeting of antigens to maturing dendritic cells via the DEC-205 receptor improves T cell vaccination. *J. Exp. Med.* **2004**, *199* (6), 815−824.

(18) Tacken, P. J.; de Vries, I. J.; Gijzen, K.; Joosten, B.; Wu, D.; Rother, R. P.; Faas, S. J.; Punt, C. J.; Torensma, R.; Adema, G. J.; Figdor, C. G. Effective induction of naive and recall T-cell responses by targeting antigen to human dendritic cells via a humanized anti-DC-SIGN antibody. *Blood* **2005**, *106* (4), 1278−1285.

(19) Schjetne, K. W.; Fredriksen, A. B.; Bogen, B. Delivery of antigen to CD40 induces protective immune responses against tumors. *J. Immunol.* **2007**, *178* (7), 4169−4176.

(20) Crispe, I. N. The liver as a lymphoid organ. *Annu. Rev. Immunol.* **2009**, *27*, 147−163.

(21) Leleux, J.; Roy, K. Micro and nanoparticle-based delivery systems for vaccine immunotherapy: an immunological and materials perspective. *Adv. Healthcare Mater.* **2013**, *2* (1), 72−94.

(22) Schlaad, H.; Kukula, H.; Rudloff, J.; Below, I. Synthesis of α,ω-Heterobifunctional Poly(ethylene glycol)s by Metal-Free Anionic Ring-Opening Polymerization. *Macromolecules* **2001**, *34* (13), 4302−4304.

(23) Gee, K. R.; Archer, E. A.; Kang, H. C. 4-Sulfotetrafluorophenyl (STP) esters: New watersoluble amine-reactive reagents for labeling biomolecules. *Tetrahedron Lett.* **1999**, *40* (8), 1471−1474.

(24) Crespy, D.; Musyanovych, A.; Landfester, K. Synthesis of polymer particles and nanocapsules stabilized with PEO/PPO containing polymerizable surfactants in miniemulsion. *Colloid Polym. Sci.* **2006**, *284* (7), 780−787.

(25) Baier, G.; Musyanovych, A.; Dass, M.; Theisinger, S.; Landfester, K. Cross-Linked Starch Capsules Containing dsDNA Prepared in Inverse Miniemulsion as "Nanoreactors" for Polymerase Chain Reaction. *Biomacromolecules* **2010**, *11* (4), 960−968.

(26) Baier, G.; Baumann, D.; Siebert, J. M.; Musyanovych, A.; Mailaender, V.; Landfester, K. Suppressing Unspecific Cell Uptake for Targeted Delivery Using Hydroxyethyl Starch Nanocapsules. *Biomacromolecules* **2012**, *13* (9), 2704−2715.

(27) Paiphansiri, U.; Dausend, J.; Musyanovych, A.; Mailander, V.; Landfester, K. Fluorescent polyurethane nanocapsules prepared via inverse miniemulsion: surface functionalization for use as biocarriers. *Macromol. Biosci.* **2009**, *9* (6), 575−584.

(28) Ziegler, A.; Landfester, K.; Musyanovych, A. Synthesis of phosphonate-functionalized polystyrene and poly(methyl methacrylate) particles and their kinetic behavior in miniemulsion polymerization. *Colloid Polym. Sci.* **2009**, *287* (11), 1261−1271.

(29) Rausch, K.; Reuter, A.; Fischer, K.; Schmidt, M. Evaluation of nanoparticle aggregation in human blood serum. *Biomacromolecules* **2010**, *11* (11), 2836−2839.

(30) Steptoe, R. J.; Fu, F.; Li, W.; Drakes, M. L.; Lu, L.; Demetris, A. J.; Qian, S.; McKenna, H. J.; Thomson, A. W. Augmentation of dendritic cells in murine organ donors by Flt3 ligand alters the balance between transplant tolerance and immunity. *J. Immunol.* **1997**, *159* (11), 5483−5491.

(31) He, Y.; Pimenov, A. A.; Nayak, J. V.; Plowey, J.; Falo, L. D.; Huang, L. Intravenous injection of naked DNA encoding secreted flt3 ligand dramatically increases the number of dendritic cells and natural killer cells in vivo. *Hum. Gene Ther.* **2004**, *11* (4), 547−554.

(32) Gehring, S.; Dickson, E. M.; San Martin, M. E.; van Rooijen, N.; Papa, E. F.; Harty, M. W.; Tracy, T. F., Jr.; Gregory, S. H. Kupffer cells abrogate cholestatic liver injury in mice. *Gastroenterology* **2006**, *130* (3), 810−822.

(33) Fichter, M.; Baier, G.; Dedters, M.; Pretsch, L.; Pietrzak-Nguyen, A.; Landfester, K.; Gehring, S. Nanocapsules generated out of a polymeric dexamethasone shell suppress the inflammatory response of liver macrophages. *Nanomedicine* **2013**, *9* (8), 1223−1234.

(34) Kuzushita, N.; Gregory, S. H.; Monti, N. A.; Carlson, R.; Gehring, S.; Wands, J. R. Vaccination with protein-transduced dendritic cells elicits a sustained response to hepatitis C viral antigens. *Gastroenterology* **2006**, *130* (2), 453−464.

(35) Talwani, R.; Gilliam, B. L.; Howell, C. Infectious diseases and the liver. *Clin. Liver Dis.* **2011**, *15* (1), 111−130.

(36) Landfester, K. Miniemulsionspolymerisation und Struktur von Polymer- und Hybridnanopartikeln. *Angew. Chem.* **2009**, *121* (25), 4556−4576.

(37) Baier, G.; Musyanovych, A.; Mailänder, V.; Landfester, K. Performing encapsulation of dsDNA and a polymerase chain reaction (PCR) inside nanocontainers using the inverse miniemulsion process. *Int. J. Artif. Organs* **2012**, *35* (1), 77−83.

(38) Chavez-Santoscoy, A. V.; Roychoudhury, R.; Pohl, N. L.; Wannemuehler, M. J.; Narasimhan, B.; Ramer-Tait, A. E. Tailoring the immune response by targeting C-type lectin receptors on alveolar macrophages using "pathogen-like" amphiphilic polyanhydride nanoparticles. *Biomaterials* **2012**, *33* (18), 4762−4772.

(39) Torrelles, J. B.; Schlesinger, L. S. Diversity in Mycobacterium tuberculosis mannosylated cell wall determinants impacts adaptation to the host. *Tuberculosis (Edinburgh)* **2010**, *90* (2), 84−93.

(40) Wijagkanalan, W.; Kawakami, S.; Takenaga, M.; Igarashi, R.; Yamashita, F.; Hashida, M. Efficient targeting to alveolar macrophages by intratracheal administration of mannosylated liposomes in rats. *J. Controlled Release* **2008**, *125* (2), 121−130.

(41) Van der Linden, P.; Ickx, B. E. The effects of colloid solutions on hemostasis. *Can. J. Anaesth.* **2006**, *53* (6 Suppl), S30−39.

(42) Sirtl, C.; Laubenthal, H.; Zumtobel, V.; Kraft, D.; Jurecka, W. Tissue deposits of hydroxyethyl starch (HES): dose-dependent and time-related. *Br. J. Anaesth.* **1999**, *82* (4), 510−515.

(43) Kraft, D.; Sirtl, C.; Laubenthal, H.; Scheiner, O.; Parth, E.; Dieterich, H. J.; Szepfalusi, Z.; Trampisch, H. J.; Gerlach, E.; Peter, K. No Evidence for the Existence of Preformed Antibodies against Hydroxyethyl Starch in Man. *Eur. Surg. Res.* **1992**, *24* (3), 138−142.

(44) Thompson, B. S.; Chilton, P. M.; Ward, J. R.; Evans, J. T.; Mitchell, T. C. The low-toxicity versions of LPS, MPL adjuvant and RC529, are efficient adjuvants for CD4+ T cells. *J. Leukocyte Biol.* **2005**, *78* (6), 1273−1280.

(45) Reed, S. G.; Bertholet, S.; Coler, R. N.; Friede, M. New horizons in adjuvants for vaccine development. *Trends Immunol.* **2009**, *30* (1), 23−32.

(46) Movita, D.; Kreefft, K.; Biesta, P.; van Oudenaren, A.; Leenen, P. J.; Janssen, H. L.; Boonstra, A. Kupffer cells express a unique combination of phenotypic and functional characteristics compared with splenic and peritoneal macrophages. *J. Leukocyte Biol.* **2012**, *92* (4), 723−733.

(47) Petrasek, J.; Csak, T.; Szabo, G. Toll-like receptors in liver disease. *Adv. Clin. Chem.* **2013**, *59*, 155−201.

(48) Liaskou, E.; Wilson, D. V.; Oo, Y. H. Innate immune cells in liver inflammation. *Mediators Inflammation* **2012**, *2012*, 949157.

(49) Ribes, S.; Ebert, S.; Regen, T.; Agarwal, A.; Tauber, S. C.; Czesnik, D.; Spreer, A.; Bunkowski, S.; Eiffert, H.; Hanisch, U. K.; Hammerschmidt, S.; Nau, R. Toll-like receptor stimulation enhances phagocytosis and intracellular killing of nonencapsulated and encapsulated Streptococcus pneumoniae by murine microglia. *Infect. Immun.* **2010**, *78* (2), 865−871.

(50) Jaeschke, H.; Smith, C. W. Cell adhesion and migration. III. Leukocyte adhesion and transmigration in the liver vasculature. *Am. J. Physiol.* **1997**, *273* (6 Pt 1), G1169−1173.

6.3   Publication 3

Monophosphoryl lipid A coating of hydroxyethyl starch nanocapsules drastically increases uptake and maturation by dendritic cells while minimizing the adjuvant dosage

Published in: *Vaccine*, 2015. **33**(7): p. 838-46.

Monophosphoryl lipid A coating of hydroxyethyl starch nanocapsules drastically increases uptake and maturation by dendritic cells while minimizing the adjuvant dosage

CrossMark

Michael Fichter[a,1], Marvin Dedters[a,1], Anette Pietrzak-Nguyen[a], Leah Pretsch[a], Claudius U. Meyer[a], Susanne Strand[b], Fred Zepp[a], Grit Baier[c], Katharina Landfester[c], Stephan Gehring[a,*]

[a] *Children's Hospital, University Medical Center, Johannes Gutenberg University, Langenbeckstraße 1, 55131 Mainz, Germany*
[b] *I. Department of Internal Medicine, University Medical Center, Johannes Gutenberg University, Langenbeckstraße 1, 55131 Mainz, Germany*
[c] *Max-Planck Institute for Polymer Research, Ackermannweg 10, 55128 Mainz, Germany*

Summary:

Coating of monophosphoryl lipid A (MPLA) led to a significantly increased uptake of hydroxyethyl starch nanocapsules (HES-NCs) by human monocyte-derived dendritic (moDCs) cells. Furthermore, MPLA-coated NCs induced activation of moDCs in terms of CD80 or CD83 expression and dramatically enhanced secretion of pro-inflammatory cytokines IL-6, TNFα or IL-12. In addition, the relevance of Toll-like receptor 4 (TLR4) ligation for the observed effects was examined using antibody-mediated blocking. By adsorption of MPLA onto the NC surface, the applied concentration of MPLA was reduced 22-fold compared to MPLA in solution. Therefore, the application of adjuvant-supplemented polymeric nanocapsules for the activation of dendritic cells inducing T_h1-mediated immunity is a very suitable approach in order to reduce MPLA-associated side effects.

Author contribution:

- Design, conduction and evaluation of all biological experiments
- Preparation of graphs and figures
- Preparation of the manuscript together with Prof. Dr. Stephan Gehring

Monophosphoryl lipid A coating of hydroxyethyl starch nanocapsules drastically increases uptake and maturation by dendritic cells while minimizing the adjuvant dosage

Michael Fichter [a],[1], Marvin Dedters [a],[1], Anette Pietrzak-Nguyen [a], Leah Pretsch [a],
Claudius U. Meyer [a], Susanne Strand [b], Fred Zepp [a], Grit Baier [c],
Katharina Landfester [c], Stephan Gehring [a],*

[a] Children's Hospital, University Medical Center, Johannes Gutenberg University, Langenbeckstraße 1, 55131 Mainz, Germany
[b] I. Department of Internal Medicine, University Medical Center, Johannes Gutenberg University, Langenbeckstraße 1, 55131 Mainz, Germany
[c] Max-Planck Institute for Polymer Research, Ackermannweg 10, 55128 Mainz, Germany

ARTICLE INFO

ABSTRACT

Enhancing delivery of antigens to dendritic cells (DCs) is essential for the induction of vigorous antigen-specific cellular immune responses. Aim of the present study was to evaluate the properties of hydroxyethyl starch nanocapsules (HES-NCs) functionalized with anti-CD40, anti-DEC205, interferon-γ (IFNγ) and/or monophosphoryl lipid A (MPLA) with respect to the overall uptake, the released cytokine profile, and the influence on phenotypic maturation of human monocyte-derived DCs using flow cytometry, confocal microscopy and enzyme-linked immunosorbent assays.

NC uptake by DCs was significantly enhanced by functionalizing NCs with anti-CD40 or MPLA. With respect to the cytokine profile and the maturation status, coating with MPLA evoked a strong T_h1-type cytokine response and significantly increased CD80 and CD83 expression on DCs, contrasting the moderate effects of MPLA in solution. Notably, an at least 20 fold higher amount of MPLA in solution was needed compared to the dosage of MPLA attached to HES-NCs in order to induce comparable effects, evidencing the intense dose-sparing potential of particle-bound MPLA.

Reducing the amount of the vaccine adjuvant MPLA, while maintaining or even surpassing the effects on human DCs, reveals the potential of HES-NCs as a promising carrier system for the simultaneous delivery of antigen along with compounds promoting a T_h1-prone cellular immune response.

© 2014 Elsevier Ltd. All rights reserved.

1. Introduction

Nanomedicine is a rapidly growing research area with multiple applications, including imaging [1], vaccination [2,3], biosensoring [4], and drug delivery systems [5–7]. Due to the potential of nanocarriers to promote cell-specific targeting and to protect drugs on its way to the desired cell/organ/tissue, nanocarriers play an important role as drug delivery systems. There are many different preparation techniques for nanocarriers. However, miniemulsion is the preparation method of choice for many applications, which is owed to its excellent properties, including the tuning of size and size distribution, surface functionalization opportunities and the high payload efficiency. In the present study hydroxyethyl starch (HES) was chosen as biopolymer for nanocapsule synthesis, based on its biocompatible properties and its established use in various clinical applications [8]. In previous investigations we observed, that HES nanocapsules without any surface functionalization display a diminished unspecific cell uptake [9], a liver specific deposition [10], and excellent release properties [11]. In particular, we could demonstrate in an *in vitro* murine model, that hydroxyethyl starch-based nanocapsules (HES-NCs) are efficiently ingested by resident liver macrophages (Kupffer cells) and that they are able to release their content (dexamethasone) followed by a significant suppression of cytokine release [11].

The latter observation prompted the present study focusing on the interaction of functionalized HES-NCs with human dendritic cells (DCs), which would potentially qualify HES-NCs as a vaccine platform. A critical obstacle in the development of vaccines against viral pathogens is the induction of vigorous and

---

* Corresponding author. Tel.: +49 6131 17 3560.
  E-mail address: stephan.gehring@uni-mainz.de (S. Gehring).
[1] Both authors contributed equally to this manuscript.

long-lasting, antigen-specific cellular immune responses [12]. DCs – professional antigen presenting cells – are a key cell population linking the innate with the adaptive immune system and are essential for the initiation of cellular immune responses [13]. Accordingly, DCs have become a primary target for novel vaccine formulations, such as virus-like particles, replicons, and nanoparticles [14].

Tailor-made nanocarriers for vaccination with encapsulated antigen have a number of advantages, including (a) prevention of proteolytic degradation [15]; (b) prolonged antigen presentation [16]; (c) enhanced phagocytosis by antigen presenting cells (APCs) [17]; (d) promotion of endosomal release of antigen, leading to enhanced cross-presentation [18]; (e) co-delivery of antigen and adjuvant, promoting T_h1 responses [19]; and (f) receptor-mediated targeting of DCs by immobilization of antibodies on the polymer surface [20].

Commonly targeted DC receptors [21] include CD205 (DEC205) [22], CD209 (DC-SIGN) [23], and CD40 [24]. Importantly, receptor mediated targeting not only enhances uptake but is also capable to induce activation of cells; *e.g.* in CD40-mediated phagocytosis.

In the present study we investigated the effects of HES-NCs functionalized with commonly used targeting receptors (anti-DEC205 and anti-CD40) and compare the latter with monophosphoryl lipid A-(MPLA) and interferon-γ-(IFNγ) coated HES-NCs. MPLA was chosen since it is a commonly used vaccine adjuvant, known to induce maturation of dendritic cells [25,26]. Notably, MPLA has been approved by US and European authorities as a vaccine adjuvant, *e.g.* in a Hepatitis B vaccine (Fendrix, GlaxoSmithKline). In addition, we have recently observed that coating of HES-NCs with MPLA promotes uptake by macrophages and DCs in a murine model [10]. Importantly, combining MPLA with IFNγ is a particular suitable approach to induce IL-12 secretion by human monocyte-derived DCs [27,28]. In summary, we aimed to investigate how MPLA and IFNγ immobilized on HES-NCs affects phagocytosis and maturation of human DCs, with the particular interest to induce a cytokine environment promoting T_h1 T cell responses. Anti-DEC205- and anti-CD40-coated HES-NCs served as a reference.

2. Material and methods

2.1. Nanocapsule synthesis and characterization

2.1.1. Materials used for the NCs synthesis

Materials purchased included: hydroxyethyl starch (HES, $M_w = 200,000 \, g \, mol^{-1}$; Fresenius Kabi), 2,4-toluene diisocyanate (TDI) and cyclohexane (>99.9%; Sigma Aldrich), sodium dodecylsulfate (SDS; Fluka), *N*-ethyl-*N'*-(3-dimethylaminopropyl)-carbodiimide (EDC), monochloroacetic acid (MCA; Aldrich), and Cy5-labeled oligonucleotides (5′-Cy5-CCACTCCTTTCCAG-AAAACT-3′, Thermo Scientific). The surfactant poly((ethylene-*co*-butylene)-*b*-(ethylene oxide)), P(E/B-*b*-EO) [29] and 4-sulfotetrafluorophenyl (STP) were synthesized at the Max-Planck Institute for Polymer Research [30].

Antibodies and other materials for coupling onto the NCs surface were: anti-DEC205 (BD Pharmingen; clone MG38), anti-CD40 (eBioscience; clone 5C3), unspecific anti-human IgG (BD Pharmingen; clone 27–35), interferon-γ (IFNγ; Peprotech) or monophosphoryl lipid A (MPLA; Sigma Aldrich).

2.1.2. Preparation of nanocapsules

HES nanocapsules were synthesized by a polyaddition reaction performed at the miniemulsion droplet's interface according to previously published protocols [9,10] as shown in Fig. 1. Nanocapsules were labeled with Cy5-oligonucleotides in order to assess NC uptake by DCs *in vitro*. Afterwards, HES nanocapsules were

functionalized by a carboxymethylation procedure as previously published [31]. Coupling of anti-DEC205, anti-CD40, IFNγ or IgG, adsorption of MPLA onto HES nanocapsules and their subsequent characterization were performed using a method previously described [10].

2.2. Biological analysis

2.2.1. Generation of human monocyte-derived dendritic cells

Adult peripheral blood mononuclear cells (PBMCs) were isolated from fresh buffy coats, obtained from healthy voluntary donors (blood bank of the University Medical Center Mainz), upon informed and signed consent, by centrifugation through Histopaque-1077 density gradient media (Sigma-Aldrich) for 20 min at $900 \times g$ and 20 °C. The interphase consisting of PBMCs were subsequently extracted and washed with Hank's balanced salt solution (Sigma-Aldrich). CD14$^+$ monocytes were isolated from the PBMC fraction by positive selection using CD14 MicroBeads, MACS LS columns and a magnetic cell separator (MACS; Miltenyi Biotec) in accordance with the manufacturer's instructions. CD14 positive monocytes were washed in X-Vivo 15 medium (Lonza). Subsequent flow cytometric analysis (LSR II; BD Biosciences) verified a high purity of CD14$^+$ monocytes (>98%). Purified monocytes were cultured at a concentration of 10^6 cells per ml in 6-well plates (Greiner Bio-One) in X-Vivo 15 medium supplemented with L-glutamine, $100 \, U \, ml^{-1}$ penicillin and $100 \, \mu g \, ml^{-1}$ streptomycin. Finally, GM-CSF ($200 \, U \, ml^{-1}$) and IL-4 ($200 \, U \, ml^{-1}$) was added to the medium following 6 days of culture at 37 °C and 5% CO_2 with addition of 1 ml fresh medium at days 2 and 4. Immature moDCs were obtained by harvesting the non- or loosely adhering cell population (approx. 30% of CD14$^+$ monocytes). Incubation of moDCs with different nanocapsule formulations was performed using X-Vivo 15 medium supplemented with antibiotics and cytokines as described above.

2.2.2. Confocal laser scanning microscopy (CLSM)

Nanocapsule uptake by moDCs was evaluated using a Zeiss LSM 710 NLO confocal laser scanning microscope. Immature DCs were harvested as described above and cultured with a density of $3 \times 10^5 \, ml^{-1}$ in 8-well chamber slides (ibidi) at 37 °C for 4 h in the presence of $7.5 \, \mu g \, ml^{-1}$ HES-IgG nanocapsules. Nuclei were stained with $2 \, \mu g \, ml^{-1}$ Hoechst 33342 (Life Technologies) for 30 min. Immediately before analysis $2 \, \mu g \, ml^{-1}$ CellMask Orange (Life Technologies) was added for plasma membrane staining.

2.2.3. In vitro loading of moDCs with nanocapsules and flow cytometric analysis

In vitro uptake of nanocapsules by moDCs and maturation analysis were performed by coincubation of immature moDCs in a density of $10^6 \, ml^{-1}$ with $7.5 \, \mu g \, ml^{-1}$ of Cy5-labeled nanocapsules (HES-IgG, HES-αCD40, HES-αDEC205, HES-IFNγ, HES-MPLA, HES-IgG-MPLA, HES-αCD40-MPLA, HES-αDEC205-MPLA, HES-IFNγ-MPLA) or without nanocapsules (control) for 4 and/or 24 h in 48-well plates (Nunclon Surface; Nunc—Thermo Scientific). Cell culture supernatants were collected after 24 h of incubation at 37 °C and stored at −20 °C for subsequent cytokine analysis. Uptake, maturation and toxicity were analyzed by flow cytometry using the multi-channel cytometer BD LSR II (BD Biosciences) equipped with FACSDiva software (BD Biosciences). Data analysis was performed with FlowJo software (Tree Star). Approximately 5×10^5 moDCs were incubated with excess human polyvalent IgG antibody (Sandoglobulin Liquid; CSL Behring) in order to block the Fc receptor and avoid unspecific binding of primary antibodies, followed by a 30 min incubation with fluorochrome-conjugated antibodies CD14 (PerCP; clone MφP9), CD40 (PE; clone 5C3), CD80 (FITC; clone BB1), CD83 (PE; clone HB15e), CD86 (FITC; clone

1. Carboxymethylation process (NaOH, ClCH₂COOH, NaOH)
2. Coupling of antibody or IFNγ (EDC, STP, pH 6.5)
3. Adsorption of MPLA
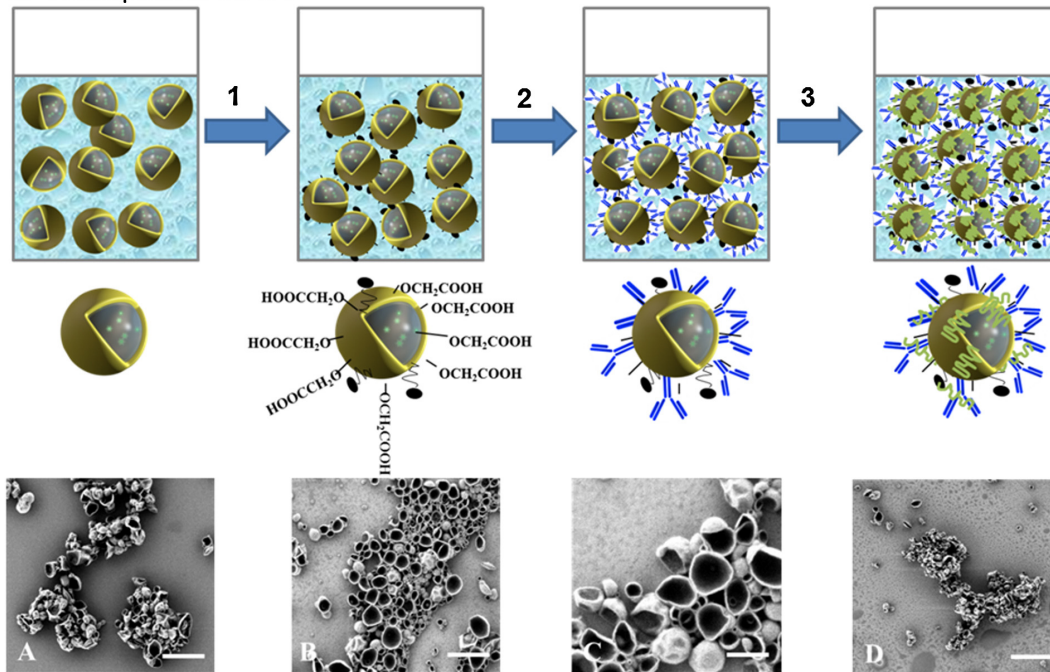
Scalebar corresponds to 500 nm (B and C) and 1 µm (A and D).

Fig. 1. Nanocapsule synthesis and scanning electron microscopic evaluation. (A) HES, (B) HES-COOH, (C) HES-αDEC205 and (D) HES-αDEC205-MPLA.

MMRI-7), HLA-A,B,C (FITC; clone G46-2.6), HLA-DR (PerCP; clone G46-6), or CD11c (V450; clone B-ly6).

2.2.4. Measurement of cytokine secretion

In order to quantify the secretion of IL-6, TNFα and IL-12p70, cell culture supernatants collected after 24 h incubation in the presence of nanocapsules were analyzed using a commercial enzyme-linked immunosorbent assay kit (IL-12p70; eBiosciences) and a Cytometric Bead Array Kit (Human Th1/Th2 Cytokine Kit II; BD Biosciences) in accordance with the manufacturer's instructions followed by data analysis using FCAP Array software (Soft Flow).

2.2.5. Toll-like receptor 4 blocking

The involvement of the Toll-like receptor 4 (TLR4) in the activation of moDCs induced by MPLA-coated nanocapsules was evaluated through antibody-mediated blocking. Briefly, moDCs (10^6 ml^{-1}) were preincubated with different concentrations of a human TLR4 antibody (Invivogen; clone W7C11) for one hour followed by incubation with 7.5 µg ml^{-1} HES-IFNγ, HES-MPLA, HES-IFNγ-MPLA capsules or 4 µg ml^{-1} MPLA. After 24 h incubation, moDCs were harvested and analyzed for nanocapsule uptake and maturation marker expression by flow cytometry. Furthermore, culture supernatants were obtained and analyzed using a Cytometric Bead Array Kit (Human Th1/Th2 Cytokine Kit II; BD Biosciences).

2.2.6. Statistical analysis

Experiments were performed in triplicates and analyzed using SigmaPlot 11 software (Systat Software Inc). When more than two groups were compared with each other, a one way ANOVA test

Table 1
Characterization of nanocapsules.

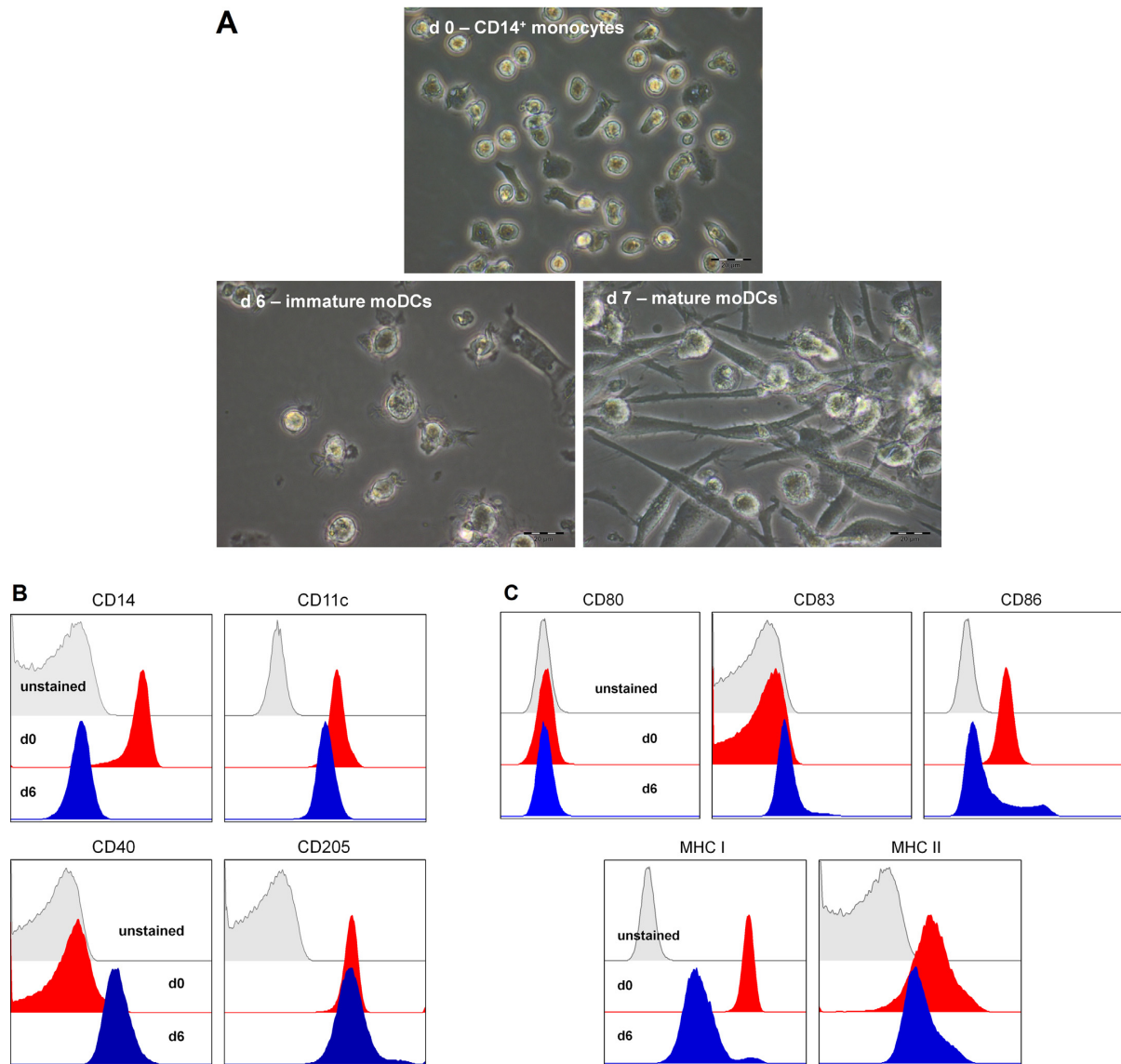| Samples	Average diameter [nm]/standard deviation [%]			Zeta potential (pH 7) [mV]
	In water phase	After antibody coupling	After MPLA adsorption	
HES	230/28	–	–	−24
HES-MPLA		–	235/32	−32
HES-αDEC205		240/30	–	−14
HES-αDEC205-MPLA			240/32	−30
HES-αCD40		220/29	–	−18
HES-αCD40-MPLA			235/33	−30
HES-IgG		235/30	–	−18
HES-IgG-MPLA			235/30	−32
HES-IFNγ		220/31	–	−17
HES-IFNγ-MPLA		–	235/30	−32

Fig. 2. (A) Phase contrast microscopic images of CD14+ monocytes (d0), immature monocyte-derived dendritic cells (moDCs; d6) and matured moDCs (d7). CD14+ monocytes were cultured for six days in the presence of GM-CSF and IL-4. (B and C) Phenotypic characterizations of CD14+ monocytes (d0) and moDCs (d6) were performed using flow cytometry.

was performed followed by a Holm–Sidak test to determine which groups differed significantly (* $p < 0.05$; ** $p < 0.01$; *** $p < 0.001$). For comparisons between two groups only a non-paired Student's *t*-test was performed (* $p < 0.05$; ** $p < 0.01$; *** $p < 0.001$).

3. Results

3.1. Nanocapsule synthesis

HES-NCs were synthesized by interfacial polyaddition resulting in a core-shell structure as confirmed by SEM images (Fig. 1). The polymeric shell consists of HES and inside the aqueous core,

Cy5 oligonucleotides were encapsulated for fluorescently labeling of NCs.

Carboxymethylation and antibody binding including its effect on size, polydispersity and zeta potential has been recently described by our group [10]. The characteristics of the synthesized NCs are summarized in Table 1. The average size of NCs was between 220 nm and 240 nm. The percentage of MPLA adsorbed to hydroxyethyl starch nanocapsules was calculated based on the quantities applied in the adsorption procedure. Therefore, a percentage of 2.4% could be calculated assuming optimal conditions with an adsorption efficacy of 100%. Thus, 7.5 μg HES-MPLA-NCs carried a maximum load of 0.18 μg MPLA corresponding to an average of 760 molecules per nanocapsule.

3.2. Characterization of human monocyte-derived dendritic cells

CD14$^+$ monocytes were isolated from PBMCs and subsequently cultured for six days in the presence of IL-4 and GM-CSF resulting in the generation of immature monocyte-derived dendritic cells (moDCs) (with a yield of 25% to 35%). MoDCs were characterized by flow cytometry and phase contrast microscopy displaying the typical morphology of immature moDCs which appeared round, non- or slightly-adherent with few cytoplasmic projections (Fig. 2A). Non-moDCs appeared flat and strongly adherent; therefore, only non-adherent cells were harvested and used for further experiments. Flow cytometric analysis was performed to verify the phenotype of immature moDCs which was CD14$^-$, CD11c$^+$, CD40$^+$, CD205$^+$, CD80$^-$, CD83$^-$, CD86^{intermediate}, MHC I^{intermediate} and MHC II^{intermediate} (Fig. 2B and C).

3.3. Uptake of nanocapsules by moDCs

In order to confirm nanocapsule uptake rather than adherence to the plasma membrane, confocal laser scanning microscopy was performed. Fig. 3A clearly documents the intracellular uptake of Cy5-labeled nanocapsules (red), which appear to be compartmentalized. Furthermore, the uptake behavior of different nanocapsule formulations (HES-IgG, HES-αCD40, HES-αDEC205, HES-IFNγ, HES-MPLA, HES-IgG-MPLA, HES-αCD40-MPLA, HES-αCD205-MPLA and HES-IFNγ-MPLA) was quantified with HES-IgG serving as a control. Fig. 3B shows a significantly increased uptake of moDCs when HES-NCs were coated with the targeting antibody anti-CD40 compared to capsules coupled to the isotype control (IgG). However, coupling of anti-DEC205 or IFNγ to HES-NCs exhibited only a minute and non-significant effect with respect to the uptake intensity of moDCs *in vitro*. Interestingly, coating with MPLA induced the most pronounced effect on the ingestion of nanocapsules with up to 58% of moDCs being NC positive after 24 h of coincubation. Notably, a combined coating with IgG, anti-DEC205 or IFNγ rather reduced the effects of MPLA-coating regarding the uptake capacity.

3.4. Nanocapsule-induced maturation and cytokine secretion

Nanocapsules were cocultured with moDCs and analyzed for their potential to induce maturation and secretion of proinflammatory cytokines. Flow cytometric analysis revealed a significant increase in CD83 and CD80 expression induced by MPLA-coated HES-NCs from a baseline expression of 8% to 32.5% (Fig. 4A) and from 1.2 to 3.9% (Fig. 4B), respectively. Nanocapsules without MPLA did not trigger any increase in CD83 or CD80 expression, even when anti-CD40 or IFNγ was coupled to the surface. MPLA in solution and a combination of MPLA and IFNγ served as positive controls and lead to a comparable upregulation of CD83 and CD80 expression when compared to MPLA-coated nanocapsules. Supernatants of HES-MPLA capsules after the adsorption procedure served as a control and showed no activation compared to HES-IgG (data not shown). In addition to the phenotypic maturation status of moDCs, cytokine secretion analysis was performed using a multiplex assay. In parallel to the maturation experiments, HES-MPLA-NCs induced a massive secretion of the pro-inflammatory cytokines IL-6 and TNFα, whereas nanocapsules without MPLA-coating did not induce any cytokine response by moDCs (Fig. 5A and B). In order to evaluate whether the different MPLA nanocapsules elicit a T$_h$1-directed cytokine secretion, IL-12p70 levels were measured after coincubation with moDCs (Fig. 5C). Similar to analysis of IL-6 and TNFα, only MPLA-coated nanocapsules induced remarkable levels of IL-12. Interestingly, HES-MPLA capsules showed a 4.5 fold increased IL-12 secretion compared to HES-IgG-MPLA capsules, whereas a
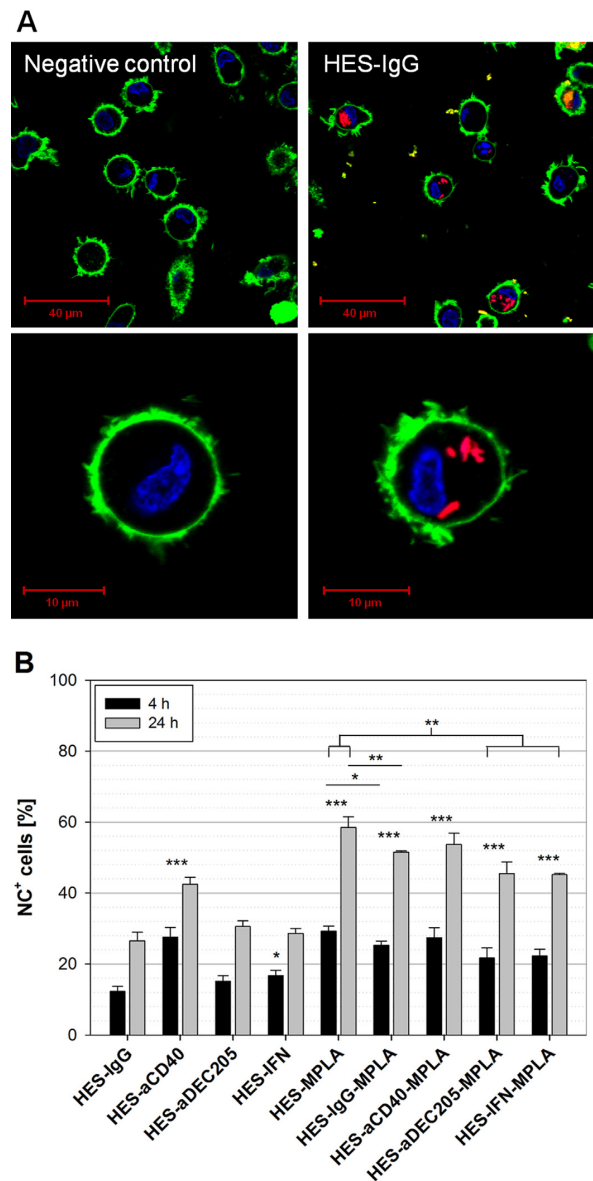
Fig. 3. (A) Confocal laser scanning microscopy (CLSM) was performed in order to document the uptake of HES-IgG nanocapsules (red) by moDCs. Cells incubated without nanocapsules served as negative control. Plasma membrane was stained with CellMask Orange (green) and nuclei were stained using Hoechst 33342 (blue). Flow cytometric analysis was performed to quantify the uptake of nanocapsules by moDCs after 4 and 24 h of coincubation (B). Data shown in (B) are representative of four individual experiments and are expressed as mean ± SD. All NC formulations were compared to HES-IgG and MPLA-coated NCs were additionally compared to HES-MPLA. Significance was given with $p < 0.05$ (*), $p < 0.01$ (**), $p < 0.001$ (***) (One way ANOVA). (For interpretation of the references to color in this figure legend, the reader is referred to the web version of this article.)

coincubation with HES-IFNγ-MPLA-NCs led to an increase of 30%. However, HES-αCD40-MPLA and HES-αDEC205-MPLA capsules reduced the IL-12 secretion by 33% and 41%, respectively.

Notably, MPLA in solution did not elicit a significant effect on IL-12 secretion, contrasted by the overwhelming IL-12 secretion caused by MPLA and IFNγ in solution.
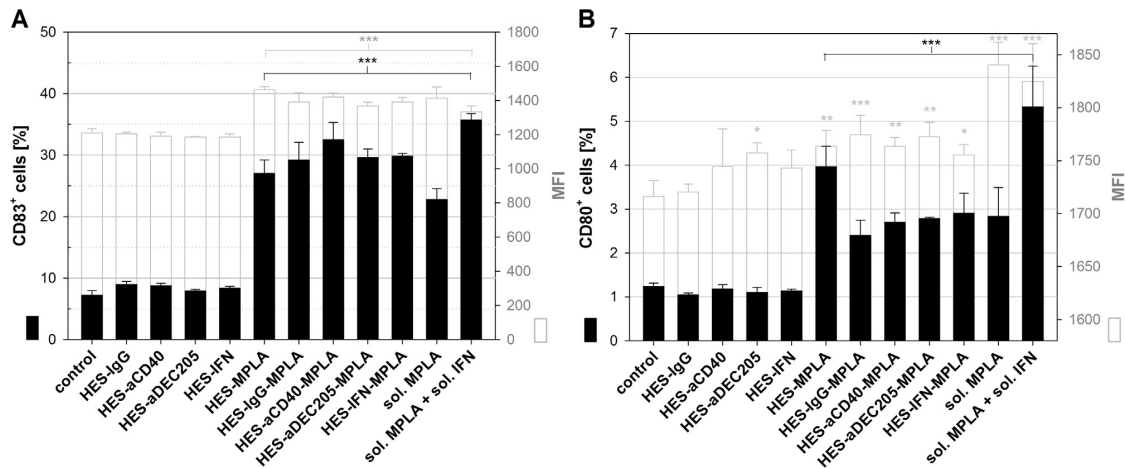
Fig. 4. Phenotypic maturation of moDCs after coincubation with different nanocapsule formulations for 24 h. IFNγ (50 U ml^{-1}) and/or MPLA (4 μg ml^{-1}) in solution served as positive controls. CD83 (A) and CD80 (B) expression was analyzed using flow cytometry. Percentages of moDCs positively stained for CD83 or CD80 are shown as black bars, median fluorescence intensities (MFI) are displayed as transparent bars. The experiment was performed four times and results are expressed as mean ± SD. All conditions were compared to the negative control (moDCs without stimulation) and significance was given with $p < 0.05$ (*), $p < 0.01$ (**), $p < 0.001$ (***) (one way ANOVA).

3.5. Blocking of Toll-like receptor 4 (TLR4)

Preincubation with a TLR4-blocking-antibody showed no effect regarding the uptake of MPLA-coated nanocapsules by moDCs *in vitro* (Fig. 6A). However, an antibody concentration-dependent decrease in CD83 expression was observed after incubation with HES-MPLA and HES-IFNγ-MPLA capsules (Fig. 6B). MPLA in solution served as a positive control and led to a similar reduction after blocking of TLR4. Cytokine analysis of culture supernatants paralleled these findings with a pronounced statistically significant decrease in IL-6 and TNFα secretion even after incubation with low blocking antibody concentrations (Fig. 6C).

4. Discussion

The lack of efficient vaccines against pathogens such as HCV or HIV underlines the need for novel, tailor-made vaccine delivery platforms. Particulate vaccines like virus-like particles (VLPs) have proven to be successful in inducing protective immunity against Human Papilloma and Hepatitis B virus [32,33]. Other innovative vaccine formulations include liposomes, immunostimulating complexes (ISCOMs), polymeric nanocapsules and nanogels [34,35]. Nanocapsules are of particular interest because they combine all essential components needed for a successful vaccine like adjuvants, antigen and antibodies for targeting purposes [35]. Targeting antigen to antigen-presenting cells (APCs), especially dendritic cells is crucial for the induction of antigen-specific immune responses [20]. Several studies show, that a broad intrahepatic CD8$^+$ and CD4$^+$ T cell response is needed for the eradication of HCV [36,37], whereas a missing CD4$^+$ T cell help is associated with a chronification of the infection [38]. In particular, a T_h1-directed immune response was observed in HCV-infected patients who displayed a sustained virological response and eliminated the virus [39]. The liver is prone to tolerance, which in part explains the susceptibility to chronic infections with HBV and HCV [40]. Thus, formulating vaccine nanoparticles containing antigens in combination with adjuvants overcoming the state of tolerance is a promising approach for the development of therapeutic/prophylactic vaccines.

Therefore, the aim of the present study was the development of a nanocapsule delivery platform composed of hydroxyethyl starch characterized by an efficient uptake, and maturation of human moDCs *in vitro*, as well as the induction of T_h1-related cytokine secretion patterns. We made use of monocyte-derived dendritic cells as a model system in order to obtain sufficient numbers of human dendritic cells [41]. Phenotypic characterization of generated immature moDCs displayed a CD14$^-$CD11c$^+$CD40$^+$CD205$^+$CD80$^-$CD83$^-$CD86^{intemediate} phenotype and a round morphology with few small dendrites. In a first step, the uptake of hydroxyethyl starch nanocapsules by moDCs was documented by confocal microscopy, evidencing intracellular uptake of HES-NCs rather than attachment.

Quantification of the overall uptake by FACS analysis revealed an enhanced phagocytosis when NCs were equipped with the targeting antibody anti-CD40 (Fig. 3B). To our surprise anti-DEC205-coating had only a minute effect on the uptake behavior of human DCs. Interestingly, NCs coated with the TLR4 ligand MPLA were taken up by moDCs to a significant higher level compared to all other capsule formulations. This finding is in parallel to our previous study where murine liver DCs expanded *in vivo* with hFlt3-ligand were preferentially ingesting MPLA-coated nanocapsules [10]. Remarkably, murine DCs showed an even higher uptake when HES-NCs were additionally coupled with targeting antibodies anti-CD40 or anti-DEC205, which was not the case for human moDCs.

Besides an enhanced uptake of HES-NCs, activation and maturation of moDCs reflected by the expression of the maturation marker CD83 and the costimulatory molecule CD80 could also be induced by MPLA-coated NCs. HES-αCD40-MPLA-NCs appeared as the best inducer of CD83 expression.

In a preliminary dose finding study an optimal concentration of 7.5 μg ml^{-1} in terms of neglectable toxicity caused by nanocapsules was determined (data not shown). MPLA-coated nanocapsules at this concentration feature just a small fraction of MPLA related to the weight of the capsule (max. 2.4%) that is at least 22 times lower than the concentration of the applied positive control with 4 μg ml^{-1} pure MPLA in solution. Stimulation of DCs with 4 μg ml^{-1} MPLA in solution was determined in a dose finding study to be optimal in terms of the induction of IL-12p70 secretion and thus used as positive control (Supplementary Fig. 1). Remarkably, the effect of MPLA-NCs upon maturation and especially upon the secretion of pro-inflammatory cytokines was even higher compared to the positive control (MPLA in solution). This finding documents the benefit
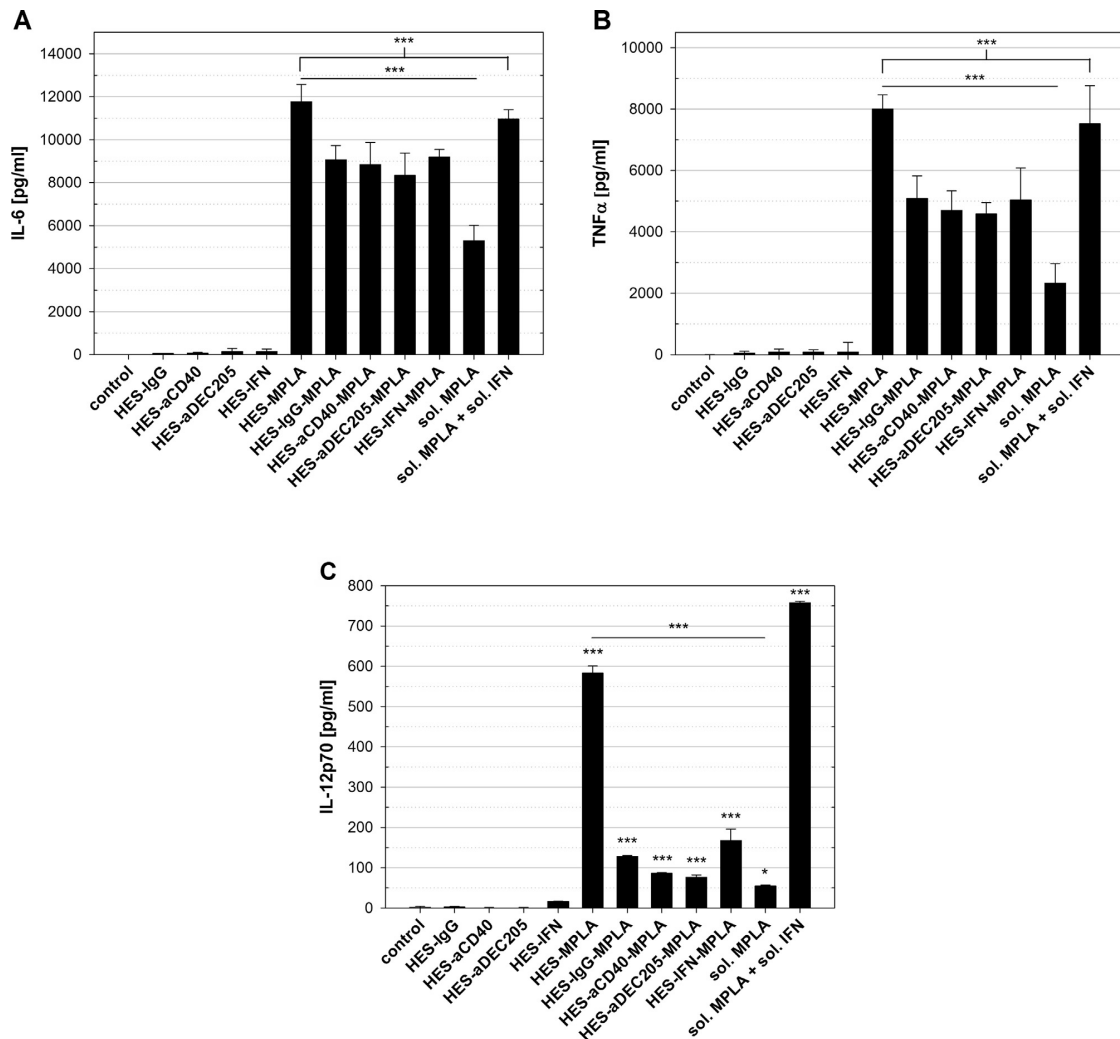
Fig. 5. Cytokine release of moDCs pulsed with NCs was analyzed using a Cytometric Bead Array for IL-6 (A), TNFα (B) and an ELISA for IL-12p70 (C). 7.5 μg ml^{-1} NCs were cocultured with moDCs for 24 h. Data are representative of four individual experiments and are expressed as mean ± SD. All conditions were compared to the negative control and HES-MPLA NCs were additionally compared to MPLA in solution. Significance was given with $p < 0.05$ (*), $p < 0.001$ (***) (one way ANOVA, Student's *t*-test).

of particle-bound MPLA in contrast to MPLA in solution. Furthermore, targeting dendritic cells with antigen- and adjuvant-loaded nanoparticles provides the opportunity to reduce the amount of adjuvant up to 100 times [42]. Such dose-sparing strategies are essential for the development of novel vaccines, reducing systemic and/or local side-effects caused by MPLA. The size of nanocapsules in combination with the presentation of the TLR4 ligand resembles pathogen-like structures inducing antigen-specific immunity [43].

In order to determine whether the applied nanocapsules induce a T$_h$1-type response we analyzed the IL-12p70 secretion levels after incubation with NCs and identified a reasonable secretion for all MPLA-coated nanocapsule formulations. However, in contrast to IL-6 or TNFα secretion and expression of maturation markers, HES nanocapsules solely coated with MPLA induced a massive, 4.5× increased IL-12 secretion as compared to NCs additionally coated with targeting antibodies or interferon-γ. This could be due to a reduced coating efficacy caused by prior coupling of antibodies or IFNγ on the nanocapsule surface resulting in a diminished surface

area available for MPLA adsorption. Furthermore, we hypothesize that an equipment of nanocapsules with antibodies or proteins hinders the TLR4 ligand to bind to its receptor on the cell plasma membrane, therefore, leading to a decreased IL-12 secretion.

Monophosphoryl lipid A as an agonist of the Toll-like receptor 4 mediates through TRIF-based pathway leading to a T$_h$1-directed response [44]. Blocking of TLR4 led to a significant reduction in the maturation state of moDCs and their secretion of pro-inflammatory cytokines after treatment with MPLA-coated nanocapsules. This finding indicates that the activation of moDCs by MPLA-NCs is mediated through TLR4 ligation. Furthermore, Toll-like receptor 4 seems to be involved in the phagocytic process induced by MPLA-coated nanocapsules as has been described for murine macrophages [45] and bone marrow-derived dendritic cells [46]. As shown in Fig. 3, the uptake of HES nanocapsules by moDCs could be increased when MPLA was coated onto the capsule surface. However, the uptake intensity could not be reduced by blocking TLR4 (Fig. 6). Therefore, we hypothesize that other receptors like
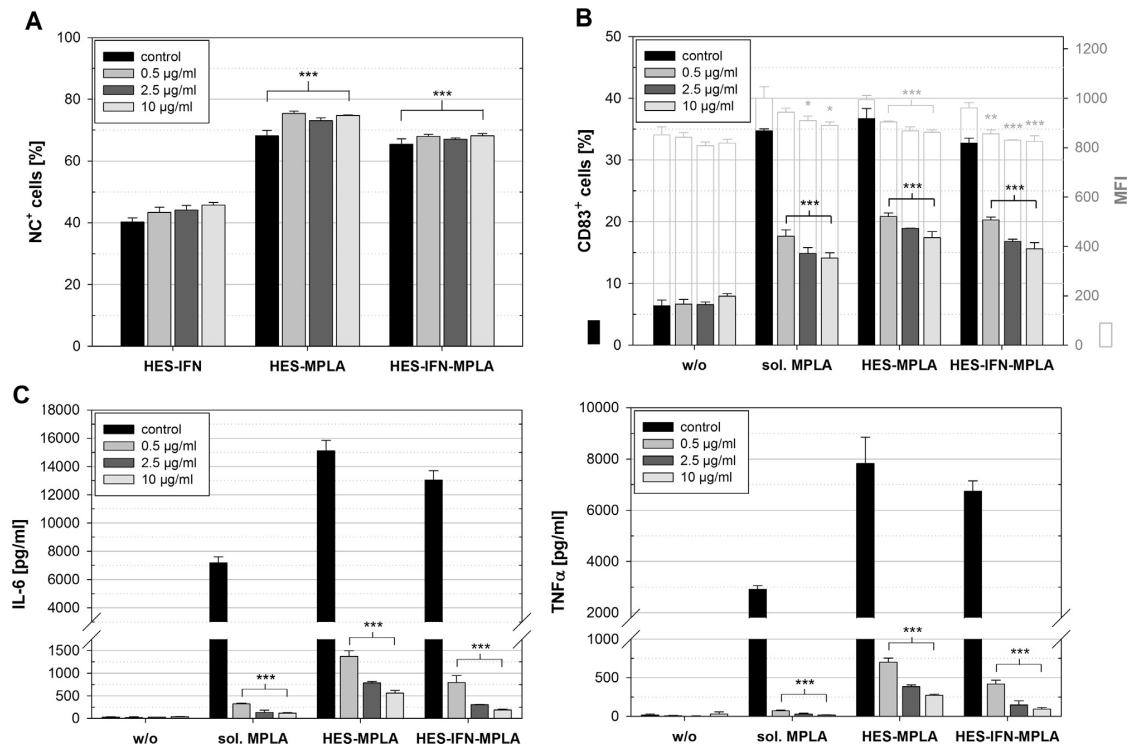
Fig. 6. Blocking of Toll-like receptor 4 (TLR4) was performed by preincubation with a neutralizing antibody (0.5, 2.5, 10 µg ml^{-1}) against TLR4 followed by coculturing with different nanocapsule formulations at a concentration of 7.5 µg ml^{-1}. Effects of TLR4 blocking on nanocapsule uptake (A), on phenotypic maturation displayed by CD83 expression (percentages of positively stained cells in black bars, median fluorescence intensities – MFI – in transparent bars) (B) and on the secretion of IL-6 or TNFα (C) was analyzed using flow cytometry. The experiment was performed five times and results are expressed as mean ± SD. All conditions were compared to the negative control of each condition (without blocking antibody) (B and C) or to HES-IFNγ NCs (A) and significance was given with $p < 0.05$ (*), $p < 0.01$ (**), $p < 0.001$ (***) (Student's *t*-test).

scavenger receptors could have been responsible for the compensation of TLR4 blockade leading to an unaltered uptake behavior by moDCs. The class A scavenger receptors type I and II are capable of recognition of lipopolysaccharide moieties like lipid A and thus could be the target of MPLA-coated nanocapsules [47,48].

5. Conclusion

In conclusion, this publication presents a nanocarrier platform based on hydroxyethyl starch nanocapsules with a diameter between 220 and 240 nm. Coating with the vaccine adjuvant MPLA effectively enhanced nanocapsule phagocytosis by dendritic cells and led to maturation and the induction of IL-12 secretion as an indicator for a T_h1-directed response. Notably, the amount of MPLA attached to the HES-NCs was at least 20 fold lower than soluble MPLA used for maturation of DCs evidencing the intense dose-sparing potential of particle-bound MPLA.

Conflict of interest statement

The authors have no conflict of interest to disclose.

Appendix A. Supplementary data

Supplementary material related to this article can be found, in the online version, at http://dx.doi.org/10.1016/j.vaccine. 2014.12.072.

References

[1] Qazilbash MM, Brehm M, Chae BG, Ho PC, Andreev GO, Kim BJ, et al. Mott transition in VO$_2$ revealed by infrared spectroscopy and nano-imaging. Science 2007;318(5857):1750–3 (Epub 2007/12/15).
[2] Koppolu B, Zaharoff DA. The effect of antigen encapsulation in chitosan particles on uptake, activation and presentation by antigen presenting cells. Biomaterials 2013;34(9):2359–69 (Epub 2013/01/01).
[3] Vallhov H, Gabrielsson S, Stromme M, Scheynius A, Garcia-Bennett AE. Mesoporous silica particles induce size dependent effects on human dendritic cells. Nano Lett 2007;7(12):3576–82 (Epub 2007/11/03).
[4] Maxwell DJ, Taylor JR, Nie S. Self-assembled nanoparticle probes for recognition and detection of biomolecules. J Am Chem Soc 2002;124(32):9606–12 (Epub 2002/08/09).
[5] Horcajada P, Chalati T, Serre C, Gillet B, Sebrie C, Baati T, et al. Porous metal–organic-framework nanoscale carriers as a potential platform for drug delivery and imaging. Nat Mater 2010;9(2):172–8 (Epub 2009/12/17).
[6] Min KH, Park K, Kim YS, Bae SM, Lee S, Jo HG, et al. Hydrophobically modified glycol chitosan nanoparticles-encapsulated camptothecin enhance the drug stability and tumor targeting in cancer therapy. J Control Release 2008;127(3):208–18 (Epub 2008/03/14; official journal of the Controlled Release Society).
[7] Vila A, Gill H, McCallion O, Alonso MJ. Transport of PLA-PEG particles across the nasal mucosa: effect of particle size and PEG coating density. J Control Release 2004;98(2):231–44 (Epub 2004/07/21) (official journal of the Controlled Release Society).
[8] Van der Linden P, Ickx BE. The effects of colloid solutions on hemostasis. Can J Anaesth 2006;53(6 Suppl.):S30–9 (Epub 2006/06/13).

[9] Baier G, Baumann D, Siebert JM, Musyanovych A, Mailander V, Landfester K. Suppressing unspecific cell uptake for targeted delivery using hydroxyethyl starch nanocapsules. Biomacromolecules 2012;13(9):2704–15 (Epub 2012/08/01).

[10] Pietrzak-Nguyen A, Fichter M, Dedters M, Pretsch L, Gregory SH, Meyer C, et al. Enhanced in vivo targeting of murine non-parenchymal liver cells with monophosphoryl lipid A functionalized microcapsules. Biomacromolecules 2014 Jul 14;15(7):2378–88 (Epub 2014/06/06).

[11] Fichter M, Baier G, Dedters M, Pretsch L, Pietrzak-Nguyen A, Landfester K, et al. Nanocapsules generated out of a polymeric dexamethasone shell suppress the inflammatory response of liver macrophages. Nanomed: Nanotechnol, Biol, Med 2013 Nov;9(8):1223–34 (Epub 2013/06/04).

[12] Levitz SM, Golenbock DT. Beyond empiricism: informing vaccine development through innate immunity research. Cell 2012;148(6):1284–92 (Epub 2012/03/20).

[13] Steinman RM. Decisions about dendritic cells: past, present, and future. Annu Rev Immunol 2012;30:1–22 (Epub 2011/12/06).

[14] Nabel GJ. Designing tomorrow's vaccines. N Engl J Med 2013;368(6):551–60 (Epub 2013/02/08).

[15] Waeckerle-Men Y, Groettrup M. PLGA microspheres for improved antigen delivery to dendritic cells as cellular vaccines. Adv Drug Delivery Rev 2005;57(3):475–82 (Epub 2004/11/25).

[16] Waeckerle-Men Y, Allmen EU, Gander B, Scandella E, Schlosser E, Schmidtke G, et al. Encapsulation of proteins and peptides into biodegradable poly(D,L-lactide-co-glycolide) microspheres prolongs and enhances antigen presentation by human dendritic cells. Vaccine 2006;24(11):1847–57 (Epub 2005/11/18).

[17] Leleux J, Roy K. Micro and nanoparticle-based delivery systems for vaccine immunotherapy: an immunological and materials perspective. Adv Healthc Mater 2013;2(1):72–94 (Epub 2012/12/12).

[18] Nembrini C, Stano A, Dane KY, Ballester M, van der Vlies AJ, Marsland BJ, et al. Nanoparticle conjugation of antigen enhances cytotoxic T-cell responses in pulmonary vaccination. Proc Natl Acad Sci USA 2011;108(44):E989–97 (Epub 2011/10/05).

[19] Trumpfheller C, Longhi MP, Caskey M, Idoyaga J, Bozzacco L, Keler T, et al. Dendritic cell-targeted protein vaccines: a novel approach to induce T-cell immunity. J Intern Med 2012;271(2):183–92 (Epub 2011/12/01).

[20] Cruz LJ, Tacken PJ, Rueda F, Domingo JC, Albericio F, Figdor CG. Targeting nanoparticles to dendritic cells for immunotherapy. Methods Enzymol 2012;509:143–63 (Epub 2012/05/10).

[21] Tacken PJ, de Vries IJ, Torensma R, Figdor CG. Dendritic-cell immunotherapy: from ex vivo loading to in vivo targeting. Nat Rev Immunol 2007;7(10):790–802 (Epub 2007/09/15).

[22] Bonifaz LC, Bonnyay DP, Charalambous A, Darguste DI, Fujii S, Soares H, et al. In vivo targeting of antigens to maturing dendritic cells via the DEC-205 receptor improves T cell vaccination. J Exp Med 2004;199(6):815–24 (Epub 2004/03/17).

[23] Tacken PJ, de Vries IJ, Gijzen K, Joosten B, Wu D, Rother RP, et al. Effective induction of naive and recall T-cell responses by targeting antigen to human dendritic cells via a humanized anti-DC-SIGN antibody. Blood 2005;106(4):1278–85 (Epub 2005/05/10).

[24] Schjetne KW, Fredriksen AB, Bogen B. Delivery of antigen to CD40 induces protective immune responses against tumors. J Immunol 2007;178(7):4169–76 (Epub 2007/03/21).

[25] Massa C, Seliger B. Fast dendritic cells stimulated with alternative maturation mixtures induce polyfunctional and long-lasting activation of innate and adaptive effector cells with tumor-killing capabilities. J Immunol 2013;190(7):3328–37 (Epub 2013/03/01).

[26] Alving CR, Peachman KK, Rao M, Reed SG. Adjuvants for human vaccines. Curr Opin Immunol 2012;24(3):310–5.

[27] Ten Brinke A, Karsten ML, Dieker MC, Zwaginga JJ, van Ham SM. The clinical grade maturation cocktail monophosphoryl lipid A plus IFNgamma generates monocyte-derived dendritic cells with the capacity to migrate and induce Th1 polarization. Vaccine 2007;25(41):7145–52.

[28] Krumbiegel D, Zepp F, Meyer CU. Combined Toll-like receptor agonists synergistically increase production of inflammatory cytokines in human neonatal dendritic cells. Hum Immunol 2007;68(10):813–22.

[29] Schlaad H, Kukula H, Rudloff J, Below I. Synthesis of α,ω-heterobifunctional poly(ethylene glycol)s by metal-free anionic ring-opening polymerization. Macromolecules 2001;34(13):4302–4.

[30] Gee KR, Archer EA, Kang HC. 4-Sulfotetrafluorophenyl (STP) esters: new water-soluble amine-reactive reagents for labeling biomolecules. Tetrahedron Lett 1999;40(8):1471–4.

[31] Paiphansiri U, Dausend J, Musyanovych A, Mailander V, Landfester K. Fluorescent polyurethane nanocapsules prepared via inverse miniemulsion: surface functionalization for use as biocarriers. Macromol Biosci 2009;9(6):575–84.

[32] Roldao A, Mellado MC, Castilho LR, Carrondo MJ, Alves PM. Virus-like particles in vaccine development. Expert Rev Vaccines 2010;9(10):1149–76 (Epub 2010/10/07).

[33] Ambrosch F, Wiedermann G, Kundi M, Leroux-Roels G, Desombere I, Garcon N, et al. A hepatitis B vaccine formulated with a novel adjuvant system. Vaccine 2000;18(20):2095–101 (Epub 2000/03/15).

[34] Correia-Pinto JF, Csaba N, Alonso MJ. Vaccine delivery carriers: insights and future perspectives. Int J Pharm 2013;440(1):27–38 (Epub 2012/05/09).

[35] De Temmerman ML, Rejman J, Demeester J, Irvine DJ, Gander B, De Smedt SC. Particulate vaccines: on the quest for optimal delivery and immune response. Drug Discovery Today 2011;16(13–14):569–82 (Epub 2011/05/17).

[36] Diepolder HM, Zachoval R, Hoffmann RM, Wierenga EA, Santantonio T, Jung MC, et al. Possible mechanism involving T-lymphocyte response to non-structural protein 3 in viral clearance in acute hepatitis C virus infection. Lancet 1995;346(8981):1006–7 (Epub 1995/10/14).

[37] Thimme R, Oldach D, Chang KM, Steiger C, Ray SC, Chisari FV. Determinants of viral clearance and persistence during acute hepatitis C virus infection. J Exp Med 2001;194(10):1395–406 (Epub 2001/11/21).

[38] Thimme R, Binder M, Bartenschlager R. Failure of innate and adaptive immune responses in controlling hepatitis C virus infection. FEMS Microbiol Rev 2012;36(3):663–83 (Epub 2011/12/07).

[39] Flynn JK, Dore GJ, Hellard M, Yeung B, Rawlinson WD, White PA, et al. Maintenance of Th1 hepatitis C virus (HCV)-specific responses in individuals with acute HCV who achieve sustained virological clearance after treatment. J Gastroenterol Hepatol 2013;28(11):1770–81 (Epub 2013/05/15).

[40] Thomson AW, Knolle PA. Antigen-presenting cell function in the tolerogenic liver environment. Nat Rev Immunol 2010;10(11):753–66 (Epub 2010/10/26).

[41] Sallusto F, Lanzavecchia A. Efficient presentation of soluble antigen by cultured human dendritic cells is maintained by granulocyte/macrophage colony-stimulating factor plus interleukin 4 and downregulated by tumor necrosis factor alpha. J Exp Med 1994;179(4):1109–18 (Epub 1994/04/01).

[42] Tacken PJ, Zeelenberg IS, Cruz LJ, van Hout-Kuijer MA, van de Glind G, Fokkink RG, et al. Targeted delivery of TLR ligands to human and mouse dendritic cells strongly enhances adjuvanticity. Blood 2011;118(26):6836–44 (Epub 2011/10/05).

[43] Smith DM, Simon JK, Baker Jr JR. Applications of nanotechnology for immunology. Nat Rev Immunol 2013;13(8):592–605 (Epub 2013/07/26).

[44] Mata-Haro V, Cekic C, Martin M, Chilton PM, Casella CR, Mitchell TC. The vaccine adjuvant monophosphoryl lipid A as a TRIF-biased agonist of TLR4. Science 2007;316(5831):1628–32 (Epub 2007/06/16).

[45] Blander JM, Medzhitov R. Regulation of phagosome maturation by signals from toll-like receptors. Science 2004;304(5673):1014–8 (Epub 2004/05/15).

[46] Amiel E, Alonso A, Uematsu S, Akira S, Poynter ME, Berwin B. Pivotal advance: toll-like receptor regulation of scavenger receptor-A-mediated phagocytosis. J Leukoc Biol 2009;85(4):595–605 (Epub 2008/12/30).

[47] Hampton RY, Golenbock DT, Penman M, Krieger M, Raetz CR. Recognition and plasma clearance of endotoxin by scavenger receptors. Nature 1991;352(6333):342–4 (Epub 1991/07/25).

[48] Peiser L, Mukhopadhyay S, Gordon S. Scavenger receptors in innate immunity. Curr Opin Immunol 2002;14(1):123–8 (Epub 2002/01/16).

6.4   Publication 4

Biodegradable protein nanocontainers

Published in: *Biomacromolecules*, 2015. **16**(3): p. 815-21.

Biodegradable Protein Nanocontainers

Keti Piradashvili, Michael Fichter, Kristin Mohr, Stephan Gehring, Frederik R. Wurm,*
and Katharina Landfester*

Max Planck Institute for Polymer Research, Ackermannweg 10, Mainz 55128, Germany

Children's Hospital, University Medical Center, Johannes Gutenberg University, Mainz 55131, Germany

Ⓢ *Supporting Information*

Summary:

To our knowledge, the present study documents, for the first time, the synthesis of polymeric nanocarriers exclusively made of protein, here: ovalbumin (OVA) or bovine serum albumin (BSA). The prepared nanocarrier formulations had core-shell morphology and exhibited high encapsulation efficiencies of fluorescent dyes while avoiding aggregation. OVA nanocarriers were efficiently taken up by human monocyte-derived dendritic cells *in vitro* and demonstrated degradation by incubation with proteases leading to protein release. Since the method of synthesis is easily transferable to other proteins, polymeric protein nanocarriers are an excellent platform for the delivery of therapeutically relevant proteins.

Author contribution:

- Contribution to the study design
- Design, conduction and evaluation of all biological experiments
- Preparation of graphs and figures based on cell culture assays
- Preparation of the biological part of the manuscript

Biodegradable Protein Nanocontainers

Keti Piradashvili, Michael Fichter, Kristin Mohr, Stephan Gehring, Frederik R. Wurm,* and Katharina Landfester*

Max Planck Institute for Polymer Research, Ackermannweg 10, Mainz 55128, Germany

Children's Hospital, University Medical Center, Johannes Gutenberg University, Mainz 55131, Germany

S *Supporting Information*

ABSTRACT: The application of synthetic polymers for drug delivery often requires tremendous efforts to ensure biocompatibility and -degradation. To use the body's own substances can help to overcome these problems. Herein, we present the first synthesis of nanocontainers entirely composed of albumin proteins. These protein nanocontainers (PNCs) were loaded with hydrophilic compounds and release of the payload is triggered through natural lysis in vitro in human monocyte-derived dendritic cells (moDCs). No aggregation of PNCs in human blood plasma was observed, indicating stability for blood circulation. As the PNCs were readily taken up by moDCs, they are considered as a promising delivery platform for vaccination strategies and could minimize the risk of side effects caused by foreign carrier substances.
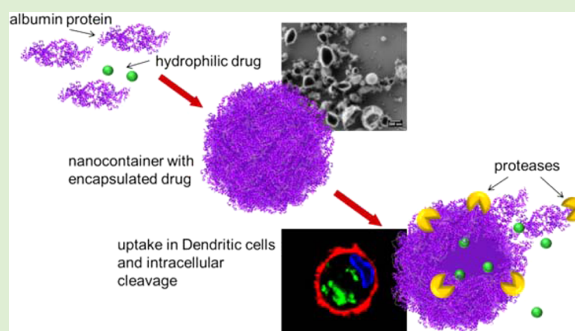
■ INTRODUCTION

In the field of targeted drug delivery the design of nanocarriers is particularly interesting as these systems open up ways of directed and personalized medication with reduction of side effects.[1,2] Drug delivery vehicles should protect sensitive cargo and be able to safely transport the medication to the pathological site overcoming biological barriers within the body.[3,4] Additionally, a facile, controlled, and naturally driven way of release must be guaranteed once the target site is reached.[5] Thus, nanocontainers for the use as drug carriers have to meet certain requirements such as low toxicity, high loading efficiency, and a sustained release.[6]

Several efforts have been undertaken to provide such drug delivery systems with materials that are known for their biocompatibility and -degradability, such as poly(lactide-co-glycolide)s or poly(lactone)s.[7,8] However, these materials still remain a foreign material within a biological system exhibiting certain drawbacks as, for example, a fast clearance by the immune system, toxicity, or low pH of the degradation products.[9,10] Nanocontainers based on biopolymers such as polysaccharides[11−13] and proteins,[14,15] on the contrary, have been proven to be more effective as they often show a higher drug-loading capacity and a better biocompatibility compared to the synthetic ones.[11]

Proteins are particularly interesting as they are easily accessible, water-soluble, in general, associated with low toxicity, and biodegradable.[13,16,17] Moreover, due to their defined molecular weight and known primary structure, further chemical modifications are possible.[18−20] In recent studies, for example, the chemotherapeutic agent paclitaxel was bound to albumin nanoparticles (*nab*-paclitaxel), increasing the efficacy of the drug compared to solvent-based formulations and lowering the side effects.[21]

Herein we report the synthesis of nanocontainers composed exclusively of bovine serum albumin (BSA) or ovalbumin (OVA). The nanocontainers were prepared via the inverse miniemulsion technique (see Figure 1).

This process enables the production of stable capsules in size ranges of 50−500 nm via a polyaddition reaction at the interface of stable nanosized droplets in emulsion.[22−24] The advantage of this method is that, with water representing the dispersed phase, it is possible to encapsulate water-soluble compounds with high loading efficiency.[25,26] Additionally, via functional groups on the nanocontainer surface (such as hydroxyl or amino moieties), the nanocontainers can be further modified, for example, with antibodies, for targeting of specific organs or cell types.[27−29] Polysaccharide-based nanocarriers, for example, functionalized with antibodies and adjuvants were taken up more efficiently by Kupffer cells and dendritic liver cells compared to the untargeted constructs.[29] Polyurethane nanocapsules with an amino-functionalized surface showed an increased uptake by HeLa cells, demonstrating their potential use as biocarriers.[26]

In the present study, BSA and OVA were chosen as model proteins. These proteins are well studied, easily available, exhibit a wide acceptance in the pharmaceutical industry, and
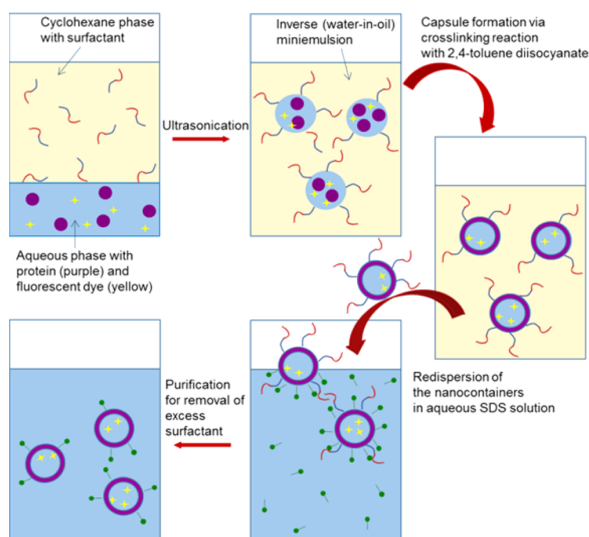
Figure 1. Synthetic procedure for protein nanocontainers via a miniemulsion process.

are already used in several drug delivery systems.[19,30−32] A representative from serum albumins was chosen as these proteins are the most abundant plasma proteins in mammals and play an important role in the transport of small molecules due to the extraordinary high ligand binding capacity.[18,33] BSA nanoparticles can be used as suitable agents for liver-targeting drug delivery systems. It was found that BSA nanoparticles prepared via the pH-coacervation method and loaded with the anticancer drug methotrexate exhibited a significant higher accumulation in the murine liver, lung and spleen compared to the free drug.[34] Furthermore, studies have shown that nanoparticles modified with serum albumin have less undesired interactions in serum and thus can be used as suitable agents for gene therapy.[35,36]

As BSA is extracted from bovine blood and can therefore be, despite purification, contaminated with pathogens, ovalbumin is preferentially used for medical testing.[37] Especially for immunization experiments, ovalbumin is widely used as a model antigen for vaccine studies. OVA and BSA share a number of common properties, including low toxicity, and they are biodegradable, chemically rather stabile and capable to stabilize emulsions.[18]

Protein nanocontainers were characterized regarding their loading efficiency by encapsulating the dye SR101 as a hydrophilic drug model. Further, the uptake of the PNCs in human dendritic cells was examined along with the degradation of PNCs by proteolysis both in a cell-free assay and in a dendritic cell culture system. In addition, the behavior of the PNCs in human blood plasma was investigated.

■ EXPERIMENTAL SECTION

Materials. All chemicals and materials were used as received.

Bovine serum albumin (>96% purity) and albumin from chicken egg white (grade VII) were purchased from Sigma-Aldrich, as well as 2,4-toluene diisocyanate (TDI) and dimethyl sulfoxide (DMSO; >99%). Cyclohexane (HPLC grade) and the osmotic reagent sodium chloride were purchased from VWR. The block copolymer poly-((ethylene-*co*-butylene)-*b*-(ethylene oxide) P(E/B)-*b*-EO) used as the oil soluble surfactant was synthesized as described in literature[38] and consists of a poly((ethylene-*co*-butylene) block (NMR: M_n = 3900 g/

mol) and a poly(ethylene oxide) block (NMR: M_n = 2700 g/mol). The anionic surfactant sodium dodecyl sulfate (SDS) was purchased from Alfa Aesar. The sodium chloride solution (NaCl 0.9%) was purchased from B. Braun. CellTracker Green CMFDA and DQ ovalbumin (D-12053) were purchased from Molecular Probes. Sulforhodamine 101 (SR101) was purchased from BioChemica, Aldrich. The cy5-labeled oligonucleotide with the sequence cy5-CCA CTC CTT TCC AGA AAA CT-3′ was synthesized by Thermo Scientific. Amicon Ultra-2 centrifugal filter devices and the GS200 nm filters were purchased from Merck Millipore (100000 nominal molecular weight limit (NMWL)). The human blood plasma, prepared according to the standard guidelines, was obtained from the University Clinic of Mainz (Germany). Due to the high variation of protein composition of different patients, a pool of plasma obtained by the mixture of serum of several healthy donors was used for all measurements. Demineralized water was used for all experiments. For cell experiments, Histopaque-1077 from Sigma-Aldrich was used. CD14 microbeads were purchased from Miltenyi Biotec, X-Vivo 15 medium from Lonza and GM-CSF and IL-4 from ImmunoTools. Propidium iodide solution was purchased from eBiosciences. The magnesium and calcium free phosphate-buffered saline, Hoechst 33342 and CellMask Orange were purchased from Life Technologies.

Instrumentation. For ultrasonication, a Branson Sonifier W-450-Digital was used with a 1/2" tip, operating under ice cooling for 3 min at 70% amplitude with pulse cycles of 20 s sonication and 10 s pauses.

For centrifugation, the Sigma 3 k-30 from Sigma Centrifuges, U.K., was used.

Morphological studies were performed with transmission electron microscopy (TEM) and scanning electron microscopy (SEM). For the measurements, one drop of diluted PNC dispersion was placed either onto a silica wafer (for SEM) or onto a 300 mesh carbon-coated copper grid (for TEM) and allowed to dry under ambient conditions. The SEM measurements were performed with a 1530 Gemini LEO (Zeiss) field emission microscope, with an accelerating voltage of 170 V. For TEM measurements, Jeol 1400 transmission electron microscope was used with an accelerating voltage of 120 kV.

The average size and size distribution of the PNCs were measured via dynamic light scattering (DLS) at 25 °C using a Nicomp 380 submicron particle sizer (Nicomp Particle Sizing Systems, U.S.A.) at an angle of 90°.

FT-IR measurements were performed with the PerkinElmer Spectrum BX FT-IR spectrometer. For the measurements, approximately 3 mg of the freeze-dried sample was pressed with KBr to a pellet, and the spectrum was recorded between 4000 and 400 cm^{-1}.

Zeta potential measurements were performed in 10^{-3} M potassium chloride solution at pH 6.8 and 25 °C with Malvern Zeta sizer (Malvern Instruments, U.K.).

All dynamic light scattering experiments in human blood plasma were performed on a commercially available instrument from ALV GmbH consisting of a goniometer and an ALV-5000 multiple-tau full-digital correlator with 320 channels. A helium−neon laser (JDS Uniphase with a single mode intensity of 25 mW operating at a laser wavelength of λ_0 = 632.8 nm) was used as the light source. All solutions for light scattering experiments were prepared in dust-free quartz light scattering cuvettes (inner diameter 18 mm, Hellma, Müllheim), which were cleaned prior to use with distilled acetone.

Fluorescence intensity measurements were performed with the Infinite M1000 plate reader from Tecan, Austria using 96-well plates.

Flow cytometric analysis of PNC$^+$ moDCs was performed on the BD LSR II flow cytometer (BD Biosciences).

Confocal laser scanning microscopy was performed on the Zeiss LSM 710 NLO.

Methods. *Protein Nanocontainer (PNC) Synthesis.* The protein nanocontainers were prepared, adopting a previously described procedure from Landfester et al., using a polyaddition reaction in an inverse miniemulsion process.[12] First, 50 mg of the appropriate protein were dissolved in 0.5 g demineralized water and 7.2 mg NaCl were added to the mixture. A total of 35.7 mg surfactant P((E/B)-*b*-EO) was dissolved in 7.5 g cyclohexane, and the mixture was added dropwise to the stirred aqueous solution. The so-prepared pre-
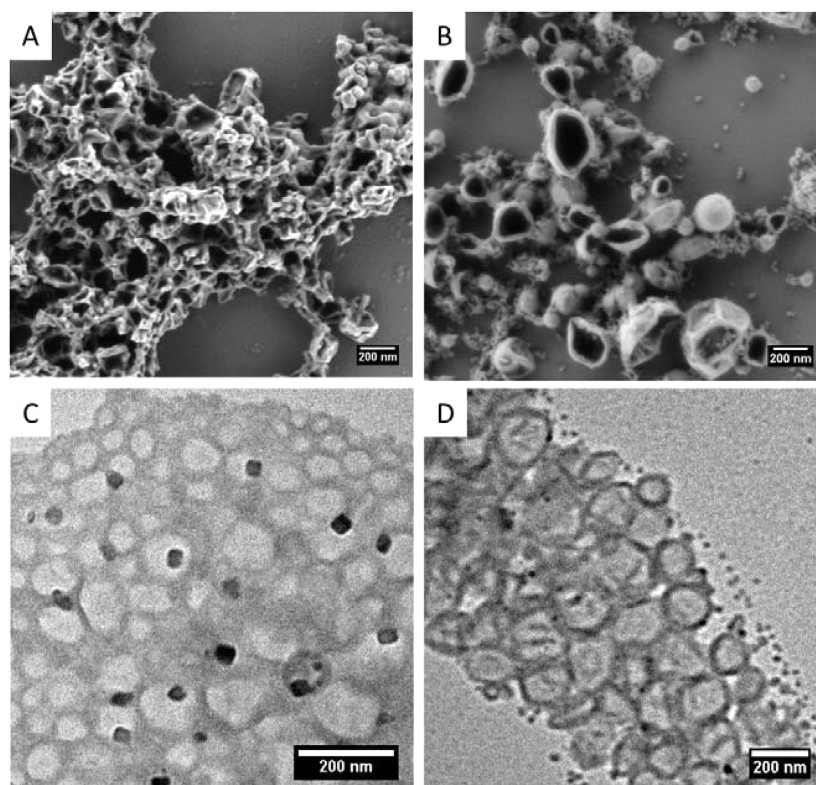
Figure 2. Scanning electron microscopy (SEM) images of (A) BSA-nanocontainers and (B) OVA-nanocontainers; Transmission electron microscopy (TEM) images of (C) BSA-nanocontainers (black spots: NaCl crystals) and (D) OVA-nanocontainers.

emulsion was homogenized by ultrasound as described above. A solution of 10.7 mg P((E/B)-*b*-EO) and 11.4 mg TDI in 5 g of cyclohexane was then added dropwise over a period of 2 min to the miniemulsion, and the mixture was allowed to stir at 25 °C for an additional 24 h.

The synthesized PNCs were purified by repetitive centrifugation (3 times for 20 min, RCF 1664) to remove the excess of the surfactant and redispersed in pure cyclohexane. For transfer into the aqueous phase, 500 μL of PNC dispersion in cyclohexane was added dropwise to 5 g of an aqueous SDS solution (0.1 wt %) under mechanical stirring, and the samples were subjected afterward to an ultrasound bath for 3 min at 25 °C (25 kHz). Subsequently, the samples were stirred open for 24 h at 25 °C to evaporate cyclohexane. To remove the excess SDS, the dispersion was further purified via Amicon Ultra-2 centrifugal filter (3 times for 20 min, RCF 1664) and redispersed in NaCl solution (0.9 wt %).

Modification of PNCs for Biological Analysis. For the measurement of cellular uptake, the PNCs were loaded with the cy5-labeled oligonucleotides by using 130 μL of the fluorophore dissolved in PBS and 0.370 g distilled water proceeding as described above.

The PNCs modified with DQ ovalbumin were synthesized by the addition of 300 μL of a DQ ovalbumin solution in PBS buffer (with a concentration of 1 mg/mL) to the aqueous phase. PNCs labeled with CellTracker CMFDA were synthesized by the addition of 160 μL of CellTracker CMFDA (with a concentration of 1 mg/mL in DMSO) to the aqueous phase and proceeding as described above.

Measurements in Human Blood Plasma. The PNCs were measured in PBS buffer solution at physiological pH (7.4) and salinity (0.152 M). For measurements of nanocontainer-plasma mixtures, 10 μL of PNC dispersion (0.2%) was pipetted unfiltrated into the light scattering cuvette containing 200 μL of undiluted human plasma, which was filtered into the cuvette through a GS200 nm filter. The protein/PNC ratio was kept constant to the respective in vivo

experiments (600 mg protein per mg PNC). The mixture was then diluted up to 1 mL total sample volume by filtering PBS into the light scattering cuvette. For DLS analysis of the nanocontainers alone, 10 μL of the PNC solution (0.2%) was added (without filtration) in 990 μL of filtered PBS. Plasma alone was prepared adding 800 μL of PBS to maintain the same dilutions.

After mixing, the samples were incubated for 20 min on a shaker at room temperature (20 °C) prior to the measurement. All DLS measurements were performed at 20 °C.

Determination of PNC Permeability and Encapsulation Efficiency. The permeability of the PNC-shell was studied by encapsulation of the fluorescent dye SR 101, which shows an absorption maximum at 550 nm and an emission maximum at 605 nm. A total of 0.5 mg SR101 was mixed with the aqueous phase, and the reaction was carried out as described above. After redispersion in the aqueous SDS solution, the PNCs were sedimented by centrifugation with the Amicon Ultra-2 centrifugal filter devices, and the fluorescence intensity of the permeate was measured by a plate reader. The encapsulation efficiency was calculated by correlating the obtained fluorescence intensity to the intensity of the starting concentration of SR101. To determine the permeability, the experiment was repeated over a given period of time, and the fluorescence signal was compared to the initial value. The experiment was conducted two times with three single measurements.

Intracellular Uptake of PNCs. Human monocyte-derived dendritic cells (moDCs) were generated as previously described.[39] Briefly, peripheral blood mononuclear cells (PBMCs) were isolated from buffy coats of healthy human donors upon informed consent using density gradient centrifugation. Subsequently, CD14^{+} monocytes were isolated using the magnetic-activated cell sorting technique and CD14 microbeads. Purified CD14^{+} monocytes were cultured in X-Vivo 15 medium supplemented with L-glutamine, 100 U/mL penicillin, 100 μg/mL streptomycin, 200 U/mL GM-CSF, and 200 U/mL IL-4 for 6

days. After 6 days of culture, immature moDCs were collected and cocultured with 25 μg/mL cy5-labeled OVA PNCs in 8-well chamberslides (ibidi) for 24 h at 37 °C. Nuclei were stained with 2 μg/mL Hoechst 33342 for 30 min, and 4 μg/mL CellMask Orange was added immediately before analysis for plasma membrane staining. In order to evaluate intracellular uptake of OVA PNCs by moDCs, confocal laser scanning microscopy was performed.

In addition, PNC-uptake was quantified using flow cytometry. Therefore, immature moDCs were cocultured with or without various concentrations of cy5-labeled OVA PNCs (7.5/25/100 μg/mL) for 24 h.

Biodegradability of PNCs. The degradation of DQ ovalbumin and CellTracker CMFDA-labeled PNCs was studied with the serine protease trypsin. A concentration of 2 mg/mL trypsin was used and the measurements were performed in PBS buffer. Control measurements of the PNCs in PBS buffer were carried out additionally. The changes in fluorescence intensity were recorded over 1 h at 37 °C. In addition, the biodegradability of PNCs was evaluated using a cell culture system as described above. MoDCs were coincubated with or without 25 μg/mL OVA-DQ PNCs for 24 h, subsequently stained with Hoechst 33342 and CellMask Orange, and analyzed by confocal laser scanning microscopy.

Toxicity Evaluation of PNCs. Human moDCs were cultured in the presence of different concentrations of OVA-cy5 PNCs (2.5/7.5/25/ 100 μg/mL) or without PNCs for 24 h, as described above. Subsequently, moDCs were harvested and incubated with 10 μL of propidium iodide solution for 2 min in order to stain nuclei of dead cells, followed by flow cytometric analysis.

■ RESULTS AND DISCUSSION

Synthesis of Protein Nanocontainers. Protein nanocontainers were synthesized by a polyaddition reaction at the interface of nanodroplets in water-in-oil miniemulsions: the isocyanate groups of the cross-linker 2,4- toluene diisocyanate (TDI) react with the nucleophilic groups of the respective protein (hydroxyls and amines), which results in the formation of water-insoluble nanocontainers with a dense and cross-linked polypeptide shell. FT-IR spectra (see Figure S1 in the Supporting Information) show the characteristic C=O vibration signals of urethane and urea groups (1600−1700 cm^{-1}), indicating the formation of a polyurethane/polyurea shell. SEM and TEM images confirm the core−shell morphology of the obtained PNCs (see Figure 2). For studies of cellular uptake and degradation, the OVA-PNCs were modified with fluorescent dyes cy5, CellTracker CMFDA (CT), and fluorescently labeled ovalbumin (DQ; see below).

The average size of the particles was determined via dynamic light scattering (DLS) and the data is shown in Table 1 (for the

Table 1. Characterization of the Protein Nanocontainers

sample	avg diameter in cyclohexane (nm)	avg diameter in water (nm)	ζ (mV)
OVA-cy5	164	175	−19.3
OVA-DQ	179	173	−16.0
OVA-CT	169	182	−11.5
BSA	186	190	−17.5

size distribution diagrams see Figure S2 in the Supporting Information). PNCs with a diameter of about 170 nm were obtained which were redispersed in aqueous SDS solution. After purification zeta potentials in the range of −10 to −20 mV were measured (see Table 1). The negative values are due to the residual negatively charged anionic surfactant used for stabilization of the particles during the redispersion process.

Encapsulation Efficiency. Encapsulation efficiency is an essential characteristic determining the value of PNCs as drug delivery systems. Therefore, the fluorescent, hydrophilic dye sulforhodamine 101 (SR101) was chosen as a water-soluble drug representative (structure, see Figure S3). The advantage of SR101 is that it does not influence the cross-linking reaction.[25] Notably, SR101 is a relatively small molecule (1.0−1.4 nm),[40] enabling the assessment of the endurance and the shell density. Additionally, due to its fluorescence, the leakage of the nanocontainers can be easily determined by measuring the residual fluorescence intensity in the aqueous phase after removal of the PNCs. The resulting values were correlated with the initial amount of the encapsulated dye. A release over time was also monitored by measuring the change in fluorescence intensity over a period of 22 days ($t = 0$ days is 12 h after redispersion; Figure 3). For both protein nanocontainers very
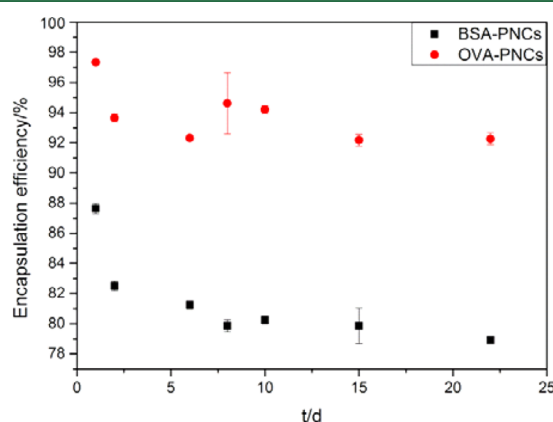

Figure 3. Encapsulation efficiencies and density measurements for PNCs in aqueous dispersion (measured via fluorescence of SR101). Depicted values were determined through two experiments with three single measurements per sample.

high encapsulation efficiencies were detected with 88% for BSA-PNCs and 97% for OVA-PNCs. After redispersion into water, an initial leakage (less than 10%) was detected. However, it reached a plateau after 8 days indicating that in the remaining observation period only very limited release of the encapsulated dye took place.

After 22 days, a total leakage of 8.7% for BSA-PNCs and 5.1% for OVA-PNCs compared to the initial value was observed. Thus, both PNCs, especially OVA-PNCs, can be used to encapsulate hydrophilic molecules stressing the density of the synthesized shell, which impedes the diffusion of the encapsulated compound.

Aggregation Behavior in Blood Plasma. The aggregation behavior of the PNCs in blood plasma was studied via DLS by applying the method after Rausch et al.[41] For light scattering experiments, the protein to PNC ratio was set constant to the in vivo experiments. Figure 4 displays the self-autocorrelation function of the plasma/PNC mixture which can be perfectly described by the so-called force fit. This means that the sum of the individual correlation functions with the known parameters of the two compounds (plasma/PNC) is kept fixed and the intensity contributions for plasma and PNC are the only fit parameters.[41] The result indicates that no sizes larger than the largest size of either plasma or PNCs are formed in the mixture.
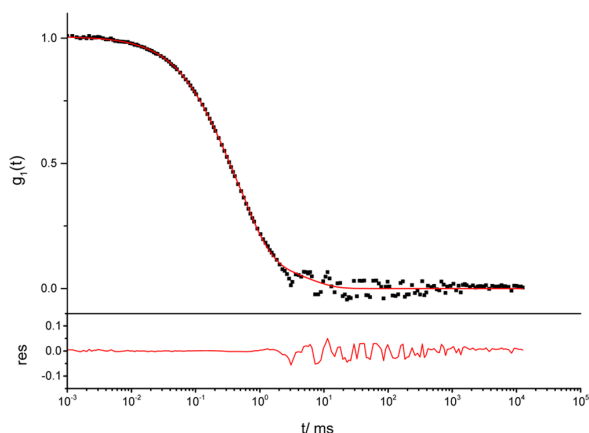
Figure 4. Self-autocorrelation function of the plasma/OVA-nanocapsule mixture. Black squares depict the data points of the plasma/OVA-nanocapsule mixture. The red curve represents the force fit of the mixture and the residue of the fit. Scattering angle 60°, T = 20 °C.

It has to be noted that the presented method is not able to detect changes in the size distribution caused by a monolayer of proteins on the nanoparticle surface.[42]

Intracellular Uptake. Intracellular uptake of OVA-PNCs was analyzed by an in vitro cell culture system using human monocyte-derived Dendritic cells (moDCs) due to their capability to phagocytize particles in the nanometer range. In addition, dendritic cells are specialized antigen presenting cells that play a role in the induction of immune responses.[43] Confocal laser scanning microscopy (CLSM) revealed an intracellular uptake of cy5-labeled OVA-PNCs by moDCs after incubation for 24 h rather than just adherence to the plasma membrane (Figure 5). Furthermore, the uptake of OVA-cy5 by moDCs was quantified using flow cytometry after coincubation for 24 h. Figure 5B shows a concentration-dependent increase from 16.8% of PNC$^+$ moDCs up to 87.4% for 7.5 μg/mL and 100 μg/mL OVA-cy5, respectively, documenting an efficient uptake of PNCs by moDCs in vitro.

Cytotoxicity. In order to examine a potential toxicity of the PNCs, human moDCs were coincubated with OVA-cy5 PNCs with concentrations from 2.5 to 100 μg/mL for 24 h. As can be seen in Figure S5, no cytotoxicity could be detected. This finding suggests that potential toxic substances used for the synthesis of PNCs do not exceed critical concentrations in the resulting nanocontainer dispersion.

Degradation. The degradation of OVA-PNCs was studied with a method resembling physiologically occurring biodegradation. Accordingly, OVA-PNCs were loaded with the fluorescent markers DQ ovalbumin (DQ) and CellTracker CMFDA (CT), which do not emit fluorescence signals in their natural states. DQ ovalbumin is composed of the protein ovalbumin which is conjugated to multiple BODIPY molecules leading to a quenching of fluorescence. Proteolytic degradation of the protein into BODIPY-labeled peptides, however, leads to a restoration of fluorescence.[44] CellTracker CMFDA is a low-molecular weight fluorescent dye of about 465 Da that is colorless and nonfluorescent (structure of CT, see Supporting Information). Upon cleavage of acetate groups by esterases, the resulting product is activated and can emit fluorescence signals. Due to its esterase activity,[45] we chose the serine protease trypsin as the enzyme for the degradation of both substrates, DQ ovalbumin as well as CellTracker CMFDA.

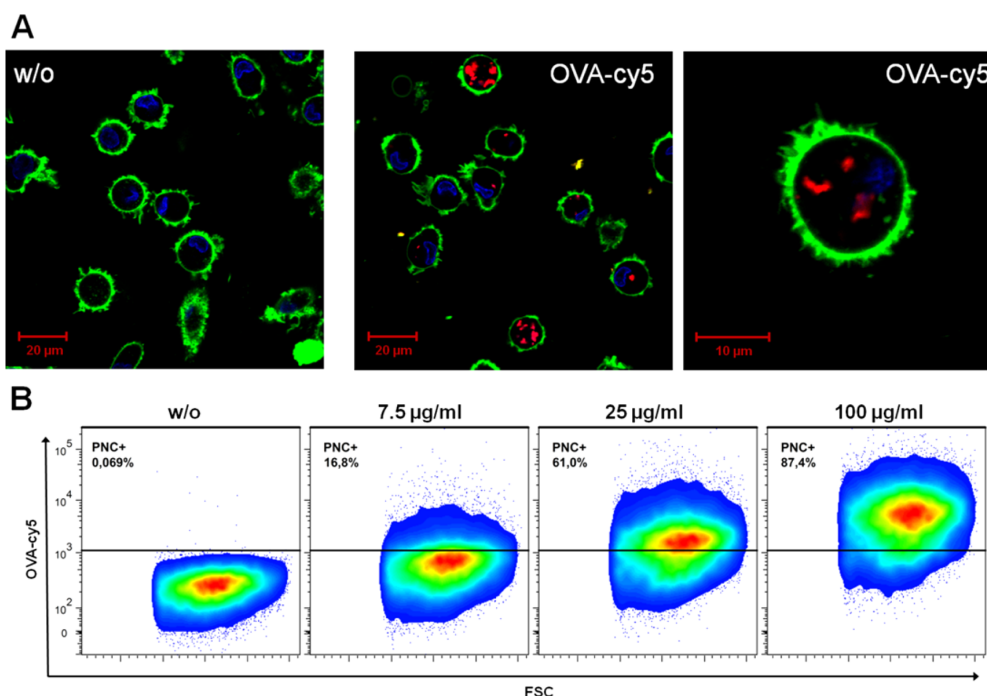**Figure 5.** Confocal laser scanning microscopy images (A) and dot plots obtained by flow cytometry (B) of moDCs incubated without or with different concentration of OVA-cy5 PNCs for 24 h. (A) Plasma membrane was stained with CellMask Orange (green), nuclei were stained with Hoechst 33342 (blue), OVA-PNCs were labeled with cy5 (red). (B) moDCs that incorporated PNCs were quantified and indicated with "PNC+".

The diagrams in Figure 6 show the increase in fluorescence intensity of the aqueous surrounding immediately after addition
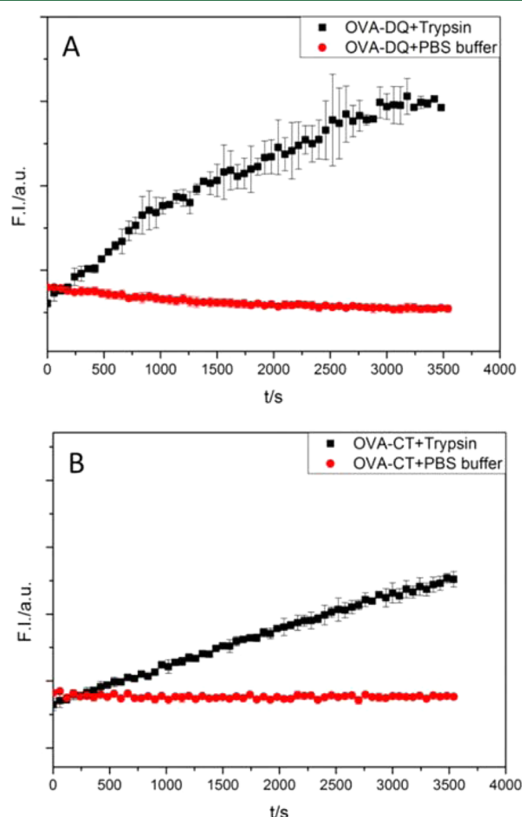

Figure 6. Time-dependent change of fluorescence intensity due to trypsin degradation of DQ ovalbumin (A) and CellTracker-labeled OVA-PNCs (B).

of trypsin both for DQ ovalbumin and CT-modified OVA-PNCs. The controls without trypsin display no change in intensity. Thus, the release of PNC content is dependent on proteolytic degradation of the capsule shell.

These results demonstrate that despite cross-linking of the proteins by urethane and urea linkages and the resulting conformational changes, PNCs are still accessible to proteolytic degradation by proteases.

In order to confirm these observations in an in vitro setting, cell-culture experiments using human monocyte-derived dendritic cells cocultured with OVA-DQ PNCs were performed. This experimental approach revealed an intracellular release of DQ ovalbumin (Figure 7) after coincubation for 24 h. In consequence, ovalbumin nanocontainers inherit the potential to release protein into the cytoplasm, resulting in further degradation into peptides.

CONCLUSION

In the present work, nanocontainers composed of albumin proteins were successfully synthesized using an inverse miniemulsion protocol. The PNCs have a dense shell and possess loading capabilities between 79 and 92% which were determined by encapsulation of the hydrophilic dye SR101 as model substance. PNCs subjected to human blood plasma showed no aggregation behavior. In order to determine the
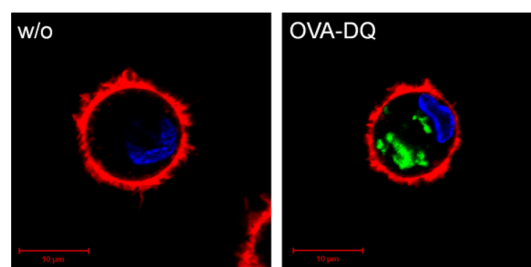

Figure 7. Confocal laser scanning microscopic images of moDCs incubated with (right) or without (left) OVA-DQ PNCs for 24 h (plasma membrane was stained with CellMask Orange (red), nuclei were stained with Hoechst 33342 (blue), and OVA-DQ PNCs were stained with DQ ovalbumin (green)).

biodegradability, PNCs were treated with the serine protease trypsin. A successful degradation was observed through the release of fluorescent markers incorporated both in the PNC shell and in the core. Importantly, PNCs were efficiently taken up by moDCs, resulting in intracellular cleavage of PNCs and subsequent release of protein content. Since the method of synthesis is transferable to other proteins, PNCs bear the potential for the application as an antigen delivery system, for example, in vaccine development.

ASSOCIATED CONTENT

Ⓢ Supporting Information

FT-IR spectra of PNCs, size distribution diagrams of PNCs obtained by DLS. Chemical structures of SR 101 and CellTracker CMFDA. This material is available free of charge via the Internet at http://pubs.acs.org.

AUTHOR INFORMATION

Notes

The authors declare no competing financial interest.

ACKNOWLEDGMENTS

REFERENCES

(1) Karp, J. M.; Langer, R. Development and therapeutic applications of advanced biomaterials. *Curr. Opin. Biotechnol.* **2007**, *18* (5), 454–459.

(2) Landfester, K.; Mailänder, V. Nanocapsules with specific targeting and release properties using miniemulsion polymerization. *Exp. Opin. Drug Delivery* **2013**, *10* (5), 593–609.

(3) Torchilin, V. P., Drug targeting. *Eur. J. Pharm. Sci.* **2000**, *11*, Supplement 2, (0), S81–S91.

(4) Song, Y.; Zhou, Y.; van Drunen Littel-van den Hurk, S.; Chen, L. Cellulose-based polyelectrolyte complex nanoparticles for DNA vaccine delivery. *Biomater. Sci.* **2014**, *2* (10), 1440–1449.

(5) Allen, T. M.; Cullis, P. R. Drug delivery systems: entering the mainstream. *Science* **2004**, *303* (5665), 1818–1822.

(6) Singh, R.; Lillard, J. W., Jr. Nanoparticle-based targeted drug delivery. *Exp. Mol. Pathol.* **2009**, *86* (3), 215–23.

(7) Amass, W.; Amass, A.; Tighe, B. A review of biodegradable polymers: uses, current developments in the synthesis and characterization of biodegradable polyesters, blends of biodegradable polymers and recent advances in biodegradation studies. *Polym. Int.* **1998**, *47* (2), 89–144.

(8) Luckachan, G.; Pillai, C. K. S. Biodegradable polymers: a review on recent trends and emerging perspectives. *J. Polym. Environ.* **2011**, *19* (3), 637−676.

(9) Knop, K.; Hoogenboom, R.; Fischer, D.; Schubert, U. S. Poly(ethylene glycol) in drug delivery: pros and cons as well as potential alternatives. *Angew. Chem., Int. Ed.* **2010**, *49* (36), 6288−6308.

(10) Ulery, B. D.; Nair, L. S.; Laurencin, C. T. Biomedical applications of biodegradable polymers. *J. Polym. Sci., Part B: Polym. Phys.* **2011**, *49* (12), 832−864.

(11) Liu, Z.; Jiao, Y.; Wang, Y.; Zhou, C.; Zhang, Z. Polysaccharides-based nanoparticles as drug delivery systems. *Adv. Drug Delivery Rev.* **2008**, *60* (15), 1650−1662.

(12) Baier, G.; Musyanovych, A.; Dass, M.; Theisinger, S.; Landfester, K. Cross-linked starch capsules containing dsDNA prepared in inverse miniemulsion as "nanoreactors" for polymerase chain reaction. *Biomacromolecules* **2010**, *11* (4), 960−968.

(13) Wurm, F. R.; Weiss, C. K. Nanoparticles from renewable polymers. *Front Chem* **2014**, *2*, 49.

(14) Schoonen, L.; van Hest, J. C. M. Functionalization of protein-based nanocages for drug delivery applications. *Nanoscale* **2014**, *6* (13), 7124−7141.

(15) Gayakwad, S. G.; Bejugam, N. K.; Akhavein, N.; Uddin, N. A.; Oettinger, C. E.; D'Souza, M. J. Formulation and in vitro characterization of spray-dried antisense oligonucleotide to NF-κB encapsulated albumin microspheres. *J. Microencapsulation* **2009**, *26* (8), 692−700.

(16) Wartlick, H.; Spänkuch-Schmitt, B.; Strebhardt, K.; Kreuter, J.; Langer, K. Tumour cell delivery of antisense oligonuclceotides by human serum albumin nanoparticles. *J. Controlled Release* **2004**, *96* (3), 483−495.

(17) Rhodes, B. A.; Zolle, I.; Buchanan, J. W.; Wagner, H. N., Jr Radioactive albumin microspheres for studies of the pulmonary circulation. *Radiology* **1969**, *92* (7), 1453−1460.

(18) Elzoghby, A. O.; Samy, W. M.; Elgindy, N. A. Albumin-based nanoparticles as potential controlled release drug delivery systems. *J. Controlled Release* **2012**, *157* (2), 168−82.

(19) Hawkins, M. J.; Soon-Shiong, P.; Desai, N. Protein nanoparticles as drug carriers in clinical medicine. *Adv. Drug Delivery Rev.* **2008**, *60* (8), 876−885.

(20) Arnedo, A.; Espuelas, S.; Irache, J. M. Albumin nanoparticles as carriers for a phosphodiester oligonucleotide. *Int. J. Pharm.* **2002**, *244* (1−2), 59−72.

(21) Gradishar, W. J. Albumin-bound paclitaxel: a next-generation taxane. *Expert Opin. Pharmacother.* **2006**, *7* (8), 1041−1053.

(22) Landfester, K. Synthesis of colloidal particles in miniemulsions. *Annu. Rev. Mater. Res.* **2006**, *36*, 231−279.

(23) Landfester, K. Polyreactions in miniemulsions. *Macromol. Rapid Commun.* **2001**, *22* (12), 896−936.

(24) Landfester, K.; Musyanovych, A. Hydrogels in Miniemulsions. In *Chemical Design of Responsive Microgels*; Pich, A., Richtering, W., Eds.; Springer: Berlin; Heidelberg, 2011; Vol. *234*, pp 39−63.

(25) Paiphansiri, U.; Dausend, J.; Musyanovych, A.; Mailänder, V.; Landfester, K. Fluorescent polyurethane nanocapsules prepared via inverse miniemulsion: surface functionalization for use as biocarriers. *Macromol. Biosci.* **2009**, *9* (6), 575−584.

(26) Landfester, K.; Musyanovych, A.; Mailänder, V. From polymeric particles to multifunctional nanocapsules for biomedical applications using the miniemulsion process. *J. Polym. Sci., Part A: Polym. Chem.* **2010**, *48* (3), 493−515.

(27) Badiee, A.; Davies, N.; McDonald, K.; Radford, K.; Michiue, H.; Hart, D.; Kato, M. Enhanced delivery of immunoliposomes to human dendritic cells by targeting the multilectin receptor DEC-205. *Vaccine* **2007**, *25* (25), 4757−66.

(28) Bandyopadhyay, A.; Fine, R. L.; Demento, S.; Bockenstedt, L. K.; Fahmy, T. M. The impact of nanoparticle ligand density on dendritic-cell targeted vaccines. *Biomaterials* **2011**, *32* (11), 3094−105.

(29) Pietrzak-Nguyen, A.; Fichter, M.; Dedters, M.; Pretsch, L.; Gregory, S. H.; Meyer, C.; Doganci, A.; Diken, M.; Landfester, K.;

Baier, G. Enhanced in vivo targeting of murine non-parenchymal liver cells with monophosphoryl lipid A functionalized microcapsules. *Biomacromolecules* **2014**, *15* (7), 2378−2388.

(30) Weber, C.; Coester, C.; Kreuter, J.; Langer, K. Desolvation process and surface characterisation of protein nanoparticles. *Int. J. Pharm.* **2000**, *194* (1), 91−102.

(31) Merodio, M.; Arnedo, A.; Renedo, M. J.; Irache, J. M. Ganciclovir-loaded albumin nanoparticles: characterization and in vitro release properties. *Eur. J. Pharm. Sci.* **2001**, *12* (3), 251−259.

(32) Lin, W.; Coombes, A.; Davies, M.; Davis, S.; Illum, L. Preparation of sub-100 nm human serum albumin nanospheres using a pH-coacervation method. *J. Drug Target.* **1993**, *1* (3), 237−243.

(33) Hu, Y.-J.; Liu, Y.; Sun, T.-Q.; Bai, A.-M.; Lü, J.-Q.; Pi, Z.-B. Binding of anti-inflammatory drug cromolyn sodium to bovine serum albumin. *Int. J. Biol. Macromol.* **2006**, *39* (4−5), 280−285.

(34) Santhi, K.; Dhanaraj, S.; Koshy, M.; Ponnusankar, S.; Suresh, B. Study of biodistribution of methotrexate-loaded bovine serum albumin nanospheres in mice. *Drug Dev. Ind. Pharm.* **2000**, *26* (12), 1293−1296.

(35) Simões, S.; Slepushkin, V.; Pires, P.; Gaspar, R.; Pedroso de Lima, M. C.; Düzgüneş, N. Human serum albumin enhances DNA transfection by lipoplexes and confers resistance to inhibition by serum. *Biochim. Biophys. Acta* **2000**, *1463* (2), 459−469.

(36) Brzoska, M.; Langer, K.; Coester, C.; Loitsch, S.; Wagner, T. O. F.; Mallinckrodt, C. v. Incorporation of biodegradable nanoparticles into human airway epithelium cells: in vitro study of the suitability as a vehicle for drug or gene delivery in pulmonary diseases. *Biochem. Biophys. Res. Commun.* **2004**, *318* (2), 562−570.

(37) Tetzner, T. A. D.; Saraiva, N. Z.; Perecin, F.; Niciura, S. C. M.; Ferreira, C. R.; Oliveira, C. S.; Garcia, J. M. The effects of ovalbumin as a protein source during the in vitro production of bovine embryos. *Rev. Bras. Zootec.* **2011**, *40* (10), 2135−2141.

(38) Schlaad, H.; Kukula, H.; Rudloff, J.; Below, I. Synthesis of α,ω-heterobifunctional poly(ethylene glycol)s by metal-free anionic ring-opening polymerization. *Macromolecules* **2001**, *34* (13), 4302−4304.

(39) Fichter, M.; Dedters, M.; Pietrzak-Nguyen, A.; Pretsch, L.; Meyer, C. U.; Strand, S.; Zepp, F.; Baier, G.; Landfester, K.; Gehring, S. Monophosphoryl lipid A coating of hydroxyethyl starch nano-capsules drastically increases uptake and maturation by dendritic cells while minimizing the adjuvant dosage. *Vaccine* **2015**, DOI: 10.1016/j.vaccine.2014.12.072.

(40) Ishizaka, S.; Nakatani, K.; Habuchi, S.; Kitamura, N. Total internal reflection fluorescence dynamic anisotropy of sulforhodamine 101 at a liquid/liquid interface: rotational reorientation times and interfacial structures. *Anal. Chem.* **1998**, *71* (2), 419−426.

(41) Rausch, K.; Reuter, A.; Fischer, K.; Schmidt, M. Evaluation of nanoparticle aggregation in human blood serum. *Biomacromolecules* **2010**, *11* (11), 2836−2839.

(42) Hemmelmann, M.; Mohr, K.; Fischer, K.; Zentel, R.; Schmidt, M. Interaction of pHPMA−pLMA copolymers with human blood serum and its components. *Mol. Pharmaceutics* **2013**, *10* (10), 3769−3775.

(43) Banchereau, J.; Steinman, R. M. Dendritic cells and the control of immunity. *Nature* **1998**, *392* (6673), 245−252.

(44) Santambrogio, L.; Sato, A. K.; Carven, G. J.; Belyanskaya, S. L.; Strominger, J. L.; Stern, L. J. Extracellular antigen processing and presentation by immature dendritic cells. *Proc. Natl. Acad. Sci. U.S.A.* **1999**, *96* (26), 15056−61.

(45) Schwert, G. W.; Neurath, H.; et al. The specific esterase activity of trypsin. *J. Biol. Chem.* **1948**, *172* (1), 221−39.

6.5 Publication 5

Heparin-based nanocapsules as potential drug delivery systems

Published in: *Macromol Biosci*, 2015. **15**(6): p. 765-76.

Heparin-Based Nanocapsules as Potential Drug Delivery Systems

Grit Baier, Svenja Winzen, Claudia Messerschmidt, Daniela Frank,
Michael Fichter, Stephan Gehring, Volker Mailänder, Katharina Landfester*

G. Baier, S. Winzen, C. Messerschmidt, D. Frank, V. Mailänder, K.
Landfester
Max Planck Institute for Polymer Research, Ackermannweg 10,
Mainz 55128, Germany
E-mail: landfester@mpip-mainz.mpg.de
Fax: +49(0)6131 379-370
M. Fichter, S. Gehring
University Medicine of the Johannes Gutenberg University,
Children's Hospital, Langenbeckstr. 1, Mainz 55131, Germany
V. Mailänder
University Medicine of the Johannes Gutenberg University, III.
Medical Clinic, Langenbeckstr. 1, Mainz 55131, Germany

Summary:

Heparin-based nanocapsules (HEP-NCs) with different chain-densities were synthesized using the method of miniemulsion polymerization at the droplets interface leading to nanocapsules with an average diameter of about 180 nm. The developed NCs displayed good stability in physiological solutions regarding the emission of fluorescent dyes or aggregation of NCs. Anti-coagulative properties of heparin-based nanocapsules were demonstrated by measurement of the activated clotting time of human blood. In addition, HEP-NCs were efficiently ingested by different cell lines leading to an accumulation in endosomal compartments.

Author contribution:

- Assistance in the conduction of coagulation experiments
- Proofreading of the manuscript

Heparin-Based Nanocapsules as Potential Drug Delivery Systems

Grit Baier, Svenja Winzen, Claudia Messerschmidt, Daniela Frank,
Michael Fichter, Stephan Gehring, Volker Mailänder, Katharina Landfester*

Herein, the synthesis and characterization of heparin-based nanocapsules (NCs) as potential drug delivery systems is described. For the synthesis of the heparin-based NCs, the versatile method of miniemulsion polymerization at the droplets interface was achieved resulting in narrowly distributed NCs with 180 nm in diameter. Scanning and transmission electron microscopy images showed clearly NC morphology. A highly negative charge density for the heparin-based NCs was determined by measuring the electro-kinetic potential. Measuring the activated clotting time demonstrated the biological intactness of the polymeric shell. The ability of heparin-based NCs to bind to antithrombin (AT III) was investigated using isothermal titration calorimetry and dynamic light scattering experiments. The chemical stability of the NCs was studied in physiological protein-containing solutions and also in medically interesting fluids such as sodium chloride 0.9%, Ringer's solution, and phosphate buffer saline using dynamic light scattering and measuring the fluorescence intensity. The impressive uptake of NCs in different cells was confirmed by fluorescence-activated cell sorting, confocal laser scanning microscopy, and transmission electron microscopy. The low toxicity of all types of NCs was demonstrated.

Heparin based nanocapsules
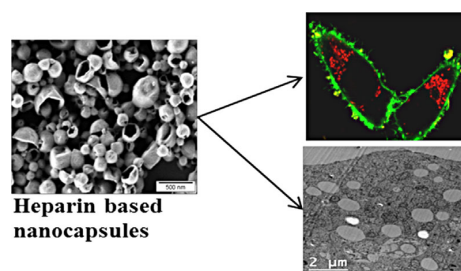
1. Introduction

Promising methods to synthesize nanocarriers with stealth effects or prolonged circulating times are the modification of their surfaces with flexible, highly hydrophilic polymers, such as poloxamers, or polysaccharides. Besides that, the grafting, coating, or binding of complement inhibitors on the nanocarrier's surface serves as alternative methods to create a system with stealth effect properties.[1–3]

Several manuscripts describe heparin as a compound with stealth effect properties in combination with antithrombogenic characteristics and as potential drug release systems. Bajpai et al. studied the controlled release of heparin from cross-linked starch microspheres. They

G. Baier, S. Winzen, C. Messerschmidt, D. Frank, V. Mailänder, K. Landfester
Max Planck Institute for Polymer Research, Ackermannweg 10, Mainz 55128, Germany
E-mail: landfester@mpip-mainz.mpg.de
Fax: +49(0)6131 379-370
M. Fichter, S. Gehring
University Medicine of the Johannes Gutenberg University, Children's Hospital, Langenbeckstr. 1, Mainz 55131, Germany
V. Mailänder
University Medicine of the Johannes Gutenberg University, III. Medical Clinic, Langenbeckstr. 1, Mainz 55131, Germany

investigated different parameters on heparin release such as the effect of percentage of loading, starch, cross-linker (epichlorohydrin), pH, physiological fluid, and the effect of α-amylase on the degradation of these swellable starch microspheres.[4] Wang et al. studied the entrapping of the hydrophobic agent taxol in heparin–PEG–folate nanoparticles and their cellular specific targeting in KB-3-1 cells, a folate receptor overexpressing cell line.[5] Socha et al. studied the release of insulin-loaded particles with a heparin-coated surface, characterized these particles *in vitro* (diameter, zeta potential, encapsulation efficiency, and release kinetics) and studied the pharmacokinetics after intravenous injection.[6] They found an increase in the elimination half-life of insulin showing a limitation in recognition by the mononuclear phagocytosis system *in vivo*. Passirani et al. compared nanoparticles bearing heparin or dextran covalently bound to the surface. They observed a stealth effect of the heparin particles' which was increased by its inhibition of complement activation.[7,8]

Heparin is a polysaccharide consisting of a pentasaccharide sequence. The abundance of sulfate groups on glucosamine residues leads to a high negative charge density. This high negative charge density of the heparin molecules is crucial for their anticoagulant properties. Heparin is widely used in acute thrombotic diseases, in vascular disease, and in cardiac surgery. The well investigated antithrombogenic activity is mediated by binding to antithrombin (AT III), a serine protease-inhibitor in plasma. This neutralizes thrombin ultimately preventing the cleavage of fibrinogen to fibrin. Moreover, the interaction between heparin and AT III is highly specific, and this affinity of heparin to AT III is influenced by strongly negative ions.[9] Heparin binds to many naturally occurring neutral and acidic proteins peptides. This interaction together with the well-known anticoagulant activity of heparin could be exploited for developing heparin-containing materials. In one study, good anticoagulant action, better cell adhesion properties, lower cell toxicity, and shortened clotting time of the heparin-grafted hybrid materials was observed, compared with heparin itself.[10] Ran et al. synthesized a heparin-like structured macromolecule for the modification of non-coagulating biomaterials.[11] Another publication showed that a drug-eluting coating, consisting of heparin-loaded microspheres was effective in suppressing platelet adhesion, the film showed better anticoagulation, better biocompatibility with human umbilical veins endothelial cells (HUVECs), and an improvement in hemocompatibility.[12] The effect of functionalization of poly(lactide-*co*-glycolide) (PLGA) nanoparticles by heparin-conjugated Pluronic on tumor targeting was studied in *in vitro* and *in vivo* experiments.[13] Recently, heparin-coated silica nanoparticles were used for an efficient binding to antithrombin as an anticoagulant drug delivery system.[14]

Synthesizing nanocapsules (NCs) using the inverse miniemulsion process allows one to obtain core-shell nanocarriers in a size range between 100 and 500 nm with defined properties like average size, morphology, and surface functionality.[15] Under carefully chosen conditions of mini-emulsification, it is possible to encapsulate efficiently fragile molecules. The high stability of the system allows performing reactions inside the droplets and at their interface.[16,17]

Up to now, heparin war only used as shell material of *micro*capsules or as modification of *nano*particles. NCs consisting of heparin-based shell and an aqueous core would be highly advantageous since (i) hydrophilic active components can be encapsulated; (ii); due to the size an injection in blood would possible; and (iii) heparin would serve as functional shell material.

In the current publication, heparin-based NCs as potential drug delivery were obtained with the inverse miniemulsion technique. The activated clotting time (ACT) demonstrated the biological intactness of the polymeric shell. The chemical stability of the NCs was studied in various physiological and biological fluids. The binding properties of AT III to heparin-based NCs were studied using isothermal titration calorimetry (ITC) and dynamic light scattering (DLS). The uptake of NCs in different cells was confirmed by fluorescence-activated cell sorting (FACS), confocal laser scanning microscopy (CLSM), and by transmission electron microscopy (TEM). The low toxicity of all types of NCs was investigated by a MTS assay.

2. Experimental Section

2.1. Chemical Reagents

All chemicals or materials were used without further purification, and sterile water (Ampuwa®) was used through all experiments. Heparin-Natrium® (12–15 kDa) was purchased from B. Braun Melsungen AG. The magnesium- and calcium-free phosphate buffered solution (PBS buffer) was purchased from Gibco, Germany. Hexanediol, 2,4-toluene diisocyanate (TDI) and cyclohexane (>99.9%) were from Sigma–Aldrich. The oil soluble block copolymer surfactant poly[(ethylene-*co*-butylene)-*b*-(ethylene oxide)], P(E/B-*b*-EO), was synthesized according to the procedure described in the literature.[18] The fluorescent dye sulforhodamine 101 (SR101) was from BioChemica. AT III (Kybernin® P500) was purchased from CSL Behring GmbH. Sodium chloride (NaCl 0.9%) and the Ringer's solution were from Fresenius Kabi. The magnesium- and calcium-free phosphate-buffered solution (PBS) was from Invitrogen. The anionic surfactant sodium dodecylsulfate (SDS) was purchased from Fluka.

2.1. Preparation of the Nanocapsules

Heparin and hexanediol-based (served as control) NCs were synthesized via interfacial polyaddition reaction using the inverse

miniemulsion technique.[19–21] Briefly, an aqueous phase consisting of heparin (5 000 IE · mL^{-1}, 12–15 kDa), 1 000 mg heparin/400 mg PBS buffer (HEP-001) or 700 mg heparin/700 mg PBS buffer (HEP-002) or hexanediol 142 mg/1 400 mg PBS buffer (HEX, control sample) was mixed with 1 mg sulforhodamine SR101 (M_w = 606.71 g · mol^{-1}). The amphiphilic block copolymer P(E/B-b-EO) (100 mg) was dissolved in 7.5 g cyclohexane and mixed with the previously prepared aqueous solution. The obtained emulsion was stirred over 1 h at 25 °C and then ultrasonicated for 180 s at 90% amplitude in a pulse regime (20 s sonication, 10 s pause) using a Branson Sonifier W-450-Digital and a ½″ tip under ice cooling to prevent the evaporation of the solvent. A solution consisting of 5.0 g cyclohexane, 30 mg P(E/B-b-EO), and 100 mg of TDI was added dropwise over 5 min to the earlier prepared emulsion maintaining the temperature at 25 °C. The reaction proceeded for 24 h at 25 °C under stirring. After the synthesis, the NCs were purified by repetitive centrifugation (Sigma 3k-30, RCF 3300, 20 min, twice) in order to remove the residues of P(E/B-b-EO) and the pellet was re-suspended in cyclohexane. Afterwards, the NCs were transferred into an aqueous phase using the following procedure: 1 g (polymer solid content 3%) of the NC dispersion in cyclohexane was mixed with 5 g SDS aqueous solution (0.1 wt.-%) and kept under mechanical stirring for 24 h at 25 °C. Then, the samples were treated for 20 min in a sonication bath (power 50%, 25 kHz). After redispersion, the NCs were dialyzed (MWCO: 12 000 g · mol^{-1}) for 12 h in order to remove residues of SDS.

2.2. Stability of Nanocapsules in Biological Media

These experiments were performed to ensure that the NCs' stability was not affected by the presence of the three different media. The colloidal and chemical stability of heparin and hexanediol NCs was studied in sodium chloride (NaCl) 0.9%, Ringer's solution, and DPBS buffer. Therefore, the NC dispersion was centrifuged, the supernatant was removed, and the pellet was redispersed either in NaCl 0.9%, in Ringer's solution or in DPBS buffer. In a first experiment, all obtained dispersions were investigated in terms of size and size distribution using dynamic light scattering (DLS). In a second experiment, the release of the encapsulated fluorescent dye SR101 out of the NCs was studied by measuring the fluorescence intensities in the supernatant. For these experiments, 500 μL of NCs (1 · 10^{10} NCs per mL, solid content 1%) were mixed with 500 μL of NaCl 0.9%, Ringer's solution, or DPBS, incubated at 37 °C for 24 h under gentle shaking conditions, centrifuged (Sigma 3k-30, RCF 1467, 20 min) and the fluorescence intensities in the supernatant were measured.

2.3. Isothermal Titration Calorimetry (ITC) Experiments

The calorimetric measurements were performed using a MicroCal VP-ITC (GE Healthcare, Piscataway, USA). In an experiment, 250 μL of an AT III solution (9.5 g · L^{-1}, 0.163 mM in water) was titrated to a dispersion of NCs (0.5–0.55 g · L^{-1}, 6.5 · 10^{-6} mM in water). The experimental temperature was kept constant at 25 °C. Additionally, the same amount of AT III solution was titrated into pure water to determine the heat of dilution for reference. The number and

injected volume of the titration steps were the same for all measurements (25 × 10 μL). The interval between injections was set to 300 s. Prior to the main titration steps, an initial injection of 1.5 μL was performed to eliminate deviations due to diffusion. Accordingly, the area of the first peak was not considered in the data evaluation. The integrated heats of dilution were then subtracted from the integrated heats of the adsorption experiments.

2.4. Determination of the Activated Clotting Time (ACT)

The biologic activity of the heparin-based NCs was determined with a Medtronic ACT II™ device (Automated Coagulation Timer II, Medtronic Hemotec Inc., Engelwood, CO, USA). The activated clotting time (ACT) test is commonly used to monitor the effect of high-dose heparin, e.g., in patients undergoing surgery that requires intense anticoagulant administration.[22] The LR-ACT cartridges were purchased from Medtronic (Cat-N# 402-01) and kaolin was used as the activating agent. The measurement endpoint was the time (in seconds) until detection of clot formation. Whole blood samples from healthy adults aged 21–45 years were collected after obtaining informed consent. The double-tube LR-ACT Cartridges (Low Range Activated Clotting time Cartridges) were loaded with a total of 1 mL blood (0.5 mL per channel). Each measurement was performed at 37 °C with a capsule/blood ratio of 1/100 and repeated three times resulting in six ACT values/sample. Hexanediol-based NCs served as control.

2.5. Cell Culture and CLSM Studies

The cellular uptake of the NCs was confirmed by confocal laser scanning microscopy (CLSM) and flow cytometry. For these experiments, human cervix carcinoma cells (HeLa cells), estrogen receptor-positive breast cancer cells (Michigan Cancer Foundation-7 [MCF-7] cells) and prostate cancer cells (PC3)[23–25] were used. HeLa cells and MCF-7 cells were kept in Dulbecco's Modified Eagle Medium (DMEM, Invitrogen, Germany). Cultivating MCF-7 cells additionally affords the supplementation of 10 μg · mL^{-1} human recombinant insulin (Gibco, Germany) and 1 mM sodium-pyruvate (Sigma–Aldrich, Germany). PC3 cells were kept in Roswell Park Memorial Institute Medium (RPMI, Invitrogen, Germany) with 1 mM sodium-pyruvate and 2 mM GlutaMAX (Invitrogen, Germany). All cells were supplemented with 10% fetal calf serum (FCS), 100 units penicillin and 100 mg · mL^{-1} streptomycin, (all from Invitrogen, Germany). Cells were grown in a humidified incubator at 37 °C and 5% CO$_2$. On the day prior to the experiments, the adherent cells were detached by trypsin (Gibco, Germany) and seeded in a FCS-supplemented medium at a density of 50 000 cells · cm^{-2} in 6-well plates (Greiner, Germany) for flow cytometry and 10 000 cells · cm^{-2} in ibiTreat μ-slides (IBIDI, Germany) for CLSM analysis. On the following day, the NCs (75 μg · mL^{-1}, labeled with SR101) were added to the medium in presence of 10% FCS without using a transfection agent. Incubation periods had been carried out in a humidified incubator (37 °C, 5% CO$_2$). For CLSM, the cells were analyzed on the ibiTreat μ-slides and washed twice with phosphate buffered saline without calcium and magnesium (PBS, Invitrogen, Germany) before membrane staining and analysis. For

flow cytometry analysis, six-well plates were used; the cells were washed with PBS, trypsinized, centrifuged (3 min, 3 000 rpm = 956 $\times$ g [m $\cdot$ s^{-2}]) and finally resuspended in PBS. The cell viability was confirmed by a MTS assay (CellTiter 96$^{\circledR}$ Aqueous One Solution Cell Proliferation Assay, Promega, USA), performed according to the product insert in 96-well assay plates (Corning Incorporated costar$^{\circledR}$ 3603, Corning, Germany). Each well was seeded with 10 000 cells the day before the experiment (addition of NCs: 75 μg $\cdot$ mL^{-1}). Absorbance (490 nm) of this assay was measured with a microplate reader (Infinite M1000, Tecan, Switzerland).

2.6. Transmission Electron Microscopy (TEM)

To visualize the NCs at a high resolution in their cellular environment, we applied transmission electron microscopy of HeLa cells treated with 150 μg $\cdot$ mL^{-1} of HEP-001 NCs for 24 h. Before treatment, cells were left to grow for 48 h after seeding onto sapphire discs (diameter 3 mm) at a density of 15 000 cells $\cdot$ cm^{-2} in a 24-well plate. At the end of the incubation period, cells were fixed by means of high-pressure freezing using a Compact 01 HPF machine (Wohlwend GmbH, Switzerland). Subsequent freeze-substitution was conducted using a Leica EM AFS 2 device (Leica Microsystems, Germany). The substitution medium contained acetone p.a., 0.2% osmium tetroxide, 0.1% uranyl acetate, and 5% water and was pre-cooled to $-90\,^{\circ}$C before the samples were added. After freeze-substitution, the samples were washed twice with acetone p.a. and finally embedded into EPON 812 resin. Ultrathin sectioning of the embedded samples was performed using a Leica Ultracut UCT (Leica Microsystems, Germany) and a diamond knife.

Examination of thin sections was conducted using a FEI Tecnai F20 transmission electron microscope (FEI, USA) operated at an acceleration voltage of 200 kV. Bright field images were acquired using a Gatan US1000 slow scan CCD camera (Gatan Inc., USA).

2.7. Characterization of the Nanocapsules

The average size and the size distribution of the NCs were measured by means of dynamic light scattering (DLS) in diluted solutions (0.05 g $\cdot$ L^{-1}). DLS experiments were performed on an ALV instrument consisting of a goniometer and an ALV-5000 multiple-tau full-digital correlator with 320 channels. A helium–neon laser (JDS Uniphase with a single mode intensity of 25 mW operating at a laser wavelength of $\lambda_0 = 632.8$ nm) was used as the light source. All samples were filtered through polyethersulfone filters with a pore size of 5 μm (Chromafil Xtra PES-500/25, Macherey-Nagel, Germany) prior to the measurements. The zeta potential of the NCs was measured in 10^{-3} M potassium chloride solution with a Zeta Nanosizer (Malvern Instruments, U.K.) at 20 $^{\circ}$C. Scanning electron microscopy (SEM) studies were done on a field emission microscope (LEO [Zeiss] 1530 Gemini, Oberkochen, Germany) working at an accelerating voltage of 170 V. Generally, the samples were prepared by diluting the capsule dispersion in cyclohexane or demineralized water (for redispersed samples) to about 0.01% solid content. Then, one droplet of the sample was placed onto a silica wafer and dried under ambient conditions overnight. No additional contrast agent was applied. Additionally, NCs were embedded into EPON resin for examination by TEM operated at an acceleration voltage of 200 kV

(FEI Tecnai F20). For contrast enhancement, the capsule suspension was incubated with OsO$_4$ (aq) and then centrifuged to create a pellet. After discarding the supernatant and two washing steps with distilled water, an alcohol dilution series was performed. Finally, the sample was embedded into EPON 812 resin and cut into 60 nm slices using an ultramicrotome (Leica Ultracut UCT). The solid content of the capsule dispersion was measured gravimetrically.

2.8. Confocal Laser Scanning Microscopy and Flow Cytometry

The confocal laser scanning microscopy (CLSM) experiments were performed to determine the intracellular localization of the NCs. The images were taken using a commercial setup (LSM SP5 STED Leica Laser Scanning Confocal Microscope, Leica, Germany), consisting of an inverse fluorescence microscope DMI 6000 CS, equipped with a multi-laser combination, and five detectors operating in the range of 400–800 nm. A HCX PL APO CS 63x/1.4–0.6 oil-immersion objective was used in these studies. For the excitation of the NCs, a DPSS $\lambda = 561$ nm ($\approx$20 mW) laser was used. The emission was detected at 580–620 nm. The NCs are pseudocolored in red in the obtained images (see below). The cell membrane was stained with CellMask$^{\text{TM}}$ Deep Red plasma membrane stain (1.25 μg $\cdot$ mL^{-1}, Invitrogen, Germany). In these images, the cell membrane is shown pseudo-colored in green (excited with HeNe laser: $\lambda = 633$ nm $\sim$10 mW and detected at 660–750 nm).

The quantification of the NCs' cellular uptake was analyzed by flow cytometry. Measurements were performed with a CyFlow ML using FlowMax 2.57 software (Partec, Germany). SR101-labeled heparin NCs were excited with a 561 nm laser, and the fluorescence was detected with a 610–630 nm band pass filter in the FL5 channel. For the analysis, cells were selected on a forward scatter/sideward scatter plot (488 nm laser), thereby excluding cell debris. These gated events were then further analyzed using the FL5 channel (FCS Express, De Novo Software, USA). The median in the FL5 was determined from 1D histograms. This corresponds to the amount of NCs taken up or associated with individual cells. All values are triplicates with the standard deviation and confirmed in two independent experiments with the two identically synthesized heparin NCs (HEP-001 and HEP-002).

3. Results and Discussion

The formation of polymeric NCs was achieved through a cross-linking reaction between the OH groups of the hydrophilic heparin or hexanediol and the NCO groups of 2,4-toluene diisocyanate (TDI), resulting in a polyurethane shell. The reaction took place at the interface of mini-emulsion droplets and highly cross-linked NCs were obtained. In order to monitor the release from the NCs, the fluorescent dye SR101 was encapsulated inside each of the NCs. The formulation process of the NCs is shown in Figure 1. In all cases, no precipitation, coagulation, or flocculation of the NCs was observed throughout the preparation of the NCs.
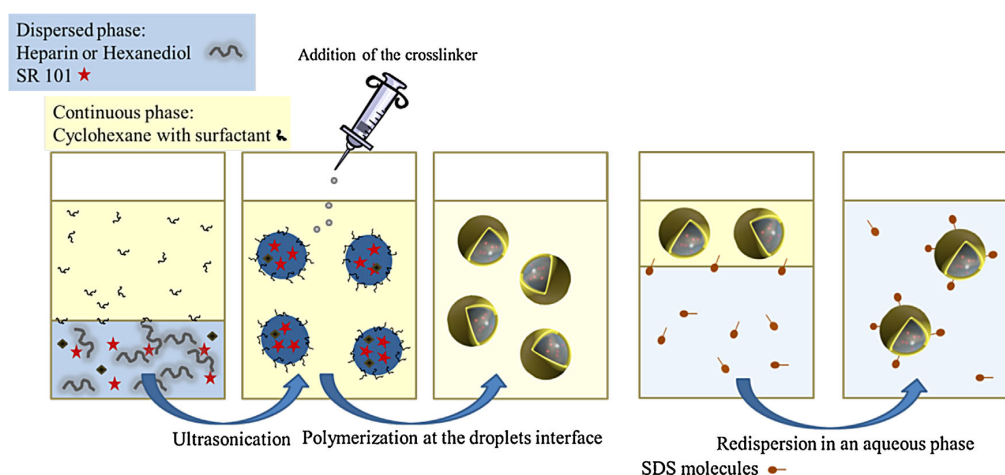
Figure 1. Schematic illustration of the NCs formation through interfacial polyaddition reaction in the inverse miniemulsion system.

After the NC formation and their redispersion in aqueous SDS solution, the size, size distribution, and morphology of the NCs were studied using DLS and SEM. The average size of the initial droplets/final NCs in the cyclohexane phase and later on in the water phase was found to be around 180 nm (in diameter), with a standard deviation of about 27% independent of the used shell material. The SEM and TEM images (see Figure 2) show a clear NC morphology in all cases. The collapse of the NCs' wall (like deflated balls) as detected by SEM is due to the electron beam. The average NC size in the SEM and TEM images is slightly smaller than that measured by DLS, as a result of the drying effects.
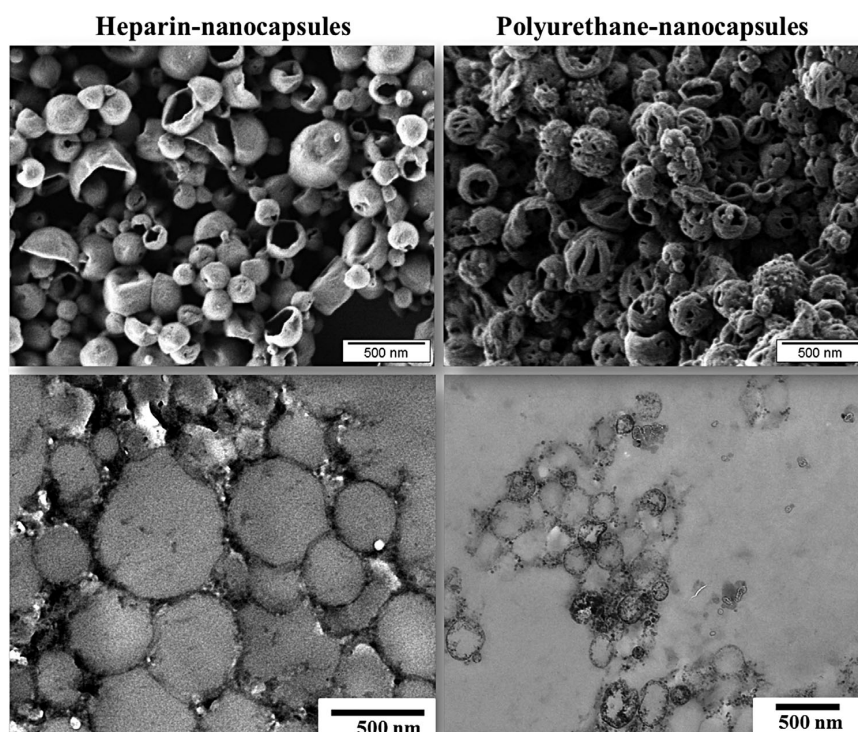

Figure 2. SEM (first row) and TEM images (second row) of cross-linked heparin (HEP-001) and hexanediol (HEX, control sample) NCs.

The zeta potentials (measured in 10^{-3} M potassium chloride solution, pH 6.8) of the redispersed and purified heparin-based and hexanediol-based NCs are negative (HEP-001-NCs: -51 mV, HEP-002-NCs: -48 mV, and HEX-NCs: -27 mV) due to the presence of sulfate groups on the surface NCs. The zeta potential of the heparin-based NCs is much more negative since sulfate groups originate from SDS and heparin.

3.1. Stability of Nanocapsules in Biological Media

In the view of potential biomedical applications, the stability of NCs was analyzed in 0.9% NaCl solution, Ringer's solution, and DPBS buffer solution. The experiments were performed to ensure that the NCs' stability is not affected by the presence of the three different media. Sodium chloride (NaCl) was chosen because it is often used in various areas of biology and biochemistry experiments because of its isotonic character. Ringer's solution is isotonic compared to extracellular body fluid and is intended for intravenous administration. The experiments with DPBS were performed because this buffer is commonly used as a minimal buffer in biological applications.

On one hand, the NCs that were treated with the different solutions were analyzed in terms of size and size distribution by DLS. The obtained results revealed that the NCs are basically stable in all investigated media. A small increase of the sizes (20 nm in diameter) and size distributions (3%) was observed, but those variations can be assigned to the preparation method. Nevertheless, no aggregate formation or precipitation was visible.

On the other hand, the release of SR 101 from the NCs which is related to the stability of the NCs' shell was studied by fluorescence spectroscopy. The measured fluorescence intensities of the supernatant that were obtained after precipitation of the NCs treated with 0.9% NaCl, Ringer's solution, and DPBS were compared with the non-treated ones. The results are triplicates and show the fluorescence intensities of the treated and non-treated (NCs in water phase, dark grey column) NC samples, see Figure 3. The fluorescence signals measured in the supernatant for the NaCl 0.9%, Ringer's solution, and DBPS are almost identical as the ones for the control samples, indicating the high stability of all polymeric NCs under the investigated conditions (incubation time 24 h at 37 °C).

3.3. Interaction of Heparin-Based Nanocapsules With AT III: ITC and DLS Experiments

To determine the interaction of heparin groups of the surface of the heparin NCs with AT III, ITC binding experiments were carried out with the NCs containing two different amounts of heparin (HEP-001 with a high
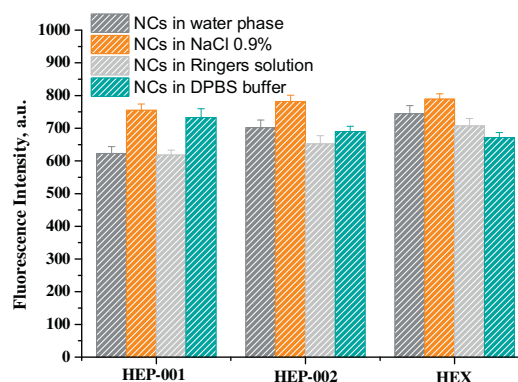

Figure 3. Amount of fluorescent dye SR101 released from the NCs after incubation for 24 h at 37 °C in 0.9% NaCl solution, Ringer's solution, and DPBS buffer.

heparin chain density and HEP-002 with a low chain density) as well as the hexanediol NCs (HEX) as control. A solution of AT III was titrated into dispersions of the different NCs and the resulting heat change monitored overtime (Figure 4A). The change in heat was then integrated and related to the concentration of titrate (Figure 4B). To correct for the heat of the AT III dilution, data from a reference titration of AT III into water were subtracted from each measurement.

For both types of heparin NCs, an exothermic interaction with AT III is observed, because the released heat is much higher than the heat of dilution. The initial heat release during the first titration steps differs between the two capsule types, whereas toward the end of the titration, both isotherms follow the same trend. In contrast to the heparin NCs, the titration of hexanediol NCs looks very similar to the reference measurement, resulting in an adsorption isotherm not showing any heat of interaction. This clearly indicates that AT III is not, or only very poorly, interacting with the hexanediol NCs.

The titration isotherms of the heparin NCs reveal a similar curve progression, indicating a two-step interaction process. The initial disparity of the two different capsule systems could be the reason of a fast unspecific adsorption of AT III onto the NCs, which seems to be stronger when less heparin is present on the capsule surfaces. In addition, there is a second interaction process visible, which is similar for the different heparin contents. This process most likely represents the binding of AT III to the pentasaccharide region of heparin that was identified as the interaction domain.[26] The binding of AT III to heparin normally takes place in two stages which involve a conformational change of AT III.[27] However, these two stages cannot be resolved in the ITC experiments. A reason for this might be that the heat generated or absorbed by the conformational change is too small to be detected in these measurements. Additionally, it
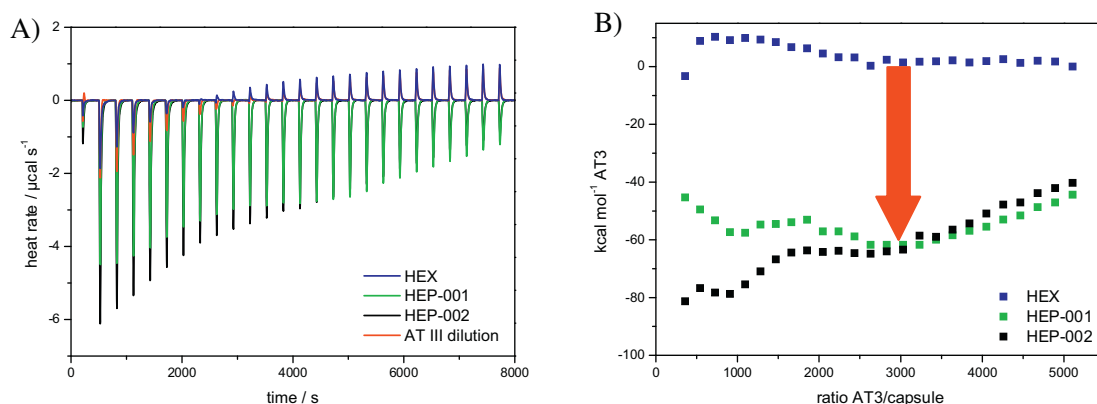
Figure 4. ITC data for the interaction of heparin and hexanediol NCs with AT III. A) Raw heat rate; negative peaks represent exothermic processes. B) Integrated heat of each peak (titration isotherms); the red arrow indicates the difference between heparin and hexanediol NCs.

Table 1. Investigation of size and zeta potential of nanocapsules before and after interaction with AT III.

Capsule	−AT III		+AT III	
	Zeta-potential [mV]	Diameter [nm]	Zeta-potential [mV]	Diameter [nm]
HEX	−27	180 ± 18	−30	150 ± 15/600 ± 60
HEP-001	−51	170 ± 17	−4	800 ± 80
HEP-002	−48	180 ± 18	−32	660 ± 66

is not clear which parts of the heparin molecules are actually present on the capsule surface, so that the binding process might not proceed as expected.

Still, it is obvious that the heparin NCs possess a biological activity in contrast to the hexanediol-based NCs. Indeed, the different amounts of heparin used in the NC synthesis did not lead to a significant change in the heat measurements, but this might be based on sensitivity issues as the difference is only small compared to the hexanediol NCs.
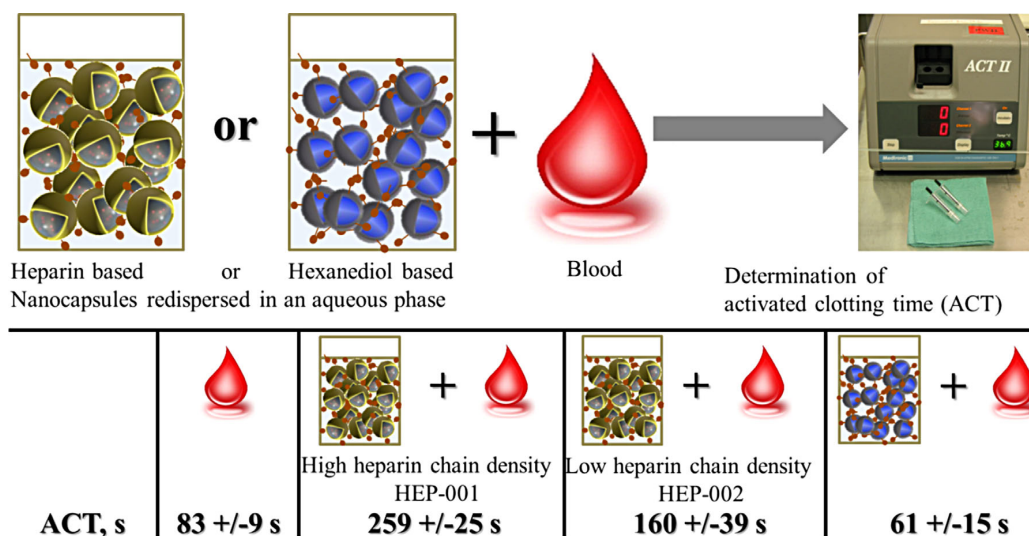

Figure 5. Scheme of the experimental setup and ACT-results of heparin-based NCs, of hexanediol-based NCs (control sample), and of blood.
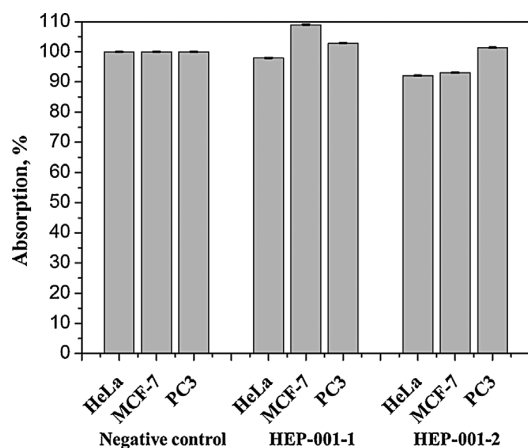
Figure 6. MTS assay: absorption of HeLa, MCF-7 and PC3 cells without heparin NCs (negative control, NC) and incubated with HEP-001 and HEP-002.

To support the information obtained via ITC and to distinguish between the two types of heparin NCs, DLS and zeta potential measurements were performed before and after the interaction of the NCs with AT III. The results are presented in Table 1.

Concerning the size and zeta potential data of the hexanediol NCs as a control, it is quite obvious that no strong interaction with AT III is taking place. There is no change of the zeta potential, which means that the surface of the NCs is not or only sparely covered with proteins. The light scattering data also reveal a diffusing process that falls within the size range of the NCs. A second type of diffusing process with a diameter of around 600 nm can be assigned to some aggregates formed, though it cannot be distinguished between aggregates only formed of NCs and AT III-containing ones. Those results match with the previously obtained information. The heparin NCs clearly show signs of AT III adsorption, which was already suggested by the ITC
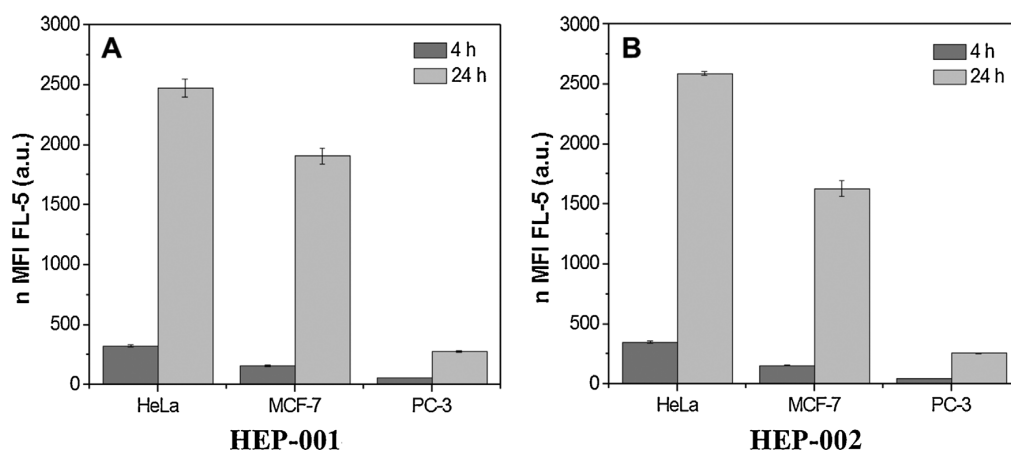
Figure 7. Flow cytometric analysis of HeLa, MCF-7, and PC3 cells after 4 h (gray) and 24 h (lighter gray), HEP-001 (A) and HEP-002 (B). The normalized median (nanocapsules · per mL) of fluorescence intensity (n MFI) is shown.
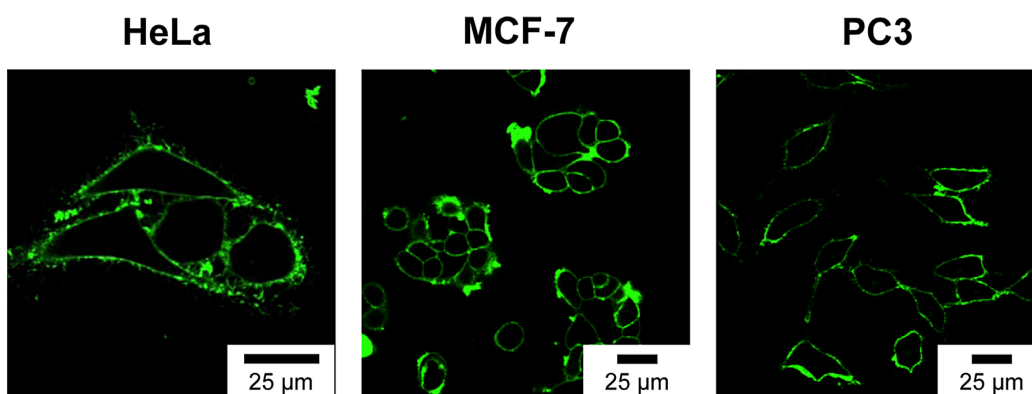
Figure 8. CLSM images: negative controls (without NCs) of HeLa, MCF−/ and PC3 cells after 24 h. The cell membrane is pseudocolored in green (CellMask™ Deep Red).

772

Macromolecular
Journals

Macromol. Biosci. **2015**, *15*, 765–776
© 2015 WILEY-VCH Verlag GmbH & Co. KGaA, Weinheim

Materials
Views
www.MaterialsViews.com

Figure 9. CLSM images of (a) HeLa, (b) MCF-7, and (c) PC3 cells after incubation with HEP-001-1 (upper row) and HEP-001-2 (lower row) for 4 and 24 h. Cell membranes (CellMask™ Deep Red) are pseudocolored in green and heparin NCs (SR 101) in red.

data. Changes in size and zeta potential can even resolve the influence of heparin content. The zeta potential of both NCs increases significantly, indicating coverage with AT III. As AT III is only slightly negatively charged at pH 7, the higher zeta potential of HEP-001 implies a higher amount of AT III adsorbed to the surface. Those data are supported by the DLS measurements, showing a higher diameter for the NCs with higher heparin content. So, clearly the capsule's potency of interaction with AT III can be tuned by the amount of heparin used in the synthesis.

3.4. Determination of the Activated Clotting Time (ACT)

The activated clotting time was studied to confirm biological active residues of heparin chains attached onto the NCs surface. For that reason, the two types of heparin NCs with different heparin chain densities already analyzed with ITC (HEP-001, high chain density; HEP-002, low chain density) were exami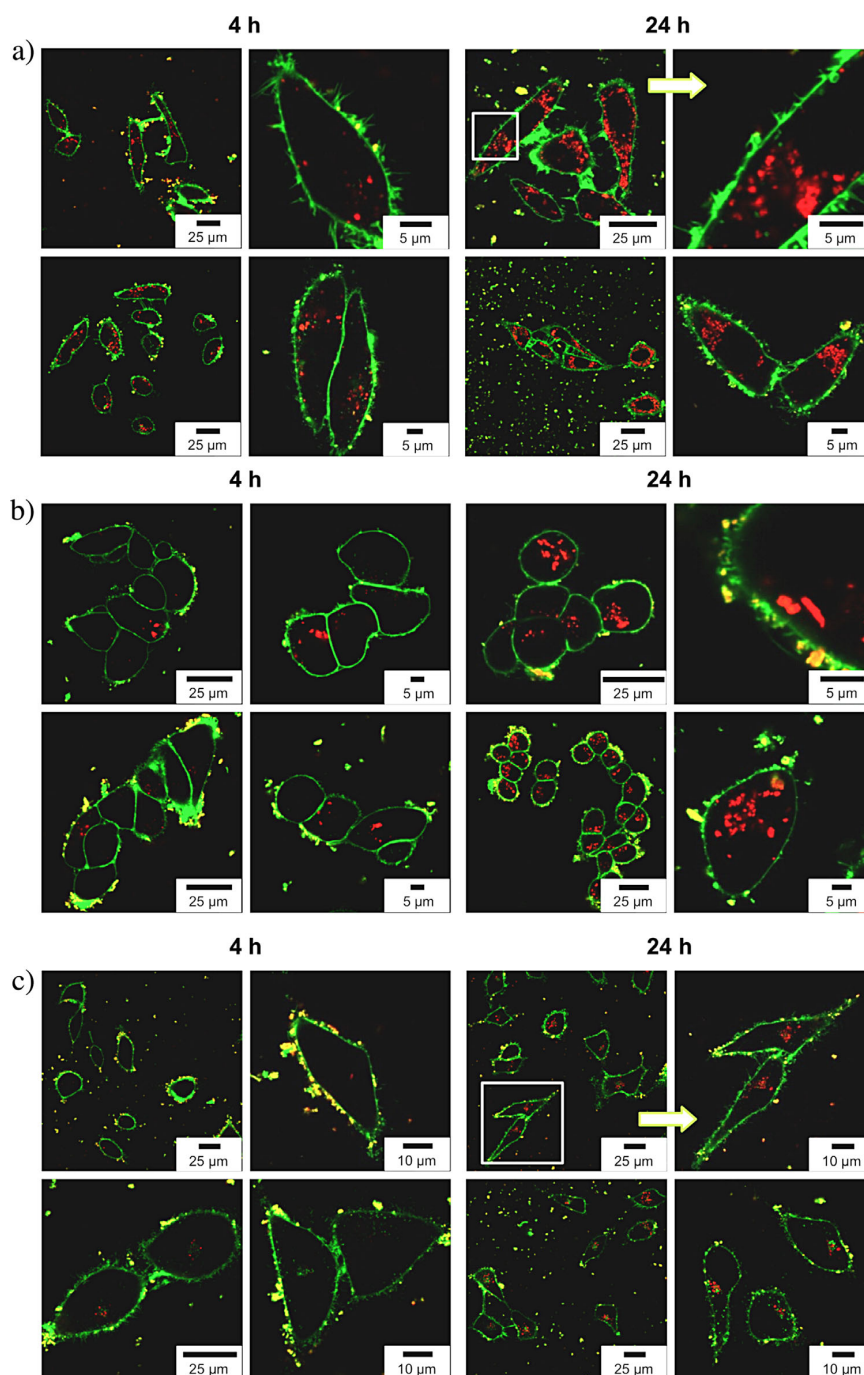ned. Hexanediol NCs served as control. The scheme of the experimental setup and the ACT-results are depicted in Figure 5. It can be seen that the ACT determined from blood (83 s) is nearly the same as in the control sample (hexanediol NCs, 61 s). Furthermore, the ACT of NCs with high chain density is higher (259 s) than with low chain density NCs (160 s). This shows that using more heparin for the synthesis results in higher ACT values which are followed by a higher heparin chain density onto the NCs' surface. From these results, it can be seen that the determination of the activated clotting time (ACT) is a nice tool to monitor the heparin chain density onto the NCs surface on one side and it displays the biological intactness of the polymeric shell on the other side.
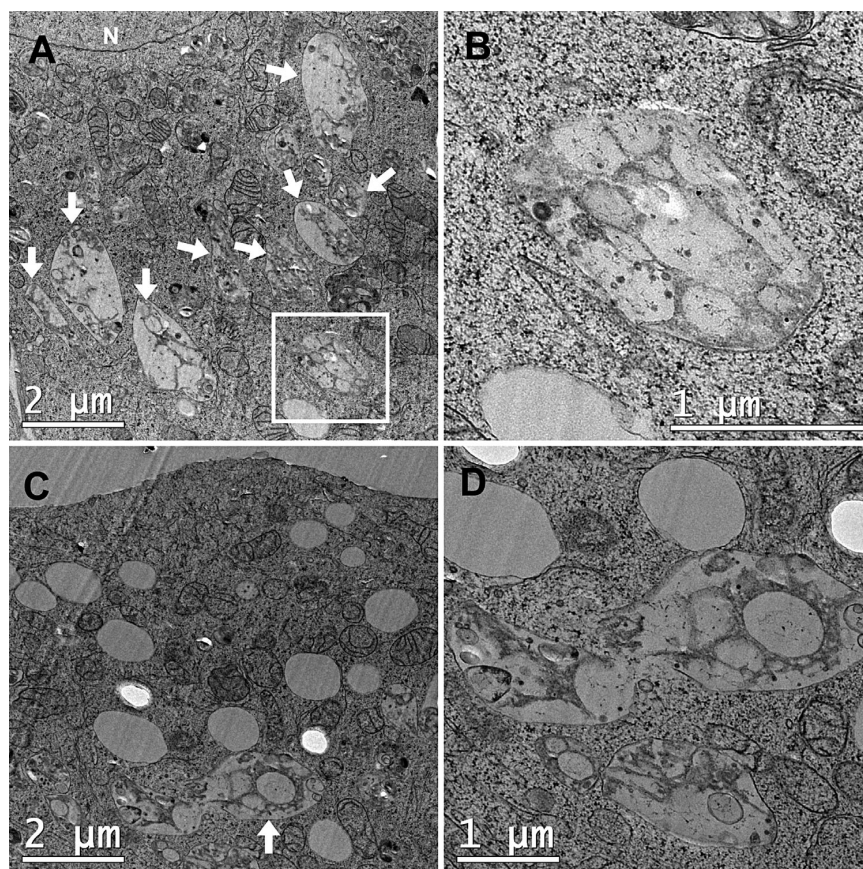

Figure 10. TEM bright field images of HEP-001 NCs inside HeLa cells. (A) shows an overview with the nucleus marked with ''N'' and white arrows indicating capsule-containing endosomes. (B) is a close-up of the region in (A) marked with a square and shows an endosome that is tightly packed with NCs. (D) is a close-up of the vesicle marked with an arrow in (C).

3.5. Investigation of the Cellular Uptake in Different Cell Lines by FACS Measurements and CLSM

Due to the high negative charge density, caused by the sulfate groups of the heparin, a good cellular uptake level was expected for the heparin NCs in different cell lines. To compare cellular uptake efficiency in diverse tumor cell lines, HeLa cells were analyzed as well as MCF-7 and PC3 cells. The cell viability was checked via MTS assay after a NC incubation period of 24 h (75 $\mu g \cdot mL^{-1}$) and showed absorption/absorbance rates of over 90% among all samples, compared to the untreated negative controls (Figure 6). No remarkable decrease in metabolism functions of all cell lines was caused by the cellular uptake of HEP-001 and HEP-002.

The results of the flow cytometry analysis are shown in Figure 7 after 4 h (dark grey) and 24 h (light grey). The fluorescence intensity of HEP-001 and HEP-002 is normalized to the number of NCs per mL. Therefore, a direct comparison between the two heparin NCs is possible (Figure 7A and B). Very good reproducibility of the results was achieved both with HEP-001 and HEP-002 for all cell lines.

CLSM-images are shown in Figure 8 (negative controls), Figure 9a (HeLa cells), 9b (MCF-7 cells), and 9c (PC3 cells). HEP-001 and HEP-002 NCs are internalized by all observed cell lines. Heparin NCs show intracellular localization and sporadic adherence/association with the cell membrane. These associations are shown in yellow (overlap of pseudocolored green cell membrane and red NCs).

3.6. Transmission Electron Microscopic Evaluation of HEP-001 in HeLa Cells

TEM evaluation shows that HEP-001 NCs are taken up by HeLa cells and are found in endosomal structures after an incubation period of 24 h (Figure 10). Cells usually contain several capsule-containing vesicles and each of these vesicles contains several NCs. The NCs appear as circles that are slightly stretched or deformed, maybe due to processes inside the cells or due to the fixation method which uses high pressure to freeze cells in an instant.

4. Conclusion

In the present work, heparin-based NCs, containing two different amounts of heparin as well as the hexanediol NC for control, were synthesized via miniemulsion polymerization at the droplets interface. Narrowly distributed NCs with 180 nm in size were obtained. The biological intactness of the polymeric shell was shown by measuring the activated clotting time. From isothermal titration measurements, an exothermic interaction with antithrombin is observed. In contrast to the heparin-based NCs, the titration of control hexanediol based NCs was very similar to the reference measurement, resulting in an adsorption isotherm not showing any heat of interaction. The chemical stability of the NCs was shown in 0.9% NaCl, Ringer's solution, and PBS. The uptake of NCs in different cells was confirmed by FACS, by confocal laser scanning microscopy, and by transmission electron microscopy using cryo-substitution preparation for showing the uptake of NCs in cells. The low toxicity of all types of NCs was displayed by a MTS assay.

[1] D. Jain, R. Athawale, A. Bajaj, S. Shrikhande, P. N. Goel, R. P. Gude, *Colloids Surf. B* **2013**, *109*, 59.

[2] R. Gref, M. Luck, P. Quellec, M. Marchand, E. Dellacherie, S. Harnisch, T. Blunk, R. H. Muller, *Colloids Surf. B* **2000**, *18*, 301.

[3] T. Verrecchia, G. Spenlehauer, D. V. Bazile, A. Murrybrelier, Y. Archimbaud, M. Veillard, *J. Control. Release* **1995**, *36*, 49.

[4] A. K. Bajpai, S. Bhanu, *J. Mater. Sci-Mater. M* **2007**, *18*, 1613.

[5] Y. Wang, Y. Wang, J. Xiang, K. Yao, *Biomacromolecules* **2010**, *11*, 3531.

[6] M. Socha, P. Bartecki, C. Passirani, A. Sapin, C. Damge, T. Lecompte, J. Barre, F. El Ghazouani, P. Maincent, *J. Drug Target* **2009**, *17*, 575.

[7] C. Passirani, G. Barratt, J. P. Devissaguet, D. Labarre, *Life Sci.* **1998**, *62*, 775.

[8] C. Passirani, G. Barratt, J. P. Devissaguet, D. Labarre, *Pharmaceut. Res.* **1998**, *15*, 1046.

[9] G. Oshima, K. Nagasawa, *Thromb. Res.* **1986**, *42*, 375.

[10] K.-J. Wang, H.-X. Li, Y.-M. Song, N.-N. Luan, P. Xian, *Biopolymers* **2010**, *93*, 887.

[11] F. Ran, S. Nie, J. Li, B. Su, S. Sun, C. Zhao, *Macromol. Biosci.* **2012**, *12*, 116.

[12] H. J. Wang, Z. X. Lin, X. M. Liu, S. Y. Sheng, J. Y. Wang, *J. Control. Release* **2005**, *105*, 120.

[13] Y.-I. Chung, J. C. Kim, Y. H. Kim, G. Tae, S.-Y. Lee, K. Kim, I. C. Kwon, *J. Control. Release* **2010**, *143*, 374.

[14] C. Argyo, V. Cauda, H. Engelke, J. Raedler, G. Bein, T. Bein, *Chem-Eur. J.* **2012**, *18*, 428.

[15] K. Landfester, *Angew. Chem.* **2009**, *121*, 4556.

[16] G. Baier, A. Musyanovych, V. Mailaender, K. Landfester, *Int. J. Artif. Organs* **2012**, *35*, 77.

[17] G. Baier, J. M. Siebert, K. Landfester, A. Musyanovych, *Macromolecules* **2012**, *45*, 3419.

[18] H. Schlaad, H. Kukula, J. Rudloff, I. Below, *Macromolecules* **2001**, *34*, 4302.

[19] G. Baier, D. Baumann, J. M. Siebert, A. Musyanovych, V. Mailaender, K. Landfester, *Biomacromolecules* **2012**, *13*, 2704.

[20] G. Baier, A. Cavallaro, K. Vasilev, V. Mailaender, A. Musyanovych, K. Landfester, *Biomacromolecules* **2013**, *14*, 1103.

[21] D. Crespy, M. Stark, C. Hoffmann-Richter, U. Ziener, K. Landfester, *Macromolecules* **2007**, *40*, 3122.

[22] M. I. Hug, S. Di Bernardo, F. Berger, U. Bauersfeld, M. Weiss, *Acta Anaesth. Scand.* **2004**, *48*, 211.

[23] A. S. Levenson, V. C. Jordan, *Cancer Res.* **1997**, *57*, 3071.

[24] L. Bonaccorsi, M. Muratori, V. Carloni, S. Zecchi, L. Formigli, G. Forti, E. Baldi, *Int. J. Androl.* **2003**, *26*, 21.

[25] M. E. Kaighn, K. S. Narayan, Y. Ohnuki, J. F. Lechner, L. W. Jones, Invest. *Urol.* **1979**, *17*, 16.

[26] R. Carrell, R. Skinner, M. Wardell, J. Whisstock, *Mol. Med. Today* **1995**, *1*, 226.

[27] S. T. Olson, I. Bjork, R. Sheffer, P. A. Craig, J. D. Shore, J. Choay, *J. Biol. Chem.* **1992**, *267*, 12528.

www.MaterialsViews.com

6.6   Publication 6

Glutathione responsive hyaluronic acid nanocapsules obtained by bioorthogonal interfacial "click" reaction

Published in: *Biomacromolecules*, 2016. **17**(1): p. 148-53.

Glutathione Responsive Hyaluronic Acid Nanocapsules Obtained by Bioorthogonal Interfacial "Click" Reaction

Grit Baier,[†] Michael Fichter,[‡] Andreas Kreyes,[†] Katja Klein,[†] Volker Mailänder,[†,§] Stephan Gehring,[‡] and Katharina Landfester[*,†]

[†]Max Planck Institute for Polymer Research, Ackermannweg 10, 55128 Mainz, Germany

[‡]Children's Hospital and [§]III. Medical Clinic, University Medical Center of the Johannes-Gutenberg University, Langenbeckstr. 1, 55131 Mainz, Germany

Summary:

The focus of this study was the synthesis of glutathione-responsive polytriazol nanocapsules composed of hyaluronic acid using "click" reaction polymerization. The introduction of disulfide-functionalized dialkyne resulted in an incorporation of disulfide bonds. The release of different fluorescent dyes after incubation with glutathione was verified following incubation with human monocyte-derived dendritic cells *in vitro*. Glutathione-sensitive nanocapsules, which release their cargo in intracellular compartments, are of great interest for the development of targeted drug delivery systems with highly efficient release properties.

Author contribution:

- Design, conduction and evaluation of all biological experiments
- Preparation of graphs and figures based on cell culture assays
- Preparation of the biological part of the manuscript
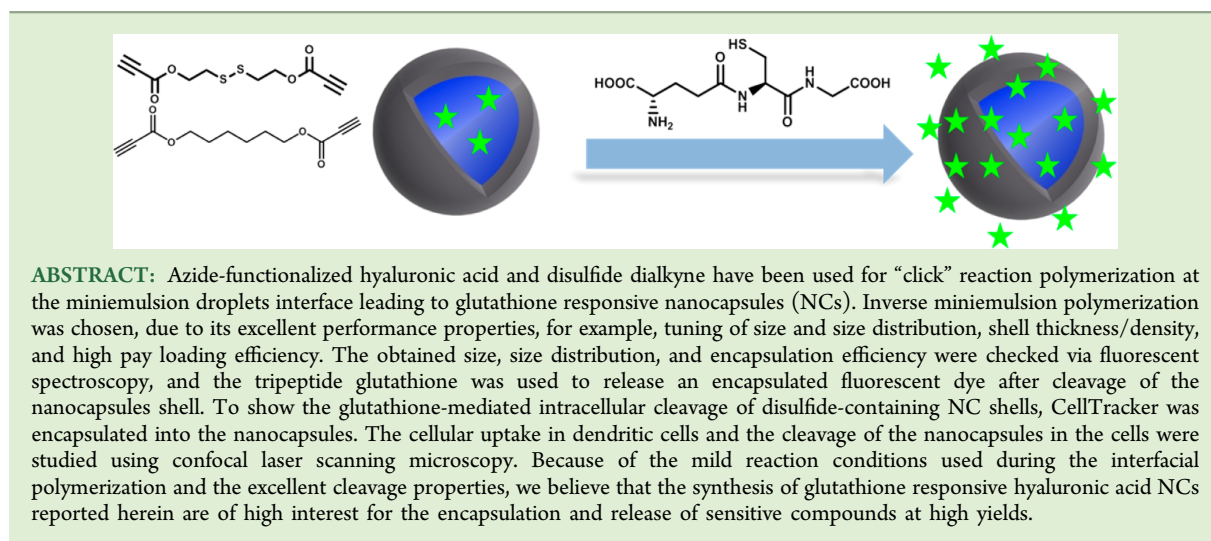- Proofreading of the manuscript

Glutathione Responsive Hyaluronic Acid Nanocapsules Obtained by Bioorthogonal Interfacial "Click" Reaction

Grit Baier,[†] Michael Fichter,[‡] Andreas Kreyes,[†] Katja Klein,[†] Volker Mailänder,[†,§] Stephan Gehring,[‡] and Katharina Landfester*,[†]

[†]Max Planck Institute for Polymer Research, Ackermannweg 10, 55128 Mainz, Germany

[‡]Children's Hospital and [§]III. Medical Clinic, University Medical Center of the Johannes-Gutenberg University, Langenbeckstr. 1, 55131 Mainz, Germany

S *Supporting Information*

ABSTRACT: Azide-functionalized hyaluronic acid and disulfide dialkyne have been used for "click" reaction polymerization at the miniemulsion droplets interface leading to glutathione responsive nanocapsules (NCs). Inverse miniemulsion polymerization was chosen, due to its excellent performance properties, for example, tuning of size and size distribution, shell thickness/density, and high pay loading efficiency. The obtained size, size distribution, and encapsulation efficiency were checked via fluorescent spectroscopy, and the tripeptide glutathione was used to release an encapsulated fluorescent dye after cleavage of the nanocapsules shell. To show the glutathione-mediated intracellular cleavage of disulfide-containing NC shells, CellTracker was encapsulated into the nanocapsules. The cellular uptake in dendritic cells and the cleavage of the nanocapsules in the cells were studied using confocal laser scanning microscopy. Because of the mild reaction conditions used during the interfacial polymerization and the excellent cleavage properties, we believe that the synthesis of glutathione responsive hyaluronic acid NCs reported herein are of high interest for the encapsulation and release of sensitive compounds at high yields.

INTRODUCTION

Recently, several groups reported having performed the Huisgen 1,3-dipolar cycloaddition of terminal electron-deficient alkynes to azides at room temperature without the use of a copper catalyst.[1−6] This reaction enables mild conditions for life science application and can be performed in the absence of an inert atmosphere that is needed to protect the copper(I) catalyst from being oxidized. For example, copper salts themselves reduce the stability of emulsions through interaction with surfactants, thus, limiting the range of applicable surfactants. Furthermore, copper complexes can be highly toxic to living systems and can induce changes in the cellular metabolism.[7] The impact of multiple reactions that are named "click" reaction and the developed applications of the "click" chemistry have been previously described in many publications.[8,9] Polysaccharide chemistry is often used to modify polysaccharides (e.g., cellulose, dextran, chitosan, starch, guar, hyaluronan) to achieve structures with specific properties for a 1,3-dipolar azide alkyne cycloaddition.[8,10,11] Moreover, the functionalization of nanocarriers with drug-derived clickable biomimetic anchor units is currently part of numerous studies.[12] Since "click" chemistry has been shown to work well for protein functionalization, the introduction of azides and

acetylenes into biomolecules has become of great interest.[13] To form a stable triazole ring, 1,3-dipolar cycloaddition as a highly atom-efficient reaction is well suited since no side products are produced. This makes the reaction suitable for many applications (e.g., biomedical application, drug delivery systems, cosmetics, food chemistry). Hyaluronic acid (HA) is composed of D-glucuronic acid and D-*N*-acetylglucosamine, linked via alternating β-1,4- and β-1,3-glycosidic bonds. It is biocompatible, biodegradable, has a very low level of immune response, and exhibits a fast degradation profile and clearance within the body. During the last years HA has been modified using different procedures to obtain nanocarriers for various applications (e.g., hydrogels for tissue engineering).[14]

To perform reactions inside the droplets and at their interface, the miniemulsion technique is a versatile method to obtain nanometer-sized (100−500 nm) and narrowly distributed polymeric nanocapsules. Under carefully chosen conditions of miniemulsification, on one hand, it is possible to encapsulate fragile molecules, and on the other hand, it is

Table 1. NCs Characteristics: Molecular Weights, Diameter, and Standard Deviation Obtained from DLS Measurements, Zeta Potential, and Encapsulation Efficiency

samples	HA-N$_3$, deg of azidation[a] (%)	amt of HDDP or HDDP-S-S (mg)	Z-avg[a] (nm)/std dev (%)	zeta potential (mV, pH 7.2)	encapsulation efficiency (wt %)
001 HA-N$_3$-HDDP	40	33.9	no capsule morphology found		
002 HA-N$_3$-HDDP	60	50.8	180/24	−34	68
003 HA-N$_3$-HDDP	73	62.4	170/24	−36	71
004 HA-N$_3$-HDDP	80	67.4	162/23	−34	96
005 HA-N$_3$-HDDP-S-S	40	42.1	no capsule morphology found		
006 HA-N$_3$-HDDP-S-S	60	62.2	165/25	−39	76
007 HA-N$_3$-HDDP-S-S	73	77.4	165/25	−40	82
008 HA-N$_3$-HDDP-S-S	80	85.2	150/24	−39	98
HA-N$_3$HDDP-S-S (CellTracker)	80	85.2	160/26	−35	94

[a]Substitution degree per 1 unit HA.

possible to functionalize the surface of these nanocontainers during the synthesis or afterward. Recently, we reported the use of "click" reactions to form nanocapsules of low molecular weight difunctional monomers through polymerization at the interface of miniemulsion droplets and we achieved nanocontainers through the interfacial thiol—disulfide exchange reaction between dithiol DNA oligonucleotides and disulfide groups of a comonomer.[15,16] The concept of interfacial step growth addition of electron-deficient alkynes and a water-soluble azide showed that there is no need of a (copper) catalyst, and all polymerizations could be conducted at room temperature, resulting in a high degree of polymerization. Due to its excellent biological properties, including nonimmunogenicity, which is an essential prerequisite for biocompatibility, hyaluronic acid and its derivatives are broadly used in pharmacy and medicine. Recently, we synthesized hyaluronic acid-based nanocapsules containing the antimicrobial agent polyhexanide. These nanocapsules are specifically cleaved in the presence of hyaluronidase, an enzyme that is produced by bacteria like *Staphylococcus aureus* and *Escherichia coli*.[17]

Glyconanocapsules were prepared with an oily core by copper(I)-catalyzed azide—alkyne cycloaddition interfacial step growth polymerization in oil-in-water miniemulsion conditions.[18] Herein, the formation of NCs consisting of a polytriazole shell designed from an electron-deficient disulfide dialkyne and hyaluronic acid azide is shown. The miniemulsion "click" reaction polymerization took place at the droplets interface under ambient conditions. Cleavage of pendant disulfide linkages introduced in the polytriazole shell was obtained by glutathione titration. Glutathione as a natural tripeptide is the most abundant thiol species in the cytoplasm and the major reducing agent in biochemical processes.[19] As a cellular reducing agent it is found at different concentrations in intracellular (~10 mM) and extracellular (<10 μM) compartments as well as the elevated concentration in cancer cells promotes glutathione in the development of drug delivery systems.[20−22] The intracellular uptake of disulfide containing NC shells was confirmed by confocal laser scanning microscopy resulting in the distribution of the encapsulated fluorescent CellTracker dye.

■ EXPERIMENTAL SECTION

Materials. All chemicals or materials were used without further purification. Demineralized water was used during the experiments. Hyaluronic acid sodium salt (M_w = 140000 g·mol^{-1}) was purchased Sigma-Aldrich. The magnesium- and calcium-free phosphate buffered solution (PBS buffer) was purchased from Gibco, Germany. The oil

soluble block copolymer surfactant poly[(ethylene-*co*-butylene)-*block*-(ethylene oxide)], P(E/B-*b*-EO), consisting of a poly(ethylene-*co*-butylene) block (M_w = 3700 g·mol^{-1}) and a poly(ethylene oxide) block (M_w = 3600 g·mol^{-1}) was synthesized according to the procedure described in the literature.[23] The fluorescent dye sulforhodamine 101 (SR101) was purchased from BioChemica. The sodium chloride (NaCl 0.9%) was purchased from Fresenius Kabi and phosphate-buffered saline without calcium and magnesium (PBS) was purchased by Invitrogen, Germany. CellTracker Green CMFDA (5-chloromethylfluorescein diacetate) was purchased from "Life Technologies" (Thermo Fisher), bis(2-hydroxyethyl) disulfide, propiolic acid (both Alfa Aesar), *p*-toluene sulfonic acid (Fluka), hyaluronic acid (Aldrich), ethyl chloroformate (Aldrich), 3-bromopropylamine hydrobromide (Acros), sodium azide (AppliChem), DOWEX 50WX8 cation exchange resin (Aldrich), dry DMSO (Aldrich), dry DCM (Acros), and benzene (VWR) were used as received.

Synthesis of Azide-Functionalized Hyaluronic Acid (HA-N$_3$). 3-Azidopropylamine was synthesized according to a literature procedure:[24] To a solution of 3-bromopropylamine hydrobromide (8.0 g, 36.5 mmol) in H$_2$O (40 mL), NaN$_3$ (7.8 g, 120 mmol) was added, and the reaction was stirred overnight at 90 °C. The solution was then cooled to 0 °C and Et$_2$O (30 mL) was added. KOH (10 g) was added portionwise under vigorous stirring. The organic phase was separated and the aqueous phase extracted with Et$_2$O (2 × 10 mL). The combined organic phases were dried over anhydrous NaSO$_4$. After removal of the solvent, 3-azidopropylamine was obtained as slightly yellow oil (2.5 g, 68%). ^{1}H NMR spectrum (300 MHz, CDCl$_3$), δ [ppm]: 3.35 (t, J = 6.7 Hz, 2H, NH$_2$-C$\underline{H}_2$), 2.78 (t, J = 6.8 Hz, 2H, N$_3$-CH$_2$), 1.75−1.66 (m, 2H, CH$_2$-C$\underline{H}_2$-CH$_2$), 1.31 (bs, 2H, N$\underline{H}_2$), see SI, Figure 1.

Azidation of hyaluronic acid was performed in a modified two-step procedure based on Huerta-Angeles et al.:[25] Hyaluronic acid was dissolved in H$_2$O (200 mL). Dowex 50WX8 was added, and the mixture was stirred for 2 h. The resin was then removed by centrifugation, and the solution was freeze-dried. The acid form of HA (0.74 g) was dissolved in dry DMSO (70 mL). Triethylamine (2.7 mL, 19.5 mmol) was added, and the solution was stirred for 15 min. Ethyl chloroformate (0.58 mL, 6 mmol) was then added. After stirring for 1 h, 3-azidopropylamine (0.45 g, 4.1 mmol) was added, and the reaction was stirred overnight. A 50 mL aliquot of water was added, and the mixture was dialyzed against water for 3 days and finally freeze-dried. HA-N$_3$ was obtained as a white solid with a DS of 80%, as detected by ^{1}H NMR spectroscopy.

Synthesis of 1,6-Hexanediol Dipropiolate (HDDP). A total of 11.8 g of hexanediol (0.1 mmol, 1.0 equiv), 28 g propiolic acid (0.4 mmol, 4.0 equiv), and *p*-toluene sulfonic acid (1 g, 5 mol %) were charged together with 300 mL of dry toluene under an argon atmosphere into a flame-dried, three-neck flask equipped with a water separator and condenser. The solution was refluxed for 120 h using an oil bath, and the excess of water and propiolic acid was azeotropically distilled out and collected. After cooling, the organic phase was washed with 300 mL of saturated NaHCO$_3$ solution and 300 mL of water. The

organic phase was separated and dried over anhydrous magnesium sulfate and filtered, and the solvent was distilled out using a rotoevaporator and dried under vacuum. A total of 19.5 g (87%, 0.087 mmol) of a colorless oil was obtained, which solidified upon standing.

^{1}H NMR (CDCl$_3$, 300 MHz, δ in ppm): 4.15 (t, 4 H, ^3J = 6.0 Hz), 2.87 (s, 2H), 1.86 (m, 4H), 1.37 (m, 4H). ^{13}C NMR (CDCl$_3$, 75 MHz, δ in ppm): 152.9, 74.9, 74.8, 66.3, 28.3, 25.6. IR (ν in cm^{-1}): 2945 (C$_{aliph}$-H), 2114 (C$_{sp}$-C$_{sp}$), 1702 (C=O), 1249 (C−O). R_f (Et$_2$O): 0.76. ESI-MS (m/z): 245 [M + Na]$^+$.

Synthesis of Disulfide 1,6-Hexanediol Dipropiolate (HDDP-S-S). Propiolic acid (5.4 g, 78.0 mmol), bis(2-hydroxyethyl) disulfide (3.0 g 19.5 mmol), and p-toluene sulfonic acid monohydrate (0.36 g, 2.0 mmol) were dissolved in benzene (150 mL). The reaction was stirred under reflux with a water separator for 3 days. After cooling to room temperature, saturated NaHCO$_3$ solution was added. The organic phase was separated, and the aqueous phase was washed twice with Et$_2$O. The combined organic phases were dried over anhydrous NaSO$_4$. After removal of the solvent, the crude product was purified by column chromatography (n-hexane: EtOAc = 3:1). The product was obtained as a colorless liquid that solidified upon standing (2.3 g, 46%). ^{1}H NMR (300 MHz, CDCl$_3$), δ [ppm]: 4.41 (t, J = 6.6 Hz, 4H, O-CH$_2$), 2.96−2.92 (m, 6H, S-CH$_2$ and alkyne-CH). ^{13}C NMR (75 MHz, CDCl$_3$), δ [ppm]: 152.3, 75.5, 74.3, 63.9, 36.7. MS (FD) m/z Calcd for C$_{10}$H$_{10}$O$_4$S$_2$, 258.00; found, 258.6. Elem. anal.: Calcd for C$_{10}$H$_{10}$O$_4$S$_2$: C, 46.50; H, 3.90. Found: C, 46.52; H, 3.91.

Synthesis of Nanocapsules. For the nanocapsules synthesis, in the aqueous phase, 25 mg HA-N$_3$ was dissolved in 500 μL of PBS solution together with the fluorescent dye sulforhodamine 101 (SR101, 2 mM). In the continuous phase, 65 mg of the surfactant poly((ethylene-co-butylene)-$block$-(ethylene oxide)), P(E/B-b-EO) was dissolved in 6.25 g cyclohexane, mixed with either HDDP or HDDP-S-S (amounts see Table 1), and stirred for 1 h under ambient conditions. Afterward, the emulsion was ultrasonicated for 180 s at 90% amplitude (Branson Sonifier W-450-Digital, 1/2″ tip) under ice cooling in order to prevent evaporation of the solvent. The polymerization reaction was carried out 24 h at 40 °C. The resulting nanocapsule dispersion was purified two times by centrifugation (Sigma 3k-30, RCF 1467, 20 min) in order to remove the residuals of P(E/B-b-EO) and was redispersed in cyclohexane. The purified nanocapsules dispersion was transferred into an aqueous phase using the following procedure: 0.5 g of the nanocapsules dispersion in cyclohexane (polymer solid content around 1.7 wt %) was mixed with 2.5 g SDS aqueous solution (0.1 wt %) under mechanical stirring for 24 h at 25 °C. Afterward, the samples were redispersed for 5 min in a sonication bath (power 50%, 25 kHz), centrifuged at 4000 rpm for 20 min (Sigma 3k-30, RCF 1467), and the pellet was resuspended in Ampuwa. Finally, the samples were dialyzed (MWCO: 8000 g·mol^{-1}) in order to remove residues of SDS. For the encapsulation of the CellTracker Green, 1 mg was dissolved in 500 μL of DMSO, and 150 μL of the resulting clear solution was used for the synthesis. The purification and redispersion procedure was the same as described above.

Characterization of Nanocapsules. The average size and the size distribution of the nanocapsules were measured by means of dynamic light scattering (DLS) with diluted dispersions (40 μL sample were diluted in 1 mL water) on a PSS Nicomp Particle Sizer 380 (Nicomp Particle Sizing Systems, U.S.A.) equipped with a detector at 90° scattering mode at 20 °C. The zeta potential of the nanocapsules was measured in 10^{-3} M potassium chloride solution with a Zeta Nanosizer (Malvern Instruments, U.K.) at 20 °C. Scanning electron microscopy (SEM) studies were done on a field emission microscope (LEO (Zeiss) 1530 Gemini, Oberkochen, Germany) working at an accelerating voltage of 170 V. Generally, the samples were prepared by diluting the nanocapsule dispersion in cyclohexane or demineralized water (for redispersed samples) to about 0.01% solid content. Then one droplet of the sample was placed onto silica wafer and dried under ambient conditions overnight. No additional contrast agent was applied. Transmission electron microscopy (TEM) studies were done by freeze-drying the nanocapsule dispersion and mixing with Epon.

Afterward, the samples were cut into 60 nm thick pieces (LEICA Ultramikrotom UCT), stained with ruthenium, and placed on a carbon-coated TEM grid. Images were recorded on a ZEISS 912 working at an accelerating voltage of 120 kV. The solid content of the capsule dispersion was measured gravimetrically. The fluorescence intensities for all mentioned experiments were measured using a microplate reader (Infinite M1000, Tecan, Switzerland).

Determination of the Encapsulation Efficiency. After the encapsulation and redispersion process, the polymeric NCs were sedimented by centrifugation (20 min using Sigma 3 k-30, RCF 1467). The nonencapsulated amount of SR 101 dye (580/610 nm) was measured in the supernatant. For the calculations, a calibration curve obtained from different amounts of dissolved SR101 in SDS solution (0.1%) was used. For the data normalization, a total amount of 1 × 10^{10} NCs/mL (solid content 5 mg/mL) was used for each experiment. For each sample, the release of SR 101 was calculated from three single measurements, and the entire experiment was repeated two times.

Analysis of Glutathione Responsive Properties of Nanocapsules. The glutathione responsive properties of the disulfide containing polytriazols (HDDP-S-S) were studied on SR 101 containing nanocapsules redispersed in an aqueous phase. After the encapsulation and redispersion process, the polymeric nanocapsules were sedimented by centrifugation (20 min at 14000 rpm). In a first experiment, the nanocapsules prepared with HA and HDDP were compared with nanocapsules synthesized with HA and HDDP-S-S. Therefore, both types of nanocapsules were treated with a glutathione solution (25 mM). In a second experiment, both types of nanocapsules were treated with PBS buffer, which serves as a control experiment. The polymeric nanocapsules were shaken gently for 260 h at 37 °C. After a certain period of time, the amount of released SR 101 was determined in the supernatant of the sedimented nanocapsules, the fluorescent intensity was calculated from three single experiments, and the whole experiment was repeated three times.

Generation of Human Monocyte-Derived Dendritic Cells. Adult peripheral blood mononuclear cells (PBMCs) were isolated from fresh buffy coats (University of Mainz, Germany), obtained from a healthy voluntary donor upon informed consent, by centrifugation through Histopaque-1077 density gradient media (Sigma-Aldrich, St. Louis, U.S.A.) for 20 min at 900g and 20 °C. The interphase consisting of PBMCs were subsequently extracted and washed with Hank's Balanced Salt Solution (Sigma-Aldrich, St. Louis, U.S.A.). CD14 positive monocytes were isolated from the PBMC fraction by positive selection using CD14 MicroBeads, MACS LS columns and a magnetic cell separator (MACS, Miltenyi Biotec, Bergisch-Gladbach, Germany), in accordance with the manufacturer's instructions. CD14 positive monocytes were cultured at a concentration of 10^6 cells per mL in 6-well plates (Greiner Bio-One, Frickenhausen, Germany) in RPMI medium (Sigma-Aldrich, St. Louis, U.S.A.), supplemented with 10% FCS, 100 U/mL penicillin, 100 μg/mL streptomycin, 1 mM L-glutamine, 1% essential and nonessential amino acids, and 50 μM 2-mercaptoethanol. Finally, GM-CSF (200 U/mL) and IL-4 (200 U/mL) were added to the medium following 5 days of culture at 37 °C and 5% CO$_2$.

Confocal Laser Scanning Microscopy (CLSM) Experiments. CLSM experiments were performed to determine the intracellular localization of hyaluronic acid nanocapsules (rather than just adherence to the plasma membrane) and their intracellular release of encapsulated substances. Therefore, immature moDCs were harvested and plated in 8-well Chamberslides in the presence of 25 μg/mL HDDP-S-S nanocapsules containing CellTracker dye in culture medium described above. Following 3 h of incubation at 37 °C, cell nuclei were stained with 2 μg/mL Hoechst 33342 (Life Technologies) for 30 min. Plasma membrane staining was performed by adding 4 μg/mL CellMaskOrange (Life Technologies) immediately before the cells were analyzed using a Zeiss LSM 710 NLO confocal laser scanning microscope.
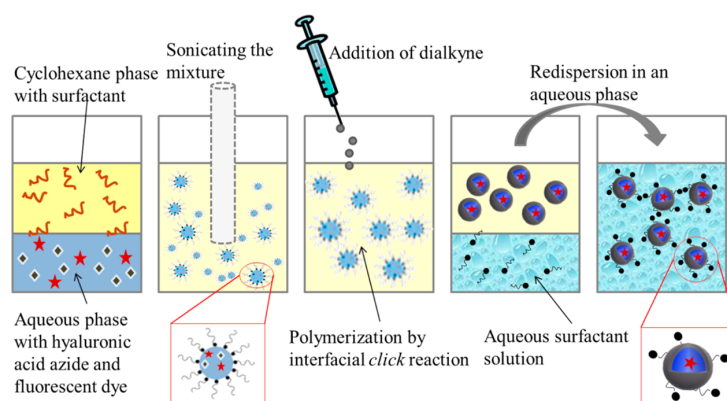
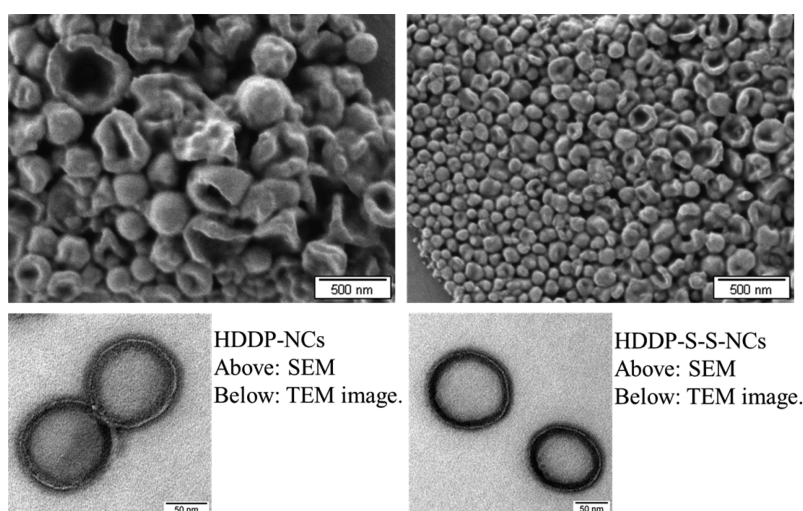**Figure 1.** Formation of NCs accomplished by bioorthogonal interfacial "click" polymerization reaction.

Figure 2. SEM and TEM micrographs of capsules achieved from interfacial "click" polymerization reaction between HA-N$_3$ and HDDP (left) or HDDP-S-S (right).

■ RESULTS AND DISCUSSION

The glutathione responsive polytriazol NCs are obtained by interfacial "click" reaction polymerization under ambient conditions from water-soluble hyaluronic acid azide (HA-N$_3$; from the droplet phase) and oil soluble disulfide functionalized dialkyne (HDDP-S-S; from the continuous phase). For comparison, a hyaluronic acid azide and a dialkyne without disulfide functionality (HDDP) were used for the "click" reaction. The "click" reaction polymerization took place at the droplets interface using a miniemulsion procedure yielding colloidal stable nanocapsules. After synthesis, the obtained polymeric nanocapsules were transferred in an aqueous phase using a SDS solution (0.1%) for stabilization of the nanocapsules. The encapsulation efficiency of the dye SR101 was studied by fluorescence spectroscopy from the amount of released SR101 found in the supernatant. The glutathione responsive properties of the disulfide containing polytriazols (HDDP-S-S) were checked by the release of the encapsulated fluorescent dye sulforhodamine SR101 using fluorescence spectroscopy. The experimental setup for the formulation of the nanocapsules is depicted in Figure 1. Additionally, CellTracker dye was encapsulated to show the glutathione

triggered release after uptake of HDDP-S-S-NCs in dendritic cells. CellTracker Green (CMFDA, 5-chloromethylfluorescein diacetate) is colorless and nonfluorescent until the acetate groups are cleaved by intracellular esterases present in the cell.

In all cases, no precipitation, no coagulation, and no flocculation of the nanocapsules was observed throughout the preparation of the nanocapsules and, under gently shaking conditions, at least within about 2 months of storage time. The morphology of the obtained nanocapsules was studied using scanning and transmission electron microscopy (SEM and TEM), see Figure 2.

The TEM images show clearly a capsule morphology in both cases. From the images it could be seen that the shell thickness is within 10−12 nm, which corresponds nicely with the expected value (calculated using the amount of reactants and the diameter of the nanocapsules), see SI. In the SEM images, the collapse of the capsules' wall is due to preparation effects. The average capsule size in the SEM and TEM images is slightly smaller than that measured by DLS (see Table 1) because of the drying effects. From DLS measurements, diameters between 150 and 180 nm were observed and the size distribution is nearly the same independent of the used

dialkyne. The zeta potentials of the HA-N$_3$-HDDP are slightly lower compared with the HA-N$_3$-HDDP-S-S NCs due to the negative character of disulfide groups.

The encapsulation efficiency of the fluorescent dye SR101 was determined by fluorescence measurements. Due to the stability of the fluorescence intensity over the broad range of pH values, SR101 was chosen as a suitable model substance to study the encapsulated amount that is related to the permeability of the wall. After the synthesis and redispersion of the nanocapsules, between 2% and 32% of the fluorescent dye was found in the supernatant, which corresponds to an encapsulation efficiency between 68% and 98%, see Table 1. It can be hypothesized that the lower release of the fluorescent dye SR101 is caused by a higher cross-link density in the shell. The shell permeability is remarkably higher using HA-N$_3$ with a degree of azidation of 60% and HDDP or HDDP-S-S for the synthesis compared with HA-N$_3$ degree of azidation of 80%. From those results it was concluded to perform the glutathione responsive and the cellular experiments with HA-N$_3$ having a degree of azidation = 80% (sample 004 and 008). To ensure working with comparable systems, the HDDP and HDDP-S-S synthesized NCs were investigated once again on their size and size distributions by dynamic light scattering measurements at different angles. The average radius of the final nanocapsules was found to be between 78 and 91 nm (diameters 156 and 182 nm) with a narrow size distribution, which are independent of the used dialkyne, see SI, Figure 2.

From those results, the nanocapsules per mL (sphere equation) were determined in order to use the same number of nanocapsules for the glutathione-triggered cleavage. For the glutathione-triggered release of SR101 encapsulated HA-N$_3$ NCs either HDDP-S-S or HDDP was used for synthesis. The nanocapsules were transferred into an aqueous phase by redispersion in 0.1% SDS solution, procedure see Experimental Part. Afterward, the nanocapsules (HA-N$_3$-HDDP-NCs and HA-N$_3$-HDDP-S-S-NCs) were treated with glutathione (25 mM) and PBS buffer (control experiments), see Figure 3.

From Figure 3, the glutathione-triggered cleavage followed by the release of the encapsulated fluorescent dye SR101 is clearly shown. Following the red line, an increase of fluorescence intensity of approximately 7 ti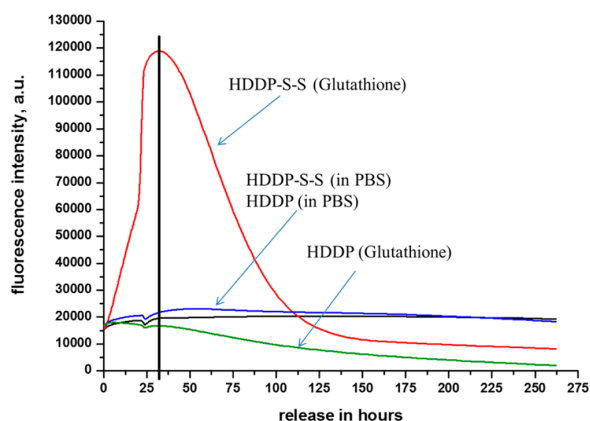mes after 30 h was detected. This result directly indicates the cleavage of the disulfide containing shell of the HA-N$_3$ NCs. No increase in fluorescence intensity was observed for HA-N$_3$-HDDP NCs, see green line. However, from the green line a decrease in the fluorescence intensity can be seen which is due to the influence of glutathione on the fluorescence intensity of SR 101. Almost no changes in fluorescence intensities were observed for the control samples (HA-N$_3$-HDDP NCs and HA-N$_3$-HDDP-S-S NCs), which were treated with PBS buffer.

For the determination of the cellular uptake of HDDP-S-S synthesized HA-N$_3$-NCs, a CellTracker dye was encapsulated. Again, the nanocapsules were transferred into the aqueous phase by redispersion in SDS solution 0.1%. The size and size distributions of the nanocapsules did not change compared to the NCs where SR101 was encapsulated, see Table 1. In addition to cell-free glutathione release experiments, we analyzed the uptake of HDDP-S-S nanocapsules by human monocyte-derived dendritic cells and studied the release of a special CellTracker dye. Dendritic cell esterases alter the CellTracker conformation leading to the emission of fluorescence. In Figure 4, confocal laser scanning microscopy
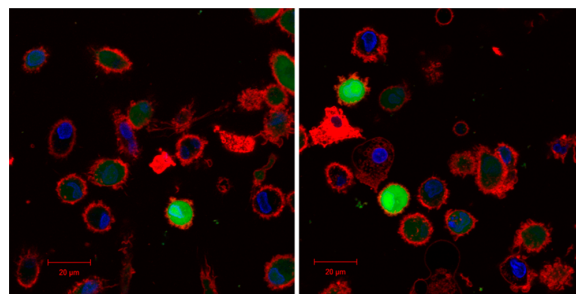

Figure 4. Cellular uptake of HDDP-SS nanocapsules containing CellTracker dye (25 μg/mL, incubation for 3 h at 37 °C). Staining of cell nuclei with 2 μg/mL Hoechst 33342 and of plasma membrane with CellMaskOrange.

clearly documents the CellTracker indicating the uptake of HDDP-S-S nanocapsules by moDCs. Furthermore, a diffuse distribution of fluorescent CellTracker dye could be detected, proving that HDDP-S-S nanocapsules have been intracellularly cleaved (by glutathione) and released the encapsulated dye leading to a whole cell staining.

CONCLUSION

Here we report the synthesis of glutathione cleavable nanocapsules consisting of a polytriazol shell synthesized from azide-functionalized hyaluronic acid, HA-N$_3$, and disulfide 1,6-hexanediol dipropiolate HDDP-S-S. In consequence, the described system is less complicated regarding the synthesis, since reaction conditions are straightforward. Furthermore, we showed that no (copper) catalyst is needed to perform the "click" reaction at the droplets interface. The resulting azide hyaluronic acid based nanocapsules synthesized with disulfide dialkyne were characterized in terms of size and size distribution. The diameter and size distribution was more or less the same independent of the degree of azidation of hyaluronic acid and the used dialkyne. Treating the nanocapsules with glutathione, a release of the encapsulated fluorescent dye after 30 h was observed. Cellular uptake experiments of HA-HDDP-S-S nanocapsules by dendritic cells

Figure 3. Fluorescence intensities achieved by glutathione-triggered (25 mM) release of SR 101 (fluorescent dye) containing HA-N$_3$ NCs synthesized either with HDDP (green line) or HDDP-S-S (red line). PBS buffer served as control (see blue and black line).

were confirmed by confocal laser scanning microscopy. The diffuse distribution of fluorescent CellTracker dye showed that the nanocapsules have been intracellular cleaved (by glutathione) and the encapsulated dye was released resulting in a cell staining. All aspects considered, the hyaluronic based nanocapsules have the potential to be used in the drug delivery field as they possess glutathione responsive properties.

■ ASSOCIATED CONTENT

Ⓢ Supporting Information

The Supporting Information is available free of charge on the ACS Publications website at DOI: 10.1021/acs.biomac.5b01279.

    NMR spectrum of the HA-azid, DLS measurements of the nanocapsules, and calculation of the shell thickness (PDF).

■ AUTHOR INFORMATION

Corresponding Author

*E-mail: landfester@mpip-mainz.mpg.de. Tel.: +49(0)6131 379-170. Fax: +49(0)6131 379-370.

Notes

The authors declare no competing financial interest.

■ ACKNOWLEDGMENTS

■ REFERENCES

(1) Codelli, J. A.; Baskin, J. M.; Agard, N. J.; Bertozzi, C. R. Second-generation difluorinated cyclooctynes for copper-free click chemistry. *J. Am. Chem. Soc.* **2008**, *130* (34), 11486−11493.

(2) Blenke, E. O.; Klaasse, G.; Merten, H.; Plueckthun, A.; Mastrobattista, E.; Martin, N. I. Liposome functionalization with copper-free "click chemistry". *J. Controlled Release* **2015**, *202*, 14−20.

(3) Nilo, A.; Allan, M.; Brogioni, B.; Proietti, D.; Cattaneo, V.; Crotti, S.; Sokup, S.; Zhai, H.; Margarit, I.; Berti, F.; Hu, Q. Y.; Adamo, R. Tyrosine-Directed Conjugation of Large Glycans to Proteins via Copper-Free Click Chemistry. *Bioconjugate Chem.* **2014**, *25* (12), 2105−2111.

(4) Takahashi, A.; Suzuki, Y.; Suhara, T.; Omichi, K.; Shimizu, A.; Hasegawa, K.; Kokudo, N.; Ohta, S.; Ito, T. In Situ Cross-Linkable Hydrogel of Hyaluronan Produced via Copper-Free Click Chemistry. *Biomacromolecules* **2013**, *14* (10), 3581−3588.

(5) Manabe, Y. Recent Advance in Copper-Free Click Chemistry Using Cyclooctynes, and Applications for Living Systems. *Yuki Gosei Kagaku Kyokaishi* **2012**, *70* (7), 754−755.

(6) Lutz, J.-F. Copper-free azide-alkyne cycloadditions: New insights and perspectives. *Angew. Chem., Int. Ed.* **2008**, *47* (12), 2182−2184.

(7) Kennedy, D. C.; McKay, C. S.; Legault, M. C. B.; Danielson, D. C.; Blake, J. A.; Pegoraro, A. F.; Stolow, A.; Mester, Z.; Pezacki, J. P. Cellular Consequences of Copper Complexes Used To Catalyze Bioorthogonal Click Reactions. *J. Am. Chem. Soc.* **2011**, *133* (44), 17993−18001.

(8) Elchinger, P. H.; Faugeras, P. A.; Boens, B.; Brouillette, F.; Montplaisir, D.; Zerrouki, R.; Lucas, R. Polysaccharides: The "Click" Chemistry Impact. *Polymers* **2011**, *3* (4), 1607−1651.

(9) Hoyle, C. E.; Bowman, C. N. Thiol-Ene Click Chemistry. *Angew. Chem., Int. Ed.* **2010**, *49* (9), 1540−1573.

(10) Eissa, A. M.; Khosravi, E.; Cimecioglu, A. L. A versatile method for functionalization and grafting of 2-hydroxyethyl cellulose (HEC) via Click chemistry. *Carbohydr. Polym.* **2012**, *90* (2), 859−869.

(11) Shey, J.; Holtman, K. M.; Wong, R. Y.; Gregorski, K. S.; Klamczynski, A. P.; Orts, W. J.; Glenn, G. M.; Imam, S. H. The azidation of starch. *Carbohydr. Polym.* **2006**, *65* (4), 529−534.

(12) Goldmann, A. S.; Schodel, C.; Walther, A.; Yuan, J. Y.; Loos, K.; Muller, A. H. E. Biomimetic Mussel Adhesive Inspired Clickable Anchors Applied to the Functionalization of Fe3O4 Nanoparticles. *Macromol. Rapid Commun.* **2010**, *31* (18), 1608−1615.

(13) van Dongen, S. F. M.; Teeuwen, R. L. M.; Nallani, M.; van Berkel, S. S.; Cornelissen, J. J. L. M.; Nolte, R. J. M.; van Hest, J. C. M. Single-Step Azide Introduction in Proteins via an Aqueous Diazo Transfer. *Bioconjugate Chem.* **2009**, *20* (1), 20−23.

(14) Nimmo, C. M.; Owen, S. C.; Shoichet, M. S. Diels-Alder Click Cross-Linked Hyaluronic Acid Hydrogels for Tissue Engineering. *Biomacromolecules* **2011**, *12* (3), 824−830.

(15) Siebert, J. M.; Baier, G.; Musyanovych, A.; Landfester, K. Towards copper-free nanocapsules obtained by orthogonal interfacial "click" polymerization in miniemulsion. *Chem. Commun.* **2012**, *48* (44), 5470−5472.

(16) Paiphansiri, U.; Baier, G.; Kreyes, A.; Yiamsawas, D.; Koynov, K.; Musyanovych, A.; Landfester, K. Glutathione-Responsive DNA-Based Nanocontainers Through an "Interfacial Click" Reaction in Inverse Miniemulsion. *Macromol. Chem. Phys.* **2014**, *215* (24), 2457−2462.

(17) Baier, G.; Cavallaro, A.; Vasilev, K.; Mailander, V.; Musyanovych, A.; Landfester, K. Enzyme Responsive Hyaluronic Acid Nanocapsules Containing Polyhexanide and Their Exposure to Bacteria To Prevent Infection. *Biomacromolecules* **2013**, *14* (4), 1103−1112.

(18) Roux, R.; Sallet, L.; Alcouffe, P.; Chambert, S.; Sintes-Zydowicz, N.; Fleury, E.; Bernard, J. Facile and Rapid Access to Glyconanocapsules by CuAAC Interfacial Polyaddition in Miniemulsion Conditions. *ACS Macro Lett.* **2012**, *1*, 1074−1078.

(19) Lim, I. I. S.; Mott, D.; Ip, W.; Njoki, P. N.; Pan, Y.; Zhou, S. Q.; Zhong, C. J. Interparticle interactions in glutathione mediated assembly of gold nanoparticles. *Langmuir* **2008**, *24* (16), 8857−8863.

(20) Arrick, B. A.; Nathan, C. F. Glutatione metabolism as s determinant of therapeutic efficacy - a review. *Cancer Res.* **1984**, *44* (10), 4224−4232.

(21) Khorsand, B.; Lapointe, G.; Brett, C.; Oh, J. K. Intracellular Drug Delivery Nanocarriers of Glutathione-Responsive Degradable Block Copolymers Having Pendant Disulfide Linkages. *Biomacromolecules* **2013**, *14* (6), 2103−2111.

(22) Saito, G.; Swanson, J. A.; Lee, K. D. Drug delivery strategy utilizing conjugation via reversible disulfide linkages: role and site of cellular reducing activities. *Adv. Drug Delivery Rev.* **2003**, *55* (2), 199−215.

(23) Schlaad, H.; Kukula, H.; Rudloff, J.; Below, I. Synthesis of alpha,omega-heterobifunctional poly(ethylene glycol)s by metal-free anionic ring-opening polymerization. *Macromolecules* **2001**, *34* (13), 4302−4304.

(24) Yameen, B.; Ali, M.; Alvarez, M.; Neumann, R.; Ensinger, W.; Knoll, W.; Azzaroni, O. A facile route for the preparation of azide-terminated polymers. "Clicking" polyelectrolyte brushes on planar surfaces and nanochannels. *Polym. Chem.* **2010**, *1* (2), 183−192.

(25) Huerta-Angeles, G.; Smejkalova, D.; Chladkova, D.; Ehlova, T.; Buffa, R.; Velebny, V. Synthesis of highly substituted amide hyaluronan derivatives with tailored degree of substitution and their crosslinking via click chemistry. *Carbohydr. Polym.* **2011**, *84* (4), 1293−1300.

6.7   Publication 7

Polymeric hepatitis C virus non-structural protein 5A nanocapsules induce intrahepatic antigen-specific immune responses

Fichter M, Piradashvili K, Pietrzak-Nguyen A, Pretsch L, Kuhn G, Strand S, Zepp F, Wurm FR, Mailänder V, Landfester K, Gehring S.

Submitted manuscript

Summary:

In the presented manuscript polymeric nanocapsules exclusively made of the hepatitis C virus non-structural protein 5A (NS5A) were developed using the miniemulsion polymerization process. The applied method led to nanocapsules with an average diameter of about 410 nm that were primarily deposited in the liver and ingested by murine non-parenchymal liver cells in a concentration-dependent manner. Surface functionalization with monophosphoryl lipid A (MPLA) led to a tremendous activation of intrahepatic dendritic cells with a T_h1 bias. Immunization of mice with MPLA-coated NS5A-NCs achieved intrahepatic antigen-specific cellular immune responses (CD4$^+$) and antibody responses. The use of nanocarrier systems solely generated out of the antigen is of great interest for the development of nanoparticulate vaccines in order to prevent unintended side effects caused by additional carrier substances.

Author contribution:

- Design, conduction and evaluation of all biological experiments
- Preparation of graphs and figures
- Preparation of the manuscript proofread by Prof. Dr. Stephan Gehring

Polymeric hepatitis C virus non-structural protein 5A nanocapsules induce intrahepatic antigen-specific immune responses

Michael Fichter [a], Keti Piradashvili [b], Anette Pietrzak-Nguyen [a], Leah Pretsch [a], Gabor Kuhn [b,d], Susanne Strand [c], Fred Zepp [a], Frederik R. Wurm [b], Volker Mailänder [b,d], Katharina Landfester [b] & Stephan Gehring [a]*

a. Children's Hospital, University Medical Center, Johannes Gutenberg University, Langenbeckstraße 1, 55131 Mainz, Germany

b. Max Planck Institute for Polymer Research, Ackermannweg 10, 55128 Mainz, Germany

c. III. Department of Internal Medicine, University Medical Center, Johannes Gutenberg University, Langenbeckstraße 1, 55131 Mainz, Germany

d. Department of Dermatology, University Medical Center, Johannes Gutenberg University, Langenbeckstraße 1, 55131 Mainz, Germany

Corresponding author (*)

Prof. Dr. med. Stephan Gehring

Zentrum für Kinder- und Jugendmedizin

Universitätsmedizin der Johannes Gutenberg-Universität Mainz

Langenbeckstraße 1

55118 Mainz, Germany

Tel.: +49 6131 17 3560

Fax.: +49 6131 17 9658

Email: stephan.gehring@uni-mainz.de

Abstract

Targeting antigen combined with adjuvants to hepatic antigen-presenting cells (APCs) is essential for the induction of intrahepatic T cellular immunity controlling and resolving viral infections of the liver. Intravenous injection of antigen-loaded nanoparticles is a promising approach for the delivery of antigens to liver APCs.

Accordingly, polymeric nanocapsules (NCs) synthesized exclusively of hepatitis C virus non-structural protein 5A (NS5A) and the adjuvant monophosphoryl lipid A (MPLA) adsorbed to the nanocapsule surface were developed. Aim of the present study was the evaluation of the *in vitro* and *in vivo* behavior of MPLA-functionalized NS5A-NCs regarding the interaction with liver dendritic cells (DCs) and the potential to induce intrahepatic immune responses in a mouse model.

Maturation of DCs was significantly increased by application of NS5A+MPLA-NCs compared to non-functionalized NS5A-NCs promoting a vigorous expression of CD40, CD80, CD86 and a strong secretion of the T_h1-related cytokine IL-12. NS5A-NCs were preferentially deposited in DCs and Kupffer cells residing in the liver after intravenous administration. Immunization with NS5A-NCs induced intrahepatic antigen-specific $CD4^+$ T cellular immune responses determined by the secretion of IFNγ and IL-2. Furthermore, supplementation with MPLA induced significant levels of NS5A-specific antibodies.

The application of polymeric nanocapsules synthesized exclusively out of antigen avoids the risk of unintended side effects caused by additional carrier substances. Functionalization with adjuvants like MPLA and the efficient targeting to liver-resident APCs inherits the potential for application of antigen nanocapsules in further vaccination approaches against pathogens affecting the liver.

1 Introduction

More than 180 million people worldwide are infected with the hepatitis C virus accounting for a global prevalence of 2.8% [1]. A particularly high prevalence of >3.5% exists in developing countries in Central and East Asia, North Africa, and the Middle East [1]. Genotype 1 is worldwide the most prevalent strain, whereas genotypes 2 and 4 are predominantly present in African countries [2, 3]. Chronic hepatitis C virus infection is associated with a significantly increased risk to develop liver cirrhosis and hepatocellular carcinoma [4] and accounts for more than 360,000 deaths each year [5].

Standard of care treatment was recently dramatically improved through the development of new therapeutic regimens with direct acting antiviral drugs (DAAs). Therapy with FDA-approved interferon- and ribavirin-free DAA combinations, such as sofosbuvir/ledipasvir, sofosbuvir/daclatasvir, and ombitasvir/paritaprevir/ritonavir + dasabuvir, resulted in sustained virological response (SVR) rates of over 95% [6-8]. However, the US price for a 12-week therapy with sofosbuvir or sofosbuvir/ledipasvir is $84,000 and $94,500, respectively [9]. Despite efforts to reduce treatment costs in low-income countries with high prevalence, overall treatment expenses will likely hinder many HCV-infected patients from getting access to DAA-based therapy prior to expiration of existing patents (expected in about 15 years) [10]. Thus, ongoing research efforts aiming to develop a prophylactic or therapeutic HCV vaccine meet an important medical need.

Recent approaches to develop an effective vaccine against HCV were challenged by the vast genetic variability of the virus [11]. Furthermore, the liver, being the primary target of HCV infection, is characterized by an inherent tolerogenic microenvironment. The latter is characterized by a suppressed IL-12 production by intrahepatic dendritic cells and a decreased stimulatory capacity to induce T_h1 polarization [12-14]. In contrast, viral clearance depends on a broad intrahepatic CD8$^+$ T cell response maintained by a vigorous, antigen-specific, T_h1-

biased CD4$^+$ T cell activity [15-18]. The discrepancy between the immune tolerance of the liver and the pattern of immune response required to eradicate HCV outlines the challenge, faced by attempts to develop potential HCV vaccine candidates.

The ability to tailor the immune response against antigens with the use of novel, well-characterized adjuvants has opened new opportunities in vaccine development. MPLA, a Toll-like receptor 4 agonist, which was recently FDA-approved for the use in hepatitis B virus and human papillomavirus vaccines, promotes T_h1-directed responses [19, 20]. Targeting antigen to dendritic cells combined with simultaneous maturation is a promising approach for the induction of antigen-specific immunity. Nanoparticulate structures, in particular polymeric nanocapsules, are perfectly suited for vaccine formulations due to several advantages: (i) encapsulated antigens can be protected from proteolytic degradation [21, 22]; (ii) nanocapsules admit a high antigen loading efficacy along with prolonged antigen presentation [23-25]; (iii) they promote enhanced cross-presentation by DCs [26-28]; (iv) nanocapsules enable co-delivery of DC maturation stimuli [29-32]. Administration of particulate antigens via intravenous injections is an unconventional but particular suitable approach in order to target antigen to the liver. Intravenous application of protein particles led to higher immunogenicity compared to traditional subcutaneous injections in mice [33]. The application of *Plasmodium falciparum* sporozoites (PfSPZ) vaccine via intravenous but not subcutaneous injection induced strong and sustained intrahepatic T cell responses in non-human primates [34]. This finding was supported by a follow-up phase I clinical trial using intravenous application of PfSPZ in healthy individuals [35].

However, antigen delivery structures are often made of additional compounds that act as carrier forming the particle-scaffold or capsule-shell, e.g. PLGA-particles or polymeric nanocapsules. The application of such structures *in vivo* can result in unintended adverse effects such as the generation of immunity against carrier compounds [22]. Formulating

4

nanocarriers exclusively made of the specific antigen will prevent possible side effects caused by carrier substances. In addition, this approach implements a high antigen payload that can be delivered to antigen-presenting cells, as a requirement for the induction of robust T cellular immune responses as recently reviewed [36]. Therefore, the aim of the present study was to synthesize nanocapsules exclusively out of the HCV non-structural protein 5A (NS5A), delivery of nanocapsules to the primary organ affected by HCV infection, and the induction of intrahepatic immunity.

2   Materials and Methods

2.1   Nanocapsule synthesis and characterization

2.1.1   Synthesis of NS5A nanocapsules

NS5A nanocapsules were synthesized adapting a modified procedure from Baier et al. in an inverse miniemulsion using a polyaddition reaction at the droplets interface for cross-linking [37, 38]. A mixture of 125 µL of the NS5A solution (6.25 mg) and 33 µL (4.89 nmol) of cy5-labeled oligonucleotides were dissolved in PBS constituting the aqueous phase. Separately, 9 mg of the surfactant P((E/B)-*b*-EO) were dissolved in 1.88 g of cyclohexane and the mixture was added to the aqueous phase under stirring. The mixture was homogenized by ultrasound. To a solution of 2.7 mg P((E/B)-*b*-EO) in 1.25 g cyclohexane, 8.5 mg 2,4-toluene diisocyanate (TDI) was added. The mixture was added dropwise to the miniemulsion and the reaction proceeded overnight at 25 °C under stirring.

Subsequently, repetitive centrifugation (3 times for 20 min, 1664 x g) and exchange of the upper phase with pure cyclohexane was performed to remove excess surfactant. In order to transfer NCs into the aqueous phase, 500 µL of the dispersion was added in 100 µL steps to 5 g of an aqueous solution containing 0.1 wt% sodium dodecyl sulfate (SDS). The mixture was subjected to an ultrasound bath for 5 min at 25°C (25 kHz). The samples were stirred open for 24 h at 25 °C to remove cyclohexane. Repetitive centrifugation (4 times for 15 min, 1817 x g) and exchange of the supernatant with aquapure water was applied for the removal of excess SDS. The synthesis of ovalbumin (OVA) nanocapsules was described elsewhere [38].

Adsorption of MPLA onto the NC surface was performed using a slightly modified method as described previously [30]. Briefly, 1 mg of a NS5A-NC dispersion was mixed with 24 µL of MPLA/DMSO solution (0.1%) and stirred for 1 day at 4 °C. Afterwards, NCs were washed

with ultrapure water two times by centrifugation at 2.500 x g for 15 min in order to remove residues of MPLA. Finally, the supernatant was removed and the NCs were redispersed in 0.9% NaCl.

2.2 Biological analysis

2.2.1 Mice

Six to 8-week old female C57BL/6J and B6N-Tyr^{c-Brd}/BrdCrCrl albino mice were obtained from Harlan Laboratories and from the Transgenic Facility Mainz, respectively. All mice were kept under a 12 h dark, 12 h light cycle (with food and water supply ad libitum) in the animal facility of the Translational Animal Research Center, University Medical Center Mainz, Germany. The animals were treated in accordance with NIH publications entitled "Principles for Use of Animals" and "Guide for the Care and Use of Laboratory Animals". All protocols have been approved by the local Animal Care and Use Committee ("Landesuntersuchungsamt Rheinland-Pfalz").

2.2.2 Expansion of the dendritic cell population *in vivo*

The dendritic cell population in the livers of mice was expanded *in vivo* via hydrodynamic tail vein injections using methods previously described [30, 39, 40]. Briefly, 10 μg of the plasmid pUMVC3-hFLex (Vector Core Laboratory, University of Michigan) encoding the secreted portion of the human Fms-like tyrosine kinase 3 ligand (hFlt3l) was dissolved in 2 mL of 0.9% NaCl and injected into tail veins of mice within 5 s. The injection was repeated on day 6; on day 12 pre-treated mice were employed for subsequent studies.

2.2.3 Isolation of non-parenchymal liver cells and splenocytes

The non-parenchymal liver cells (NPCs) of pre-treated mice, mainly consisting of dendritic cells, Kupffer cells, and lymphocytes, were isolated from livers as described previously [41,

7

42]. Splenocytes were isolated following dissection of spleens. Single cell suspensions were prepared using a 70 µm nylon cell strainer.

2.2.4 Cultivation of non-parenchymal liver cells and splenocytes and stimulation with nanocapsules

Isolated non-parenchymal liver cells and splenocytes were cultured at 1×10^6 cells/mL in culture medium composed of HEPES-buffered RPMI 1640 medium supplemented with 10% FCS, 2 mM L-glutamine, 100 U/mL penicillin, 100 µg/mL streptomycin, 1% non-essential amino acids, 1 mM sodium pyruvate and 50 µM 2-mercaptoethanol. In order to determine the influence of nanocapsules upon NPCs, different concentrations (1 / 10 / 100 µg/mL) of NS5A- or NS5A+MPLA-NCs were added to the culture medium. Cells were cultured for 3 h or 24 h and analyzed for NC uptake and cytokine production (ICCS) as described below. Culture supernatants were obtained after 24 h incubation and analyzed in terms of cytokine secretion levels by NPCs.

2.2.5 Effects of NCs after *in vivo* injection

For *in vivo* experiments 300 µg NS5A- or NS5A+MPLA-NCs were suspended in 300 µL NaCl 0.9% and intravenously injected into tail veins. Mice injected with 300 µL vehicle (0.9% NaCl) served as a negative control. NPCs from NC-treated mice were isolated 4 h after injection as described in 2.2.4 and analyzed for NC uptake and cytokine production determined by ICCS.

In vivo imaging studies were performed in order to analyze the biodistribution of NCs. Therefore, B6N-Tyr[c-Brd]/BrdCrCrl albino mice were depilated at the abdominal and thoracic zone and the corresponding dorsal areas. NS5A- or NS5A+MPLA-NCs (300 µg) labeled with IRdye 800CW (LI-COR Biosciences) were injected intravenously and mice were analyzed at

time points 30 min, 1 h, 2 h, 3 h, and 4 h using the IVIS SpectrumCT imager (PerkinElmer) and the Living Image software 4.5.

2.2.6 Flow cytometry and intracellular cytokine staining

Flow cytometric analysis was performed according to previously published methods using the multi-channel flow cytometer BD LSR II (BD Biosciences) equipped with FACSDiva software (BD Biosciences) [39, 42]. Briefly, NPCs were incubated with 5 µg of anti-mouse CD16/32 (clone 2.4G2, rat isotype) for 15 min at 4 °C in order to block unspecific antibody binding by Fc receptors. Subsequently, NPCs were stained for 30 min with antibodies specific for CD45 (V450 − clone 30-F11), CD11c (PE-Cy7 − N418), F4/80 (FITC − BM8), CD4 (APC-Cy7 − GK1.5), CD40 (PerCP-CF710 − 1C10), CD80 (FITC − 16-10A1) or CD86 (PE-Cy7 − GL1). For intracellular cytokine stainings (ICCS), isolated NPCs were cultured for 16 h in culture medium supplemented with or without different NC formulations or different concentrations of NS5A (immunization readouts). A protein transport inhibitor containing Brefeldin A (GolgiPlug - BD Biosciences) was added after 3 h of incubation in order to inhibit cytokine secretion. Cells were then harvested, fixed and permeabilized using a cytofix/cytoperm kit (BD Pharmingen) and additionally incubated with anti-mouse interleukin-6 (PE − MP5-20F3), IL-12p70 (V450 − C15.6) or IFNγ (APC − XMG1.2) followed by flow cytometric analyses.

2.2.7 Quantification of cytokine secretion

Quantification of cytokine secretion by NPCs was performed using a cytometric bead array kit (BD CBA Mouse Inflammation Kit, BD Biosciences) in accordance with manufacturer´s instructions followed by data analysis using FCAP 3.0 software (SoftFlow, Inc.). Cytokines secreted by NPCs and splenocytes derived from immunized mice were determined using commercial enzyme-linked immunosorbent assays (Read-Set-Go, eBioscience) measuring IFNγ, IL-2, and IL-4 according to manufacturer´s instructions.

2.2.8 Immunization

Following expansion of DCs *in vivo*, groups of 5 mice each were immunized as follows: (i) NS5A-NCs, (ii) NS5A+MPLA-NCs, (iii) NS5A+MPLA-NCs + αCD40, (iv) OVA+MPLA-NCs. Mice were inoculated intravenously three times at 2-week intervals with 50 μg of NCs each. In the case of group (iii) 50 μg αCD40 was injected intraperitoneally at each immunization. One week after the final inoculation, mice were sacrificed and NPCs and splenocytes were isolated for subsequent analyses. The immunization schedule is shown in Table 1.

Table 1: Immunization schedule

day 0	Hydrodynamic injection of hFlt3l
day 6	Hydrodynamic injection of hFlt3l
day 12	First immunization (NCs i.v. ± αCD40 i.p.)
day 19	Hydrodynamic injection of hFlt3l
day 26	Second immunization
day 40	Third immunization
day 48	Sacrifice mice for immunological studies

2.2.9 Sera collection and humoral immune response

Sera of immunized mice were collected by cardiac puncture and subsequent centrifugation at 10,000 x g for 5 min. Quantification of NS5A-specific antibody titers in serum samples was assessed by ELISA. Therefore, high binding microtiter plates (Greiner Bio-One) were coated with 10 μg/mL NS5A dissolved in 100 mM sodium bicarbonate buffer (pH 9.6) over night at 4 °C. Unspecific binding of antibodies was blocked by incubation with 5% bovine serum albumin for 1 h followed by a 2 h incubation of two-fold serial dilutions of serum samples. NS5A-specific antibodies present in sera were labeled with a goat anti-mouse IgG-peroxidase (1:2,000 in PBS - Sigma-Aldrich, A4416) for 2 h. Visualization of NS5A antibodies was

achieved by incubation with TMB substrate for 10 min followed by subsequent absorbance measurements at 450 nm.

2.2.10 Statistical analysis

Experiments were performed in triplicates and analyzed using SigmaPlot 11 software (Systat Software, Inc.) and GraphPad Prism 6.0 (GraphPad Software, Inc.). For comparisons between two groups only, a non-paired Student's *t*-test was performed (* $p < 0.05$; ** $p < 0.01$; *** $p < 0.001$). When more than two groups were compared to each other, a one way ANOVA test or a Kruskall-Wallis test were performed followed by a Holm-Sidak or Tukey posthoc test procedure, respectively, in order to determine which groups differed significantly.

3 Results

3.1 Synthesis of NS5A nanocapsules

Fluorescently labeled NS5A nanocapsules were obtained in an inverse miniemulsion. The nanocapsule formation was achieved through a polyaddition reaction at the oil/aqueous nanodroplet interface using TDI as a cross-linker for the NS5A protein, forming urea linkages. The nanocapsules were subsequently transferred to the water phase. The obtained core-shell morphology was verified by scanning electron microscopy (SEM) and transmission electron microscopy (TEM) as displayed in Figure 1.
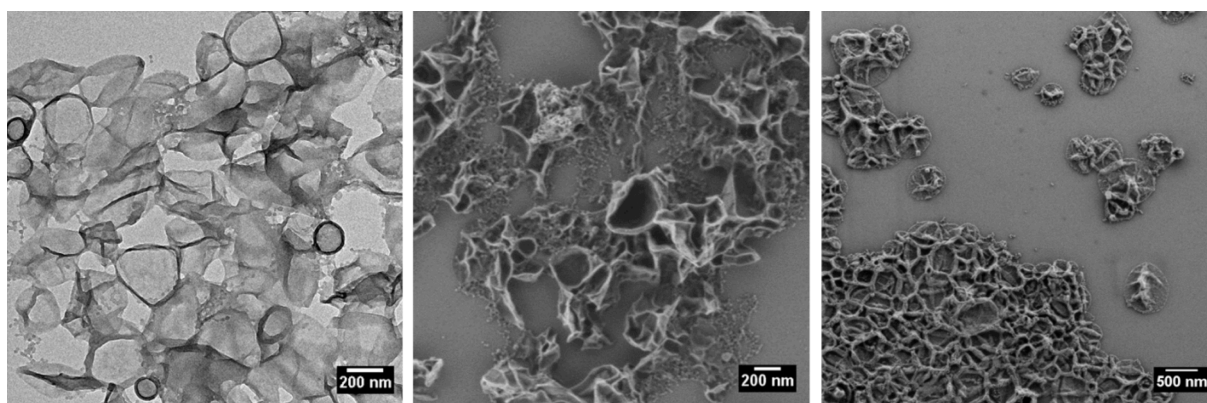

Figure 1: Electron microscopic characterization of NS5A-NCs. *left*: transmission electron microscopy (TEM) image, *middle*: scanning electron microscopy image (SEM) of NS5A nanocapsules in cyclohexane phase, *right:* SEM image of the nanocapsules in aqueous phase.

Dynamic light scattering was used to determine the size of the nanocapsules. The cy5-labeled NS5A nanocapsules had an average diameter of 370 nm in the cyclohexane phase and 410 nm in the aqueous dispersion after purification (Supporting Figure 1). Residuals of the negatively charged anionic surfactant, used for stabilization during the transfer of the nanocapsules from the organic to the aqueous phase, account for the negative zeta potential of -31.8 mV. The amphiphilic MPLA was adsorbed onto the nanocapsules in defined quantities. A loading capacity (LC) of 0.66% was documented using a limulus amebocyte lysate assay. Nanocapsules based on ovalbumin (OVA) were synthesized as described previously and applied as negative control in immunization studies [38].

3.2 Toxicity of NS5A nanocapsules

Toxicity of different NS5A nanocapsule concentrations was evaluated by coincubation with murine non-parenchymal liver cells (NPCs) for 24 h and staining of dead cells with 7-Aminoactinomycin D (7-AAD). Subsequent flow cytometric analysis revealed a percentage of dead NPCs of around 15% (Figure 2). Cocultivation with NS5A-NCs resulted in no significant increase in toxicity, whereas incubation with NS5A+MPLA-NCs (1 µg/mL and 10 µg/mL) led to a slight reduction of 7-AAD$^+$ NPCs.
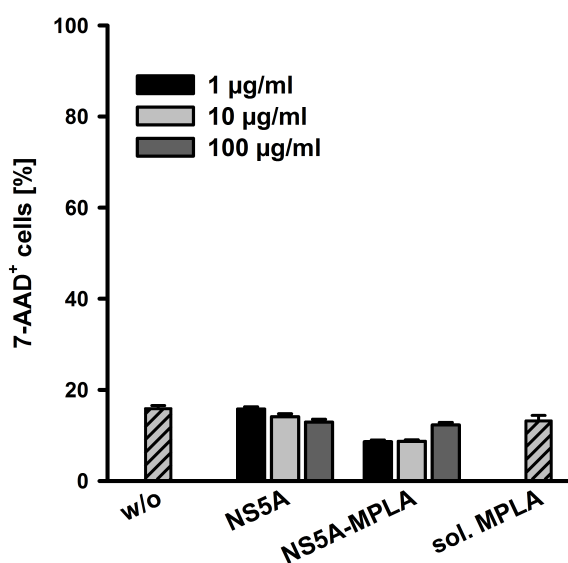

Figure 2: Toxicity of NS5A nanocapsule formulations was documented by 7-AAD-staining and subsequent flow cytometric analysis. NPCs were coincubated with NS5A- or NS5A+MPLA-NCs at different concentrations (1, 10, or 100 µg/ml) for 24 hours. Data represent the mean ± SD of four independent experiments conducted with n = 3.

3.3 NC uptake *in vitro*

Uptake of NS5A nanocapsules by NPCs derived from hFlt3l-treated mice was evaluated by two methods. First, confocal laser scanning microscopy (CLSM) was performed in order to verify intracellular uptake of NCs excluding adhesion to the cell membrane. Figure 3 A and B clearly documents the intracellular localization of cy5-labeled NS5A nanocapsules (red) after cocultivation with NPCs for 3 h *in vitro* (see also Supporting Video 1). None of the analyzed cells displayed signs of plasma membrane adherence. Internalized NCs displayed a dense,

compartmentalized fluorescence signal. Flow cytometric analysis revealed a concentration-dependent increase in NC$^+$ NPCs from 2.5% to 34.1% by incubation with 1 μg/mL or 100 μg/mL for 3 h, respectively (Figure 3 C). Prolonged incubation up to 24 h did not significantly augment the percentage of NC ingesting NPCs in comparison to the 3 h incubation period (Figure 3 D). In addition, adsorption of MPLA onto the NC shell induced a significantly enhanced uptake for NC concentration 10 μg/mL and 100 μg/mL from 10.8% to 15.0% and 27.7% to 34.1%, respectively. However, incubation with 1 μg/mL NS5A+MPLA-NCs led only to a minute and non-significant increase regarding NC ingestion by NPCs.
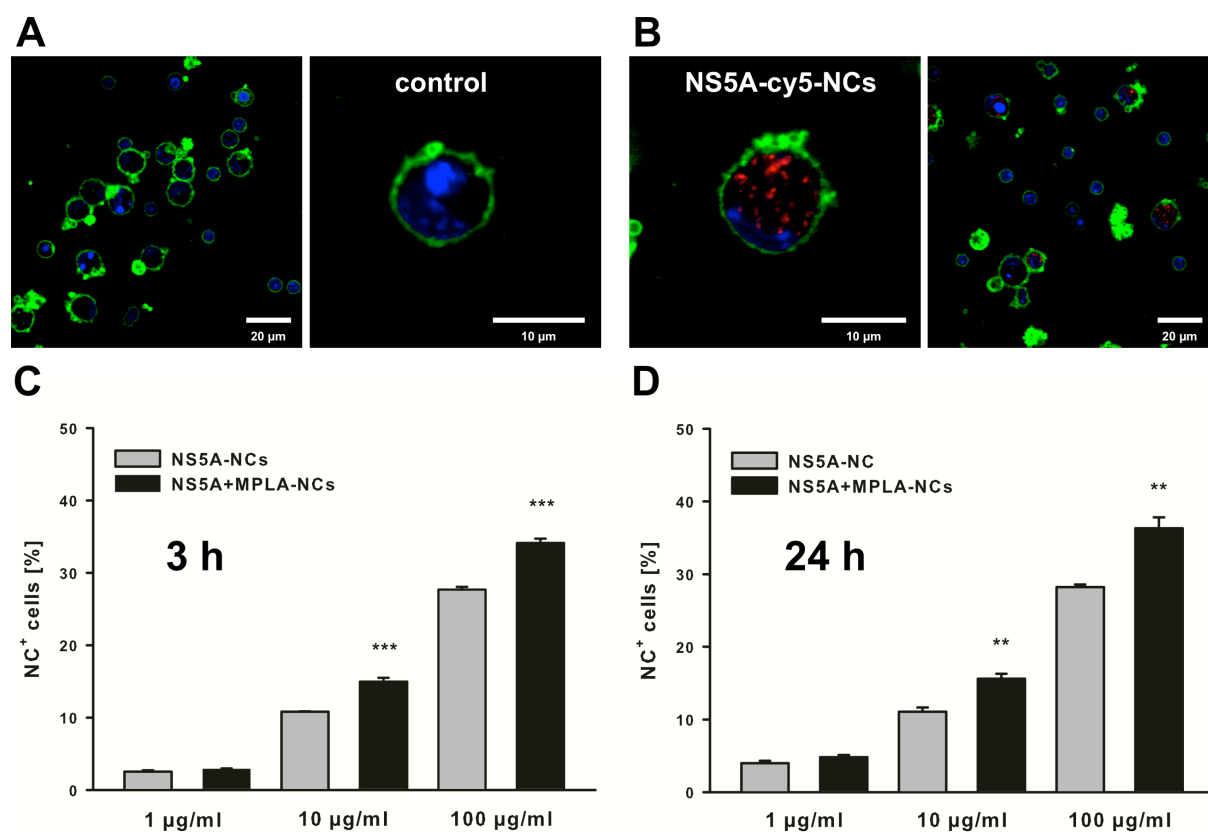

Figure 3: (A, B) Confocal laser scanning microscopy was performed in order to document the uptake of NS5A-NCs nanocapsules (red) by NPCs (B). Cells incubated without nanocapsules served as negative control (A). Plasma membrane was stained with CellMask Orange (green) and nuclei were stained using Hoechst 33342 (blue). (C, D) Flow cytometric analysis was performed to quantify the uptake of different concentrations (1, 10, or 100 μg/ml) of NS5A- or NS5A+MPLA-NCs by NPCs after 3 h (C) and 24 h (D) of coincubation. Data shown in Figure 3 C and D are expressed as mean ± SD representing five independent experiments conducted with n = 3. Comparisons between NS5A- and NS5A+MPLA-NCs were performed using a non-paired Student's t-test. Significance was given with $p < 0.01$ (**); $p < 0.001$ (***).

3.4   MPLA-induced activation of dendritic cells *in vitro*

The ability of adjuvanted NS5A nanocapsules to induce activation and maturation of dendritic cells with respect to the secretion of cytokines and the expression of surface markers *in vitro* was investigated. MPLA-adsorption on NS5A-NCs induced a significant upregulation of CD40, CD80 and CD86 expression by CD11c$^+$ NPCs (Figure 4 A). This effect depended on the applied NC concentration and even surpassed the activation state of DCs stimulated with MPLA in solution at a concentration of 1 µg/mL. Incubation with NS5A-NCs did not induce a significant upregulation of surface marker expression even at high concentrations. In addition to phenotypic analysis, the potential of NCs to induce DC activation was evaluated by measurements of the cytokines IL-6, TNFα, and IFNγ secreted by NPCs into culture supernatants. Figure 4 B and C displays a significant increase of IL-6 and TNFα levels, when NS5A-NCs were coated with MPLA in comparison to the negative control without stimulation. In contrast, no secretion of IL-6 or TNFα was detected with NS5A-NCs without MPLA. MPLA in solution served as a control leading to lower levels of both cytokines for NS5A+MPLA-NCs at a concentration of 100 µg/mL. TNFα secretion, induced by incubation with 10 µg/mL MPLA-coated NCs, even surpassed the levels induced by the positive control. Detectable levels of IFNγ could only be generated by stimulation with 10 µg/mL or 100 µg/mL NS5A+MPLA-NCs (Figure 4 D). In cell culture supernatants IL-12p70 could not be detected (data not shown). Therefore, intracellular cytokine staining of NPCs was performed documenting an increase in IL-12p70$^+$, IL-6$^+$, and double positive CD11c$^+$ cells, when NS5A-NCs were additionally coated with MPLA (Figure 4 E). This effect was even more prominent after gating on NC$^+$ cells.
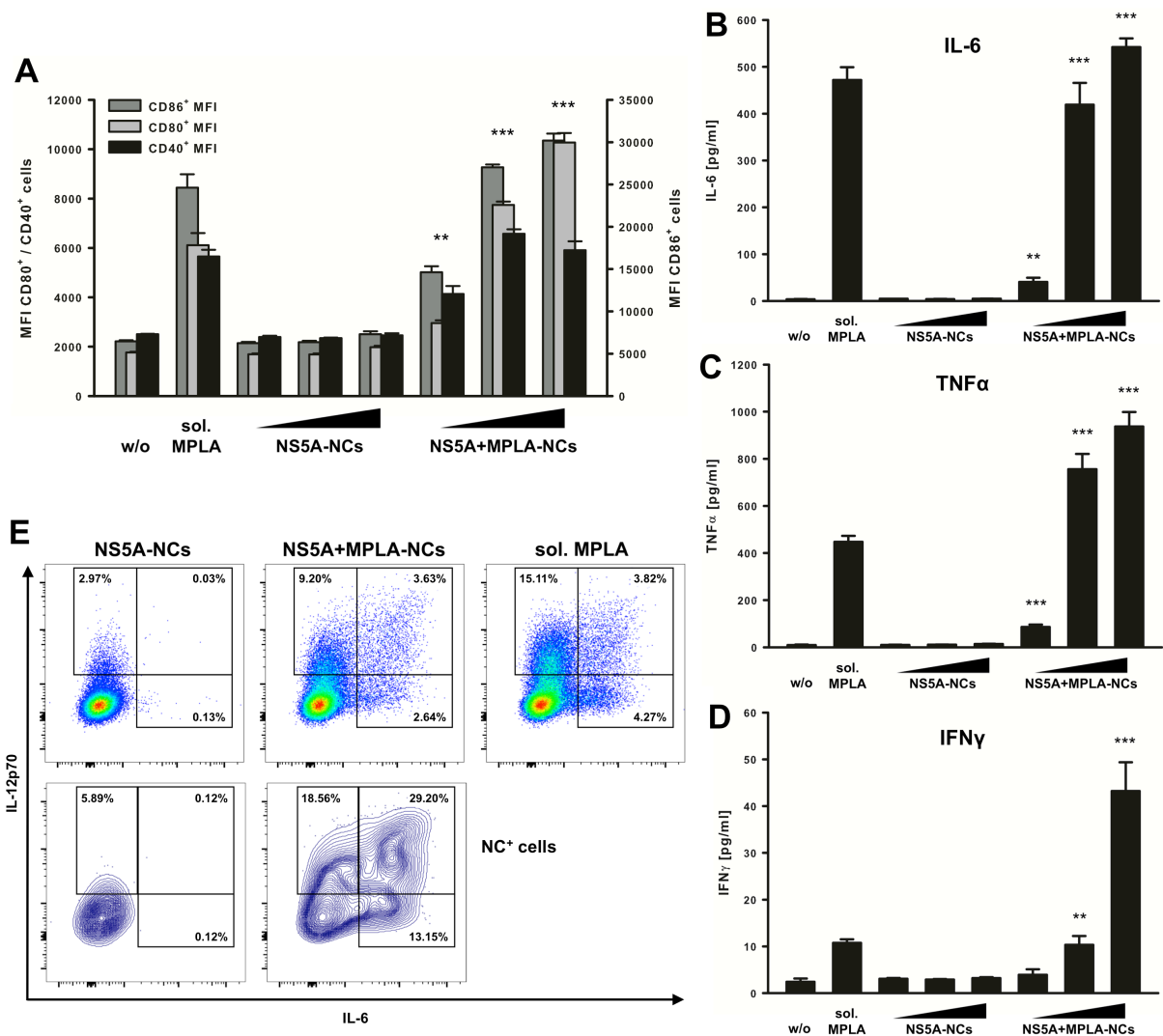
Figure 4: Phenotypic maturation of NPCs and cytokine production after coincubation with different nanocapsule formulations for 24 hours. MPLA (1 µg/ml) in solution served as positive control. (A) CD80 (light grey), CD86 (dark grey), and CD40 (black) expression was analyzed using flow cytometry and indicated as median fluorescence intensity (MFI) of positively stained cells. Cytokine secretion was evaluated using a cytometric bead array analyzing IL-6 (B), TNFα (C) and IFNγ (D). (E) Intracellular cytokine staining of IL-12p70 and IL-6 were performed followed by analysis of the CD11c^{+} NPC population (upper panel) and the NC^{+} CD11c^{+} NPCs (lower panel). Data represent mean ± SD of three independent experiments conducted with n = 3. Comparisons between NS5A- and NS5A+MPLA-NCs were performed using a non-paired Student's t-test and significance was given with $p < 0.01$ (**), $p < 0.001$ (***).

3.5 *In vivo* uptake of nanocapsules in the liver

The deposition of two NS5A nanocapsule formulations in the liver was evaluated after intravenous injections. *In vivo* imaging analysis was performed at different time points following intravenous administration of NS5A- or NS5A+MPLA-NCs. Figure 5 A displays a preferential deposition of nanocapsules in the liver also visualized in a 3D reconstruction using fluorescence imaging tomography (see Supporting Video 2). The intrahepatic

16

accumulation of NS5A-NCs was even higher after adsorption of MPLA with a significant increase at 30 min and 3 h post injection (Figure 5 A). *Ex vivo* imaging of organs isolated 4 h after NC injection confirmed an almost exclusive accumulation of both NC formulations in the liver, while a very weak signal was observed originating from the spleen. In the lung no accumulation of NCs was detectable. In addition, flow cytometric analysis of NPCs isolated 4 h after NC injection resulted in an overall uptake of about 1% for both NC formulations (Figure 5 B). Due to the pre-treatment of mice with hFlt3l, resulting in a substantial expansion of the DC population, more than 99% of isolated NPCs were positively stained for CD45. Accordingly, only a minute percentage of $CD45^-$ NPCs account for NC uptake. Further phenotypic analysis of NC ingesting NPCs demonstrated $CD11c^+$ dendritic cells and $F4/80^+$ Kupffer cells as primary target cells with about 64% and 36% of total $CD45^+$ NC^+ NPCs, respectively. A significant effect of MPLA-coating in terms of cell type targeting or overall uptake as observed *in vitro* could not be confirmed under *in vivo* conditions. However, intracellular cytokine staining of NPCs after intravenous administration of NS5A+MPLA-NCs showed an increase in $IL-12p70^+$, $IL-6^+$, and in double positive $CD11c^+$ NC ingesting cells in comparison to the application of NS5A-NCs without adjuvant (Figure 5 C).
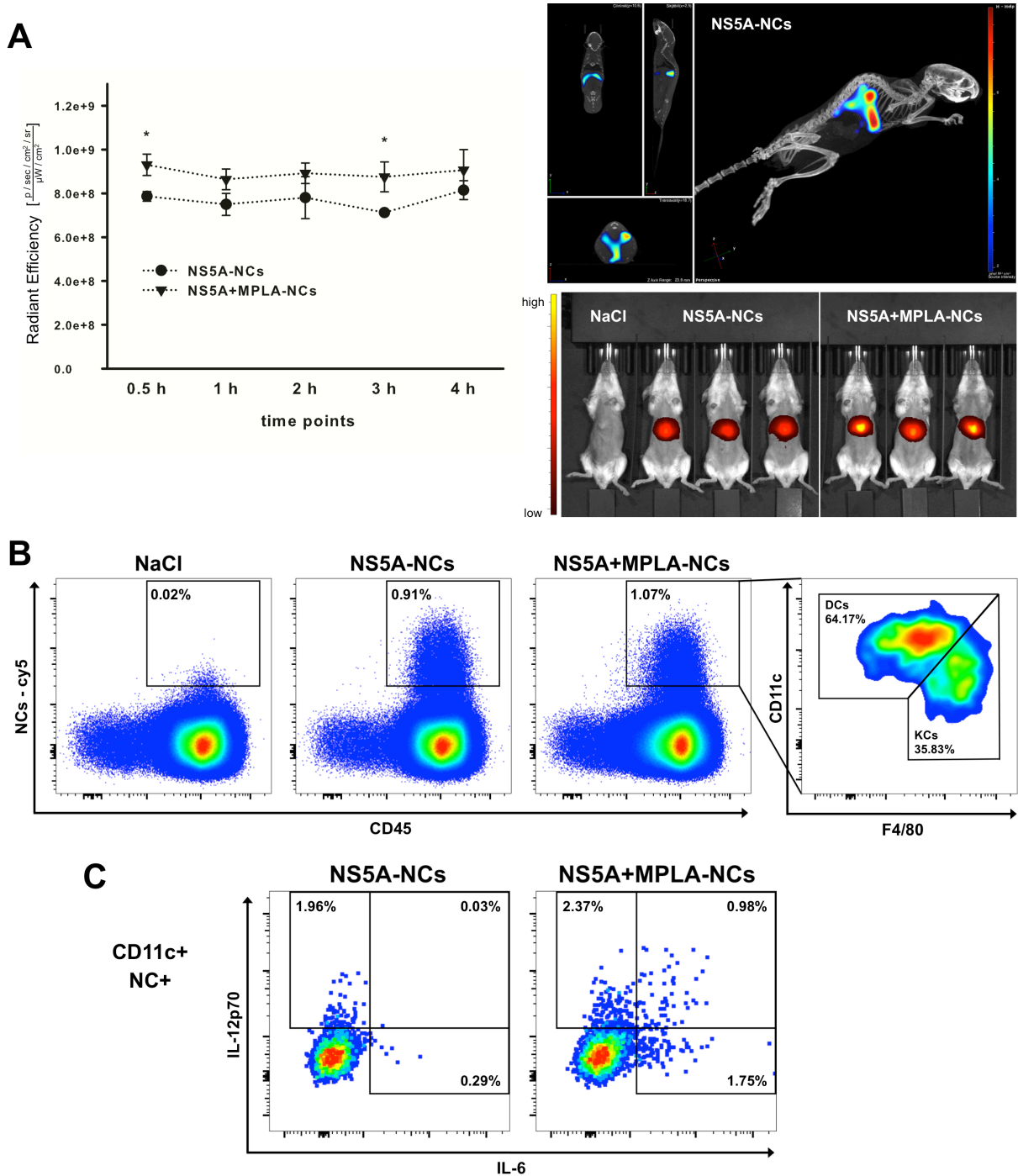
Figure 5: (A) *In vivo* imaging of NS5A- and NS5A+MPLA-NCs labeled with IRdye 800CW was performed at different time points (30 min / 1 h / 2 h / 3 h / 4 h) after intravenous injection into B6N-Tyr^{c-Brd}/BrdCrCrl albino mice (n = 3). Comparisons between NS5A- and NS5A+MPLA-NCs were performed using a non-paired Student's *t*-test and significance was given with p < 0.05 (*). *left:* fluorescence signal intensities (radiant efficiency) contributing to IRdye 800CW-labeled NCs. *Right, upper panel:* representative image of an albino mouse 4 h after injection of NS5A-NCs analyzed using fluorescence intensity tomography and 3D reconstruction. Coregistration of bones and fluorescence signals are depicted. *Right, lower panel:* epi-illumination image of mice 4 h after NC injection. (B) flow cytometric analysis of isolated NPCs following injection (4 h) with NS5A- or NS5A+MPLA-NCs and characterization of NC ingesting cells. NaCl served as negative control. (C) intracellular cytokine stainings of IL-12p70 and IL-6 after intravenous administration of NCs and flow cytometric analysis of CD11c$^+$NC$^+$ NPCs. Cells were isolated 4 h after injection and additionally incubated with GolgiPlug for 16 h prior to analysis. Representative dot plots are shown.

3.6 Immunization with NS5A-NCs

Evaluation of anti-HCV NS5A immune responses was based on previous studies demonstrating that the resolution of HCV is accompanied with intrahepatic T_h1-directed immune responses. The main focus of this study was the evaluation of cellular immune responses localized in the liver. Hence, concentrations of IFNγ and IL-2 were measured in culture supernatants of NPCs isolated from livers of immunized mice following stimulation with different concentrations of NS5A. Figure 6 A shows an increase in IL-2 and IFNγ secretion by NPCs derived from livers of mice that were vaccinated with NS5A+MPLA-NCs. Additional adjuvant supplementation with αCD40 further enhanced this effect. The immunization with OVA+MPLA-NCs did not induce any significant cytokine secretion. Splenocytes isolated from immunized mice displayed a similar pattern in terms of IFNγ secretion (Figure 6 A). NS5A-NCs without adjuvant showed a slight, concentration-dependent increase in IFNγ and IL-2 levels. These findings were confirmed by intracellular cytokine stainings represented by an elevated frequency of IFNγ-producing NPCs from 0.03%, 0.15%, and 0.05% up to 0.44% (NS5A-NCs), 0.54% (NS5A+MPLA-NCs), and 0.47% (NS5A+MPLA-NCs + αCD40), respectively (Figure 6 B). All administered NC formulations did not induce significant secretion of IL-4 after stimulation with NS5A (Supporting Figure 2).

In order to determine humoral immune responses, serum titers of NS5A-specific antibodies were measured (Figure 6 C). Immunization with MPLA-adjuvanted NS5A-NCs led to a substantial production of antigen-specific antibodies, while NS5A-NCs without MPLA or OVA+MPLA-NCs did not induce considerable titers.
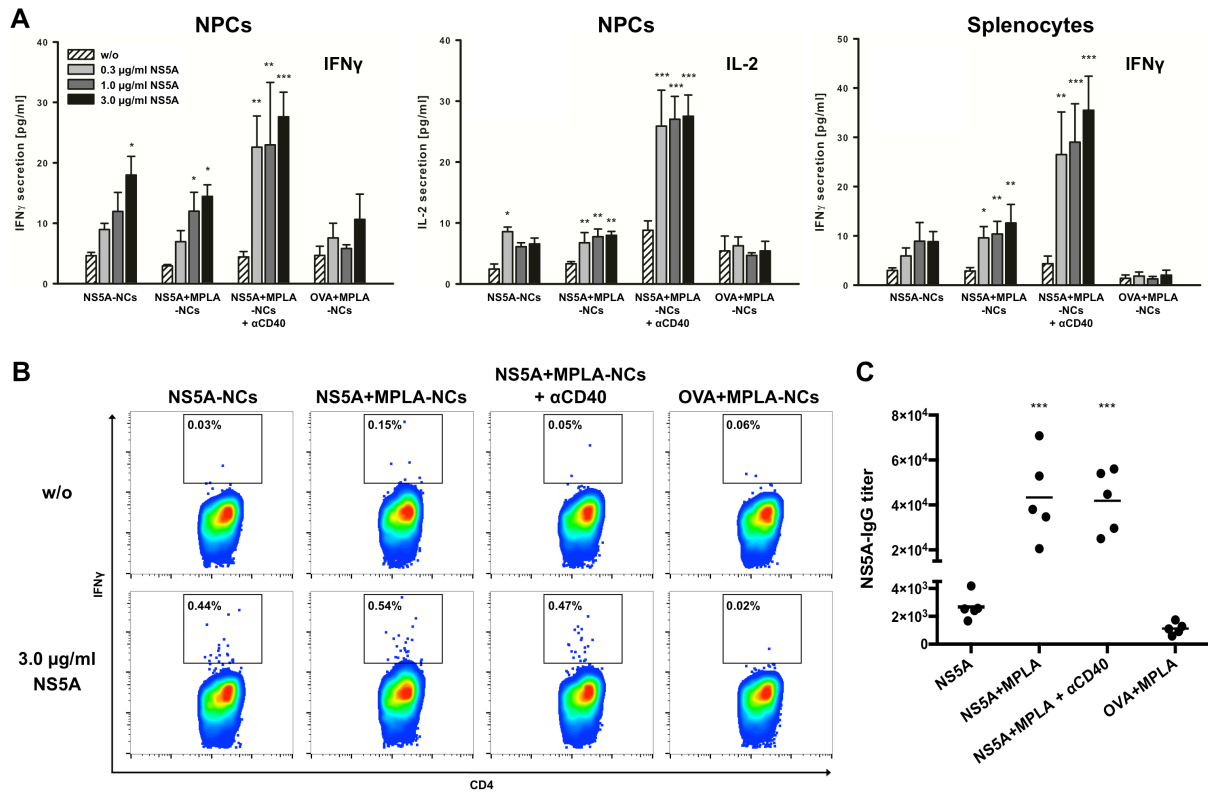
19

Figure 6: NPCs and splenocytes obtained from mice immunized three times with different NC formulations were cultured with recombinant HCV NS5A at indicated concentrations. (A) Culture supernatants were collected after 24 h; IFNγ and IL-2 concentrations were quantified by an enzyme-linked immunosorbent assay. (B) NPCs were cultured for a total of 16 h, in the presence of GolgiPlug during the last 4 h, following intracellular cytokine staining of IFNγ and flow cytometric analysis. (C) Antibody responses were evaluated after serum collection from immunized mice. NS5A-specific antibody titers were determined using an enzyme-linked immunosorbent assay. Data represent the means ± SD derived from five mice. All conditions were compared to the negative control (without stimulation) or to the OVA+MPLA-NCs group for antibody responses and significance was given with $p < 0.05$ (*), $p < 0.01$ (**), $p < 0.001$ (***) (One way ANOVA).

4 Discussion

The development of new direct acting antiviral drugs against hepatitis C virus infections, leading to SVR rates of over 95% and low risk of side effects, tremendously improved the clinical outcome of infected patients [43]. Nevertheless, high treatment costs, the possibility of emerging viral resistance to DAAs due to high mutational rates or the pre-existing variability of HCV [44, 45], and the risk of reinfection after viral clearance [46] still represent remarkable limitations in the treatment of HCV infected patients. Intravenous drug users have a high risk for HCV infections and are particularly prone to reinfections [47, 48]. Thus, the development of an HCV vaccine remains to be an essential medical need. One of the main challenges recent vaccine development efforts encountered, is the exceptional tolerogenic microenvironment predominating the liver [14]. Overcoming the state of tolerance is a key factor for the induction of antigen-specific immunity with a robust protection against hepatotropic pathogens [49, 50]. A targeted delivery of antigens to liver-resident antigen-presenting cells, such as dendritic cells or Kupffer cells, represents a particular promising approach for the induction of immune responses *in situ* [51].

Accordingly, the aim of the present proof-of-concept study was the development of a polymeric antigen delivery system consisting of the HCV non-structural protein 5A in combination with an adjuvant defined by the following characteristics: (i) low cytotoxicity, (ii) efficient ingestion and a T_h1-directed activation of dendritic cells *in vitro* and *in vivo*, (iii) accumulation in the liver after intravenous injection, (iv) induction of intrahepatic antigen-specific cellular immune responses following intravenous immunizations. In a previous study, we described the synthesis of robust and biodegradable protein nanocapsules made of albumins (ovalbumin and bovine serum albumin) using the method of miniemulsion polymerization at the droplets interface [38]. This technique is particular suitable due to its transferability for the polymerization of other proteins serving as antigens in vaccination

21

approaches. In order to avoid any unintended side effects or unspecific immune responses caused by additional carrier substances and to increase the amount of delivered antigen, often representing a limitation of polymeric particulate structures [22], nanocapsules exclusively synthesized of HCV NS5A as a model antigen were prepared. The miniemulsion technique requires approximately 10 mg of raw material per batch even after downscaling, thus the NS5A protein had to be produced at large scale in a yeast-based (Pichia pastoris) expression system. NS5A is a strongly amphiphilic protein consisting of three domains and an amphipathic α-helix of 30 aa residues located at the amino-terminus that mediates membrane association at the endoplasmatic reticulum [52, 53]. In order to avoid binding to intracellular membrane structures and to increase the yield of expressed protein, the first 33 amino acids were eliminated leading to a shortened NS5A protein (414 aa) that was used for all experiments presented in this study.

The resulting NS5A nanocapsules displayed a spherical core-shell morphology as determined by electron microscopy (Figure 1). No aggregation or flocculation was detected at any steps during synthesis and NCs remained stable at 4 °C under constant stirring. The slightly bigger size in water is possibly due to a swelling of the NCs in the water phase. A limulus amebocyte lysate assay revealed a loading capacity of 0.66% after adsorption of MPLA onto the NC surface representing a concentration of MPLA of 6.6, 66, or 660 ng/mL, depending on the applied NC concentration (1, 10, or 100 μg/mL), respectively. This finding is comparable to a LC of up to 0.86% after incorporation of MPLA in PLGA nanoparticles as reported recently [54]. The prepared nanocapsule formulations showed no significant toxicity profile even at concentrations of up to 100 μg/mL (Figure 2). This finding verified sufficient removal of potentially toxic residual substances needed during synthesis and redispersion. Mice injected with NS5A-NCs developed no clinical symptoms at all, whereas application of MPLA-coated nanocapsules was accompanied by a mild fatigue with a short duration of about 2 hours. This

observation corresponds to slightly increased side effects observed for the MPLA-supplemented hepatitis B virus vaccine (Fendrix®) [55].

Confocal laser scanning microscopy verified intracellular localization of NCs that appeared to be compartmentalized after phagocytosis (see Figure 3 and Supporting Video 1). Quantification using FACS analysis revealed a rapid (<3 h) uptake of NS5A nanocapsules *in vitro* that could not be substantially increased by extension of the incubation period of up to 24 h, assuming a phagocytic saturation after 3 h incubation. Surface modification of NS5A-NCs with MPLA led to an enhanced overall uptake, confirming previous studies with hydroxyethyl starch nanocapsules [29, 30]. In addition, MPLA coating induced a massive activation of murine dendritic cells. Intracellular cytokine staining revealed a T_h1-directed activation of DCs after internalization of NS5A+MPLA-NCs measured by production of the bioactive form of IL-12 (Figure 4 E), while a substantial production of IL-10 could not be detected. NS5A+MPLA-NCs at a concentration of 10 µg/mL feature a calculated concentration of 66 ng/mL MPLA that was applied for cell culture assays. Given the fact that 1 µg/mL MPLA in solution served as positive control and induced comparable levels of pro-inflammatory cytokines, a dose-sparing effect by more than 15 times can be hypothesized, similar to our previous finding [29]. Several studies described the importance of combining antigens along with adjuvants in nanoparticle-based immunization approaches [31, 56-58]. Encapsulation of adjuvant (R848) and antigen (OVA) promoted vigorous immune responses allowing the usage of 100-fold lower adjuvant doses in a murine model [56].

In recent studies a beneficial *in vivo* uptake of nanocapsules was reported after surface-functionalization with MPLA [30]. This finding could be confirmed using NS5A+MPLA-NCs, though not at the observed magnitude. *In vivo* imaging revealed a preferential deposition of NS5A-NCs in the liver. The hydrodynamic delivery of a human Fms-like tyrosine kinase 3 ligand (hFlt3l)-encoding plasmid led to a massive increase in liver DC frequency as published

23

previously [30]. This method was applied in order to enhance NC uptake by dendritic cells up to a frequency of 60% related to the total NPC population. The potential of MPLA-coated NCs to promote secretion of IL-12 and IL-6 after NC ingestion by liver DCs was observed even after intravenous injection, representing essential prerequisites for the induction of intrahepatic cellular immune responses [18].

In a last set of experiments the generation of intrahepatic immune responses was observed after three times injection of different NC formulations in hFlt3l-treated mice. Ovalbumin nanocapsules functionalized with MPLA (OVA+MPLA-NCs) served as an antigen control for NS5A. The synthesis and characterization of OVA-NCs has been published elsewhere [38]. The secretion of IFNγ and IL-2 in the absence of IL-4 after restimulation with NS5A suggests the induction of a T_h1-directed immune response. This finding was confirmed by intracellular cytokine staining of NPCs. In addition to the T_h1-related response, significantly higher titers of NS5A-specific antibodies (IgG) were determined, when MPLA was adsorbed to NCs. NS5A-NCs without adjuvant did not induce any substantial antibody production compared to ovalbumin-based NCs.

In conclusion, in this proof-of-concept study polymeric nanocapsules synthesized exclusively of the HCV-specific NS5A antigen and functionalized with the adjuvant MPLA proved the capability to target liver-resident antigen-presenting cells leading to an efficient maturation and activation. The induction of intrahepatic cellular immunity and humoral responses after immunization provides the basis for the development of vaccines tackling liver-associated pathogens such as hepatitis C virus or Malaria parasites. Optimizing NC synthesis and adjuvant combinations will be the challenges of future studies.

Acknowledgements

References

1. Mohd Hanafiah K, Groeger J, Flaxman AD, Wiersma ST (2013) Global epidemiology of hepatitis C virus infection: new estimates of age-specific antibody to HCV seroprevalence. *Hepatology* 57(4):1333-1342.

2. Gower E, Estes C, Blach S, Razavi-Shearer K, Razavi H (2014) Global epidemiology and genotype distribution of the hepatitis C virus infection. *J. Hepatol.* 61(1 Suppl):S45-57.

3. Messina JP, Humphreys I, Flaxman A*, et al.* (2015) Global distribution and prevalence of hepatitis C virus genotypes. *Hepatology* 61(1):77-87.

4. Lauer GM, Walker BD (2001) Hepatitis C virus infection. *N Engl J Med* 345(1):41-52.

5. Perz JF, Armstrong GL, Farrington LA, Hutin YJ, Bell BP (2006) The contributions of hepatitis B virus and hepatitis C virus infections to cirrhosis and primary liver cancer worldwide. *J Hepatol* 45(4):529-538.

6. Walker DR, Pedrosa MC, Manthena SR, Patel N, Marx SE (2015) Early View of the Effectiveness of New Direct-Acting Antiviral (DAA) Regimens in Patients with Hepatitis C Virus (HCV). *Adv. Ther.*

7. Lawitz E, Poordad FF, Pang PS*, et al.* (2014) Sofosbuvir and ledipasvir fixed-dose combination with and without ribavirin in treatment-naive and previously treated patients with genotype 1 hepatitis C virus infection (LONESTAR): an open-label, randomised, phase 2 trial. *Lancet* 383(9916):515-523.

8. Sulkowski MS, Gardiner DF, Rodriguez-Torres M*, et al.* (2014) Daclatasvir plus sofosbuvir for previously treated or untreated chronic HCV infection. *N Engl J Med* 370(3):211-221.

9. Hill A, Khoo S, Fortunak J, Simmons B, Ford N (2014) Minimum costs for producing hepatitis C direct-acting antivirals for use in large-scale treatment access programs in developing countries. *Clin Infect Dis* 58(7):928-936.

10. Hill A, Cooke G (2014) Medicine. Hepatitis C can be cured globally, but at what cost? *Science* 345(6193):141-142.

11. Bowen DG, Walker CM (2005) Mutational escape from CD8+ T cell immunity: HCV evolution, from chimpanzees to man. *J Exp Med* 201(11):1709-1714.

12. Abe M, Tokita D, Raimondi G, Thomson AW (2006) Endotoxin modulates the capacity of CpG-activated liver myeloid DC to direct Th1-type responses. *Eur. J. Immunol.* 36(9):2483-2493.

13. De Creus A, Abe M, Lau AH, *et al.* (2005) Low TLR4 expression by liver dendritic cells correlates with reduced capacity to activate allogeneic T cells in response to endotoxin. *J. Immunol.* 174(4):2037-2045.

14. Thomson AW, Knolle PA (2010) Antigen-presenting cell function in the tolerogenic liver environment. *Nat Rev Immunol* 10(11):753-766.

15. Diepolder HM, Zachoval R, Hoffmann RM, *et al.* (1995) Possible mechanism involving T-lymphocyte response to non-structural protein 3 in viral clearance in acute hepatitis C virus infection. *Lancet* 346(8981):1006-1007.

16. Thimme R, Oldach D, Chang KM, *et al.* (2001) Determinants of viral clearance and persistence during acute hepatitis C virus infection. *J Exp Med* 194(10):1395-1406.

17. Thimme R, Binder M, Bartenschlager R (2012) Failure of innate and adaptive immune responses in controlling hepatitis C virus infection. *FEMS Microbiol Rev* 36(3):663-683.

18. Flynn JK, Dore GJ, Hellard M, *et al.* (2013) Maintenance of Th1 hepatitis C virus (HCV)-specific responses in individuals with acute HCV who achieve sustained virological clearance after treatment. *J Gastroenterol Hepatol* 28(11):1770-1781.

19. Mbow ML, De Gregorio E, Valiante NM, Rappuoli R (2010) New adjuvants for human vaccines. *Curr Opin Immunol* 22(3):411-416.

20. Bohannon JK, Hernandez A, Enkhbaatar P, Adams WL, Sherwood ER (2013) The immunobiology of toll-like receptor 4 agonists: from endotoxin tolerance to immunoadjuvants. *Shock* 40(6):451-462.

21. Gregory AE, Titball R, Williamson D (2013) Vaccine delivery using nanoparticles. *Front Cell Infect Microbiol* 3:13.

22. Marasini N, Skwarczynski M, Toth I (2014) Oral delivery of nanoparticle-based vaccines. *Expert Rev Vaccines* 13(11):1361-1376.

23. Audran R, Peter K, Dannull J, *et al.* (2003) Encapsulation of peptides in biodegradable microspheres prolongs their MHC class-I presentation by dendritic cells and macrophages in vitro. *Vaccine* 21(11-12):1250-1255.

24. Waeckerle-Men Y, Groettrup M (2005) PLGA microspheres for improved antigen delivery to dendritic cells as cellular vaccines. *Adv Drug Deliv Rev* 57(3):475-482.

25. O'Hagan DT, Singh M, Ulmer JB (2006) Microparticle-based technologies for vaccines. *Methods* 40(1):10-19.

26. Shen Z, Reznikoff G, Dranoff G, Rock KL (1997) Cloned dendritic cells can present exogenous antigens on both MHC class I and class II molecules. *J. Immunol.* 158(6):2723-2730.

27. Kwon YJ, Standley SM, Goh SL, Frechet JM (2005) Enhanced antigen presentation and immunostimulation of dendritic cells using acid-degradable cationic nanoparticles. *J Control Release* 105(3):199-212.

28. Murthy N, Xu M, Schuck S, *et al.* (2003) A macromolecular delivery vehicle for protein-based vaccines: acid-degradable protein-loaded microgels. *Proc. Natl. Acad. Sci. U. S. A.* 100(9):4995-5000.

29. Fichter M, Dedters M, Pietrzak-Nguyen A, *et al.* (2015) Monophosphoryl lipid A coating of hydroxyethyl starch nanocapsules drastically increases uptake and

maturation by dendritic cells while minimizing the adjuvant dosage. *Vaccine* 33(7):838-846.

30. Pietrzak-Nguyen A, Fichter M, Dedters M*, et al.* (2014) Enhanced in vivo targeting of murine nonparenchymal liver cells with monophosphoryl lipid A functionalized microcapsules. *Biomacromolecules* 15(7):2378-2388.

31. Elamanchili P, Diwan M, Cao M, Samuel J (2004) Characterization of poly(D,L-lactic-co-glycolic acid) based nanoparticulate system for enhanced delivery of antigens to dendritic cells. *Vaccine* 22(19):2406-2412.

32. Standley SM, Mende I, Goh SL*, et al.* (2007) Incorporation of CpG oligonucleotide ligand into protein-loaded particle vaccines promotes antigen-specific CD8 T-cell immunity. *Bioconjug Chem* 18(1):77-83.

33. Christie M, Torres RM, Kedl RM, Randolph TW, Carpenter JF (2014) Recombinant murine growth hormone particles are more immunogenic with intravenous than subcutaneous administration. *J Pharm Sci* 103(1):128-139.

34. Epstein JE, Tewari K, Lyke KE*, et al.* (2011) Live attenuated malaria vaccine designed to protect through hepatic CD8(+) T cell immunity. *Science* 334(6055):475-480.

35. Seder RA, Chang LJ, Enama ME*, et al.* (2013) Protection against malaria by intravenous immunization with a nonreplicating sporozoite vaccine. *Science* 341(6152):1359-1365.

36. Burchill MA, Tamburini BA, Pennock ND*, et al.* (2013) T cell vaccinology: exploring the known unknowns. *Vaccine* 31(2):297-305.

37. Baier G, Musyanovych A, Dass M, Theisinger S, Landfester K (2010) Cross-linked starch capsules containing dsDNA prepared in inverse miniemulsion as "nanoreactors" for polymerase chain reaction. *Biomacromolecules* 11(4):960-968.

38. Piradashvili K, Fichter M, Mohr K*, et al.* (2015) Biodegradable protein nanocontainers. *Biomacromolecules* 16(3):815-821.

39. Gehring S, Gregory SH, Wintermeyer P*, et al.* (2008) Generation and characterization of an immunogenic dendritic cell population. *J Immunol Methods* 332(1-2):18-30.

40. Gehring S, Gregory SH, Wintermeyer P, Aloman C, Wands JR (2009) Generation of immune responses against hepatitis C virus by dendritic cells containing NS5 protein-coated microparticles. *Clin Vaccine Immunol* 16(2):163-171.

41. Gehring S, Dickson EM, San Martin ME*, et al.* (2006) Kupffer cells abrogate cholestatic liver injury in mice. *Gastroenterology* 130(3):810-822.

42. Fichter M, Baier G, Dedters M*, et al.* (2013) Nanocapsules generated out of a polymeric dexamethasone shell suppress the inflammatory response of liver macrophages. *Nanomedicine* 9(8):1223-1234.

43. Feeney ER, Chung RT (2014) Antiviral treatment of hepatitis C. *BMJ* 348:g3308.

44. Chayama K, Hayes CN (2015) HCV Drug Resistance Challenges in Japan: The Role of Pre-Existing Variants and Emerging Resistant Strains in Direct Acting Antiviral Therapy. *Viruses* 7(10):5328-5342.

45. Sarrazin C (2015) The importance of resistance to direct antiviral drugs in HCV infection in clinical practice. *J. Hepatol.*

46. Callendret B, Eccleston HB, Hall S*, et al.* (2014) T-cell immunity and hepatitis C virus reinfection after cure of chronic hepatitis C with an interferon-free antiviral regimen in a chimpanzee. *Hepatology* 60(5):1531-1540.

47. Ruta S, Cernescu C (2015) Injecting drug use: A vector for the introduction of new hepatitis C virus genotypes. *World J Gastroenterol* 21(38):10811-10823.

48. Hickman M, De Angelis D, Vickerman P, Hutchinson S, Martin NK (2015) Hepatitis C virus treatment as prevention in people who inject drugs: testing the evidence. *Curr Opin Infect Dis* 28(6):576-582.

49. Huang LR, Wohlleber D, Reisinger F*, et al.* (2013) Intrahepatic myeloid-cell aggregates enable local proliferation of CD8(+) T cells and successful immunotherapy against chronic viral liver infection. *Nat Immunol* 14(6):574-583.

50. Jenne CN, Kubes P (2013) Immune surveillance by the liver. *Nat Immunol* 14(10):996-1006.

51. Cruz LJ, Tacken PJ, Rueda F*, et al.* (2012) Targeting nanoparticles to dendritic cells for immunotherapy. *Methods Enzymol* 509:143-163.

52. Brass V, Bieck E, Montserret R*, et al.* (2002) An amino-terminal amphipathic alpha-helix mediates membrane association of the hepatitis C virus nonstructural protein 5A. *J. Biol. Chem.* 277(10):8130-8139.

53. Penin F, Brass V, Appel N*, et al.* (2004) Structure and function of the membrane anchor domain of hepatitis C virus nonstructural protein 5A. *J. Biol. Chem.* 279(39):40835-40843.

54. Sarti F, Perera G, Hintzen F*, et al.* (2011) In vivo evidence of oral vaccination with PLGA nanoparticles containing the immunostimulant monophosphoryl lipid A. *Biomaterials* 32(16):4052-4057.

55. Beran J (2008) Safety and immunogenicity of a new hepatitis B vaccine for the protection of patients with renal insufficiency including pre-haemodialysis and haemodialysis patients. *Expert Opin Biol Ther* 8(2):235-247.

56. Tacken PJ, Zeelenberg IS, Cruz LJ*, et al.* (2011) Targeted delivery of TLR ligands to human and mouse dendritic cells strongly enhances adjuvanticity. *Blood* 118(26):6836-6844.

57. Blander JM, Medzhitov R (2006) Toll-dependent selection of microbial antigens for presentation by dendritic cells. *Nature* 440(7085):808-812.

58. Kratky W, Reis e Sousa C, Oxenius A, Sporri R (2011) Direct activation of antigen-presenting cells is required for CD8+ T-cell priming and tumor vaccination. *Proc Natl Acad Sci U S A* 108(42):17414-17419.

59. Schlaad H, Kukula H, Rudloff J, Below I (2001) Synthesis of alpha,omega-heterobifunctional poly(ethylene glycol)s by metal-free anionic ring-opening polymerization. *Macromolecules* 34(13):4302-4304.

Supporting information

2   Materials and Methods

2.1   Nanocapsule synthesis and characterization

2.1.1   Materials

Cyclohexane (HPLC grade - VWR) and 2,4-toluene diisocyanate (TDI - Sigma-Aldrich) were used for NC synthesis. The block copolymer poly((ethylene-*co*-butylene)-*b*-(ethylene oxide) P((E/B)-*b*-EO) consisting of a poly((ethylene-co-butylene) block (NMR: M_n = 3,900 g/mol) and a poly(ethylene oxide) block (NMR: M_n = 2,700 g/mol) was used as oil soluble surfactant and was synthesized according to previously published methods [59]. The anionic surfactant sodium dodecyl sulfate (SDS - Alfa Aesar) was used for resdispersion of NCs. The cy5-labeled oligonucleotide with the sequence cy5-CCA CTC CTT TCC AGA AAA CT-3′ (Thermo Scientific) and IRdye 800CW (LI-COR Biosciences) were used for detection of NCs.

2.1.2   Instrumentation

Ultrasonication was performed using the Branson Sonifier W-450-Digital and a microtip operating under ice cooling for 3 min at 70% amplitude with a pulse regime of 20 s sonication and 10 s pauses.

Sample purification was performed with the centrifuge Sigma 3 k-30. The Jeol 1400 transmission electron microscope with an accelerating voltage of 120 kV was used for morphological studies. Sample preparation was performed by placing 20 µL of diluted NC dispersion onto a 300 mesh carbon-coated copper grid allowing to dry under ambient conditions. Scanning electron microscopy (SEM) measurements were performed with a 1530 Gemini LEO (Zeiss) field emission microscope, using an accelerating voltage of 170 V.

Sample preparation was performed as described above using silicon wafers instead of copper grids as substrate.

The average size and size distribution of the NS5A-NCs were determined via dynamic light scattering (DLS) at 25 °C using a Nicomp 380 submicron particle sizer (Nicomp Particle Sizing Systems, USA) at an angle of 90°.

Zeta potential was measured in 10^{-3} M potassium chloride solution at pH 6.8 and 25°C with the Malvern Zetasizer (Malvern Instruments, U.K.).

Quantification of MPLA adsorbed onto NS5A-NCs was performed using a Limulus Amebocyte Lysate (LAL) assay (Hycult biotech, HIT302) according to manufacturer´s instructions. Two-fold serial dilutions of NS5A+MPLA-NCs (0.54 wt%) in endotoxin-free water (1:1000 - 1:16.000) were analyzed. NS5A-NCs without MPLA served as reference. Loading capacity (LC) of MPLA was calculated by the ratio of the mass of adsorbed MPLA over the total mass of NCs.

2.2 Biological analysis

2.2.1 Antibody production

The murine CD40 antibody (clone 1C10) was purified from the supernate of a hybridoma cell line (ATCC® HB-12537™). The culture supernatant was concentrated using Centricon Plus-70 centrifugal filter units (10kDa NMWL, Merck Millipore) and antibodies were purified using a protein G purification kit (Montage Antibody Purification Kit PROSEP-G, LSK2ABG, EMD Millipore).

2.2.2 Confocal laser scanning microscopy

Confocal laser scanning microscopy (CLSM) was performed in order to visualize intracellular uptake of NS5A-NCs using a Zeiss LSM 710 NLO. NPCs (5×10^5 per well) were cultured in

8-well chamber slides (ibidi, 80827) at 37 °C for 24 h in the presence of 10 μg/mL cy5-labeled NS5A nanocapsules. Nuclei were stained with 2 μg/mL Hoechst 33342 (Life Technologies) for 30 min. Plasma membrane staining was achieved by adding 4 μg/mL CellMask Orange (Life Technologies) 5 min prior to analysis.

2.2.3 Production of HCV non-structural protein 5A

Recombinant HCV NS5A was synthesized using the yeast Pichia pastoris. The nucleotide sequence encoding aa 34 - 447 of the NS5A gene (HCV genotype 1 b) was amplified and cloned into the expression vector pPICZα A (pPICZα-NS5A - Life Technologies). The resulting clone was transformed into the Pichia pastoris strain X-33 and the recombinant NS5A protein including six amino-terminal histidine residues were expressed by secretion. Purification of the protein was performed using a nickel-chelate affinity resin (HisTrap HP – GE Healthcare) under native conditions according to manufacturer´s recommendations.
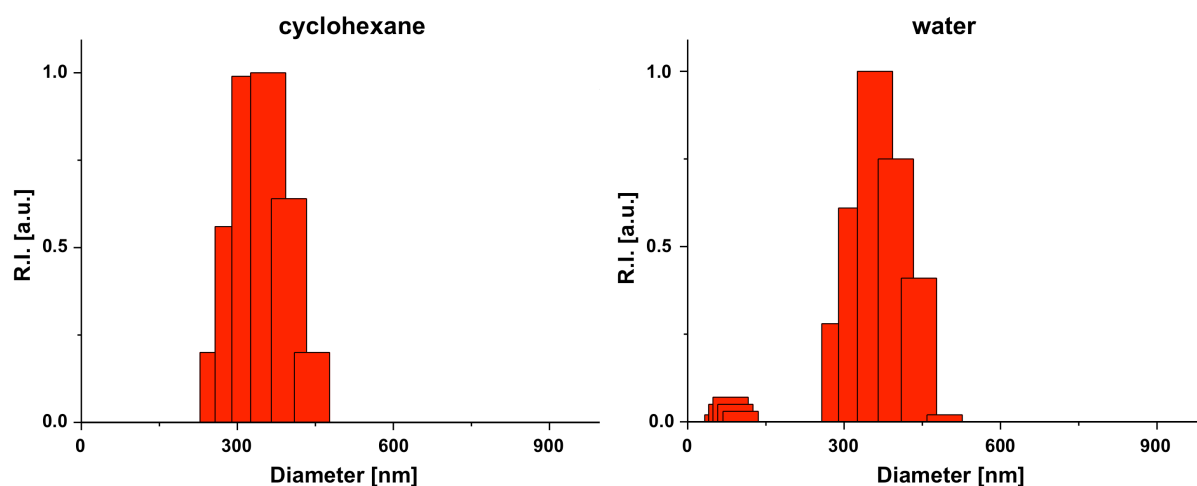

Supporting Figure 1: Size distribution diagrams of NS5A-nanocapsules in cyclohexane (*left*) and water (*right*) obtained by dynamic light scattering.
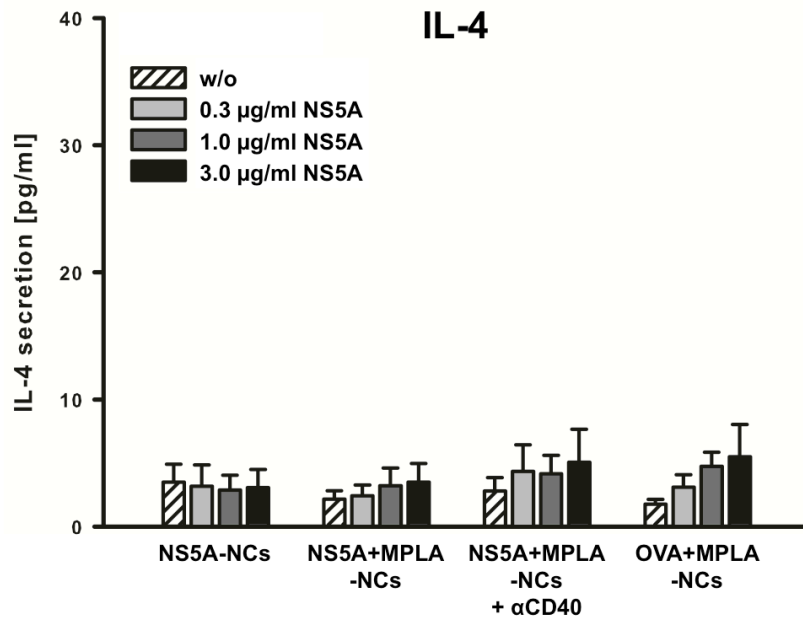
Supporting Figure 2: NPCs obtained from mice, immunized three times with different NC formulations, were cultured with recombinant HCV NS5A at indicated concentrations and culture supernatants were collected after 24 h. IL-4 concentrations were quantified using an enzyme-linked immunosorbent assay. Data represent the means ± SD derived from five mice.
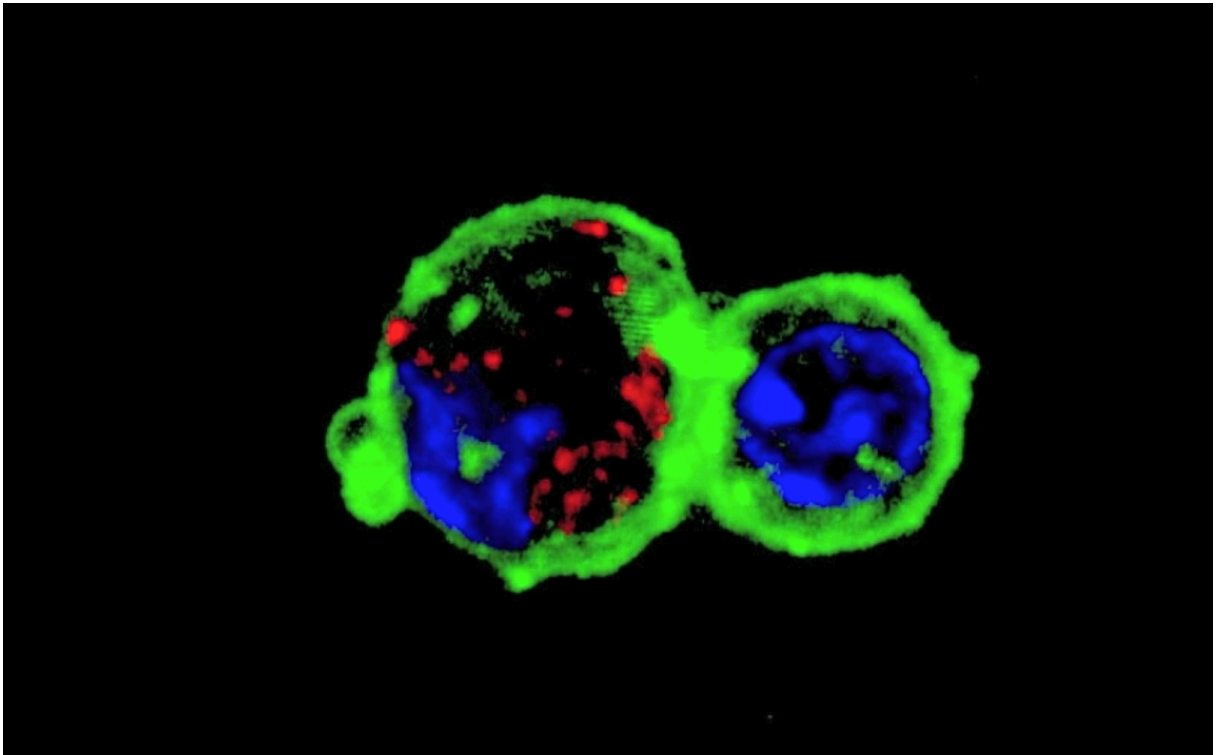
Supporting Video 1: Nanocapsule uptake by NPCs *in vitro* was evaluated using confocal laser scanning microscopy. Z-stack microscopy of a representative non-parenchymal cell ingesting nanocapsules was performed followed by 3D reconstruction and animation of the acquired data.
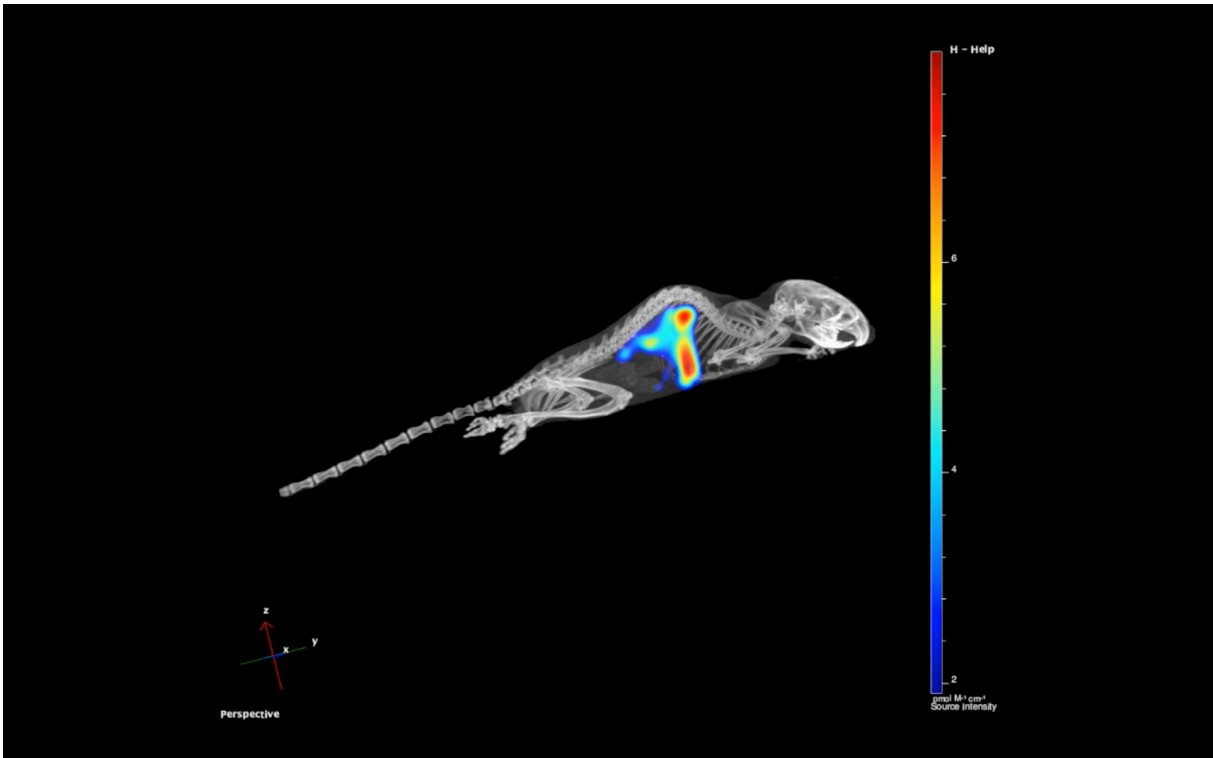
Supporting Video 2: Deposition of IRdye-labeled NS5A nanocapsules was determined using fluorescence imaging tomography 4 h after intravenous injection. Multimodality acquisition using transillumination measurements of IRdye NCs along with computed tomographic imaging was performed following 3D reconstruction of fluorescence signals and animation of the acquired data.

6.8 Abbreviations

3D	ombitasvir/paritaprevir/ritonavir + dasabuvir
ALT	alanine transaminase
alum	aluminum hydroxide/phosphate
ANOVA	analysis of variance
APC	antigen-presenting cell
AS04	Adjuvant System 04
AT III	antithrombin III
BODIPY	boron-dipyrromethene
BSA	bovine serum albumin
CD	cluster of differentiation
ChAd3	chimpanzee adenovirus type 3
CHC	chronic hepatitis C virus infection
CLSM	confocal laser scanning microscopy
CMFDA	5-chloromethylfluorescein diacetate
DAA	direct-acting antiviral drug
DC	dendritic cell
DXM	dexamethasone
E1/2	envelope protein 1/2
EMA	European Medicine Agency
FDA	Food and Drug Administration
FLIT	fluorescence intensity tomography
GBD2010	Global Burden of Disease, Injuries and Risk Factors 2010
h	hour
HA	hyaluronic acid
HAV	hepatitis A virus
HBV	hepatitis B virus
HCC	hepatocellular carcinoma
HCV	hepatitis C virus
HEP	heparin
HES	hydroxyethyl starch
hFlt3l	human Fms-like tyrosine kinase 3 ligand
HIV	human immunodeficiency virus
HPV	human papilloma virus
IFNα	interferon α
IFNβ	interferon β

IFNγ	interferon-γ
IgG	immunoglobulin G
IgM	immunoglobulin M
IL-12	interleukin-12
IV	intravenous
IVDU	intravenous drug user
KC	Kupffer cell
LPS	lipopolysaccharide
LSEC	liver sinusoidal endothelial cell
MAVS	mitochondrial antiviral-signaling protein
MC	microcapsule
min	minute
ml	milliliter
moDC	monocyte-derived dendritic cell
MPLA	monophosphoryl lipid A
mV	millivolts
MVA	modified vaccinia Ankara
MyD88	myeloid differentiation factor 88
NaCl	sodium chloride
NANBH	non-A, non-B hepatitis
NC	nanocapsule
NF-κB	nuclear factor-κB
NK (T) cell	natural killer (T) cell
nm	nanometer
NPC	non-parenchymal liver cell
NS5A	HCV non-structural protein 5A
OVA	ovalbumin
PACA	poly(cyanoacrylates)
PEG	poly(ethylene glycol)
PfSPZ	*Plasmodium falciparum* sporozoites
PGE_2	prostaglandin E_2
PLA	poly(lactic acid)
PLGA	poly(lactic-co-glycolic acid)
R848	resiquimod
RBV	ribavirin
RIG-I	retinoic acid-inducible gene 1
RNA	ribonucleic acid

SD	standard deviation
SEM	scanning electron microscopy
SR101	sulforhodamine 101
SVR	sustained virological response
TBE	tick-borne encephalitis
TEM	transmission electron microscopy
TGFβ	transforming growth factor-β
Th1/2	T helper cell 1/2
TLR3/4	Toll-like receptor 3/4
TNFα	tumor necrosis factor-α
Treg	regulatory T cell
TRIF	Toll-interleukin receptor-domain-containing adapter-inducing interferon-β
VLP	virus-like particle
µg	microgram
µM	micromolar
µm	micrometer

DECLARATION OF AUTHORSHIP

I hereby confirm that I have authored this PhD thesis independently and without use of other than the indicated resources.

Furthermore, I certify that this thesis or any part of it has not been previously submitted for a degree or any other qualification at the Johannes Gutenberg University Mainz or any other institution in Germany or abroad.

Mainz, March 9th 2016

_____

Michael Fichter